High-resolution projections of climate change over the Iberian Peninsula using a mesoscale model

Proyecciones de cambio climático de alta resolución sobre la Península Ibérica mediante un modelo de mesoscala

Memoria presentada para optar al grado de Doctor en Física por:

Daniel Argüeso Barriga

Directoras:

Dra. Yolanda Castro Díez
Dra. María Jesús Esteban Parra
Dra. Sonia Raquel Gámiz Fortis

ugr | **Universidad**
de Granada

Departamento de Física Aplicada
Facultad de Ciencias
Universidad de Granada

High-resolution projections of climate change over the Iberian Peninsula using a mesoscale model

———————

Directoras:

Dra. Yolanda Castro Díez
Catedrática
Universidad de Granada

Dra. María Jesús Esteban Parra
Profesora Titular
Universidad de Granada

Dra. Sonia Raquel Gámiz Fortis
Investigadora Contratada
Universidad de Granada

Memoria presentada para optar al grado de:
Doctor en Física
por

Daniel Argüeso Barriga
Licenciado en Física

Granada, 1 de Septiembre de 2011

Acknowledgements

Lanzarse a escribir una tesis requiere, además de ser un poco inconsciente, un grupo de gente que te apoye, te sugiera, te aconseje y te enseñe. Yo he tenido la suerte de contar con personas que han hecho eso y mucho más, y que sin ellas esta tesis difícilmente habría visto la luz.

Es necesario tener un buen capitán de barco. Y yo he tenido tres fantásticas: Yolanda, María Jesús y Sonia, mis directoras. Para empezar, ellas me han dado la oportunidad de dedicarme a lo que más me gusta. Y además han sabido apoyarme y guiarme durante estos años, haciendo que mi investigación fuera lo más productiva posible. Sin ellas este trabajo simplemente no existiría.

Durante los años que uno dedica a investigar y escribir la tesis, hay personas con las que acabas creando una gran amistad. Con Andy he compartido, además de un despacho lleno de trastos, conversaciones sobre ciencia que nunca olvidaré, repletas de naves espaciales, avioncitos de papel y bolas que se mezclan. También el gusto por cosas que nada tienen que ver con la ciencia, entre ellas *Grateful Dead*.

Cuando uno llega a un lugar, siempre hay alguien que va un pasito justo por delante, alguien que acaba de pasar por lo que tú y te entiende mejor que nadie. Poder disfrutar de los consejos de una persona así es una ayuda tremenda. ¡Muchas gracias, Penélope!.

También hay gente que llega un pasito por detrás y que con sus preguntas te enseñan cuánto te queda aún por aprender. Jose ha sido el perfecto compañero de cafés, desesperos, capitulitos y tertulias futboleras (¡¡¡no sueltes los pavos mucho, que te tengo que ver en estas dentro de un año!!!). No sé si volveremos a pasar tantas horas juntos como estos años, pero me quedo con las carcajadas (y cabreos) que hemos compartido. Te prometí que contaría las veces que me echaste una mano para ponerlas aquí luego. He perdido la cuenta. ¡Gracias, amigo!.

Gracias a toda la gente que ha hecho del despacho, más que un lugar de trabajo, una segunda casa. A Enrique, con quién compartí almuerzos y charlas todos los días (¡siempre el plato grande para tí!). A Borja, que corría por todos nosotros en el partidillo de los viernes. A Dani, que nos arreglaba los desaguisados de los ordenadores (!y hacía alguno también!). A todos los demás que pasaron

por allí e hicieron del cuartucho un lugar mucho más agradable de lo que jamás hubiera pensado.

Gracias a muchos otros que, sin apenas conocerme, me ayudaron muchísimo cuando los modelos eran para mí una selva oscura y me enseñaron a 'andar' en este mundo. Gracias a la gente de Murcia, a Juanpe y Sonia, a los de Santander, a Chus, Sixto y Lluís (nos vemos en Australia), a Jon y a muchos otros que pusieron a mi disposición su trabajo de muchos años.

Quiero recordar a la gente que dedica su tiempo y esfuerzo a crear software libre sin pedir nada a cambio. Una parte importante del avance de la ciencia computacional se la debemos a ellos. Al CSIRC de la Universidad de Granada por el tiempo de computación y a las personas que administran el UGRGRID, porque han sido claves para llevar a cabo todas las simulaciones. Al dios Google, ya sé que es una empresa y esas cosas...pero, ¿como se hacía sin él para escribir una tesis antes?.

La investigación me ha dado muchas satisfacciones y entre ellas, una de las más importantes, es haber conocido lugares y personas fascinantes. Gracias a todos ellos. Special thanks to Dr. Jimy Dudhia and the NCAR staff for all your support during my stay in Boulder and all I have learned from you. Thanks to Ulla and Rafa, my 'papitos' in the trip to Canyonlands. Gracias también a Pedro y a Jordi, que con sus charlas en la cafetería del NCAR me enseñaron que lo más importante es saber qué preguntarse, cómo plantear el problema.

Durante este tiempo ha habido mucha, muchísima gente que me han dado su apoyo y cariño, que me han enseñado y me han hecho disfrutar. A Nacho y Pablo, con los que he ido descubriendo el mundo y haciéndome mayor. A Rafca mi hermano grande y mi fuente de alegrías. A Afro (Dr. *pastaio*) y Jenny, que me han ido dejando una casa por donde he pasado y que sobre todo, han hecho de Granada un hogar; a Annalisa (¡y ahora Nina!) que durante un año y medio fue mi segunda familia; a Yoan (¡*garbancito*!), mi hermano cachaçero de entusiasmo contagioso; a Vuk, un *bon vivant* con alma de canchero (y 'teóricamente' doctorando); a Facundo y la 'Gattusa', por sus asados y por haberme pintado una franja roja en el pecho (mal momento); a Eli y Nayra que me han cuidado siempre tan bien (¿somos ricos?); A Juju, que ha compartido conmigo noches de insomnio en casa (você não imagina a companhia que me fez Devendra nesses meses). A todas la personas que me han acompañado estos años (y también antes): a los de Córdoba, a los de Módena y a los de Salamanca.

A mi familia, que han hecho que me sienta siempre querido y que cuando 'estaba' pequeño llenaron mi depósito de felicidad: a mis abuelos, mis titos y

mis primos. A mi familia brasileña: a Kaká, Mauro, Jubs, Lu, (Uh)Lelé, Nina y Olivia. Obrigado, gente!

A Bota, que me ha soportado contando las peripecias con los modelos y dando vueltas desquiciado por casa estos últimos meses. Gracias por haber estado conmigo siempre en esta montaña rusa, por tus ánimos, por tu paciencia y por tus mágicas burbujas. Océanos, flaca!

A mis padres. Ellos me han enseñado todo lo importante. Me han apoyado y exigido. Me han dado el gusto por viajar, por la literatura, por la conversación, por el cine, por la música, por la ciencia. Me han llevado a lugares maravillosos. Pero sobre todo, me han escuchado y me han dado todo el cariño y más. A mi hermano, con él he vivido y compartido de todo. No hay nadie que haya sentido más cerca que él. Hemos jugado horas y horas, hemos sido compañeros de diabluras, hemos crecido juntos poco a poco... sólo nos falta un gran viaje (escarabajo, ¿será este invierno?). Muchas gracias a los tres, os quiero!!

I would also like to thank Dr. Jason Evans and the UNSW for giving me the opportunity to continue researching in what I am passionate about and meet a new country.

Perhaps some day in the dim future it will be possible to advance the computations faster than the weather advances and at a cost less than the saving to mankind due to the information gained. But that is a dream.

Lewis F. Richardson, 1922

Abstract

Global projections of climate indicate that substantial changes might occur in the future as a consequence of global warming. Such changes would have important environmental, social and economical implications. However, the climate response to global warming strongly varies from region to region and thus it requires to be studied at scales that General Circulation Models (GCMs) cannot resolve.

In this Thesis, the Weather Research and Forecasting (WRF) model was selected to downscale GCMs information and generate physically-consistent high-resolution projections of climate change scenarios over the Iberian Peninsula (IP). A set of climate simulations over the IP were performed at 10-km resolution to explore the impact of global warming on precipitation and temperature at regional scales. At this spatial resolution, the model is able to incorporate the effects of topographical features that are know be key factors in the spatial distribution of the climate regimes and the areas within the IP that might be subjected to different changes can be identified.

Particular attention was paid to the model configuration and its evaluation with respect to the present climate. Initially, eight decadal (1990-1999) simulations were completed to conduct a sensitivity test and determine which combination of physics options better describe the Iberian climate features. The model outputs were compared with observations using an objective multi-step regionalization technique to circumvent the spatial scale disparity between the model estimates and the site-specific observations. No combination was found to outperforms the others under all circumstances and not all the physics schemes were found to be equally decisive. In fact, a compromise solution had to be selected bearing in mind factors such as the performance with respect to the different variables in the different regions, or the benefit gained with higher-complexity schemes.

The model evaluation consisted in the assessment of the model ability to simulate present climate in terms of precipitation and temperature using the Spain02 gridded dataset to compare with. Three different present climate (1970-1999)

simulations driven by three boundary data (ERA-40, ECHAM5 and CCSM3.0) covering the entire IP were completed to elucidate whether the model is suitable to study the Iberian climate. The validation reveals that, in spite of some non-negligible errors, the model is able to reproduce most of the main features of the Iberian precipitation and temperature. In particular, WRF shows particularly good agreement with the observations in terms of the probability distributions and the upper-percentiles.

Finally, the high-resolution climate change projections were obtained from an ensemble of future climate (2070-2099) simulations over the IP. In particular, three emissions scenarios (B1, A1B and A2) and two GCMs (ECHAM5 and CCSM3.0) were employed to reduce the uncertainty associated to the boundary conditions. The model estimates for temperature and precipitation were compared with those from the present climate simulations and the projected changes were analyzed. Not only the long-term means were examined, but also the high-order statistics, including different extreme indices to characterize the tails of the distributions.

The high-resolution projections of climate change scenarios over the Iberian Peninsula suggests that substantial decreases in mean precipitation might be expected over IP, but their magnitude is projected to be unevenly distributed across the IP. However, the precipitation extremes events might not be overall expected to change significantly. On the other hand, temperature increases are very likely to occur over the entire IP, particularly for maximum temperature extremes. The most affected areas by precipitation changes are projected to be the mountainous regions, whereas those affected by temperature increases cover large areas in the interior of the IP.

This Thesis represents a valuable contribution to the understanding of global warming repercussions on the Iberian climate. The spatial resolution employed in the simulations enabled the generation of climate change projections with a degree of detail that is unprecedented in the Iberian Peninsula. Furthermore, this study provides a comprehensive description of the projected changes at very different timescales, including the extreme events, which might be of greater impact than the mean climatic changes.

Contents

List of Figures

List of Tables

List of Acronyms

$ACM2$ Asymmetric Convective Model version 2

$AOGCM$ Atmosphere-Ocean Global Circulation Model

ARW Advanced Research WRF

BMJ Betts-Miller-Janjic cumulus scheme

CA Clustering Analysis

$CAM3.0$ NCAR Community Atmosphere Model version 3.0

$CAPE$ Convective Available Potential Energy

$CCSM$ NCAR Community Climate System Model version 3

$CLWRF$ Modified version of WRF v3.1.1 from University of Cantabria

$ECHAM$ Fifth-generation Max Planck Institute general circulation model

$ECMWF$ European Centre for Medium-Range Weather Forecast

GCM General Circulation Model

GHG Greenhouse Gases

IP Iberian Peninsula

$IPCC$ Intergovernmental Panel on Climate Change

$IPCC\,AR4$ IPCC Fourth Assessment Report

$IPCC\,TAR$ IPCC Third Assessment Report

KF Kain-Fritsch cumulus scheme

LAM Limited Area Model

LBC Lateral Boundary Condition

LSM Land Surface Model

MAE Mean Absolute Error

MPI Message Passing Interface

MRF Medium Range Forecast

NAO North Atlantic Oscillation

$NCAR$ National Center for Atmospheric Research

$NCEP$ National Centers for Environmental Prediction

$NNRP$ NCEP/NCAR Reanalysis Project

$NOAA$ National Oceanic and Atmospheric Administration

NWP Numerical Weather Prediction

PBL Planetary Boundary Layer

PCA Principal Components Analysis

RCM Regional Climate Model

$RMSE$ Root Mean Square Error

$SRES$ IPCC Special Report on Emission Scenarios

SST Sea Surface Temperature

$Tmax$ Maximum temperature

$Tmin$ Minimum temperature

$USGS$ U.S. Geological Survey

WPS WRF Preprocessing System

WRF Weather Research and Forecasting model

$WSM3$ WRF Single-Moment 3-class microphysics scheme

Chapter 1

Introduction

The main objective of this Thesis is to create high-resolution projections of climate change scenarios in the Iberian Peninsula and determine the impact of Global Warming on its climate. In order to achieve this goal, large-scale information is downscaled using a mesoscale model. Potential changes in both the mean and extreme values of precipitation and temperature are analyzed and discussed. Additionally, an appropriate configuration of the model for the particular region of interest is put forward, including a suitable combination of parameterizations.

A brief introduction to the problem will shed light on the obstacles and challenges that are found in the process of generating high-resolution climate change information as well as place this study within the context of the state-of-the-art research.

1.1   The Climate Change at human scales

We are already used to see pictures of glaciers that have reduced their extension dramatically, deserts that before were wetlands or striking images of floods in very diverse places. Probably as a consequence of them, the population is becoming aware of the impact that potential changes in climate might have in their lives, the media are increasingly devoting attention to the issue and governments all over the world are placing the mitigation and adaptation policies at the top of their agendas. However, these images do not constitute any scientific evidence that climate change is coming about, they are not statistically significant and they cannot even be regarded as a confirmation of a change. Indeed, consistent and statistically significant information is rather necessary to reach any robust conclusion on the matter. Despite the fact that there are still uncertainties as-

sociated to sources and mechanisms of climate change, studies in the past years have permitted to affirm that the atmosphere has been modified by humans and the effects have been observed in a range of variables (IPCC, 2007). In fact, the scientists widely agree that a change in the climate is occurring and human activity is at least partly responsible for it. Nevertheless, more information at finer scales and preciser knowledge of certain processes in the atmosphere are yet necessary to completely understand what is going on.

The climate change can overall be explained in terms of a global energy balance that is being altered through changes in the atmospheric concentration of greenhouse gases and aerosols, natural variations of solar radiation and modification of the surface albedo. These factors do not contribute to the radiative forcing in the same direction, but all together displace the radiation balance towards incoming positive values, leading to global warming. However, the information about global changes is somehow incomplete if the impact on ecosystems and population is not examined. But this has to be approached from a regional point of view. The primary question that arises out of this issue is whether the climate response to global warming varies from region to region.

Bearing in mind that the earth's climate diversity is extraordinary, it might also be expected that the projected changes in climate will vary across the globe. For example, the alteration of general circulation can produce increases in precipitation over certain areas whereas others might suffer from rainfall diminution (Fig. 1.1), as it is predicted to happen in Europe, where the strengthening of the North Atlantic Oscillation (NAO) positive phase induces a poleward displacement of the storm tracks. Furthermore, local features such as the orographic forcing, the latitude or the distance to oceans are predominant factors in defining the climate and its evolution under climate change conditions, since they might enhance or diminish global warming effects. For instance, the oceans thermal inertia might cause that the interiors of continents warm more than coastal areas. But even more, many characteristics of climate are essentially local and unevenly distributed, like extreme events, that usually depend on feedbacks between processes taking place at regional scales. Therefore, estimations of climate change projections at regional scales are crucial to determine its repercussion for both the environment and human life.

General Circulation Models (GCMs) are currently the prime source of information for future climate projections and they are extremely useful to provide comprehensive knowledge of large-scale climate and general circulation. However they are still unable to capture local features of climate and produce detailed
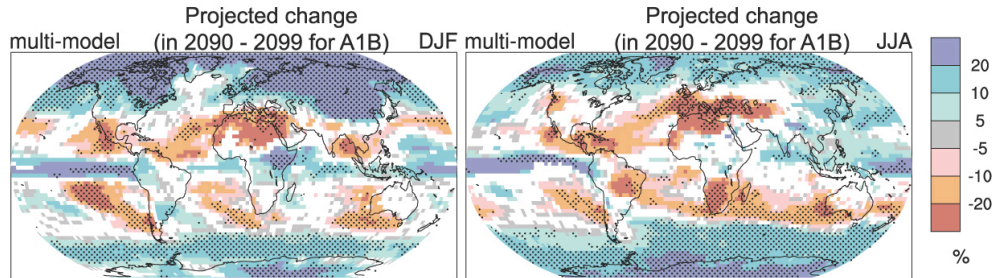
Figure 1.1: *Precipitation changes projected (in %) for the period 2090-2099 with respect to 1980-1999 and based on the SRES A1B scenario. December to February means on the left and June to August means on the right. Obtained from IPCC AR4. Figure SPM.7.*

information about climate change impact on regional scales due to their coarse resolution ($\sim 1.0°$ by $1.0°$) and their inadequate model physics to reproduce small-scale phenomena (although recent GCMs are being run at finer resolutions and employing improved parameterizations). Furthermore, GCMs grid points cannot be interpreted as representative of the place where they are located (von Storch et al., 1993) since the grid-box averages are often very different from local climate within the area (Good and Lowe, 2006) and therefore, it is inadequate to infer fine-scale results from those of large-area average (Christensen et al., 2007a). As a consequence, some decisive aspects of climate change, such as the extreme events, are absolutely impossible to address with current GCMs. An increase in GCMs resolution shoots up computational costs, but climate modeling is already one the research fields that consume more computational resources and many of the most powerful machines in the world are dedicated to climate simulations. Therefore, computational costs associated to spatial resolution increase in GCMs are still prohibitive and alternative approaches, encompassed in the term *downscaling*, have been put forward.

1.2   Downscaling: looking closer the climate change

Since General Circulations fail to describe local features of climate, dowsncaling was proposed to overcome the problem of increasing resolution at reasonable computational costs. Different types of downscaling have been suggested in the last decades, but they can be roughly classified in two groups, *statistical* (or *experimental*) and *dynamical*.

Statistical downscaling (von Storch et al., 1993; Wilby et al., 1999) is based on robust empirical relationships between large-scale variables (predictors) and local variables (predictands). These relationships are determined using observational records and are then projected to the future, retrieving local scale information from GCMs. This technique has been widely employed with remarkable results (Boé et al., 2007; Huth, 1999; von Storch et al., 1993; Wilby and Wigley, 1997) and the computational costs associated are considerably low. However, since the relationships refer to particular locations, no information can be obtained beyond the places where the observations are available. Furthermore, finding an appropriate relationship is not straightforward and sometimes it is not even possible to determine a solid connection between large-scale and local variables.

On the other hand, dynamical downscaling lies in finding an approximate solution to the equations of the atmosphere using a physical model at higher resolutions than the GCM, but imposing some restrictions. Different methods within the dynamical downscaling technique can be mentioned: 1) Those that still employ a GCM but increasing the resolution over a particular region by stretching the grid (Déqué and Piedelievre, 1995) or reorienting the grid pole (Wang et al., 1999), or during a particular short-time period (time slice technique, Cubasch et al., 1995), and 2) those that use Regional Climate Models (Giorgi and Mearns, 1999; McGregor, 1997).

The Regional Climate Models (RCMs) work by increasing GCMs resolution in a limited region of interest, numerically solving the simplifed governing equations over a finer grid with parameterizations adapted to the new spatial scale. This results in a detailed description of the orography (Fig. 1.2) and thus the processes at regional scales are likely to be captured by the model. Since RCMs are confined to a particular area, they somehow need to 'know what is happening outside' and hence they require the boundary conditions to be specified, which are usually obtained from GCM outputs or observational analysis. Moreover, GCMs employ a single configuration for the entire globe that is not necessarily the most appropriate for every region, whereas RCMs also permit to adapt their configuration to the region under survey, which might represent a considerable improvement over the GCMs.

It has been traditionally argued in favor of dynamical downscaling that it is physically consistent and thus can be used to project future climates, while statistical downscaling is exclusively based on empirical relationships that might not take place in the future. Nevertheless, this statement does not take into account that physical models are also supported by parameterizations, which
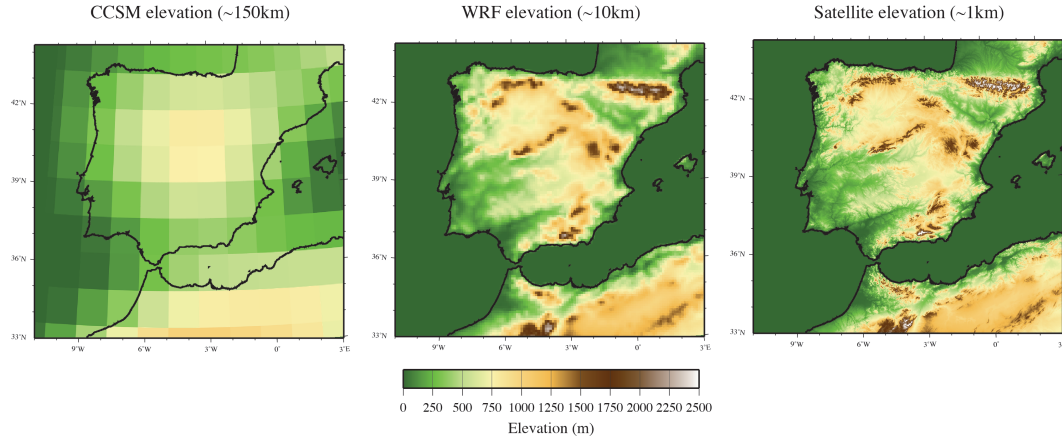
Figure 1.2: *Examples of topography from a GCM model, WRF at 10 km and an image from Satellite.*

are semi-empirical approximations of reality, and thereby prone to changes in the future. Both statistical and dynamical methods have their own advantages and shortcomings, and their choice depends directly on the study that will be conducted. Statistical downscaling can be applied not only to meteorological variables but also to other variables such as the river flow levels or the annual crops. However, the statistical downscaling results are constrained to predictands and locations with available measurements. Conversely, dynamical downscaling is able to provide a number of climate variables all through the domains, but at elevated computational costs. A positive consequence of having a broad range of variables at our disposal is their potential use as input data to local-scale models such as the hydrological ones, which constitutes an additional benefit for climate studies.

This study aims at meteorological variables over a wide area and results are desired in the entire region, including places with no observational records. Further research regarding river flow levels are also planned for the future. Therefore, dynamical downscaling using a Regional Climate Model has been selected to create high-resolution climate change scenarios projections over the Iberian Peninsula (IP).

1.3   The Iberian Peninsula

This survey presents a series of high-resolution climate change projections in the Iberian Peninsula[1]. This region was selected due to obvious personal reasons: it is the place we live in and therefore any potential change in the climate would directly impact our lives. But there are also several objective motivations.

In order to put the motivations into context, the main features of Iberian region and its climate are described. The IP is located between 36°N-44°N and 3°E-10°W (Fig. 1.3) and it is characterized by high intra-annual variability, which is typical of the midlatitudes. The large-scale precipitation is mainly modulated by the position of the Azores anticyclone that acts as a blocking structure in the summer, preventing the low pressure systems from reaching the IP, and bringing hot and dry weather. In fact, almost no rainfall is recorded during these months in the southern half of the Peninsula. Conversely, from autumn to spring, the Azores high moves toward the tropics accompanied by a southward displacement of the jet-stream letting the low pressure systems get into the IP, resulting in wetter conditions. Besides the large-scale precipitation, convective processes are also important (particularly along the east coast) and produce very confined downpours that characterize the rainfall in this area. The region is surrounded by the Atlantic Ocean to the west, the European continent to the northeast, the Mediterranean Sea to the east and the Sahara desert to the south. Depending on the origin of the air masses, their temperature and water content vary dramatically, which represents an important component of local variability not only for precipitation but also for temperature. The wide range of values that temperature reaches in the IP is indeed a distinct attribute of its climate. Surface extremes in the interior and in the main river basins yield very high temperatures during the summer (among the highest in Europe), whereas very low records are registered in the elevated mountainous areas in the winter.

Topographical features are also crucial in the configuration of climate divisions, since different high mountain ranges are distributed across the region working as barriers and passageways determining local climates (see Fig. 1.4 as a reference of the main topographical features). Actually, the IP comprises a

---

[1]To be precise, the Thesis focuses on Peninsular Spain and Balearic Islands. The terms *Spain* and *IP* are here used in the same way to refer this region for the sake of brevity. The Canary Islands are omitted because their inclusion would imply much larger domains and thus unaffordable computational costs. Although the model is here evaluated only over the Spanish territory of the IP and hence the model performance over Portugal is not examined, the climate change projections maps show the results for Portugal too. These results are not analyzed in the text and their validity is definitely limited.
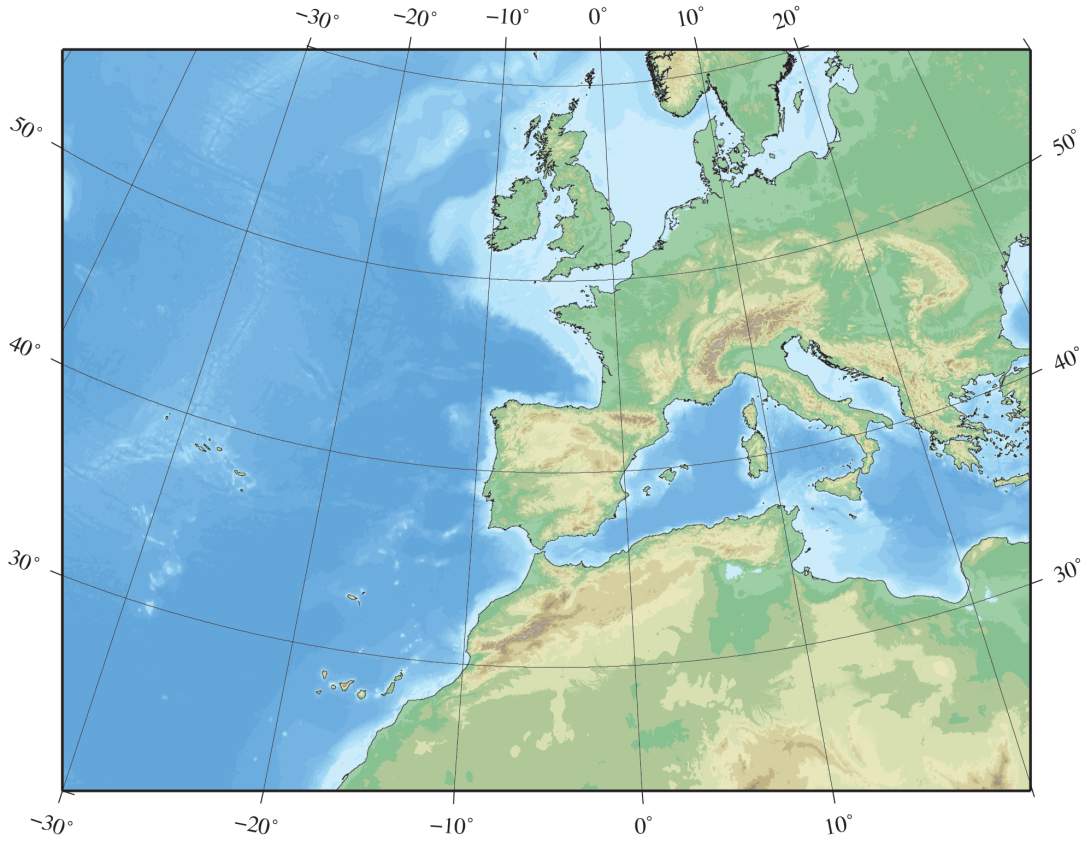
Figure 1.3: *Location of the region of interest: the IP (at the center) and the surrounding areas*

very complex orography with small but crucial geographical features such as the Strait of Gibraltar or localized mountainous systems that are completely missed in GCMs. These topographical elements exert strong influence on the climate patterns in the region and their appropriate inclusion in the model is pivotal to adequately describe the climate. The use of RCMs at high resolutions can thus provide an full picture of both the local climate and the impact of climate change on the region. A complex-topography region also represents an ideal scenario to test the model capabilities under unfavorable conditions and constitutes a challenge in terms of the model validity.

Furthermore, the IP is located in the western Mediterranean Sea, a region that is expected to be among those most affected by climate change in the globe in terms of both precipitation and summer temperature (Christensen et al., 2007a;

Figure 1.4: *Main topographical features of the Iberian Peninsula*

Giorgi, 2006a). These changes have been proven to depend not only on the atmospheric circulation but also can be attributed to land-surface processes (van Ulden et al., 2007), that in principle should be much better described at higher resolutions.

Moreover, tourism and agriculture are the two main pillars of the economy of the Iberian countries and they directly hinge on weather conditions. On that account, a detailed and accurate assessment of possible future changes, which can be obtained using RCMs, is essential to design efficient adaptation policies.

1.4   Overview of regional climate modeling research and challenges

The simulation of the atmosphere by numerical methods is by no means a new idea. In the early 20th Century, Vilhem Bjerknes (1862-1951) proposed a set of equations to describe the atmosphere. Bjerknes was convinced that meteorology could become an exact science if two conditions were fulfilled: 1) a sufficiently accurate knowledge of the state of the atmosphere at the initial time and 2) a sufficiently accurate knowledge of the laws according to which one state

of the atmosphere develops from another. His major contribution refers to the latter, proposing the so-called **primitive equations** to describe the atmosphere. Unfortunately, they constitute a non-linear system of partial differential equations that is yet to be analytically resolved and only numerical approximation of the solution are at our disposal.

Richardson (1922) attempted the first numerical approximation of the solution by hand and remained completely disappointed with the results, however his work was absolutely remarkable. It was only in the second half of the century that the first realistic solutions were obtained thanks to computer development. The earliest simulations just spread over few hours addressing the problem of weather forecasting and the technique was hence called Numerical Weather Prediction (NWP).

A regional climate simulation is at its core a prolonged numerical weather prediction. Nevertheless, the community skepticism about long-term simulations due to possible errors generated at the boundaries and the computational limitations initially hindered longer simulations. The first regional simulation that was run in climate mode' was performed in the late 1980s (Dickinson et al., 1989). Although it could not be formally considered a climate run because it barely spanned some days, the authors already stressed the importance of longer integrations so that the model becomes independent of the initial conditions. Afterwards, some other one-month simulations were completed (Giorgi, 1990; Giorgi and Bates, 1989) to evaluate the impact of initial values on different parameters. Regardless of the period they covered, these experiments laid the foundations of nested regional modeling techniques derived from numerical weather prediction.

The earliest runs extending longer periods were the perpetual January simulations (McGregor and Walsh, 1993), that consisted of several-month integrations maintaining a January typical forcing. Seasonal-varying simulations that covered various years started in the mid 1990s (Déqué and Piedelievre, 1995; Giorgi et al., 1994; Jones et al., 1995) and continued all through the decade increasing both the period studied and the resolution (Jones et al., 1997; Laprise et al., 1998; McGregor et al., 1998; Räisänen et al., 1999). Not only the resolution was improved in the successive simulations, but also the formulation of the models was gaining in complexity and they were progressively including processes that were omitted before. Computational development also contributed in a decisive way to increase the model complexity and multiply the number of simulations that were carried out over diverse regions and with different purposes in mind (Beniston et al., 2007; Castro et al., 2005; Correia et al., 2008; Jiménez et al., 2010; Solman

et al., 2008).

In the recent years, two remarkable projects focused on determining climate change impact on Europe using regional climate models, the PRUDENCE project (Christensen et al., 2007c) and the ENSEMBLES project (van der Linden and Mithchell, 2009), produced very valuable results. Other projects such as the CLARIS project (Boulanger et al., 2010), the RMIP (Fu et al., 2005) or the NARCCAP (Mearns et al., 2005) have concentrated on different regions. An ambitious project called CORDEX[1] is currently in progress and its objective is to coordinate downscaling experiments all over the globe, including both statistical and dynamical methodologies.

The reader interested in regional climate modeling is referred to Giorgi (2006b) as an excellent review that details both the status and the perspectives of the topic.

Despite the development of the models and the extraordinary evolution of the computing power, the models have to be evaluated to ascertain their potentials, which still remains a major challenge for regional modelers. Prior to make any use of RCMs for high-resolution projections, it is crucial that model estimates are validated with observational data so uncertainties can be elucidated. Validation process permits not only to assess the model reliability at regional scales, but also to determine the value-added information with respect to GCMs. In fact, the model evaluation is considered now as a compulsory step before future projections are analyzed and several works are about this subject (Antic et al., 2006; Christensen et al., 2007b; Evans and McCabe, 2010; Kusaka et al., 2010). However, validation methodologies improvement was pointed out in IPCC TAR (Giorgi et al., 2001) as an important target for future climate research and remains open to discussion until today.

The major problem is related to the scale disparity between model estimates (grid average) and site-specific measurements that hamper any direct comparison, since they do not represent exactly the same. This subject is known as the *representation error* and embodies an important challenge in the model evaluation. In order to overcome this problem, different strategies have been put forward such as the use of gridded observations. Nonetheless, the existing gridded observations are frequently created using networks that are to sparse over certain areas and therefore other methodologies have been proposed. According to Göber et al. (2008), the most appropriate way of validating the model in these cases is to perform a sort of upscaling of both the model estimates and the observations

---

[1]Available information in http://wcrp.ipsl.jussieu.fr/RCD_CORDEX.html

in order to reduce them to the same spatial scale. For instance, regionalization procedures have been suggested within the framework of RCM evaluation for different variables (Caldwell et al., 2009; Jiménez et al., 2008; Kostopoulou et al., 2009). The lack of consensual and systematic methodologies calls for objective techniques to asses the models competence and hence produce reliable climate change projections.

The evaluation is also closely related to an appropriate configuration of the model. Modern RCMs provide a large number of options to adapt the integrations to particular applications or regions. The exploration of different configurations and their performance is too often disregarded. For example the spread of the results produced with the same model using varied physics schemes can be as large as if completely different models are employed. Therefore, a thorough sensitivity test to model configuration is of paramount importance to make the most of our model.

The comprehension of sources and impacts of climate change has been capturing scientific attention in the last decades and regional modeling has become a useful tool to go into these aspects in more depth, being currently at the forefront of climate research. Regional projections have been recently carried out for many regions (Anav et al., 2010; Caldwell et al., 2009; Nuñez et al., 2008; Paeth et al., 2009; Salathé Jr et al., 2010), but there are still areas that remain to be explored or require additional studies due to their peculiarities. Indeed, the IPCC AR4 (Christensen et al., 2007a) indicated that downscaled projections adapted to specific needs are necessary and that further insight in climate features determined by topography is required because it is yet unclear how climate change will manifest at fine spatial scales.

1.5 Objectives and structure of the Thesis

This Thesis aims to generate high-resolution projections of climate change scenarios over the Iberian Peninsula to characterize possible future changes in both temperature and precipitation. To that purpose, GCMs outputs are dynamically downscaled using a mesoscale model to provide information at fine scales that otherwise cannot be explored.

In order to produce reliable projections of climate change, the model has to be adapted to the region under survey and thus an appropriate configuration suited to the region peculiarities has to be selected. To complete such a task, the sensitivity of the model results to different parameterizations is examined form

a climate point of view. Namely, a set of several-year simulations are employed to determine which combination of physics schemes better describes the climate features of the IP. To be specific, a subregion (southern Spain) has been chosen to conduct these sensitivity tests bearing in mind its particular complexity in terms of topography and climate variability.

Determining which configuration suits better the study characteristics (e.g. region, timescales, variables) is a remarkable challenge. The issue has been addressed through different timescales and using an observational dataset to compare with the model outputs. Such a comparison is hampered by certain obstacles that are attempted to overcome through a regionalization methodology.

The classification of climate regimes into divisions has been usually done via subjective procedures. A methodology that removes as much as possible the subjectivity associated to regionalization is here proposed. The delimitation of affinity areas is extremely useful not only for regional climate modeling but for many other fields (e.g. agriculture, stockbreeding, studies of wildlife habitats and migration, renewable energies).

Furthermore, the reliability of future projections are highly dependent on the model ability to reproduce present climate. Simulations that span climate reference periods (30 years) have been completed to assess the model agreement with present climate precipitation and temperature. A in-depth analysis of the model is carried out to evaluate its potentials to describe not only long-term means but also daily values or high-order statistics such as the extreme events.

These different stages make possible to generate high-resolution projections of climate change scenarios over the IP that help address possible changes in the annual, seasonal and monthly means. In addition, the probability of occurrence of particular events in the future is also analyzed. Long-term information can be inferred from GCMs up to a certain degree, but the projections of daily events, and more specifically the extreme events, require further tools such as the dynamical downscaling.

The main purpose of this Thesis is to provide climate change information at both spatial and temporal scales that are crucial to explore the impact of global warming on the people and the environment. The timescales that are explored will shed light on changes in both the mean climate and low frequency events (i.e., heavy rainfall, droughts, heat waves). The fine spatial scales enables the study of regional climate by describing small features of the region with major influence in the local circulation.

The outline of this Thesis is as follows: Chapter 2 details the principles of

dynamical downscaling and features of the mesoscale model adopted here. In Chapter 3, the observational datasets are described together with the regionalization methodology. Chapter 4 describes the configuration of the mesoscale model chosen to perform the climate runs. Chapter 5 is devoted to the model sensitivity tests and the appropriate combination of physics schemes for this study. The model ability to reproduce present climate features, namely the model evaluation is analyzed in Chapter 6. Chapter 7 provides a discussion on the future climate simulation results and the projected changes for temperature and precipitation. Finally, the last chapter summarizes the most remarkable results and the main conclusions of this study. Appendix A describes the mathematical details of the Principal Components Analysis. Appendix B provides the definition of the statistical parameters used in throughout the text.

Chapter 2

Dynamical Downscaling: the Mesoscale Model

Outside are playing fields, houses, mountains and lakes, for it was thought that those who compute the weather should breathe of it freely

Weather Prediction by Numerical Processes
Lewis Fry Richardson

Dynamical downscaling by way of a RCM has been adopted to produce high-resolution climate change information over the IP. In particular, the Weather Research and Forecasting (WRF) model has been selected to perform the climate runs. This Chapter explains the fundamentals of dynamical downscaling and then describes the WRF model.

2.1 Dynamical Downscaling using a Mesoscale Model

A mesoscale model is a numerical system that provides an approximate solution to the simplified primitive equations. The model estimates are limited to a region defined by the domain and thus the lateral boundary conditions (LBCs) must be specified at its borders, because otherwise the equations are not resolvable. This procedure is called nesting and is the starting point of dynamical downscaling by way of a regional model.

The underlying idea of dynamical downscaling using a mesoscale model is certainly not new. The problem of weather prediction was already addressed by solving the governing equations of the atmosphere with satisfactory results.

Nonetheless, the use of mesoscale models for long-term simulations entails some conceptual issues that must be examined in order to design the climate experiments adequately and hence produce reliable climate change projections.

2.1.1   Conceptual issues

In principle, a model that produces good results for short-range forecasts should also perform accurately for longer periods. However, the question is not that simple since the strategy of nesting a RCM within large-scale data is not mathematically well-posed. Namely, it does not exist a unique solution because the right conditions cannot be exactly determined. Ideally, we should have at our disposal a continuous and perfect set of boundary data to solve the equations, so that the problem would be closed and well-posed. Unfortunately, both the equations and the boundary conditions are discretized in the framework of regional modeling. Thereby, the information used to drive a regional model is incomplete and thus the problem is under-specified. To avoid the incompleteness of information, the approach is that of providing a larger number of variables that make the problem to be over-specified. If the boundary data would be error-free, then the over-specification would not be a major obstacle, because all conditions would still point to the same unique solution. But this is not true. Boundary condition datasets are subject to errors and hence they are not completely consistent.

Over-specification might thus be an added source of errors in the form of spurious waves that propagate into the domain (Staniforth, 1997). If the LBCs are over-specified and imposed in a 'hard' manner, there might be discrepancies at the domain borders that are reflected back and interfere with the model dynamics. For long-term simulations, this noise might swamp the whole domain and become increasingly important. Davies (1976) suggested a buffer zone at the domain borders where the model results are relaxed towards the driving fields and thus the discrepancies are damped. This technique successfully deals with the problem at small scales, but it does not handle larger scales correctly and long waves do reflect and alter the circulation.

An efficient solution has been proposed to manage spurious long waves and involves the adjustment of the model results all over the domain but only at larger scales, typically over 1000 km. The so-called spectral nudging (von Storch et al., 2000; Waldron et al., 1996) reduces the nesting errors and also make regional climate modeling a real downscaling procedure rather than a boundary value problem (Rummukainen, 2010). Furthermore spectral nudging provides interest-

ing consistency between large-scale defined by the GCM (or the observational reanalysis) and the regional-scale produced by the mesoscale model.

An additional aspect of dynamical downscaling that has to be considered carefully is the domain design. The domain size and location have been proven to have an effect on the model results that is not negligible at all (Jones et al., 1995; Leduc and Laprise, 2009; Liang et al., 2001; Seth and Giorgi, 1998). The quality of the observational analysis and the performance of the GCMs are not equal all over the globe, and thus depending on the placement of the domain, the accuracy of the boundary data varies. Furthermore, the domains borders should not be placed over major topographical features such as mountain ranges because they are described at different level of detail by the RCM and the GCM, and undesired artifacts can be originated. The size of the domain is a matter of discussion too. It should be large enough to allow the model to develop its own internal variability but not too extensive as to deviate in excess from the boundary data, since it might produce imbalances. The domain size is also strictly connected to computational costs and thereby it must be accommodated to the available resources.

Although the domain design implies some caveats, such as the location of the borders over homogeneous areas, spectral nudging also helps to lessen the dependence of the model on the size, location and geometry of the domains (Míguez-Macho et al., 2004). Despite the advantages of spectral nudging, it is still argued that the nudged RCMs are not able to develop their own dynamics and might be excessively forced by non-perfect boundary data. Therefore, whether to use spectral nudging is still controversial and the decision often depends on the particular application and the modeler criterium. Applying a weak nudging is a good approach to take advantage of the technique and retain RCMs internal variability.

The boundary data also deserves attention since they represent the response of the climate system to large scale forcing and thus provide the framework for RCMs. If the driving data do not adequately describe the main features of general circulation then it cannot be expected that the regional model corrects those errors, although some correction might be actually attained. On that account, the potential deficiencies of the boundary conditions is a prime driver of dynamical downscaling biases. Nonetheless, not only the quality of the LBCs is determining, but also the LBCs updating frequency and the difference between GCM and RCM resolutions play an important role.

Nesting formulation requires boundary conditions at every time step, but the

GCMs or observational analysis are only available at certain frequencies. An common practice is that of interpolate the LBCs in time to feed the regional model. Consequently, the updating frequency must be high enough to roughly reproduce the daily cycle and also capture the large-scale systems that impinge the RCM domain. Denis et al. (2002) addressed both the frequency and resolution difference issues. They showed that a 6-hour frequency suffices to correctly drive the model and no significant benefit was gained with higher frequencies. Regarding the resolution 'jump', they came to the conclusion that the resolution difference ratio should not exceed a value of 10 or else spatial inconsistencies could arises at the borders. For larger ratios, multiple nesting technique is recommended. Multiple nesting consists in using two or more domains arranged in a sort of cascade with increasing spatial resolution. Therefore, the inner domains obtains its LBC from the immediately coarser domain rather than directly from the GCM (Fig. 2.1).
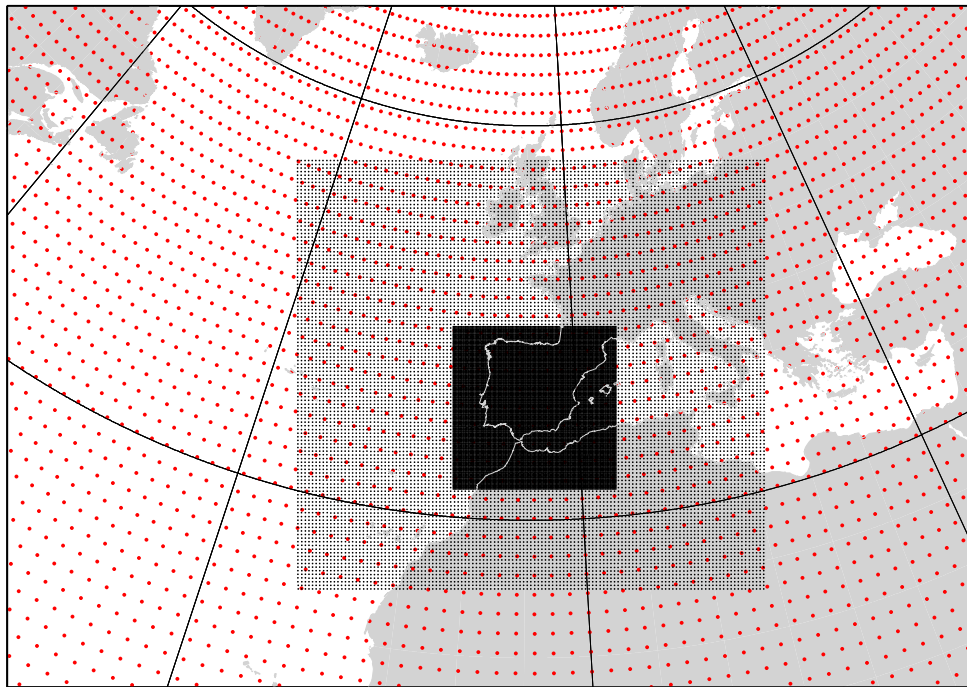
Figure 2.1: *Example of multiple nesting composed by two RCM domains (finer square grids of black dots) of 10 and 30 km respectively, and a ∼ 1.4° by 1.4° GCM grid (coarse mesh of red dots).*

No matter the resolution of a model, there are always processes that occur at sub-grid scales and have to be somehow included in the formulation. They are resolved using semi-empirical approximations called parameterizations that could be considered models themselves. The consistency in the parameterizations between the GCM and the RCM used to be a matter of dispute. The use of different schemes might cause imbalances at the borders because the sub-grid phenomena are represented dissimilarly. However, it can also been argued that even the same parameterization schemes perform very differently at varying resolutions, as it happens to convective schemes. In fact, one of the RCMs advantages is the possibility to use physics packages optimized to a particular region and resolution. In any case, the parameterization compatibility issue has been revealed to be less crucial than it was thought (Déqué et al., 2007).

Finally, the evolution of the model climatology is the result of a dynamical equilibrium between the boundary conditions and the model dynamics. In addition, regional climate modeling aims to study the climate signal regardless of the initial conditions. Despite the fact that the climate system is essentially chaotic and thus minor perturbations in the initial state might lead to different final states, long-term simulations have been proven to be insensitive to those perturbations after approximately fifteen days (Giorgi and Bi, 2000). The time required by the model to achieve an equilibrium and forget about the initial conditions is called spin-up. The choice of an appropriate length of the spin-up depends on the applications that the model will be used to, since different variables have very different inertias (i.e atmospheric fields reach a balance after few days whereas soil variables usually needs up to months to attain an equilibrium). If computational resources permits so, an extended and conservative spin-up period is then preferable, particularly when GCMs are employed as boundary conditions because many of them do not provide enough soil variables and the model has to be initialized with external datasets (see below in the model configuration, Sec. 4.2.2).

2.1.2 Dynamical downscaling uncertainties

Climate change studies are affected by a number of uncertainties that constitute a important limitation because there is no way to tell which projection is more probable. In global models, the major sources of uncertainties are related to the emissions scenarios, the model formulation and the natural variability of the climate. Other sources are also decisive but hardly to determine such as the

non-linearity of the climate system, the unexplored feedbacks, the long-term responses or unpredictable phenomena (e.g., vulcanoes). The downscaling of GCM information using a RCM introduces an additional source related to the technique itself. Namely, different model formulations, parameterizations or nesting methodologies might produce different results. Regional climate models are thus afflicted by both their own uncertainties and those inherited from GCMs, but they cannot be considered separately since the uncertainties overlap rather than simply add up.

The anthropogenic emissions of GHGs are the initial source of uncertainties. The growth of population, the society and economy development, and the technological advances are key factors in the evolution of the emissions. The anthropogenic emissions result in variations in the atmospheric GHG concentrations, which in turn produce a radiative forcing that alters the radiative balance in the Earth. For that reason, all these factors might be regarded as important and highly unpredictable climate drivers. Climate change studies have overcome their unpredictability by contemplating various plausible future evolutions of these factors (e.g., population, economic policies, energy sources) embodied in the emissions scenarios(Nakicenovic et al., 2000).

The GCMs are formulated differently and none of them provides better results under any circumstances, and hence there do not seem to be a model that is more reliable than the others. They all have their own strengths and shortcomings. The approach to reduce the uncertainty associated to the GCM formulation is to use different GCMs to constraint the regional models in order to cover a wider range of possible projections.

The third uncertainty has to do with the number of simulated years. Climate change projections span over a finite sample of years. Bearing in mind that the atmosphere is essentially chaotic and thus highly variable, a supplementary degree of uncertainty is added due to sampling limitations.

Finally, the downscaling technique introduces another uncertainty source. The RCM formulation affects the accuracy of the outputs just as for GCMs. The design of the experiment (spatial setup, model configuration, time coverage) also has an important impact on results. To progressively reduce this source of uncertainty, new simulations should be performed using various configurations over regions of different characteristics..

The sets of different simulations aimed at covering possible uncertainties are usually known as ensembles. They might include different scenarios, GCMs, RCMs or various configurations of the same regional model (physical ensemble).

The broader range of combinations are explored, the better the uncertainties can be identified and eventually reduced. However, computational costs now precludes the examination of the complete matrix of possible combinations and thus a representative selection must be made.

Far from being only a limitation, the number of uncertainty sources in climate change studies are a great incentive to produce further simulations that might reveal what are the most important sources and then would help to provide new and more reliable insight into the issue of climate change at regional scales.

2.1.3   Downscaling ability of RCMs

Despite the imperfections exposed, the RCMs have been revealed to be an extremely useful tool to provide climate information at scales that are crucial to nature and human life. They are able to produce added-value information with respect to the boundary data (Antic et al., 2006; Laprise, 2008) and improve climate simulations at the regional scale (Caldwell et al., 2009; Wang et al., 2004), evidencing RCMs downscaling ability. For instance, the experiment designed by Denis et al. (2002) employed high-resolution boundary conditions that were filtered to remove the small scale features and showed that the RCM was able to recreate those features even if they were not present in the boundary data anymore.

The regional models are able to describe in detail fine-scale characteristics of the region that are known to affect the climate such as the land-use or the vegetation (Ge et al., 2007; Hong et al., 2009; Sánchez et al., 2007), but also topographical features that might alter local circulation (e.g., intricate coastlines, steep mountain ranges, inland waters).

The affordable computational requirements of RCMs and the fact that their results are not restricted to places with available observations have made RCMs very widespread. As a result, the large number of institutions involved in climate modeling has contributed to a rapid development of the models. In spite of the large modeling community, the model evaluations are still necessary to assess their capabilities, particularly under troublesome conditions such as regions affected by very local processes induced by complex topography. In view of the benefits of employing RCMs as a supplementary tool to address the climate change problem, several studies have called for further simulations in order to produce regional climate change information (Christensen et al., 2007a; Giorgi, 2005; Rummukainen, 2010).

2.2   The Weather Research and Forecasting Model

In this Thesis, the Weather Research and Forecasting (WRF) model version 3.1.1 was selected to perform the climate runs[1]. The following description of the model should provide enough arguments to support our decision of selecting WRF among the several models at the researchers disposal.

The WRF model (Skamarock et al., 2008) is a mesoscale numerical weather prediction system develop for both operational forecast and atmospheric research needs. The WRF model is the result of a collaborative partnership that includes over 150 organizations and universities in the United States and abroad, such as the National Center for Atmospheric Research (NCAR) or the National Oceanic and Atmospheric Administration (NOAA).

Two different dynamical cores have been implemented in the model: the Non-Hydrostatic Mesoscale Model (NMM), which was primarily design for weather forecasting purposes; and the Advance Research WRF (ARW), created to be suitable for a wide range of applications at varying time and spatial scales. According to the main objective of this Thesis, the latter has been adopted and will be referred from now on as simply WRF.

The most remarkable characteristics of the model are:

A fully-compressible non-hydrostatic formulation   A non-hydrostatic version of the equations includes the vertical accelerations effect on pressure calculations, which might be very important under unstable conditions. The fully-compressible feature means that acoustic waves are also considered. Owing to sound speed, acoustic waves are extremely expensive to include in the model. Using the incompressibility assumption $\nabla \cdot \mathbf{u} = 0$ instead of the mass continuity equation filters all the acoustic modes and allows for larger time steps. As a consequence, the computational costs are dramatically reduced.

Acoustic waves are in principle of no interest to meteorology and indeed Davies et al. (2003) analyzed the performance of different simplifications of the Euler equations and concluded that the incompressibility assumption might be acceptable under particular conditions, but questioned their validity for regional climate

---

[1]The fifth-generation Penn State/NCAR Mesoscale Model (MM5, Grell et al., 1995), which is the WRF natural predecessor was initially used to conduct some preliminary simulations. Although it might be argued that they are not exactly the same model, they share many of the basic features. Hence, a valuable experience was gathered with the initial simulations that could not be deprecated in the design of WRF runs. Despite the migration from MM5 to WRF is far from being trivial, the fact that MM5 is progressively being abandoned and the improvements added to WRF encourage us to take this step.

applications.

Accordingly, WRF includes the fully-compressible equations in its formulation. In order to avoid that the calculation of acoustic waves hamper the model in excess, it also includes time-splitting (Klemp et al., 2007; Staniforth, 1997) that conserve both mass and first-order flux quantities.

Flexibility in the domain configuration   Several domains can be nested in multiple nesting levels with two-way or one-way interaction. Moving nesting is also allowed so that, for example, hurricane tracking is possible. Both regional or global runs are possible too.

Following-terrain vertical coordinates   The vertical coordinates are mass-based following terrain that range from 1.0 at the model bottom to 0.0 at the top: ARW η coordinantes (See Figure 2.2).

$$\eta = (p_h - p_{ht})/\mu, \quad \text{where} \quad \mu = p_{hs} - p_{ht} \tag{2.1}$$

p_h is the hydrostatic component of the pressure, and p_{hs} and p_{ht} represent the values along the surface and top boundaries, respectively. This way, the vertical grid is denser near the ground and gets coarser upwards. It also has the advantage that all levels are horizontally continuous, following the terrain but smoothing the perturbations in the upper levels.

Map projections   A number of map projections are available to accurately describe different regions of the globe (Polar stereographic for near-pole areas, Lambert-Conformal for the mid-latitudes areas, Mercator for the near-equator areas and latitude-longitude cylindrical for very large regions).
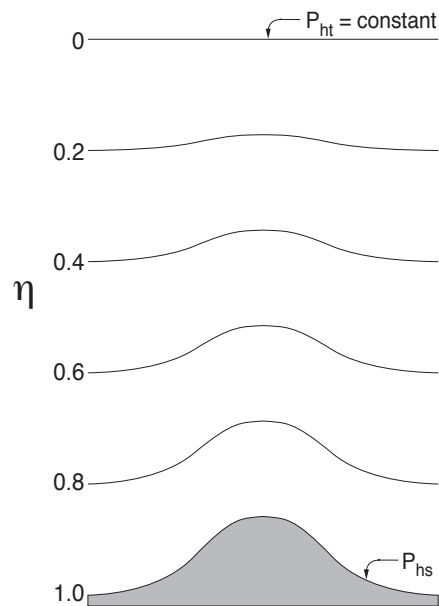
Figure 2.2: *ARW η vertical coordinate*

Horizontal discretization   The variables are located in a grid using the Arakawa-C grid staggering. Most scalars are defined on the grid center (mass points) and vectors (and also geopotential) in the grid walls (Fig. 2.3).

Figure 7.3: Arakawa-C grid staggering for a portion of a parent domain and an imbedded nest domain with a 3:1 grid size ratio. The solid lines denote coarse grid cell boundaries, and the dashed lines are the grid cell boundaries for each fine grid cell. The horizontal components ("U" and "V") are defined along the normal cell face, and the thermodynamic variables ("θ") are defined at the center of the grid cell (each square). The bold typeface variables along the interface between the coarse and the fine grid define the locations where the specified lateral boundaries for the nest are in effect.

Figure 2.3: *Arakawa-C grid staggering for two nested domains. The horizontal components of velocity (U and V) are defined along the normal cell face, and the thermodynamic variables (θ) are defined at the center of the grid cell. From Skamarock et al. (2008)*

Time integration   Runge-Kutta 2nd and 3rd order time integration options.

Equations form   Scalar-conserving flux form for prognostic equations.

Boundary conditions   Lateral boundary conditions specified using a relaxation zone to prevent boundary artifacts over the studied area.

Nudging   Observational and grid nudging, including spectral nudging. Nudging technique consists in adjusting the model outputs towards a separate set of data to improve them. Observational nudging uses *in situ* measurements whereas grid (or analysis) nudging uses upper-level and surface data gridded information.

Parameterizations   A broad choice of parameterization schemes for land-surface, planetary boundary layer, radiation, microphysics and cumulus convection.

The WRF model system is freely available online[1] and has been designed to be portable and efficient in several platforms, included parallel environments that use MPI (Message Passing Interface). These two factors have permitted a fast growth of the users community which has played a part in the model improvement via the addition of new parameterizations, the coupledom with other models and the modification of the code with new applications in mind.

A description of the WRF flowchart and structure is presented next. Afterwards, the model formulation and some additional features are detailed. The final part of this chapter overviews the physical parameterizations that were adopted in this study.

2.2.1   The WRF structure

The WRF model permits to study two different kinds of simulations: those with an ideal initialization and those using real data. The WRF core is not altered by selecting one initialization or another, but the data pre-processing is different. Ideal cases comprise simulations of very particular conditions and simplified orography, usually when individual processes in the atmosphere are to be examined (i.e., Large Eddy Simulations, sea breeze, flow over a hill). On the other hand, real-mode simulations require different atmospheric and terrain data to study an actual event on a given area. In our case, provided that the study focuses on the climate over a particular region in the globe, the real mode is selected.

The WRF software (real mode) is organized in three main modules that must be run successively: the WRF Preprocessing System, the data initialization module (*real* program) and the ARW solver. The complete flow chart is depicted in Figure 2.4, including not only the mentioned modules but also other additional software that are optional and refer to data post-processing.

WRF Preprocessing System

The role of the WRF Preprocessing System (WPS) is to prepare both geographical information and gridded meteorological data so that they can be fed into the data initialization module. It consists of a set of three programs:

- **geogrid:** It basically defines all features of the domains and interpolates the geographical data to the model grids and creates the physical environment.

---

[1]http://www.mmm.ucar.edu/wrf/users

WRF Modeling System Flow Chart
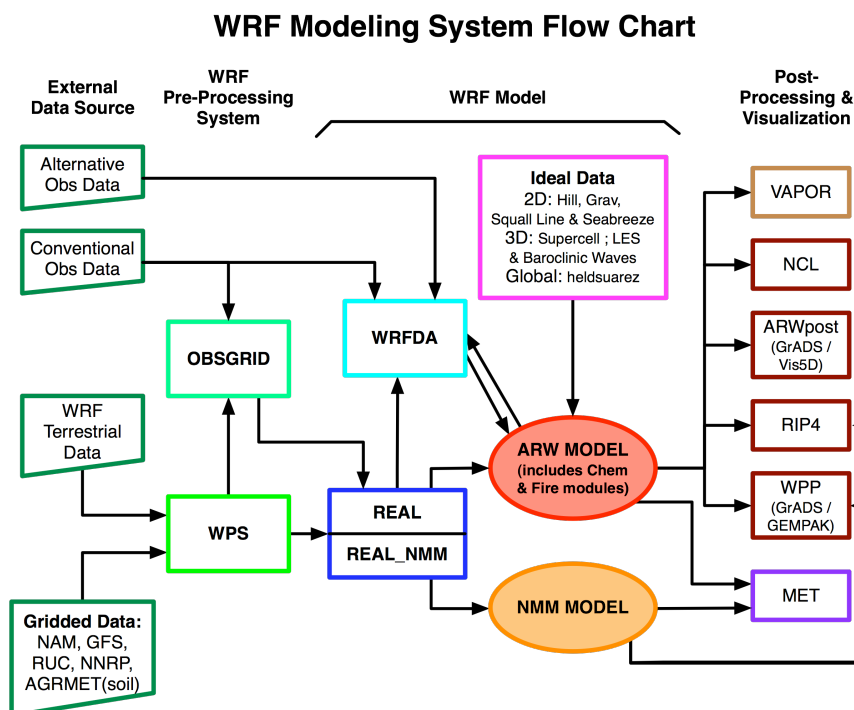
Figure 2.4: *WRF flow chart*

- **ungrib:** It reads the GRIB-formatted files with meteorological data and converts them to an intermediate format readable by the metgrid.

- **metgrid:** It horizontally interpolates the fields extracted by ungrib to the grids defined by geogrid.

The WPS also permits to specify how the domains are defined (i.e., projection, geographical data), determine the period that will be simulated or the interpolation method and the masks that are used for each variable (i.e land-mask applied to variables that are defined only over the sea). An in-depth description of WPS can be found in the ARW User's Guide[1].

The data initialization module

The data initialization module `real.exe` is actually part of WRF system, although it is explained separately because they represent different stages in the

_____

[1]http://www.mmm.ucar.edu/wrf/users/docs/user_guide_V3/contents.html

modeling process. The `real.exe` program performs the vertical interpolation from original data levels to the model vertical levels and creates the initial- and boundary-condition files. In case nudging is desired, it will also create the appropriate files for that purpose. Some other tasks are carried out by `real.exe` too, such as soil vertical interpolations and land-use mask checks.

The ARW solver

The ARW solver is the dynamic core itself (`wrf.exe`) and the responsible for resolving the equations of the atmosphere. It produces the history files that contain the results and extra output files such as the restarts files that are used to split long simulations into shorter ones. The formulation of the model that constitutes the foundations of the ARW solver is described next.

2.2.2 The WRF formulation

An atmospheric model is founded in 3 basic principles of conservation:

1. **Conservation of Momentum** expressed through a version of Navier-Stokes equations that describe inviscid fluid dynamics.

2. **Conservation of Mass** in the form of the continuity equation.

3. **Conservation of Heat (or Energy)** derived from the 1st Thermodynamic principle.

The equations associated to this set of principles are called the **Euler equations**. Additional equations can be included to conserve water or other atmospheric species (i.e., gases or aerosols). This set constitutes the fundamental equations of the atmosphere and represent a non-linear system of partial differential equations with no analytical solution. An approximation has then to be performed using a numerical method, namely an atmospheric model. However, the space in a mesoscale numerical system is discrete and hence the equations must be further adapted to this new environment embodied in the model grid.

Different approximations, most of them based on scale analysis, have been suggested over the years to facilitate the integration of the equations or attain computational stability (i.e., incompressibility, hydrostatic balance, anelastic assumption) but current numerical methods and computational resources have permitted to attempt the solution of the complete set of equations (not considering the simplifications required for discretization). The resolution of the fully-

compressible non-hydrostatic equations, and thus the inclusion of the acoustic modes, represents a considerable challenge, but it represents better the different waves in the atmosphere (Davies et al., 2003). As a consequence, the model can also be successfully run at a wide range of spatial scales from planetary to mesoscale, which is one of the final objectives of WRF.

The ARW dynamic solver integrates the fully-compressible, non-hydrostatic Euler equations in their conservative flux form and written using the η vertical coordinates. To be precise, the perturbation form of these equations is actually solved in the ARW, basically to reduce truncation errors. Two supplementary diagnostic equations are added to the system: a diagnostic relation for inverse density and the equation of state. For further details the reader is encouraged to look through Skamarock et al. (2008).

The basic prognostic variables obtained from the equations are the horizontal wind velocities (u and v), the vertical wind velocity (w), the perturbation potential temperature, the perturbation geopotential and the perturbation surface pressure[1]. However, a much larger number of variables are calculated out of these and written in the output files.

The indispensable variables to run the model at both the surface and several vertical level are the horizontal winds, the temperature, the relative humidity and the geopotential, plus the mean sea level pressure. If a soil model is used, then initial conditions for soil moisture and soil temperature are also required at various depth levels. Additionally, the use of time-varying sea surface temperature[2] is also important for climate simulations.

A time-split integration scheme is used to perform the temporal discretization consisting of a third-order Runge-Kutta (RK3) scheme for the slow modes and the high-frequency acoustic modes are integrated over smaller time steps. This approach, described in Wicker and Skamarock (2002) and in Klemp et al. (2007) for flux-form equations, permits to integrate the fully-compressible non-hydrostatic equations at reasonable computational costs and maintaining numerical stability.

The space is discretized by the ARW dynamic core using an Arakawa C-grid staggering. The spatial discretization, along with other factors, entails an issue that is probably currently regarded as one of the major challenges in the atmosphere numerical modeling: the **parameterizations**. Since parameteriza-

---

[1]The perturbation of a variable is used instead of its absolute value, which consists in providing a value with respect to a base state.

[2]Surrogates of sea surface temperature are sometimes employed with an appropriate land-sea masking, such as the skintemp.

tions represents an entire field in numerical modeling, a separate section has been dedicated ahead.

2.3   The WRF parameterizations

In the atmosphere, there are processes that take place at spatial scales below the model grid distance and thus are not explicitly resolved by the equations. They are included in the model using parameterizations, which are semi-empirical approximations of reality. Although the only pure physics in the model are the fundamental equations, the parameterizations are also called the model physics or the physics schemes. The processes that are described by parameterizations occur at small scales, but they are as decisive as the large scale defined by the equations and thus cannot be neglected. Stensrud (2007) highlighted the importance of the model physics in the paragraph below:

> *"Arguably, the most important components of any numerical weather prediction model are the the parameterization schemes. They determine the amount of energy that reaches the Earth's surface; determine the evolution of the planetary boundary layer; decide when subgridscale clouds and convection develop and produce rainfall; and determine the influence of subgrid-scale orography on the atmosphere. The analysis and understanding of parameterization schemes is a key aspect of numerical weather prediction."*

The parameterizations describe a broad range of sub-grid scale processes imposing certain assumptions and at different levels of complexity. Bearing in mind that the mesoscale models might be used for a large number of applications and at very different spatial resolutions, each of the potentially parameterized processes might be described using different approaches depending on the simulation characteristics. Furthermore, the parameterization schemes do not work independently and they usually interact. Therefore not only the physics packages themselves play an important role, but also their feedbacks should be considered. An appropriate selection of the physics schemes according to the region of interest, the resolution and the application is not a trivial task, and the choice might have a major impact on our results.

In Figure 2.5, the parameterized processes in WRF and their interactions are illustrated. Next, among the different available options to represents the processes, those examined in Thesis are enumerated and briefly described.
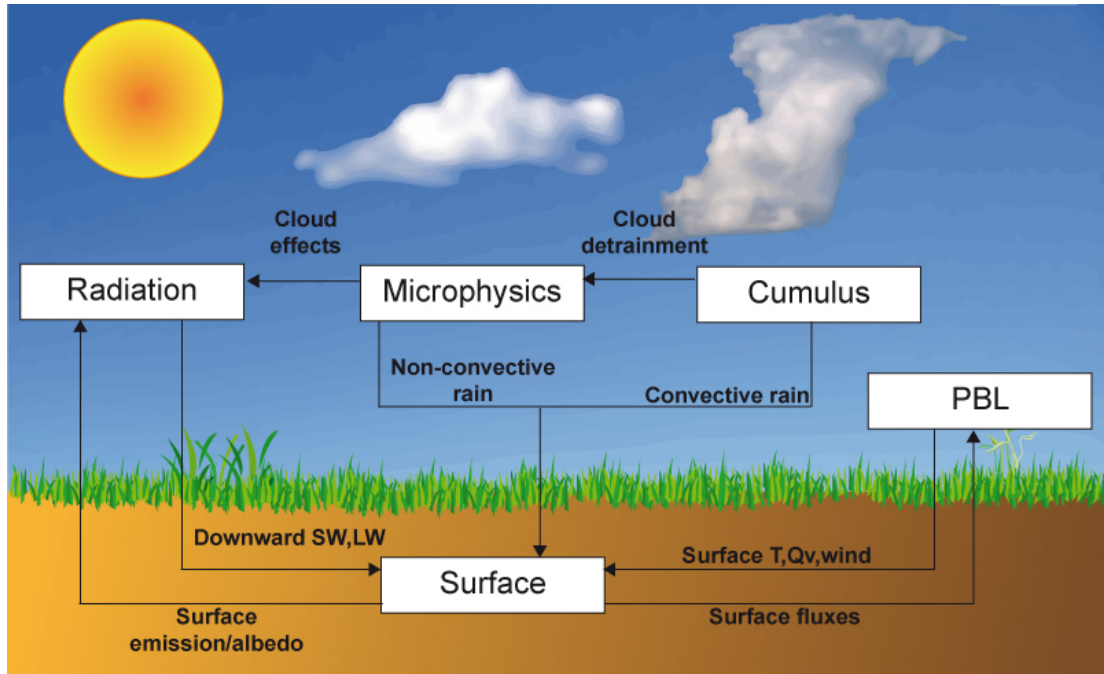
Figure 2.5: *Simple representation of sub-grid scale processes parameterized in WRF and their direct interactions*

2.3.1   Radiation

The radiation scheme represents both the atmospheric heating due to radiative flux divergence and the surface radiation for the ground heat budget.

The NCAR Community Atmosphere Model (**CAM 3.0**) has been selected to parameterize radiation processes at sub-grid scales for both longwave and short-wave (Collins et al., 2004). It is recommended for regional climate simulations because it has an ozone distribution that varies during the simulation according to monthly zonal-mean climatological data. The scheme also interacts with resolved clouds and cloud fractions. Furthermore, it handles optical properties of several aerosol types and trace gases. In fact, the main asset to choose the CAM3.0 scheme is the possibility to update GHG atmospheric concentrations depending on the SRES scenarios in order to introduce their effects on the parameterized radiation. The code had to be slightly modified to this purpose (CLWRF, Fita and Fernández, 2010).

2.3.2   Microphysics

Microphysics is responsible for the cloud microphysical processes that drive the cloud particle formation, growth and dissipation. It handles explicitly resolved water vapor, clouds and precipitation processes. The available options mostly differ in the number of phase changes of water and the number of interactions between clouds and precipitation particles (Stensrud, 2007). The selection of microphysical schemes mainly depends upon the phenomena to be simulated and the computational resources. Several choices are available in WRF, of which two are explored in this Thesis.

WRF Single-Moment 3-class (WSM3)   (Hong et al., 2004). It is a bulk[1] single-moment scheme that predicts 3 different categories of hydrometer: vapor, cloud water and rain above 0°C, and includes ice processes below 0°C (vapor, cloud ice and snow). It is a fairly simple and computational efficient scheme for the inclusion of ice processes but neither the gradual melting nor the supercooled water are considered.

Thompson et al. scheme   (Thompson et al., 2004). It is a 7-class scheme including graupel. It is a bulk single-moment scheme with double-moment for ice since the number concentration is also calculated for a more robust representation of the particle size distribution.

The use of mixed-phase schemes is not normally recommendable for grid sizes over 10 km because it adds substantial computational costs with basically no gain, because updrafts that lead to riming processes are not resolved. Since the resolution selected for our simulations is exactly that threshold, these two schemes are selected to explore the suitability of a complex scheme with respect to a simpler one under the conditions of our study.

2.3.3   Cumulus

The cumulus schemes represent the effects of convective and shallow clouds within a grid cell. They describe the vertical fluxes due to unresolved updrafts and downdrafts as well as the compensating motion outside the clouds. The cumulus schemes also provide the convective component of rainfall caused by

---

[1]In contrast with bin schemes that classifies the particles sizes in a number of fixed categories, bulk schemes describe the particle size distribution using a predefined functional form.

convective eddies that are not captured by the model. There is an evident need in developing convection adequately in both time and space, because it is a key factor in describing heavy rainfall. Therefore, a suitable cumulus scheme is of major importance since precipitation extreme events in this region are directly affected by an accurate description of convective processes. Furthermore, convection is also determinant predicting large-scale atmospheric circulations correctly, because it redistributes heat and moisture, affects radiation and overturns the atmosphere (deep convection). Two schemes have been tested in this study[1]:

Kain-Fritsch (**KF**, Kain, 2004; Kain and Fritsch, 1990). It is a mass-flux scheme with both deep and shallow convection that uses a simple cloud model with moist updrafts and downdrafts. The cloud base mass flux is determined by the amount of CAPE (Convective Available Potential Energy) in the environment that has to be removed (CAPE removal time scale closure). Entrainment and detrainment are included in the scheme. It also includes cloud, rain, ice and snow detrainment.

Betts-Miller-Janjic (**BMJ**, Betts, 1986; Betts and Miller, 1986; Janjic, 1994, 1990). It is a deep-layer control, adjustment scheme that includes both deep and shallow profiles. Rather than explicitly describe updraft and downdraft, the scheme is based on profile adjustments towards a mixing line' that represents the quasi-equilibrium thermodynamic structure that the environment tends to as a consequence of convection.

For resolutions higher than 5 km, cumulus schemes should be switched off because the model can resolve the convective eddies itself. On the other hand, for coarser resolutions (5-10 km) it is not clear to what extent the convection is explicitly resolved and thus whether cumulus schemes should be used, even if they are helpful in the activation of convection. In our case, 10-km resolution, cumulus schemes are always switched on.

2.3.4   Planetary Boundary Layer (PBL)

The land surface fluxes and the turbulence that occurs in the Planetary Boundary Layer (PBL) are crucial factors in the evolution of the atmosphere,

---

[1]Actually three schemes were analyzed since Grell3D was also employed in some preliminary studies. However, this scheme was clearly outperformed by the other parameterization options and it was thus discarded.

because their impact might propagate to the whole atmospheric column. Besides, they usually provide the conditions for certain sensible phenomena to occur, such as the deep convection. An appropriate description of the turbulence permits to distribute heat, moist and momentum all over the atmosphere, not only in the PBL. Since the PBL is directly influenced by the surface and considering that the variety of surfaces in the Earth is huge, resolving the turbulence adequately in a wide range of conditions is undoubtably a challenge.

A important problem in the description of the PBL is that of the closure, which is associated to non-linear characteristics of turbulence. Namely the number of unknowns in the set of equations for turbulent flow remains always larger than the number of equations. Consequently, the complete description of the turbulence requires an infinite set of equations (Stull, 1988). The problem of turbulence closure is solved by truncation, selecting a number of equations and calculate the remaining unknowns by semi-empirical relations in terms of the known variables. Depending on the number of terms retained, the order of the approximation is different. The first way of classifying the parameterizations of the PBL is precisely related to the order. Therefore, the 1st-order closure means that there are equations for the state variables (u, v, w, T, q) –or the first moments– and the covariance terms are parameterized. Second-order closure implies that there are equations for the state variables and their covariance terms, but the triple correlation terms are parameterized. In addition, there are also non-integer schemes, such as the half-order or the one-and-a-half-order closure, which means that the variables are truncated at different orders.

Another division that can be made refers to their local or non-local nature. When the unknown terms are parameterized according to local parameters, that is, at the same level or neighbor levels, then the scheme is local. In order to incorporate the contribution of the large-scale eddies to the total flux, parameters dependent on the whole vertical profile in the PBL are used and the scheme is called non-local. Non-local schemes tend to perform better, reproducing more accurately the structure and the depth of the PBL as well as the wind profiles within it. However, local schemes tend to produce less mixing than non-local schemes and thus might be more suitable for stable conditions such as the night time. Some schemes switch between non-local and local approaches depending upon the stability of the PBL.

Three different schemes have been analyzed in this Thesis:

Yonsei University (YSU) PBL   (Hong and Lim, 2006) It is a first-order

non-local diffusion scheme developed from Medium Range Forecast (MRF) PBL scheme (Hong and Pan, 1996) that includes countergradient flux terms to account for large eddy transport and PBL top entrainment. The YSU uses a critical bulk Richardson number of zero to determine the PBL top and so it is dependent on the buoyancy profile. In fact, it defines the PBL top as the height that a surface parcel can rise through a well-mixed layer. Afterwards, the profile of eddy viscosity is prescribed according to the PBL depth estimation. The MM5 similarity scheme was selected to parameterize the surface layer when using YSU PBL .

Mellor-Yamada-Janjic (MYJ) PBL   (Janjic, 1990, 2002; Mellor and Yamada, 1982). It is a 1.5-order local closure scheme, which means that is a simplified second-order closure scheme. The scheme is based on the prediction of generation, transport and dissipation of Turbulent Kinetic Energy (TKE). Then it uses the value of TKE to calculate the eddy viscosities and finally diffuses the different variables in the vertical. As required by the MYJ PBL scheme, it is used in combination with the Eta similarity scheme for the surface layer.

Asymmetrical Convective Model version 2 (ACM2) PBL   (Pleim, 2007). The ACM2 PBL scheme is a non-local closure model (originally based on Blackadar) that includes a first-order local eddy diffusion component. The scheme is able to smoothly change from a combination of local and non-local transport under unstable conditions to an exclusively local behavior in stable conditions. The ACM2 is then suited to reproduce rapid upwards (thermals) in convective conditions but also to simulate correctly stable situations. As for the YSU scheme, the MM5 similarity option was chose for the surface layer.

Many parameters in the PBL schemes are determined empirically over homogeneous surface and particular environmental conditions, but very few evaluations of these schemes over complex terrain or under a wide range of conditions have been performed. Therefore, the PBL schemes should be carefully tested before using them because they have been examined only for very particular situations.

2.3.5   Land surface

The land-surface models (LSMs) are responsible for the initialization of the state of the ground and account for the surface forcing in the atmosphere. They

provide the fluxes that determine the lower boundary condition for PBL schemes by describing the ground temperature, the soil moisture and temperature profiles, the canopy effects and the snow cover. The use of an appropriate sophisticated model that updates these variables is crucial from a climate point of view. In this study, the **Noah LSM** is adopted (Chen and Dudhia, 2001) mainly due to its widespread use in long-term simulations. The Noah LSM is a 4-layer (0-10 cm, 10-40 cm, 40-100 cm and 100-200 cm) soil model that estimates soil temperature and moisture, and snow cover. It includes root zone, evapotranspiration, soil drainage and runoff that depend on vegetation categories, monthly vegetation fraction and soil texture.

Chapter 3

Observational data and regionalization

> And the wind is making speeches
> And the rain sounds like a round of applause
>
> ___
>
> *Time*
> Tom Waits

In Chapter 2, the dynamical downscaling fundamentals were described and the most important steps in the generation of future projections were mentioned. Namely, the model has firstly to be suited to adequately represent present climate over the region under study. Once the model is adapted and a suitable configuration is selected, it has to be validated and the model reliability has to be addressed. If the model results are satisfactory and they reproduce the main features of climate, the future projections are finally performed.

The first two steps, the appropriate model configuration and the model validation, are carried out by examining whether the model is able to represent current climate. To that purpose, observational datasets are used to compare with the model estimates in the so-called model evaluation. Despite the importance of this stage of dynamical downscaling, there is no consensus in the evaluation methodologies and it still remains a major challenge for climate modelers.

This Chapter is devoted to describe the different datasets that were used to compare with model results, the problems that arise from direct comparison with observations and the approaches to overcome these problems.

3.1   The *representation error*

The main problem associated to the model evaluation is that the increase of RCMs resolution is much faster than the development of climate observation networks and very few regions are covered by dense observational systems. Besides, in areas where the network density is adequate, the evaluation is traditionally performed by direct comparison between model estimates and in situ observations, although this is not a like-with-like comparison (Rivington et al., 2008). The site-specific measurements describe a particular location and hence they are affected by very specific factors, they characterize a single point in the space. Conversely, the space in a RCM is discretized and a model grid point represents the mean features of its grid cell (e.g. land/water proportion, elevation, surface properties, orientation), thus the model outputs at that point represent a kind of grid-cell average.

In regions where topography is rather homogeneous, it is reasonable to expect that the grid point values are fairly representative of the entire cell. Nevertheless, current regional climate simulations are performed at resolutions that range from 10 to 50 km and the topographical diversity within a cell might be wide in complex-terrain areas. If the topographical features of a particular station are at the extremes of the grid cell diversity then the model outputs and the observations might differ substantially, not only because the model is performing inadequately but also due to the scale disparity in what they represent. The difference between model outputs and observations coming from this scale disparity is usually known as the *representation error*. The *representation error* is yet inevitable because it could only be removed if the grid-cell and observation scales would be equivalent. This means that the order of the model spatial resolution needs to be increased up to a few meters or even higher, which is absolutely unaffordable from a regional climate modeling viewpoint.

Figure 3.1 schematically illustrates this problem considering only the topographical error source. The differences between the stations altitude and the grid cell elevation is negligible at some locations, whereas at some other these differences are very significant. It must be noted that although the slope represented in Figure 3.1 might seem unrealistic, it actually takes place in several locations across the IP (*Mulhacén*, 3478m, ∼35 km to the sea; *Torre de Cerredo*, 2648m, <30 km to the sea).

Obviously, the deviations from observations have their origin at the model deficiencies too, but the *representation error* should not be disregarded in the model

evaluation. As said before, it is almost impossible to completely eliminate the *representation error*, but in order to circumvent the problem, different approaches have been put forward. For example, techniques such as the adjustment of model outputs have been proposed, either through a lapse rate depending on elevation differences between the site and the model grid point (Moberg and Jones, 2004) or using a downscaling factor calculated from deviations between observational time series and model estimates (Rivington et al., 2008). However, the comparability of these adjusted outputs with observations still remains unproven, particularly when the correction significantly modifies the model results (e.g. large altitude differences between the station and the nearest grid point).
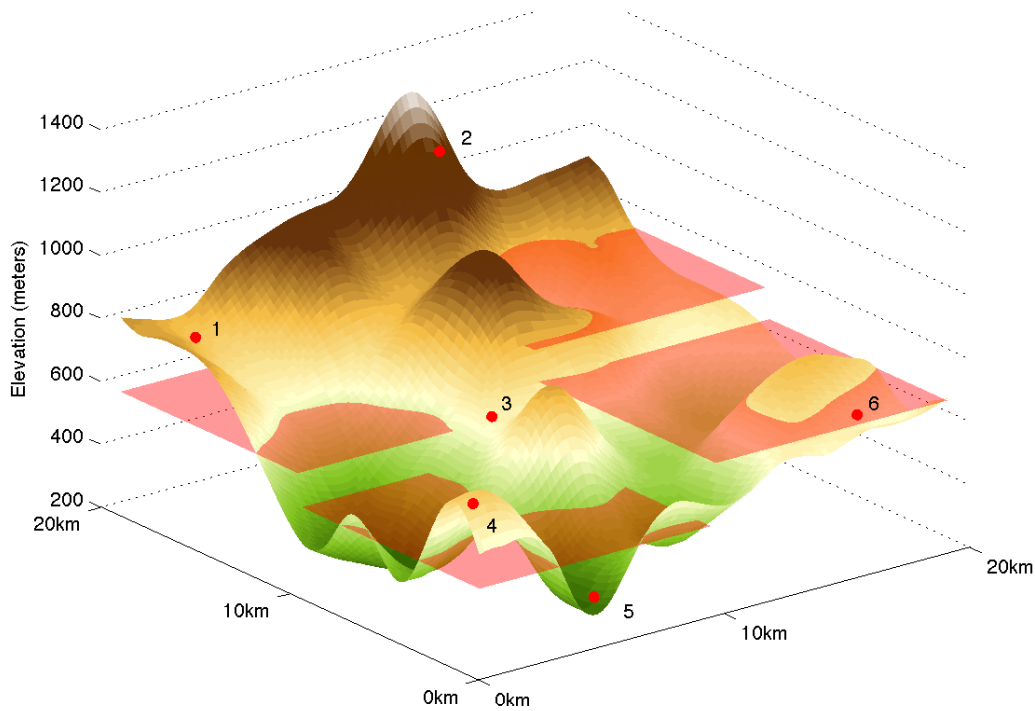
Figure 3.1: *Simplified example of the representation error due to topographical complexity. The irregular surface is the elevation in a 20-km by 20-km region. The red horizontal planes represent the elevation of 4 different grid cells for a model running at 10-km resolution. Red dots represent the location of various ideal stations.*

Otherwise, a sort of observation upscaling has been suggested as the most appropriate way to validate the model (Göber et al., 2008). For example, Osborn and Hulme (1998) grouped the information via an aggregation of the stations time series in order to compare GCMs outputs with in situ observations. An

interesting alternative that is being increasingly used and also consist in the upscaling of information is the classification of site-specific observations through different regionalization techniques to compare results by climate divisions rather than at single stations.

In the last years, a number of gridded observational datasets have been created precisely to enable comparison with model outputs (CRU TS 1.2, Mitchell et al. 2004; E-OBS, Haylock et al. 2008). The observational gridded datasets and the model estimates usually have a similar spatial scale and are thus comparable. Unfortunately, most available gridded analyses are often created with observational networks that are very sparse in certain areas like Spain and hence might be prone to substantial errors, particularly in terms of extreme events. Moreover, some gridded datasets only provide information on monthly timescales and higher frequencies cannot be explored with them. As a consequence, their use to validate the models over these regions is certainly restricted.

The observational datasets employed in the evaluation of WRF over Spain are described in the next section, including *in situ* measurements and a recently released daily gridded dataset that used an unprecedented density of observations (particularly outstanding for precipitation).

3.2 Observational data

Two sets of observational data are used in this study as a backdrop to evaluate the model outputs, an observational network and a gridded dataset.

3.2.1 Observational measurements

The site-specific observational dataset comes from a network limited to the *Comunidad Autónoma de Andalucía* in the south of Spain, and hereinafter referred as the *SubClim* dataset.

The *SubClim* dataset

The *SubClim* dataset presents a remarkable density of stations over a limited region in southern Spain, specifically in Andalusia. The dataset was provided by the *Subsistema de Climatología Ambiental* from the regional government of Andalusia (*Junta de Andalucía*). Due to its high spatial density, it is particularly useful to examine the performance of the various WRF configurations.

The dataset consist of homogeneous and quality-controlled daily temperature time series from 152 stations and daily rainfall series form 438 gauges across Andalusia (Fig. 3.2) that covers the 1990-1999 period. The quality control initially consisted in a basic check for wrong values (Tmax<Tmin, Precipitation<0 mm/day). Then the methodology followed by Hidalgo-Muñoz et al. (2011) was adopted here. The inconsistently high or low values were carefully examined. In particular, the suspicious peaks were analyzed in detail and they were confirmed using the information provided by both the nearby stations and the historical records appeared in public documents (e.g., newspapers). All those measurements that were clearly invalid were set to missing values. For the homogeneity testing, the guidance provided by the ETCCDI was applied using the RHtestV2 software[1].

The dataset originally comprised 1821 precipitation series and 850 temperature series. After the quality controls, the series were filtered on the basis of a 10% threshold of missing values for the selected 10-year period. The choice of this time lapse was made with the aim to include as much variability as possible (i.e., particularly wet/dry periods) so that the selected model configuration performs adequately under different atmospheric conditions. But the available number of observations decreases with longer periods and the computational costs associated to long WRF simulations are high; therefore, a 10-year period was considered appropriate to meet both physical and practical requirements.

3.2.2   Gridded observations

In addition to the aforementioned observational network, the Spain02 daily observational gridded dataset version 2.1 (Herrera et al., 2010b) is here adopted to evaluate the WRF model ability to represent the present climate (1970-1999) in terms of precipitation, Tmax and Tmin.

The Spain02 dataset was created using 2756 quality-controlled stations ($\sim$ 250 for temperature), which amounts to an extraordinary dense network for the precipitation dataset. Spain02 is a regular $0.2°$ ($\sim$ 20 km) daily gridded dataset that spans a 54-year period (1950-2003) and covers Peninsular Spain and the Balearic Islands (Fig. 3.3). The precipitation grid was built using a two step kriging (binary for precipitation outcomes and ordinary for amounts), whereas for temperature, thin plane splines are fitted to the monthly data considering elevation and an ordinary krigin was latter applied to the residuals. Further details

---

[1]http://cccma.seos.uvic.ca/ETCCDI/index.shtml
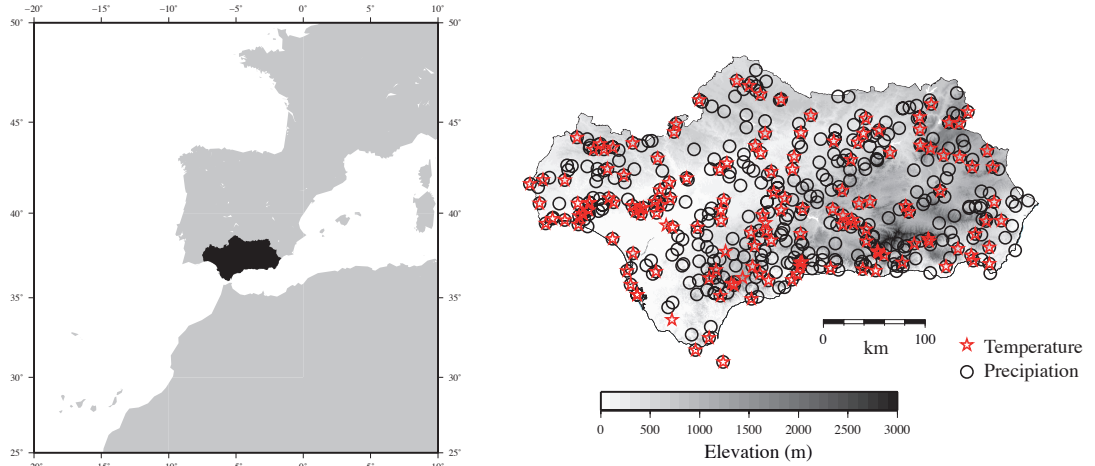
Figure 3.2: *Spatial coverage and distribution of precipitation (black circles) and temperature (red stars) stations used in this study that conforms the* Subsistema Clima *dataset.*

on the methodology can be found in the webpage of the Santander Meteorology Group[1], from University of Cantabria.

As a result of the technique adopted to generate the dataset, the final product is a sort of weighted averages of the variables over the grid cells, which replace the local measurements provided by the stations. Therefore, both Spain02 and the model outputs are representative of the grid boxes and thus are comparable because their scales are similar.

It should be noted that Spain02 is not a pure observational dataset and, besides the instrumental errors of the measurements, it might be subject to

Figure 3.3: *Spatial coverage of Spain02 gridded dataset.*

errors that come from the methodology employed to create it. Nonetheless, the quality of the grid has already been addressed by the authors not only in terms of capturing long-term means but also the upper percentiles. A discussion of the

---

[1]http://www.meteo.unican.es/en/research/datamining

Spain02 performance for precipitation is detailed in Herrera et al. (2010b). In the case of temperature, the dataset was subjected to a simple quality-control test that helped to identify some problems in the minimum temperatures over the Balearic Islands. Consequently, Spain02 was not used to conduct the WRF evaluation over this region in terms of temperature.

Finally, it is worth emphasizing that despite the fact that Spain02 and WRF grids have similar spatial scales, they are not identical and thus the *representation error* is not completely removed, although considerably reduced. Although both the gridded dataset and the WRF outputs should be ideally defined over grid points with identical characteristics (e.g. same elevation), differences between the model grid and Spain02 should not be significant in this case, and the model estimates will be simply projected onto the Spain02 grid. Nonetheless, the existence of the *representation error* should be kept in mind when interpreting the evaluation results, because it might explain minor deviations.

On the whole, Spain02 can be regarded as a remarkable effort to create a gridded daily observational dataset. The density of stations employed to create the precipitation grid is outstanding, and for temperature, it exceeds by far the number of observations used in the previous gridded datasets over the region. The spatial density together with the time frequency makes Spain02 an extraordinarily valuable tool that enables the model evaluation because it provides observational information at scales that are comparable to that of the regional model estimates.

3.3   The regionalization

In the beginning of this Chapter, it was already pointed the necessity to reduce both observations and model estimates to a similar scale so that they are comparable. Regionalization procedures have been put forward within the framework of RCM evaluation for different variables (Caldwell et al., 2009; Jiménez et al., 2008; Kostopoulou et al., 2009). The convenience of using regionalization to compare model outputs and observations have been highlighted by different authors (Bunkers et al., 1996; Reid and Turner, 2001) because it filters the very-local effects to which the stations are subject.

Regionalization as a mean to identify areas with similar climate characteristics is certainly not a new idea. Classification of stations into climate divisions have been a common practice since the early 20th century because it provides a general overview of the region under survey and permits to create comprehensive information for many purposes (e.g. examine correspondences between far

away locations, study and understand wildlife distribution or decide what to grow in the farmlands). Original methods, such as the Köppen (Köppen, 1923) and the Thornthwaite (Thornthwaite, 1931) classifications, were based on *a priori* criteria, namely on precipitation and temperature thresholds[1]. They have the advantage that provided some information from a particular station, its classification into a climate division is straightforward. In spite of their simplicity and direct applicability, they are formulated in a fairly subjective way and several methods have been recently proposed using objective procedures (Bärring, 1987; Fovell, 1997; Gerstengarbe et al., 1999; Romero et al., 1999b; Unal et al., 2003).

Among these objective methodologies, Clustering Analysis (CA, Kalkstein et al., 1987) and Principal Components Analysis (PCA, Preisendorfer, 1988) are probably the most widespread to classify stations into regional divisions (Fovell and Fovell, 1993; Lund and Li, 2009; Richman and Lamb, 1985). Both procedures have their own advantages and shortcomings in relation to climate regionalization, as detailed below for the PCA and two different CA algorithms:

1. **PCA** or Empirical Orthogonal Function analysis is an orthogonal transformation that reduces an original dataset containing a large number of possibly correlated variables to a dataset usually containing many fewer uncorrelated variables (See Appendix A for the mathematical details). These new variables are linear combinations of the original ones and are called principal components. They are chosen in such a way that they represent the maximum possible fraction of the variability contained in the original data. A significant reduction of the variables is attained when they are substantially correlated and the original dataset contains redundant information, which is typically the case of atmospheric variables.

   PCA is very useful to manage large multivariate datasets and makes possible to explore both spatial and temporal structures and variations of the fields being analyzed. Regarding regionalization, the PCA major potential is its ability to reduce information redundancy and keeps only the most important variability modes. It thus helps to generate a more comprehensive division. However, the fuzzy nature of the PCA results make it difficult to determine definite regional boundaries. It must be said that fuzzy regionalization is physically more consistent bearing in mind that particular stations might contain characteristics from two or more regions. Nonethe-

---

[1]Thornthwaite (1948) also proposed a later improvement of his climate classification using potential evapotranspiration besides precipitation and temperature.

less, the thresholds to establish whether to include or not a station within a region are virtually impossible to determine if only the PCA results are obtained and thus is not practical from a regionalization point of view.

2. **Hierarchical agglomerative CA** methods successively merge clusters based on a similarity measure. They all start from as many single-element cluster as initial objects and merge them in new cluster until one large cluster accommodating all stations is finally achieved. The main difference between hierarchical CAs lies in the similarity measure employed to determine the distance between clusters.

   As the cluster are progressively merged, several solutions that vary in the number of clusters are proposed. Let us imagine that there are n initial objects. Then the agglomerative CA suggests solutions from n single-element clusters to 1 all-inclusive cluster. These two solutions are obviously useless because they do not provide any information. However, there should be an optimal configuration that groups the objects into a reduced number of clusters that provides information about the objects affinity. The optimal configuration is selected using statistical tests that measure the cluster internal cohesion and external isolation at every step.

   The main drawback of these CA methodologies is that they do not allow for clusters recombination. Namely, the formulation prevents exchange of objects between clusters once they have been merged and therefore, in the ultimate solution, there might be certain objects that are misplaced because they do not belong to the most appropriate cluster.

3. **Non-hierarchical CA** algorithms such as *k-means* groups n objects into K groups. By contrast with hierarchical CA, which do not allow for object reallocation once it its assigned to a particular group, k-means is precisely based on reassignment.

   However, the k-means requires some previous knowledge of the data structure and the number of clusters must be specified in advanced. Furthermore, an initial guess of the groups is also required, which can be calculated as a random division of the n objects into K groups or can be provided explicitly according to some previous measure of the similarity between objects. The latter is usually preferable to determine the initial approximation because the final results tend to be much more consistent.

Regardless of the method employed to define the initial configuration, the strategy consists in:

(a) Calculate the centroids of the initial clusters as the means of the vectors that represent each object and conform each of groups.

(b) Compute the squared Euclidean distance between the the vector x_i and each of the clusters. Other distances might be used too in place of the squared Euclidean one, but this is the most widespread.

(c) Two possible situations can take place here. If the x_i vector already belongs to the closest cluster, then continue by repeating the previous step with x_{i+1}. Otherwise, assign the x_i vector to the closest one and repeat the calculation of the centroids.

The algorithm only stops when a cycle through all the n elements is completed without performing any reallocation.

The problem is that in most of the cases, the appropriate number of cluster is not know in advanced, not to mention their centroids. Therefore, this methodology is not always suitable to determine an appropriate configuration by itself and has to be used in combination with others.

In this Thesis, a multi-step methodology is proposed consisting in the consecutive application of PCA and two CA algorithms, overcoming the problems that each method presents. The procedure permits to carry out the subsequent steps using the results from each analysis, removing most of the subjectivity associated to decisions such as the number of regions or their centroids.

3.3.1   A multi-step regionalization technique

The multi-step regionalization technique first stage is a S-Mode PCA to analyze the covariance matrix of daily values. There are two main PCA decomposition modes: The spatial mode (S-mode) and the time mode (T-mode). The differences between both methods yields in the dimension we focus on. Namely, the S-mode permits to identify time series with spatial coherence and thus is useful to find spatial clusters or teleconnections, whereas the T-mode searches for similar days (or other time lapses) and helps to find synoptic or flow patterns (Compagnucci and Richman, 2008).

The majority of algorithms to conduct a PCA require that the times series are complete and no missing values are allowed. As a consequence, the stations

that present missing values must be filled somehow. Some simple approaches consist in using climatological values of the series to fill the missing values (e.g. monthly means), which might be acceptable for monthly precipitation or even daily mean temperature, but it is definitely inappropriate for daily precipitation or temperature extremes (Tmax and Tmin). In this study, the strategy to fill the missing values lies in a multiple linear regression with the five most correlated stations. For each time series, a linear combination of the five most correlated stations is computed to generate a 'reconstructed time series' using the correlation coefficient to weight them. The missing values of each station are then filled with the corresponding reconstructed series. In the case of daily precipitation, the multilinear regression introduces a small and undesired offset in the reconstructed series that is removed. The offset consists in clearly identifiable constant values that never exceeds the threshold of 1 mm/day and appear in place of rainless situations. They Figure 3.4 show two random examples of the original and the reconstructed precipitation from the *Subsistema Clima*. In these examples, one-year periods with no missing values for two different stations were selected to emphasize the suitability of the methodology, which presents high accuracy in capturing the precipitation on a daily scale.

It must be stressed that the filled series are only employed in the definition of the regions because the PCA algorithm here adopted requires complete information, but no completion of the series is performed to evaluate the model and the original series are maintained.

Once the missing values are replaced, the S-Mode PCA is computed, the principal modes of variability are retained and possible information redundancy is removed (Fovell, 1997). The North Rule of Thumb based on the eigenvalue degeneration (North et al., 1982) is adopted to determine the significant PCs. The resulting PCs are varimax rotated to increase spatial coherence. Afterwards, the stations are classified via a two-step CA (Milligan, 1980). In particular, the rotated normalized loadings are processed with an agglomerative method to set the appropriate number of clusters and their starting seeds. A non-hierarchical k-means algorithm follows the agglomerative CA to conform the final regionalization. This strategy takes advantage of both methods and reduces their respective imperfections.

Hierarchical algorithms merge clusters in new ones based on the principle of maximizing intra-cluster similarity and minimizing inter-cluster likeness. Therefore, two parameters have to be selected in order to define the clusters: a similarity measure and a method to assign objects membership to clusters according
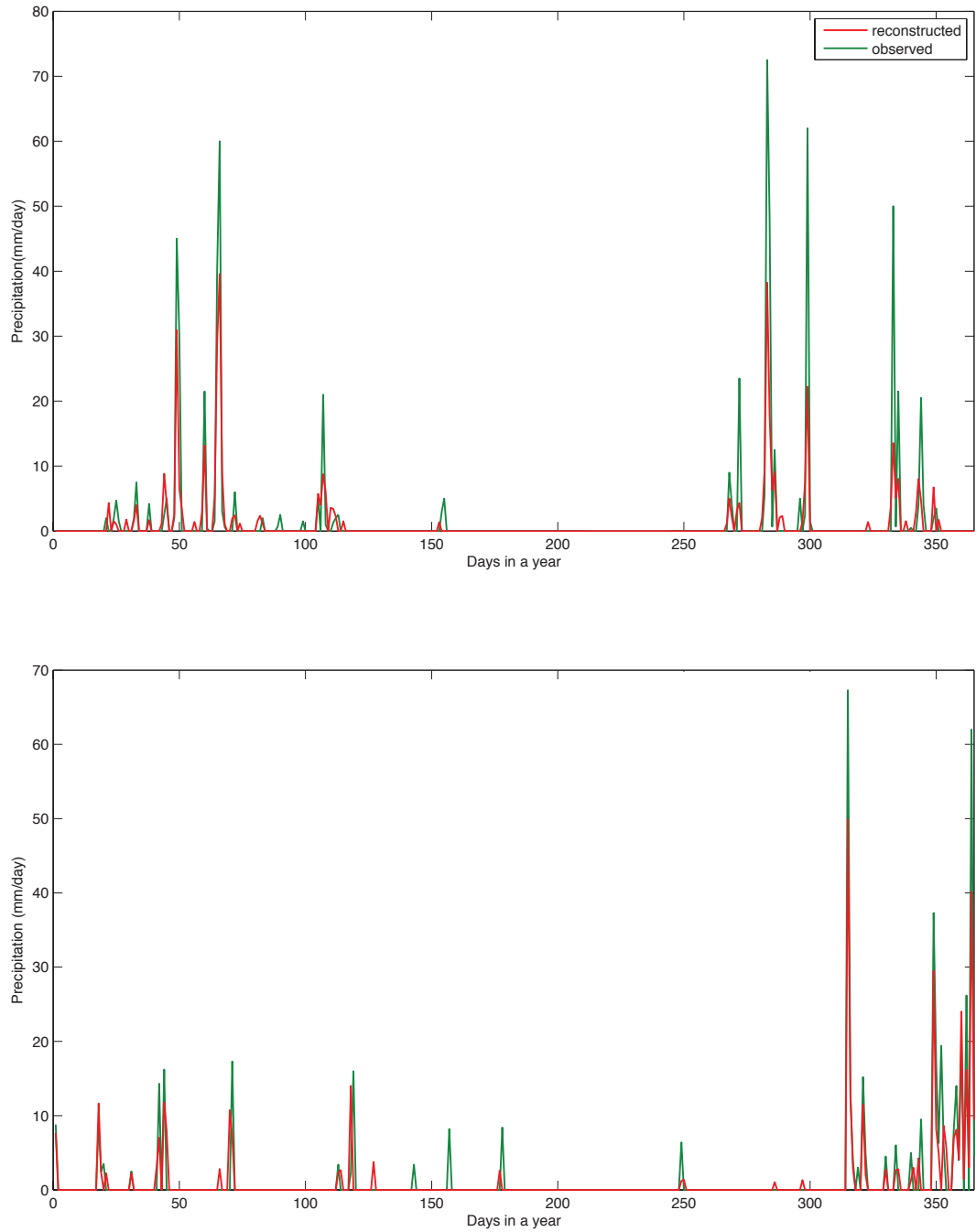
Figure 3.4: *Two examples of the original and reconstructed series from* Subsistema Clima *dataset for a one-year period using a multi-linear regression method. The series represent two different locations and two different years that were selected randomly.*

to this measure. The simplest and most extended squared Euclidean distance in the space of the rotated loadings was chosen to measure the similarity between objects and clusters. Previous works (Gong and Richman, 1995; Kalkstein et al., 1987) advocated the Average Linkage algorithm to configure the clusters in the framework of climate regionalization because it does not tend to create similar-size groups nor huge "hungry" clusters as other methods do. The Average Linkage calculates the distance between two clusters (r and s) through the average distance in each cluster as expressed below:

$$d(r,s) = \frac{1}{n_r n_s} \sum_{i=0}^{n_r} \sum_{j=0}^{n_s} dist(x_{ri}, x_{sj}) \tag{3.1}$$

and combines the two most similar clusters (least distant). The number of clusters is then reduced by 1 and the distance matrix is calculated again. This processes stops when all objects are merged in a single large cluster.

Therefore, the agglomerative CAs propose a number of configurations that ranges from as many single-element clusters as stations to an only cluster that includes all the stations. The suitability of a particular configuration can be measured through statistical parameters of which the pseudo-F seems to perform better (Milligan and Cooper, 1985). The pseudo-F test (Calinski and Harabasz, 1974) represents the ratio between the within- and the among-cluster similarity which varies as the clusters are merged. When the pseudo-F reach a local maximum, it indicates that the configuration of clusters is more robust and thus it permits to define an optimal number of divisions. However, the pseudo-F test does not always provide a single solution and further aspects must be considered. Moreover, the test sometimes is not useful at all to determine an adequate configuration because it simply decreases with the number of clusters and it is not worth of consideration in such situations. The pseudo-F test can be expressed as:

$$\text{Pseudo-F(k)} = \frac{T - \sum_k SSE_k}{\sum_k SSE_k} \frac{k-1}{n-k} \tag{3.2}$$

Where T is the total sum of squares, $\sum_k SSE_k$ is sum of squares within the clusters, k is the number of clusters and n is the number of stations. Therefore, the $T - \sum_k SSE_k$ and $\sum_k SSE_k$ represent the among- and within-cluster sum of squares respectively.

Next, the clusters centroids are calculated using the original data that was fed into the S-Mode PCA. Non-hierarchical CAs, such as the k-means, need the number of clusters to be specified and usually the initial seeds too. If not specified, the algorithm normally starts by defining random seeds, although the final results are directly affected by this initial configuration. The starting seeds required by the hierarchical k-means CA are here determined using the aforementioned centroids. Consequently the number of clusters is set by the pseudo-F test. The k-means CA checks which of the clusters is more suitable for each of the stations and relocates them accordingly, enhancing the regionalization consistency.

The interested reader is referred to Timm (2002) as an excellent overview of Clustering Analysis and Multivariate Analysis.

The regionalization is here performed to determine regions in terms of precipitation and temperature because these are two main variables that are later employed in the model evaluation. Although previous works (Fovell and Fovell, 1993; Unal et al., 2003) attempted to establish climate divisions using simultaneously precipitation and temperature, standardization problems and the rare coincidence of temperature and precipitation stations encouraged us to process them independently. The steps described above are common to both variables and thus the approaches to process them are very similar. However, some minor modifications were introduced in the data preparation (e.g precipitation was screened) due to obvious differences in the characteristics of the variables.

Precipitation preprocessing Precipitation in a wide area of Spain is concentrated in short rain events and the annual cycle is characterized by very dry summers. In order to avoid an excessive influence of this feature in the regionalization, a filter is applied and those days that were dry at most of the locations are removed. This approach of screening precipitation to reduce the influence of totally dry periods was initially suggested by Romero et al. (1999a) to define rainfall affinity areas in a region that extended over the southern and eastern Spain. It consisted in retaining only those days when precipitation was larger over a certain threshold in at least a number of stations. In particular, they selected a precipitation of 5 mm/day over at least 5% of the stations.

In this Thesis, two different precipitation observational datasets that cover Andalusia and Spain are used. The *SubClim* stations are spread all over Andalusia, a region very similar to that studied by Romero et al. (1999a) and hence the thresholds are kept to 5 mm/day and 5% of the stations. In the case of Spain02 that covers the IP, the rainfall regimes are more heterogeneous and therefore a

less restrictive threshold in the daily precipitation is selected (1 mm/day). Alternative thresholds for both the daily precipitation and the percentage of locations were examined with differences in the number of the days retained but almost negligible modifications of the climate divisions were observed. Indeed, only the boundaries of the regions were slightly displaced[1].

Temperature preprocessing Unlike precipitation, temperature was not screened and the full-length series are used to characterize the regions. The observational datasets actually include both Tmax and Tmin, and therefore both are considered in generation of climate divisions. Tmax and Tmin are initially processed separately because they are not equally affected by the same factors (i.e. stratification vs. turbulence, surface fluxes, elevation). For example, the Tmax at two stations might present a similar evolution and magnitude, but the Tmin might differ considerably. Therefore, the PCA must be computed independently for Tmax and Tmin to avoid masking the information provided by one of the temperature extremes by the other.

The PCA results, namely the rotated significant components are then merged. If Tmin is characterized by m principal components and Tmax by n, hence the new space containing all of them would have m by n dimensions, in which each station is represented by m by n components. The squared Euclidean distance that is used in the agglomerative CA is then calculated over this m-by-n dimensional space. As a result, a single regionalization that includes the attributes of both Tmax and Tmin, is obtained.

3.3.2   Regionalization of the *SubClim* dataset

The *SubClim* dataset contains precipitation, Tmax and Tmin. These three variables will then yield two independent regionalizations (one for temperature and one for precipitation).

The multiple regression method detailed above is adopted to fill the missing values for both temperature and precipitation series. For the latter, the 438 daily time series that had at least 90% of valid measurements over the 10-year period

---

[1]The thresholds are fairly arbitrary, but the different possibilities were tested evidence the method resistance. Variations in both thresholds ranged from 3 to 6% of the locations and 3 to 6 mm/day. Romero et al. (1999a) tested larger variations in the number of stations that met the rainy condition (15% and 30%). The patterns of the different regionalization were very similar when these changes are introduced and thus it can be affirmed that the method is considerably stable.

(1990-1999) are screened. Only those days when at least 5% of the stations registered precipitation larger than 5 mm are considered in the PCA.

The covariance S-mode PCA computed over this reduced precipitation dataset produces 5 significant principal modes that explained approximately 58% of the variance. These 5 significant components are rotated and the hierarchical algorithm is applied. The pseudo-F test is calculated and it indicates that a five-cluster organization is appropriate for the Andalusian precipitation, as shown in Figure 3.5. Other configurations with higher number of clusters are also suggested by the test (7,12 and 17) but the aim is to obtain a regionalization as simple as possible and thus the five-division regionalization was chosen.
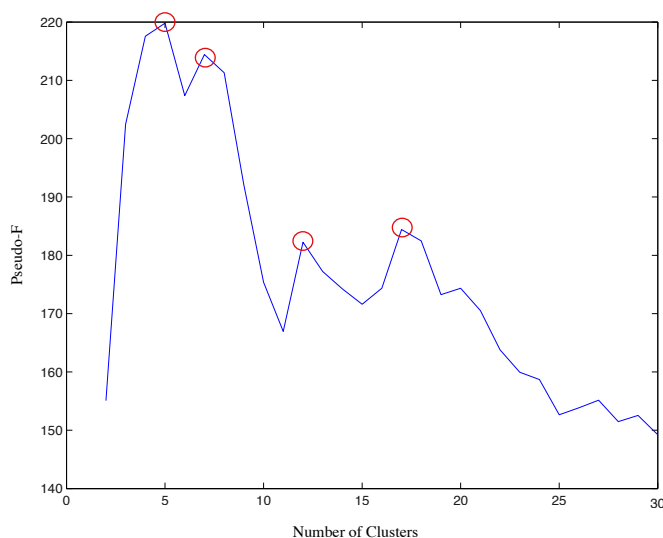
Figure 3.5: *Pseudo-F calculated for precipitation from* Subsistema Clima *dataset. A local maximum indicates a suitable number of cluster. Red circles highlight the recommended configurations.*

The screened precipitation is used to calculate the centroids of the clusters that will act as seeds to initialize the k-means. The k-means redistribute the stations in these clusters accommodating each one in the most suitable region.

The final regionalization for precipitation over Andalusia is shown in Figure 3.6a. The structure of climate divisions is coherent with topography and the main features of the dominating circulation. An evident zonal partitioning can be observed, which accounts for the gradual influence of fronts coming from the Atlantic Ocean and systems generated in the Mediterranean Sea. Moreover, topography effects can be seen in the boundaries of regions N, S and E, delimited by

the Baetic System. The eastern precipitation regime is clearly distinguished form the other Andalusian rainfall patterns; indeed this semi-arid area with markedly convective character and differentiated dynamical precipitation is accurately singled out by the regionalization technique. An almost identical regionalization was obtained in one of the solutions proposed by (Romero et al., 1999b) except for minor differences probably caused by the inclusion of the whole Spanish Mediterranean coast in their study.

Regarding temperature, 5 significant components are obtained for Tmax and 3 for Tmin that explain about 95% and 91% of the variance, respectively. The normalized loadings of these components were varimax rotated, merged and fed into the Average Linkage clustering based on a 8-D distance that includes both Tmax and Tmin rotated loadings. The pseudo-F test suggests a 4-cluster division as the simplest among those recommended. The centroids of the different regions are then calculated using Tmin and Tmax, and they are used as seeds in the k-means CA to obtain the definitive regionalization.

The configuration of the divisions is mainly driven by the elevation, which is the key factor in determining the temperature. This causes that the regions are considerably scattered and the boundaries are not as defined as they were for precipitation. Figure 3.6b illustrates the 4 different regions: a coastal (CO) region, a highlands (HL) region that includes stations at high altitudes ranging from 760 to 1350 m, stations located in the lower *Guadalquivir* basin conform the lowlands (LL), and the midlands (ML) region comprises those internal stations that are situated in the mountains but at lower elevations than HL. However the regions are labelled in terms of the altitude for the sake of readability, there are other factors such as the distance to the sea or the slope orientation that affects the regionalization. Therefore, the names assigned to each region do not strictly refer to the elevation of the single station, which would be a rather simplistic assumption, but to the overall elevation of the regions.

Summarizing, 438 rain gauges are divided into 5 regions and 152 temperature stations are classified in 4 regions (Fig. 3.6).

3.3.3   Regionalization of Spain02

Despite the fact that Spain02 is a gridded observational dataset and thus regionalization is not necessary to compare the model estimates, it facilitates the comparison in terms of certain parameters. For example, the regionalization is used to calculate and illustrate the monthly annual cycle or the percentiles of
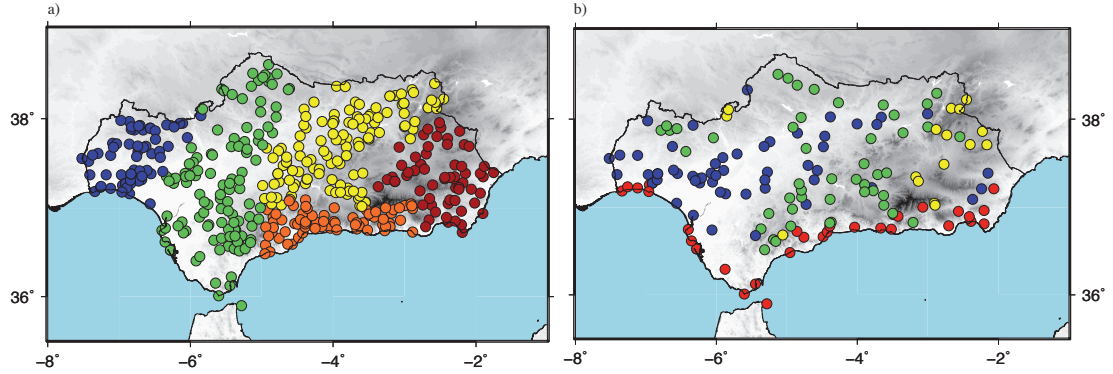
Figure 3.6: *Regions obtained with the multi-step methodology for: a) Precipitation: west (W - blue), central (C - green), north (N - yellow), south (S - orange) and east (E - red); b) Temperature: coast (CO - red), highlands (HL - yellow), midlands (ML - green) and lowlands (LL - blue).*

daily values because a single plot for every grid point is evidently impractical.

The procedure to prepare data for regionalization is analogous to *SubClim* dataset, although some differences are introduced.

In terms of precipitation, the Spain02 is initially screened to eliminate those days that were dry over the entire region with a criterion (1 mm/day in at least 5% of the locations) that slightly differs from that used in Andalusia. The filtered dataset is processed by a S-Mode PCA over the covariance matrix and the North Rule of Thumb indicates that 13 components are significant. The components retained explained about 61% of the total precipitation variance. The agglomerative CA and the subsequent pseudo-F test recommended 5, 7, 10 and 14 climate divisions as appropriate configurations. Two factors made us to prefer the 10-cluster option: 1) the coherence with the previous regionalization that divided precipitation in Andalusia (a much smaller area) into 5 regions, and 2) the pseudo-F absolute maximum attained with this configuration with respect to the other solutions. The k-means slightly moved the boundaries to yield the final climate division shown in Figure 3.7.

The regionalization obtained for Spanish precipitation agrees with the rainfall regimes distribution and the topography. The regions are broadly distributed from west to east representing the gradual influence of the fronts with origin in the Atlantic Ocean and the Mediterranean Sea. Furthermore, the areas are differentiated from north to south too, which explains the gradient in total precipitation amounts. It is also interesting to note that the mountain ranges in

the IP are in general oriented zonally and several divisions from north to south correspond to their location. Outside the IP, an additional region represents the Balearic Islands.
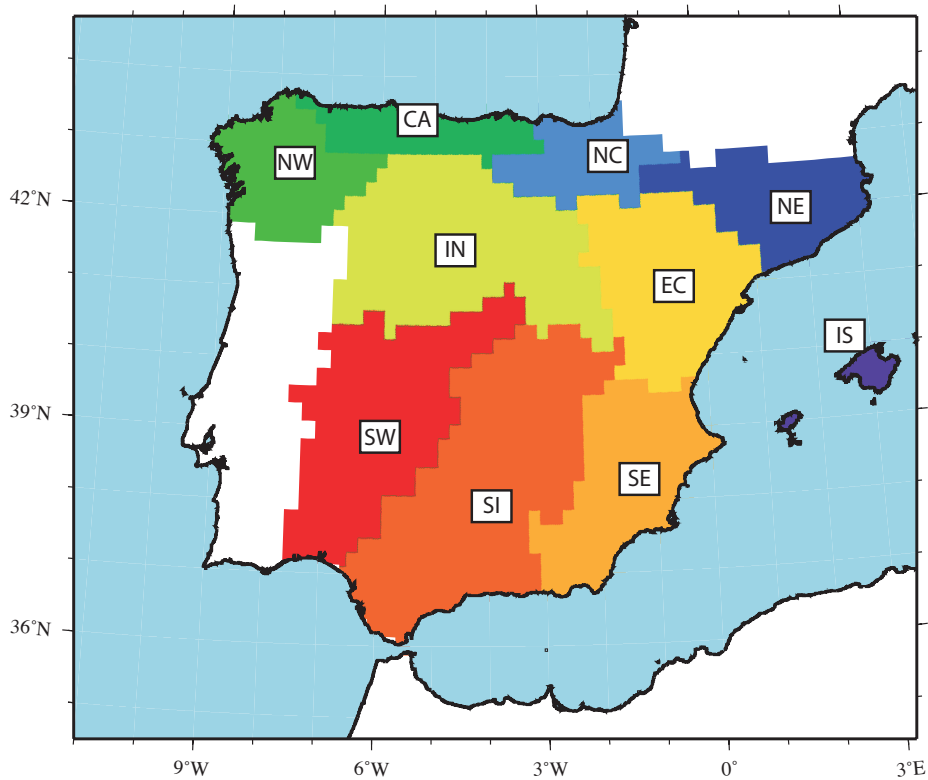
Figure 3.7: *Regions obtained with the multi-step technique for the Spain02 precipitation: northwest (NW), Cantabrian Coast (CA), north central (NC), northeast (NE), islands (IS), east central (EC), interior (IN), southwest (SW), southern interior (SI), southeast (SE).*

Regarding temperature, the same procedure that was adopted for the *SubClim* dataset is here applied. A S-Mode PCA is initially computed over the covariance matrix for both temperature extremes. The North Rule of Thumb suggested 12 principal components for Tmax that explained about 97% of the variance and 15 components for Tmin that also explained about 97% of the variance. Then, the agglomerative CA is applied to the squared Euclidean distance over the 27-D space of the rotated loadings and the pseudo-F test is carried out, which yields a local maximum at 8. The original Tmax and Tmin are processed with a k-means algorithm using the agglomerative CA results to define the appropriate number of clusters and the starting seeds. The final regionalization obtained from the

k-means non-hierarchical clustering is composed of 8 regions that characterize Spanish temperature regimes (Fig 3.8).
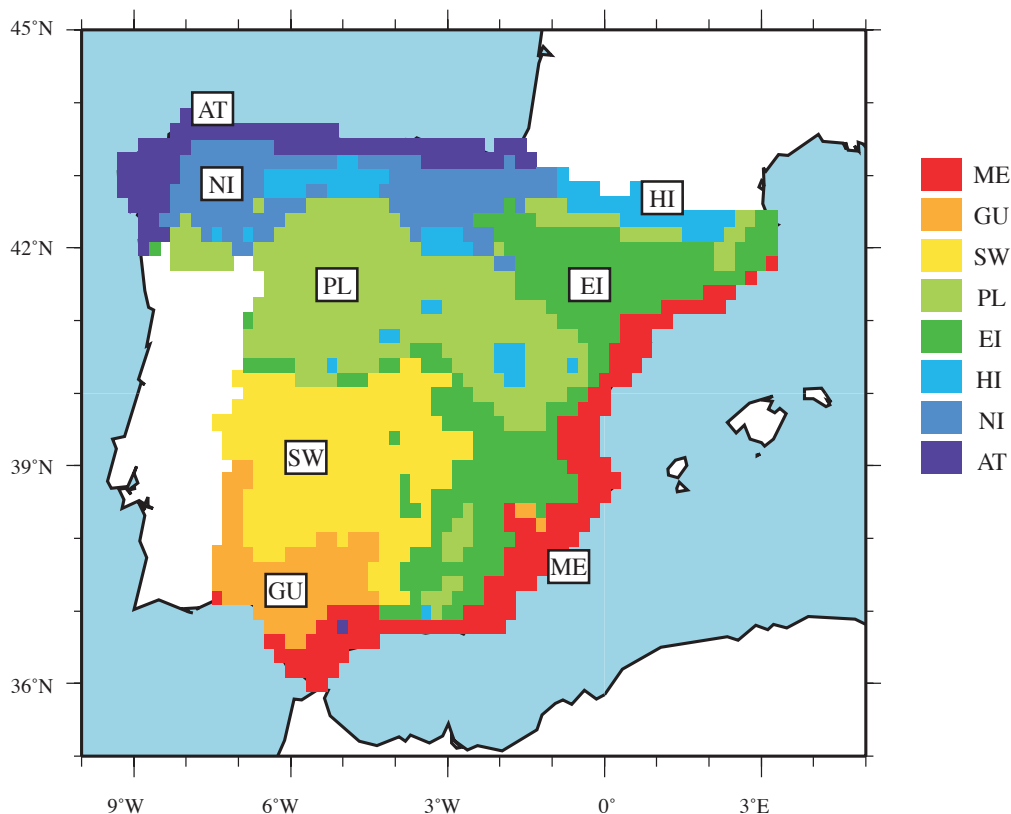
Figure 3.8: *Regions obtained with the multi-step technique for the Spain02 temperature: Mediterranean Coast (ME), Guadalquivir Basin (GU), southwest (SW), east interior (EI), plateau (PL), high mountains (HI), north interior (NI) and Atlantic coast (AT).*

The regionalization is mostly driven by elevation and distance to the sea. Two coastal regions, in the Mediterranean (ME) and in the Atlantic Ocean (AT) group the stations close to the sea. The stations located in the Guadalquivir river basin are included in the GU region. The area comprised between the Central System and the Sierra Morena, which includes the Tejo and Guadiana river basins is represented by the southwest (SW) region. The NI region is made up of locations in the nothern interior. The Northern Central Plateau forms the PL region that extends almost until the Mediterranean coast. The Ebro river basin and some areas in the eastern interior are included in the EI region. Finally ,the HI region defines the regimes associated to high-mountain climate and is spread across the

IP, from an isolated grid point in the southern Baetic Systems to the Pyrenees or the Cantabrian range.

Chapter 4

The WRF configuration

> The greatest challenge to any thinker is stating the problem in a way that will allow a solution.

> Bertrand Russell

One of the principal stages in the generation of future climate change projections through dynamical downscaling is the regional model setup. This chapter details the configuration of WRF to perform the present and future simulations. The domain design, the static fields used by the model, the running options and the driving data are herein described. These parameters where selected according to preliminary tests that qualitatively helped to design the experiments. Additional features of the model configuration that required in-depth analyses such as the parameterizations, are addressed in the next Chapter (5).

4.1 The domains design

The domains basically specify the area to be simulated, which is usually determined in advance by the region under survey. However, several factors must be considered in the domain design.

Number of domains and feedback

It is already well-known that a large resolution difference between the driving data and the RCM might have an important impact on the results (Denis et al., 2003). Given this fact, a usual approach is that of using an intermediate coarser domain where to nest the finer domain in order to reduce the disparity. As for

WRF, the grid distance ratio between the parent and nested domains is typically 3/1. Therefore, a 10-km resolution domain is usually nested in a 30-km domain. If the scale disparity between the coarse domain and the boundary conditions data is still large, then an additional domain could be added.

In the preliminary tests[1], different approaches using three-domain (90-, 30- and 10-km resolutions) and two-domain (30- and 10-km resolutions) configuration where analyzed and the two-domain option seemed to produce similar or even better results in terms correlation, RMSE and Bias with respect to observations. The resolution was chosen upon the available computational resources and the purpose of producing high-resolution projections. A climate run at 10-km (or even coarser) is currently considered a state-of-the-art high-resolution climate simulation (Caldwell et al., 2009; Evans and McCabe, 2010; Rummukainen, 2010).

Not only the number of domains must be explored but the communication between them as well. Essentially, there are two possible communication techniques between the domains, namely the one-way and the two-way nesting. The difference between them derives from whether there is feedback or not. In the one-way nesting, the boundary conditions are fixed at the borders of the coarser domain that in turn passes this information to the finer domain. On the other hand, in the two-way nesting the information generated within the finer domain is also passed into the coarser domain and therefore there is a feedback between the two domains. The two-way nesting might be highly beneficial in short-term simulations, but in the case of long-term simulations it might cause instabilities. Indeed, WRF 3.1.1 is unstable in the long term when using two-way nesting because very large vertical velocities occur in the relaxation zone where the information is shared. In addition, the ability of the one-way technique to reproduce fine scale features of atmospheric fields have already been demonstrated by several authors (Denis et al., 2002; Dimitrijevic and Laprise, 2005; Harris and Durran, 2010). In this scenario and bearing in mind that this is probably the most widespread approach in climate simulations(Antic et al., 2006; Borge et al., 2008; Bukovsky and Karoly, 2011; Frei et al., 2006; Moberg and Jones, 2004; Salathé Jr et al., 2008), the one-way procedure was chosen.

Domains position

Another subject that should be considered carefully is that of locating the domain borders adequately. The aforementioned resolution disparity between

---

[1]These are the preliminary tests that were performed using MM5 (see Sec. 2.2).

the driving data and the model itself suggest that orographic inhomogeneities should be placed far from the domain borders to avoid the generation of artifacts. However, it is not always possible to design a domain with the borders located over completely homogeneous areas and the mountainous regions are sometimes inevitable. Whenever this happens, different positions of the border should be examined to reject configurations that might induce too large errors. Moreover, the atmospheric dynamical features of the region must also be taken into account when deciding the domain location. For example, the IP is directly affected by the frontal systems that are generated in the Atlantic Ocean and hence a large portion of it should be included in the coarser domain. Nonetheless, the initial simulations indicated that a significant part of the western Mediterranean must also be included in the parent domain to correctly capture the mechanisms that produce precipitation in the eastern Spain.

All these factors led us to define two domains using one-way nesting at 30 and 10-km resolution respectively, and located as illustrated in Figure 4.1. The coarser domain consists of 130 by 120 grid points, equivalent to 3900 km (W-E) by 3600 km (S-N), and the nested one comprises 135 by 135 grid points, which amounts to 1350 km (W-E) by 1350 km (S-N).

The vertical grid

In addition to the horizontal configuration of the domains that is described above, the vertical grid has also to be defined. The soil is divided in four levels where the soil variables are defined (0-7, 7-28, 28-100 and 100-255 cm). Over the ground, both domains have 35 levels in the vertical with the top of the atmosphere located at 50hPa. Since WRF uses a η vertical coordinate system (see Sec. 2.2) the vertical resolution depends on the surface pressure and thus varies with time and space. Nonetheless, Figure 4.2 shows the position of the levels calculated using the base state pressure as a reference.

The static fields

Besides the boundary conditions that WRF needs to run, different static fields are also used as input to define the domain. These fields mainly describe the topography, the soil type and the land use. In the simulations performed here, the U.S. Geological Survey (USGS) dataset is selected to define the topography (GTOPO30, Gesch et al., 1999) and the land-use category. The USGS dataset has 24 land-use categories and a 30" resolution ($\sim$ 1 km) that is converted to
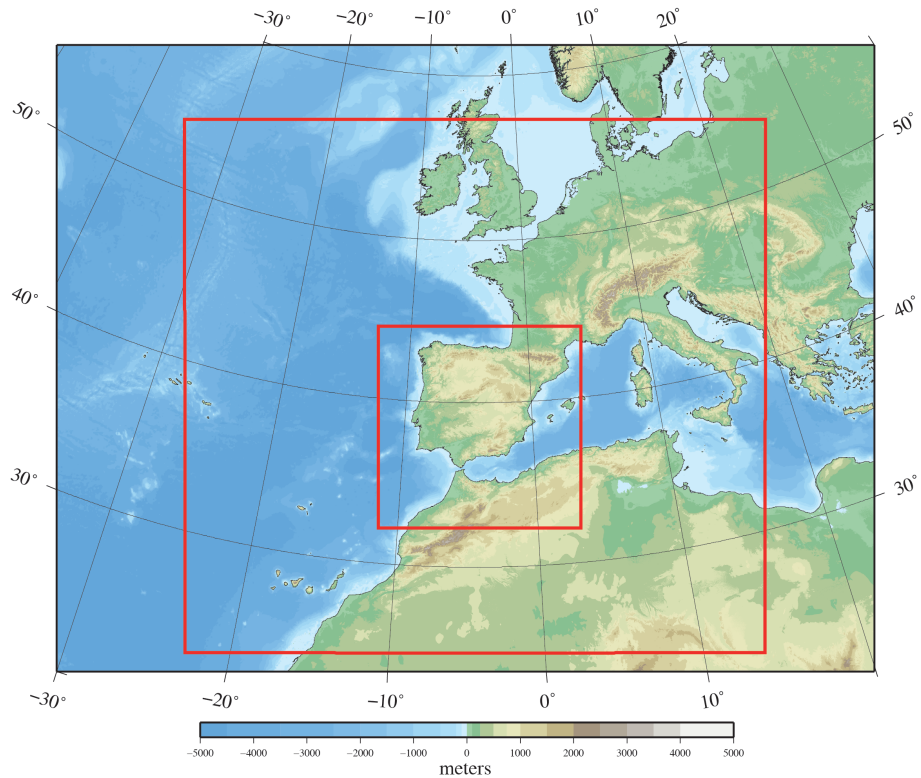
Figure 4.1: *The WRF domains configuration for present and future climate simulations. The red lines delimit the coarser (30-km) and the finer (10-km) domains.*

the model grid resolution by means of interpolation. Each of the 24 categories is characterized by a number of properties (e.g., albedo, roughness length, emissivity).

Apart from the aforementioned static fields, the Sea Surface Temperature (SST), the vegetation fraction and the albedo are also ingested by the model and usually kept constant during short-term simulations. However, in climate runs it is recommendable to enable the option that makes these fields to vary. The SST is then obtained from the driving data and updated with the same frequency as the boundary conditions, whereas the albedo and the vegetation fraction are characterized by monthly values.
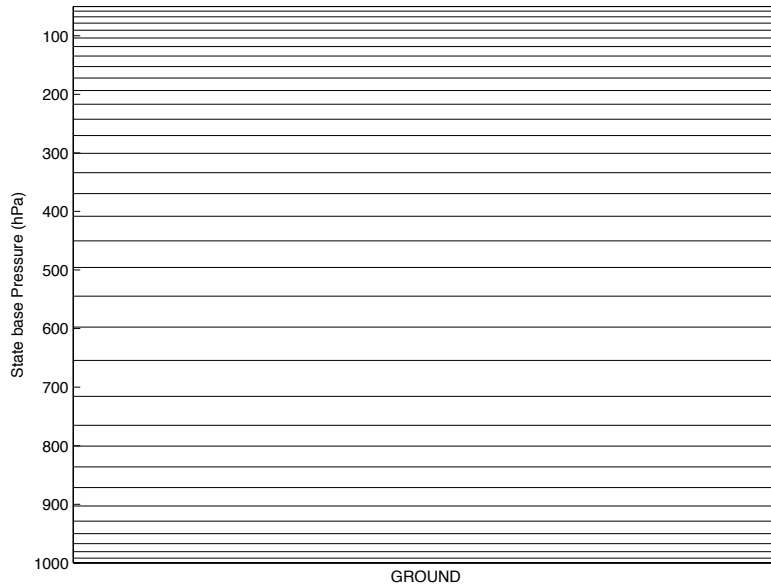
Figure 4.2: *Position in pressure coordinates of the η vertical levels using the base state pressure as a reference.*

4.2 The boundary conditions

The driving data are a crucial component in dynamical downscaling because they are the prime source of information. Indeed, the WRF model downscales the low-resolution climate information that the boundary conditions provide. Under these circumstances, the future climate projections should be produced using different data sources to generate a sort of ensembles to reduce the uncertainty by covering a wide range of possibilities. The boundary conditions can be divided into two main groups, the observational reanalyses that describe current climate to evaluate the model and the GCMs that simulate the Earth climate under present and potential future conditions.

4.2.1 The observational reanalyses

The observational reanalyses are also known within the RCMs framework as 'perfect boundary conditions' because they embody the better global representation of present climate in the form of a mesh. A reanalysis of the observations is an objective combination of instrumental measurements and a numerical model to generate a synthesized estimate of the state of the atmosphere (from reanal-

yses.org). Using reanalysis to feed the regional model, it is driven as close as possible to the actual evolution of recent-past climate. Two of the most prominent examples of global reanalyses are the National Centers for Environmental Prediction (NCEP)/NCAR Reanalysis Project (NNRP, Kalnay et al., 1996) and the ERA-40 Reanalysis (Uppala et al., 2005).

Despite the fact that this kind of driving data are usually referred as 'perfect boundary conditions', it is obvious that the reanalysis are not free of errors, and hence their reliability has to be examined. An striking example of this topic is related to NNRP skin temperature over the westernmost Mediterranean.

The boundary data reliability: the Alboran Sea example

The skin temperature is defined as the temperature of the surface at radiative equilibrium and it is often used in the place of SST[1]. The sea points where the skin temperature works as SST are identified by a land-sea mask. However, the NNRP land-sea mask is deficient in the south of Spain due to its coarse resolution (about 2.5° by 2.5°) as shown in Figure 4.3a. The Alboran Sea is then represented as a inland sea with SST values that are substantially lower than in the surrounding sea. This produces unrealistic gradients and large deviations in the skin temperature (up to 5°C) that WRF uses as lower boundary conditions, as highlighted with black ellipses in Figures 4.3b and 4.3c. As a consequence, 2m temperature along the coast might be poorly simulated and precipitation might be also affected because lower SST values hinder convective processes. This feature of the NNRP reanalysis obviously discourage us from using it to drive the WRF model, although it does not mean that the same applies for other regions in the globe.

The ERA-40 reanalysis

The ERA-40 dataset from the European Centre for Medium-range Weather Forecasting (ECMWF) has been chosen because they are fairly accurate in the surroundings of the IP and due to their widespread in dynamical downscaling

---

[1]The skin temperature is identical to the SST over sea points but it is defined also over land points, which prevents some stability problems that arise from the misinterpretation that WRF makes of the missing values if they are not precisely masked. If the land-sea mask is not accurate enough, it might include land points as sea points and the SST will not be defined over them. Actually, a missing value ($\sim 10^{-31}$) is assigned to these points that WRF understand as a real value which causes, besides the unrealistic results, severe problems of numerical instability

a)   b)   c)

275   280   285   290   295   300
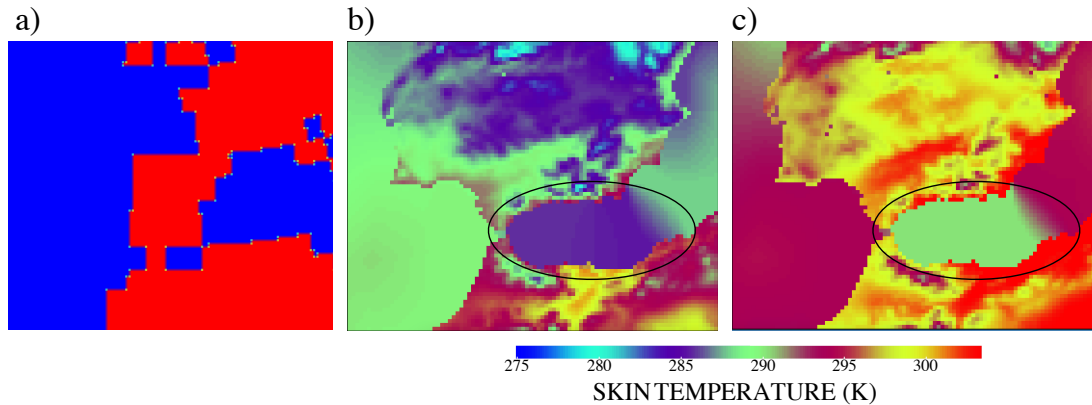
SKIN TEMPERATURE (K)

Figure 4.3: *(a) The NNRP land-sea mask and two different snapshot of skin temperature from NNRP-WRF boundary conditions in: (b) January 1st 1990 at 00h and (c) September 1st 1990 at 18h.*

studies over Europe (Christensen et al., 2007c; Fernández et al., 2007; Heikkilä et al., 2010; Rauscher et al., 2010; van der Linden and Mithchell, 2009).

ERA-40 is a reanalysis of meteorological observations that spans from September 1957 to August 2002 with a 1.125° by 1.125° spatial resolution. The observations incorporated in ERA-40 come from many different sources that include satellites, radiosondes, aircrafts, ocean-buoys and other surface platforms. It has 60 vertical levels of which 15 are selected to drive WRF (50, 70, 100, 150, 200, 250, 300, 400, 500, 600, 700, 775, 850, 925, 1000 hPa). The variables used to create the boundary conditions in the vertical levels are temperature, geopotential, U and V winds, and relative humidity. Additionally, a number of surface variables were used as well: 2m temperature, 10m U and W winds, dew point temperature, mean sea level pressure (PSML), skin temperature and sea ice. Finally, the soil temperature and moisture are also employed at four levels (0-7, 7-28, 28-100 and 100-255 cm).

It has already been mentioned that the skin temperature is often used instead of SST and an accurate land-sea mask must be provided to identify sea points. However, the default ERA-40 land-sea mask seem to be defective and some land/sea points are wrong. Thereby, when the WPS look up the land-sea mask to interpolate skin temperature over sea points, there are some areas where it generates spurious values near the coast. In Figure 4.4, both the default ERA-40 land-sea mask (a) and the ERA-40 skin temperature for a particular time are shown. The coastline is clearly visible in certain regions and comparing with the

land-sea mask map, the inconsistencies are manifest (black circles).
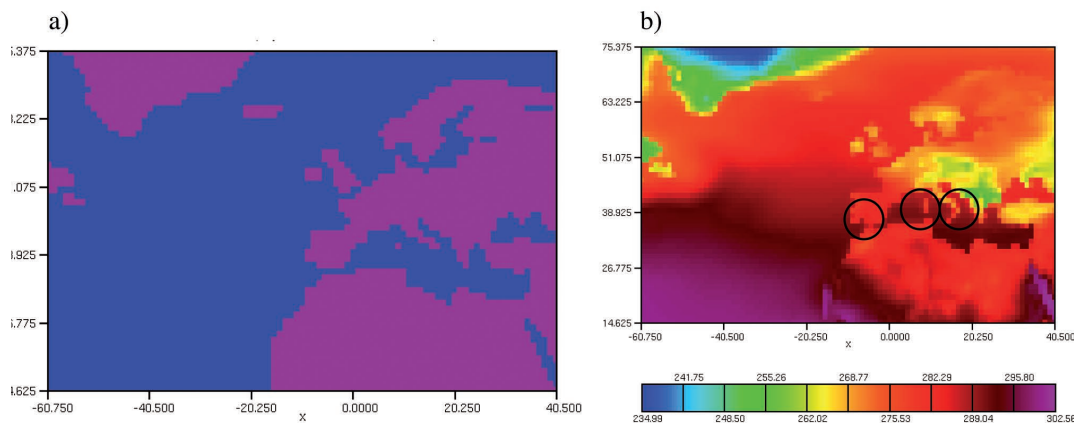
Figure 4.4: *(a) The ERA-40 skin temperature in December 1st 1989 at 00h and (b) the ERA-40 default land-sea mask.*

Nevertheless, the SST field is only defined over sea points and therefore, the land points appear as missing values and hence the land-sea mask is already incorporated in the data. Retrieving those missing values, a SST-derive land-sea mask can be obtained (Fig. 4.5). The alternative land-sea mask seems to be much more consistent that the default one and the effects of such a change can be observed in Figure 4.6, where the skin temperature is interpolated using the default ERA-40 mask (a) and the ERA-40 SST-derived mask (b). Although there are still areas with values that might be spurious (Ligurian Sea), remarkable improvements are noticeable in the western coast of the IP, in the Strait of Gibraltar, in the Strait of Bonifacio and in the south of Brittany.

Once the problem concerning the land-sea mask is fixed, the ERA-40 is used to describe the large-scale features of the atmosphere and hence to specify the boundary conditions for the simulations of present climate.

4.2.2   The General Circulation Models

The GCMs are numerical models that simulate the Earth system. Their complexity varies depending on the components of the Earth system that are included. The atmospheric or oceanic models represent only a facet of the entire system, namely the general circulation of the atmosphere or the ocean. Moderns GCM, also known as AOGCMs, tend to incorporate increasingly more processes
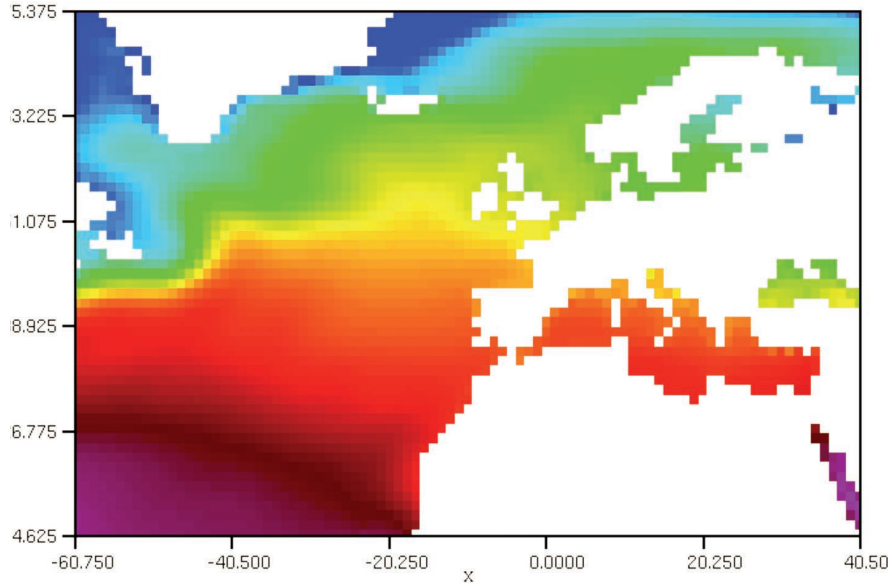
Figure 4.5: *ERA-40 land-sea mask obtained from SST.*
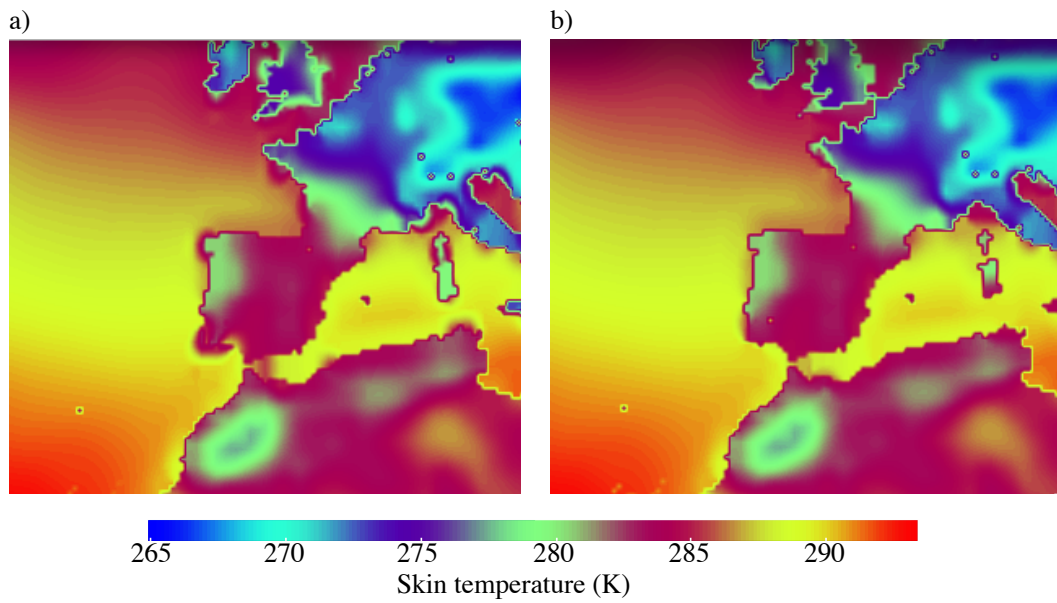
Figure 4.6: *Skin temperature interpolated using (a) the default ERA-40 land-sea mask and (b) the ERA-40 SST-derived land-sea mask.*

martes 24 de mayo de 2011

in their formulation and now most of them represent a coupled system where ocean, atmosphere, land surface, cryosphere and biosphere interact.

GCMs are currently the primary generators of climate change information. The Earth System is forced towards potential future changes (GHGs and aerosols concentration, land use, solar activity) and the climate responses are examined. The GCMs outline the climate evolution of the Earth as a whole and set up the framework where regional models produce high-resolution climate change information. Therefore, they are a cornerstone of dynamical downscaling.

The global models are certainly not perfect and thus their ability to capture climate features over a particular region has to be analyzed. The errors that GCMs might be prone to are inherited by RCMs in dynamical downscaling and hence both the GCM and the RCM performance can be assessed by the examination of the RCM outputs. The only method to examine such a performance is to carry out present climate simulations and compare the estimates with observations. This way, it is possible to delimit the uncertainties associated to future climate projections.

Nonetheless, the fact that WRF shows a good agreement with present climate when driven by a particular GCM does not completely guarantee that future climate will be simulated as adequately. Consequently, it is recommendable that different boundary conditions are used to drive the model, so that different possible evolutions of the climate are studied. This includes not only various GCMs but different emission scenarios as well.

In this Thesis, two global models included in the last IPCC AR4 (Solomon et al., 2007) and widely used by the dynamical downscaling community are employed: The Max Planck Institute ECHAM5/MPI-OM coupled model (Jungclaus et al., 2006; Roeckner et al., 2003) and the CCSM model (Collins et al., 2006) from NCAR. This models were chose on the basis of two main assets: (1) The outputs are available and the required variables to run WRF are provided at a satisfactory frequency and spatial resolution, and (2) they work reasonably well for the IP. The ECHAM5/MPI model is able to correctly capture both temperature and precipitation over the IP. The CCSM model presents some deficiencies in capturing precipitation in this region, but reproduces temperature fields very well (Errasti et al., 2010; Nieto and Rodríguez-Puebla, 2006). In addition, three different emission scenarios from those proposed by the IPCC (SRES scenarios, Nakicenovic et al., 2000). Both the GCMs details in their use as boundary conditions and the emission scenarios are briefly described below.

Max Planck Institute ECHAM5/MPI-OM model

The fifth-generation ECHAM model coupled with the Max Planck Institute Ocean Model (MPI-OM, Marsland et al., 2003) is adopted here[1] and from now on will be referred as simply ECHAM5. The ECHAM5 model is based on the global forecast models developed at the ECMWF. Besides the approximation of the Navier-Stokes equations for the atmosphere, several factors and components of the climate system are considered in the model, such as the atmospheric radiation processes, water cycle, vegetation or orbital variations.

The ECHAM5 model outputs were provided by the Deutches Klimarechen-zentrum (DKRZ) through the CERA portal[2] upon registration. A large number of variables are available of which the following were selected to drive the model: geopotential height (GPH), relative humidity (RELHUM), temperature (STP), zonal wind velocity (U) and meridional wind velocity (V) at 16 vertical levels; and 2m temperature (TEMP2), surface temperature (TSURF), 10m zonal wind velocity (U10), 10m meridional wind velocity (V10), surface pressure (APS), mean sea level pressure (MSLP) and near surface dew point temperature (DEW2) at the lower vertical level[3]. The model has 31 vertical levels of which 17 pressure levels are provided by DRKZ. All levels except for the top 10hPa level were retained to generate the boundary conditions. These vertical levels are located at: 1000, 925, 850, 775, 700, 600, 500, 400, 300, 250, 200, 150, 100, 70, 50 and 30hPA. In the horizontal, ECHAM5 in the version included in the IPCC AR4 has a T63 spectral resolution, which corresponds to an horizontal grid spacing of 1.9°(approximately 210 km in the N-S direction and 150 km in the W-E direction at mid-latitudes).

The original ECHAM5 relative humidity had to be adapted. The relative humidity is stored as parts per unit instead of the usual percent. However, WPS interprets the relative humidity in the traditional way and so ECHAM5 records had to be multiplied by 100, otherwise WRF is forced towards very low humidity values producing unrealistic results.

Moreover, the ECHAM5 dataset include soil temperature at five layers but lacks soil moisture, which is also necessary to run the Noah LSM. Therefore, a detour had to be made to overcome this obstacle. The Noah Land Surface

---

[1]There are available model results from different runs that basically differ in the forcing and the initial conditions. In this Thesis, the simulation that incorporates all forcing (anthropogenic plus natural) and starting from the pre-industrial control run was selected (run1_all) to simulate present conditions.

[2]http://cera-www.dkrz.de/CERA/

[3]The acronyms in bracket correspond to those used within the ECHAM5 model.

Model (LSM) just needs this information in first time step and after some slight modifications of the WPS code, it was possible to create the boundary conditions providing only the initial state of the soil. The procedure to obtain the initial conditions was that of retrieving both soil moisture and temperature from ERA-40 data and create a sort of climatological state of the soil. For example, if the model run starts on June 1st at 00h, a 30-year average (1970-1999) of the ERA-40 soil variables during May and June was calculated and used as initial conditions. Then the model runs for a several-month period to 'forget' about these initial conditions and permit the LSM to reach its own equilibrium. Only after the spin-up period of several months the results are retained.

The NCAR CCSM.0 model

The Community Climate System Model version 3 (CCSM) is a coupled climate model with components representing the atmosphere, ocean, sea ice and land surface connected by a flux coupler (Collins et al., 2006). The model was run at different horizontal resolutions but the version selected here has a T85 spectral resolution, which is equal to about 1.4° resolution (approximately 110 km in the N-S direction and 150 km in the W-E direction at mid-latitudes). The vertical dimension is divided into 26 levels of which 17 (1000, 925, 850, 700, 600, 500, 400, 300, 250, 200, 150, 100, 70, 50, 30, 20 and 10hPa) were used to generate the boundary conditions. The variables obtained at each of these levels are temperature (TT), zonal wind velocity (UU), meridional wind velocity (VV), relative humidity (RH) and geopotential height (GHT). Additionally, the variables sea ice (SEAICE), surface pressure (PSFC), mean sea-level pressure (PMSL), temperature (TT), zonal wind velocity (UU), meridional wind velocity (VV), relative humidity (RH), skin temperature (SKINTEMP) and sea surface temperature (SST) were defined at the lowest level[1]. As for ECHAM5, the CCMS3 lacks soil variables that are required to run the Noah LSM. Therefore the same methodology mentioned for ECHAM5 to generate the initial soil conditions was followed here.

The model outputs[2] are provided by the Earth System Grid (ESG) in their website[3] after registration.

---

[1]The acronyms in bracket correspond to those used within the CCSM model.

[2]As for ECHAM5, outputs from several runs are available for CCSM. For present climate simulations the *b30.030e* run was chosen. Whereas for future climate simulations the *b30.040e*, *b30.041e* and *b30.042e* runs were opted for.

[3]www.earthsystemgrid.org

The emissions scenarios from SRES

Three different emission scenarios from SRES (Nakicenovic et al., 2000) were selected aimed at covering a wide range of possible future evolutions of the human activity that might influence the climate. The SRES scenarios are assumptions about possible future population growth, economic activity, energy resources, society developments and technological advances that might have a substantial impact on climate. It was already mentioned in Sec. 2.1.2 that GHG emissions are the first element in the causal chain of climate change and thus those factors that directly affect the GHG emissions can be regarded as prime drivers of global warming. It is not among the objectives of this Thesis to explore the uncertainties associated to future scenarios, but they are such a paramount component of climate change studies that a brief description of them is essential.

The SRES scenarios are classified into four families depending on the development pathways of the aforementioned factors. Figure 4.7 schematically illustrates the classification of scenarios. Two main parameters are used to define the families: (1) the global vs. regional development that generates an homogeneous or heterogeneous world, and (2) the evolution towards a more economical or environmental development. These four families are subdivided into different scenarios that amount for a total of 40 different possible situations.
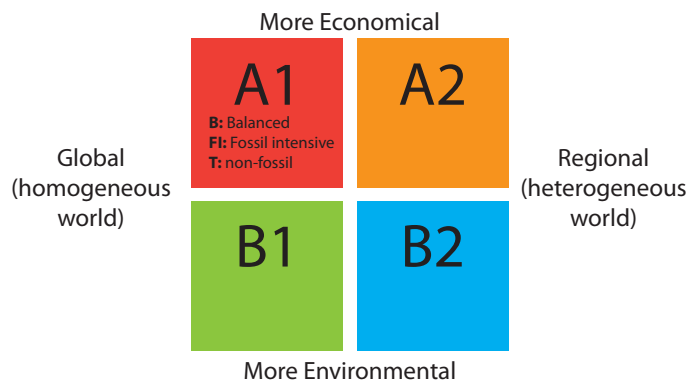
Figure 4.7: *Schematic representation of the 4 SRES scenarios families with the criteria to classify them. The global and regional character refers to the evolution towards an homogeneous or heterogeneous world, whereas the environmental or economical nature indicates the direction of developments. A subset of A2 family is also shown and includes three different divisions according to the energy sources (A1B, A1FI and A1T). From IPCC AR4.*

72   4. The WRF configuration
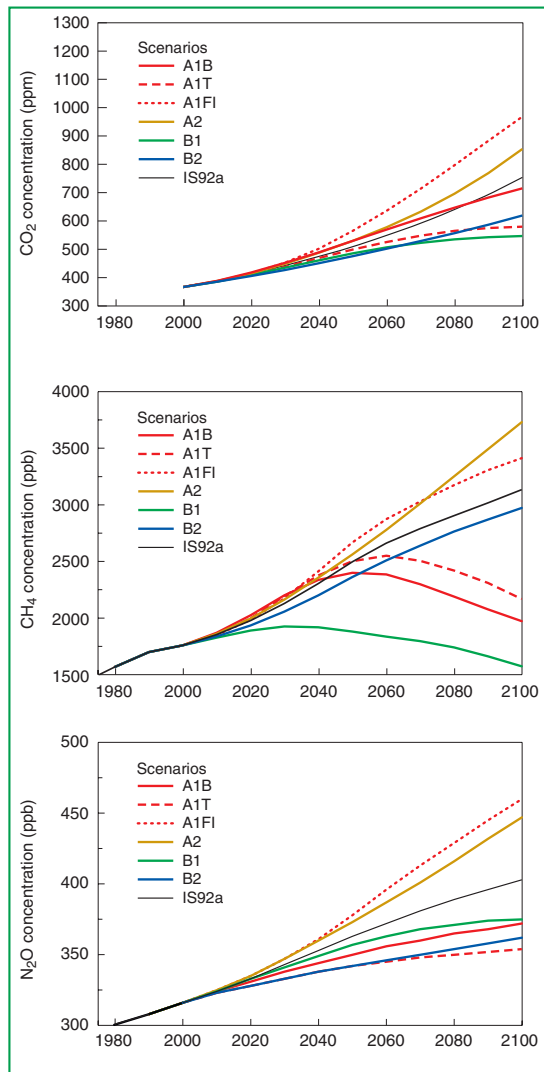
Figure 4.8: *Evolution of the atmospheric concentration of CO_2, CH_4 and N_2O during the 21st Century according to six different SRES scenarios and the old IS92a scenario (Leggett et al., 1992). From IPCC, 2001.*

Figure 18: Atmospheric concentrations of CO_2, CH_4 and N_2O resulting from the six SRES scenarios and from the IS92a scenario computed with current methodology. [Based on Figures 3.12 and 4.14]

The IPCC AR4 focuses on six possible scenarios (B1, A1T, B2, A1B, A2, and A1FI) and devotes particular attention to three of them (B1, A1B and A2). The emissions associated to each scenario are translated into GHG concentrations that in turn are interpreted as a radiative forcing. In order to provide a picture of these six scenarios, the evolution of GHG concentration in the atmosphere all through the 21st Century is shown in Figure 4.8. The corresponding radiative forcings from 1850 to 2100 are depicted in 4.9a and the anthropogenic global surface temperature changes are shown in Figure 4.9b for the six SRES scenarios. Some additional scenarios from previous IPCC reports (Leggett et al., 1992) are also included in Figure 4.9.

In line with the IPCC AR4, the scenarios selected in this study are B1, A1B, and A2. These scenarios are not only those that IPCC AR4 explore in detail, but also the most widespread in the regional climate modeling community, and therefore, their selection makes possible to compare our results with other regional climate projections. Furthermore, this set of scenarios cover a range of future possibilities for the end of this century: a low-emission (B1), an intermediate-emission (A1B) and a high-emission (A2) scenarios.

The B1 scenario describes a future world of global population that peaks in the mid-century and decreases thereafter. The economy presents rapid changes towards a service and information economy, with reductions in material intensity and the introduction of clean and resource-efficient technologies.

Projections of Future Climate Change

Figure 4.9: *(a) Evolution of the radiative forcing under six different SRES scenarios followed by radiative forcing for the model ensemble averages of the anthropogenic global mean temperature change for the different scenarios. From IPCC, 2001.*

Figure 9.13: Simple model results: (a) Estimated historical anthropogenic radiative forcing, followed by radiative forcing for the four illustrative SRES marker scenarios and for two additional scenarios from the A1 family illustrating different energy technology options. The blue shading shows the envelope of forcing that encompasses the full set of thirty-five SRES scenarios. The method of calculation closely follows Chapter 6 except where explained in the text. The values are based on the radiative forcing for a doubling of CO_2 from seven AOGCMs as given in Appendix 9.1, Table 9.A1. The IS92a, IS92c and IS92e forcing is also shown following the same method of calculation. (b) Historical anthropogenic global mean temperature change and future changes for the six illustrative SRES scenarios using

mission

nean tempera-
ES emissions
Nakićenović *et*
ted range of
se of several
ered in these
porate all the
sidered. These
1 and B2 and
y representing
T (see Section
lso shown for
9.3.1.3 some
the four draft
rature change
rios, a simple
OGCM results
The tuning of
CM results is
niCAM (Mini
west National
ssions for the
ć *et al.*, 2000).
odelling team

nthropogenic
.12, tabulated
ćenović *et al.*
. It is evident
missions. Note
emissions for
cenario.
RES emission
here follows
, with some
he forcing for
en by Wigley

The A1B scenario belongs to the A1 family. The A1 family describes a world with the same population trajectory as in the B1 family, but with very rapid economic growth. It also predicts a rapid introduction of new and more efficient technologies. In terms of global distribution, it describes a substantial reduction over time in regional differences a convergence among regions of the globe. Regarding the energy sources, the A1B scenario corresponds to a balance across al sources.

The A2 scenario describes a very heterogeneous world with preservation of local identities and self-reliance. Global population increases continuously, economic development is regionally oriented and economic growth and technological change are more fragmented and slower than in the other storylines.

The description of the scenarios is obtained from IPCC 2007. For further details on the emission scenarios the interested reader is referred to the original report (SRES, Nakicenovic et al., 2000).

4.2.3   Spectral nudging and buffer zone

In addition to the driving data sources, other variables concerning the boundary data are configurable in the WRF model.

In order to resolve the ill-posedness of the boundary conditions specification (see Sec. 2.1.1) and reduce the impact of the domain design in the results, the spectral nudging is proposed. Spectral nudging adjusts the RCM to keep the large scale consistent with the driving data. The use of spectral nudging is still somehow controversial and many studies have discussed its value (Alexandru et al., 2008; Heikkilä et al., 2010; Míguez-Macho et al., 2004; Radu et al., 2008; Zahn et al., 2008). Most of them agree that although spectral nudging might be beneficial, the adjusted scales must be chosen carefully because too strong nudging could hamper the development of the model internal variability. That being the case, a relatively weak spectral nudging is adopted over the coarser domain of our simulations. In particular, the wavenumber chosen was 3, which corresponds to adjust only waves larger than 1300 km. The spectral nudging switched off in the PBL and only the levels above are adjusted with a frequency of 24 h. All variables (U, V, T and PH –geopotential perturbation–) are nudged except for moisture. Humidity is not nudged following Míguez-Macho et al. (2005) because its spatial gradients can be very pronounced and thus might be missed by coarse resolution reanalyses.

Aside from the spectral nudging, the problems derived from the specification

of the boundaries are also prevented using a buffer zone instead of fixing the boundary conditions in a 'hard' manner. The model outputs are relaxed towards the boundaries over the buffer zone to damp any possible discrepancies between the model and the driving data. Here the boundaries are fixed at the outer grid points and the buffer zone extends 5 grid points.

The boundary conditions are updated with a frequency of 6 hours and they are linearly interpolated in time to feed the model at intermediate time steps. Denis et al. (2003) found that a 6-hour updating frequency was enough to drive a run with domain characteristics (45-km resolution, 100 by 100 grid points) that were similar to our coarser domain. Higher frequencies did not seem to provide further benefits and lower frequencies did not capture accurately the systems trajectories. On top of that, most reanalysis and GCMs are only available at a 6-hour frequency and thus the WRF boundary conditions were updated with that frequency.

4.3   Time configuration and spin-up

In order to allow the model reach an equilibrium between the external forcing and the internal dynamics, a 7-month spin-up is adopted. Although previous studies (Fernández, 2004; Giorgi and Mearns, 1999) have proven that initial values have minor effects on results after approximately one week , a longer spin-up period was chosen here to ensure that not only atmospheric fields become reasonably independent of the initial condition but soil variables as well, which normally require several months to do so. Bearing in mind that soil information in GCM-driven simulations is obtained from a surrogate created out of ERA-40, the selection of a several-month spin-up is even more important to remove the initial condition influence on the model results.

This study analyzes simulations that span 10 and 30 years. The shorter simulations are employed to determine an appropriate configuration of the model, whereas the 30-year ones (climate runs) are used to describe present and future climate. Both simulations include the 7-month spin-up, however, the climate runs are design differently to optimize computational resources. In principle, the simulations should be run continuously to preserve the consistence of the integrations in time. However, this implies that a given year can only be simulated if the previous one has already been completed. This approach is rather inefficient from a computational point of view. An alternative procedure is here adopted to reduce the time required to complete the 30-simulations and consists in splitting

the climate runs into decadal simulations that are performed simultaneously.

Each decadal simulation is then started using a 7-month spin-up to ensure independency from initial conditions and reduce the impact of model restarting. Figure 4.10 illustrates the design of the simulations in terms of time configuration for the climate runs. Additionally, Figure 4.11 illustrates the surface and soil temperature provided by two different runs: (1) A simulation that was started 10 years before and thus it is considered as 'continuous', and (2) a simulation that was started at that particular moment. It can be observed that after the 7-month period they both yield nearly identical values for the surface temperature and even the very deep soil temperature (100-200 cm) show a good agreement. This figure indicates that the selected spin-up length is adequate to reach internal equilibrium even in terms of soil variables[1], but also that the strategy to split the simulations and efficiently use the computational resources has minor effects on results.

Figure 4.10: *Time diagram of the 30-year integrations. The period is divided into three 10-years simulations with a 7-month spin-up (grey). The decadal runs are then integrated simultaneously. This example refers to present climate simulations. Future climate simulations are analogous but for the period 2070-2099.*

4.4   Other parameters

Besides the aforementioned parameters, many other options are provided by WRF and are briefly commented here.

- The equations of the atmosphere are discretized in both space and time. The temporal discretization is determined by the time step, which is an important factor to reproduce the evolution of the atmosphere, especially

---

[1]The atmospheric fields are not shown, but they usually require much shorter spin-ups to reach the dynamical equilibrium
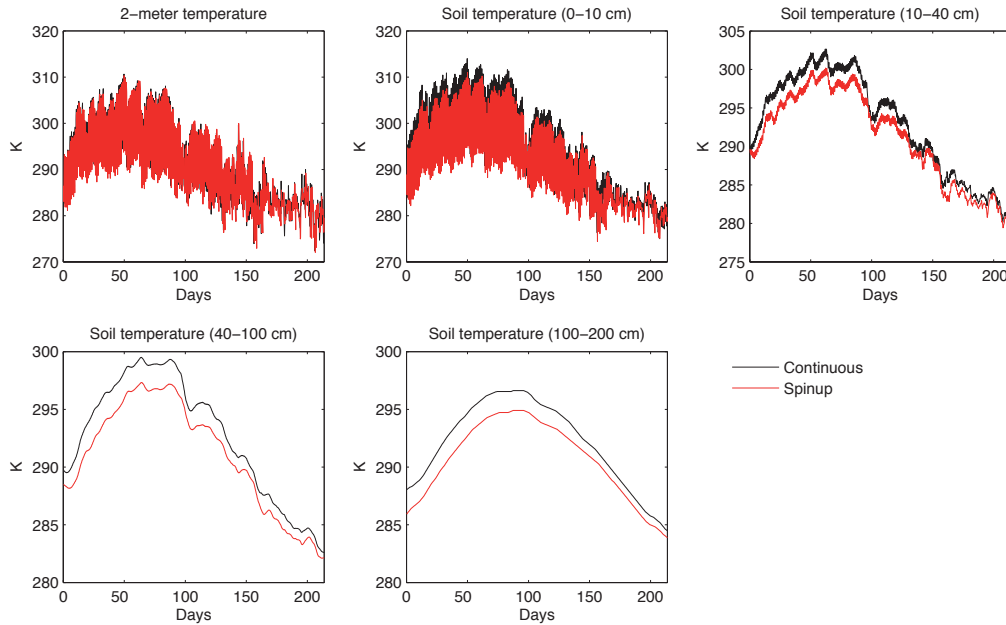
Figure 4.11: *Surface and soil temperatures obtained from a continuous run (black) and the restarted run (red) during the spin-up period. This is a random point in the IP located at 39.14° N-3.31° W*

when it changes rapidly. The recommended time step for the selected horizontal resolution[1] is here employed and was 180 and 60 s in the coarser and finer domains respectively.

- The WRF formulation is design to run the model in parallel computers. The simulations of this study were entirely performed in the Sun Fire X2200/X4600 Cluster (UGRGRID) with 1264 cores. All simulations were configured to use 64 processors.

- The model outputs were stored at a 6-hour frequency (00, 06, 12 and 18 h). In a supplementary file, precipitation is stored at 7 h on a daily basis to compare with observations.

- The CLWRF (Fita and Fernández, 2010) version of WRF 3.1.1 was here used. In CLWRF, the concentration of some gases (CO_2, N_2O, CH_4, CFC-11 and CFC-12) is modified according to the emission scenario and the information is passed to the CAM radiation model instead of using the prescribed A1B concentrations. Additionally, it enables a temperature check at every time step to calculate the Tmax and Tmin at daily timescales.

---

[1]The recommended time step is, in seconds, 6 times the horizontal resolution in km.

One of the major strengths of WRF concerns the parameterizations. A wide range of physics options is available in WRF and makes it extremely flexible in this respect. As a result, WRF sensitivity to parameterization schemes must be address and the model has to be tuned for the particular purpose of the survey. The physics choice is of such importance that a separate Chapter (5) is dedicated to that subject in order to find a suitable combination of schemes for this study.

Chapter 5

WRF parameterization tests

> Big whirls have little whirls, that feed on their
> velocity; And little whirls have lesser whirls, and so
> on to viscosity.

<div align="right">Lewis Fry Richardson</div>

This chapter continues the issue of WRF configuration that was previously raised. Although most of the parameters concerning WRF configuration were reviewed in Chapter 4, there is still an aspect that remained unaddressed and requires special attention: the physics parameterizations. Physics parameterizations comprise all processes occurring at scales that remain unresolved by the model discretized equations. One of the major strengths of WRF is precisely the wide range of available parameterization options that makes possible to adapt the model to specific conditions. Nevertheless, the model results using different combinations of physics packages might vary considerably and thus the performance of various configurations has to be explored to choose an appropriate one for our purposes. This Chapter is devoted to analyze the model precipitation and temperature estimates using different parameterizations in order to assess their validity and select a suitable configuration[1].

5.1 Sensitivity tests for climate studies

A large number of studies have dealt with the selection of an appropriate configuration of WRF physics for varying conditions and applications (Deb et al.,

---

[1]The results presented in this Chapter are part of a study published in *Journal of Climate* (Argüeso et al., 2011)

2008; Gallus Jr and Bresch, 2006; Hong et al., 2009; Hu et al., 2010; Jankov et al., 2005; Kain et al., 2006; Kwun et al., 2009; Li and Pu, 2009; Nolan et al., 2009; Ruiz et al., 2010), but due to computational costs, little effort has been devoted to this topic for long-term runs and analyzing different parameterized processes (Bukovsky and Karoly, 2009). Indeed, regional climate modeling has too often disregarded the issue of an appropriate model configuration specifically suited for the region and the time scale under survey.

Surveys on the model response to different parameterizations have usually been performed using few-day runs and thus the conclusions are restricted to that particular situation. For example, if the model is examined for the summer months, there is no saying about the model performance during the winter because the processes that take place in these seasons are completely different. In order to determine an adequate model configuration from a climate point of view, that is to say a model configuration that compares well with the observations in general and not only under certain atmospheric conditions, the analysis simulations that span several years is crucial.

Despite the fact that the choice of the parameterizations is too often made with no physical foundations and using the default configuration, it might have a dramatic impact on the model results. It is worth mentioning to this respect that most of the physics schemes are semi-empirical approximations that have been tuned to very particular environments and they have rarely been evaluated in complex terrain or under highly variable conditions, as it happens with the PBL (Stensrud, 2007). Hence, the assumption that the combination of schemes might not have a substantial effect on the results is at least dangerous, especially over regions where subgrid scale processes play an important role. That is the case of the IP and consequently, the evaluation of different WRF schemes represents a paramount stage in the generation of reliable future projections.

Ideally, all possible combinations of physics options should be tested because the accuracy of the model cannot be uniquely attributed to a single parameterization but rather to the combination of them, since feedbacks are usually as important as the schemes themselves. However, bearing in mind the number of possibilities, this still remains an utopia due to current computational limitations. An alternative approach is that of choosing a number of schemes that are different in formulation and complexity, and combine them to generate a representative sample.

Table 5.1: *Combination of parameterization schemes for sensitivity tests*

Cumulus	PBL	Microphysics	ID
BMJ	MYJ	WSM3	**BM3**
BMJ	MYJ	Thompson et al.	**BMT**
BMJ	ACM2	WSM3	**BA3**
BMJ	ACM2	Thompson et al.	**BAT**
BMJ	YSU	WSM3	**BY3**
BMJ	YSU	Thompson et al.	**BYT**
KF	MYJ	WSM3	**KM3**
KF	MYJ	Thompson et al.	**KMT**

5.1.1 Description of the simulations

Eight combinations of physics options are here analyzed in detail (Table 5.1). The eight simulations were identical except for the parameterizations. As already mentioned, the physics packages were chosen with the aim to include options with enough differences in their formulation as to consider the set of simulations to be a representative sample. The land surface model is here fixed to Noah-LSM and the radiation to CAM3.0 (see Sec. 2.3). Besides the combinations here presented, additional parameterization were tested in the preliminary tests but they were discarded at the first stages of the study because they either produced very similar results to other simulations (WRF single moment 5-class) or were clearly outperformed by other schemes (Grell 3D cumulus and five-layer soil model).

The model outputs are compared with the *SubClim* dataset to determine which configuration is more appropriate. The *SubClim* dataset presents two advantages that made us opt for it to conduct this analysis, (1) the inclusion of both temperature extremes and precipitation, and (2) the remarkable density of stations[1]. The density of the observational network is actually a key factor that enables a thoroughly evaluation of the parameterizations. In return, the examination is performed only over the area covered by the observational dataset (Andalusia - southern Spain).

Although it might be argued that this analysis cannot be projected to the entire IP, an examination of the model performance over southern Spain can be regarded as a fair approximation. Southern Spain is far from being an homoge-

---

[1] The *SubClim* dataset was actually the only available dataset that had an acceptable density when these simulations were performed. The Spain02 dataset became available only in the end of 2010.

neous region and it contains very different climate regimes as can be observed in the Spain02 regionalizations (Figs. 3.7 and 3.8). For instance, southern Spain includes a wide range of precipitation regimes (from one of Spanish wettest in *Grazalema* to the driest in *Almería*) and most of the processes producing precipitation in the IP such as the Atlantic frontal systems, the orographic rainfall or the typically Mediterranean convective phenomena. The temperature conditions are also varied because there are stations at very different elevations spread all over Andalusia (7 out of the 8 temperature regions of Spain02 have representation in southern Spain). Fernández et al. (2007) found that southern Spain presents a noteworthy diversity in terms of the optimal physics configuration. Hence, it can be affirmed that a physics configuration that compares well with the *SubClim* dataset performs adequately under a broad variety of conditions.
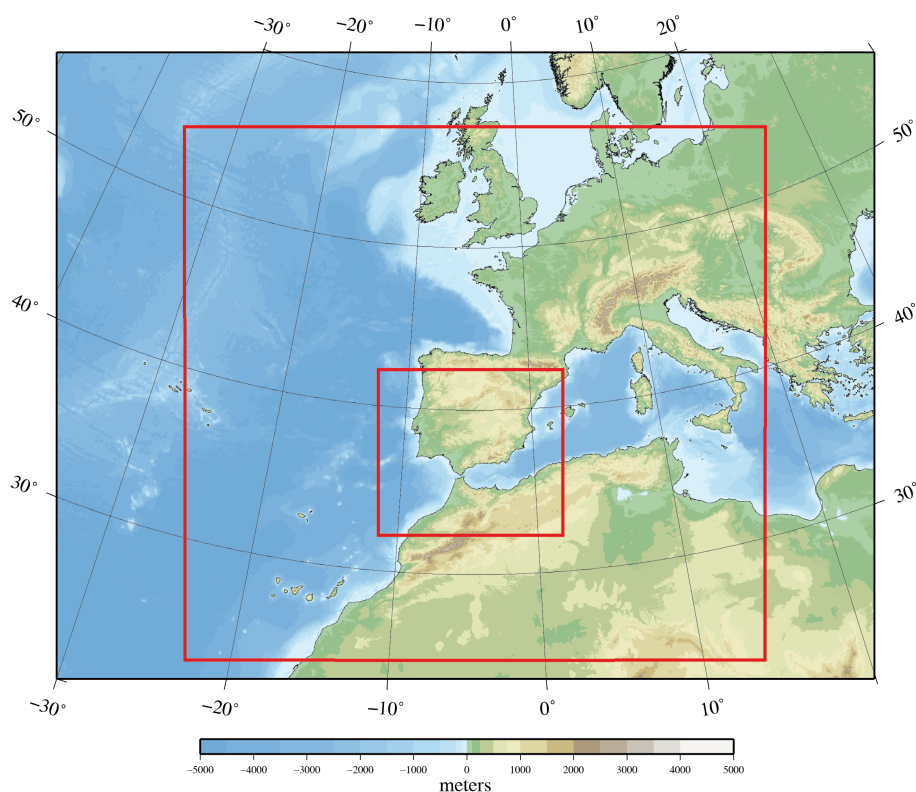
Figure 5.1: *The WRF domains configuration for the parameterization tests simulations. The red lines delimit the coarser (30-km) and the finer (10-km) domains.*

The simulations completed to conduct this examination were design in accordance with the description of the previous chapter with the exception that the

nested domain covers a slightly smaller region. The coarser domain is exactly the same (Fig. 5.1). The aim of these simulations is to represent the present climate as accurately as possible and thus they were driven by ERA-40 reanalysis. The eight runs span a 10-year period (1990-1999), which constitutes a sufficiently long interval to capture the main climate features of the region at affordable computational costs. The period was selected to coincide with the time lapse covered by the *SubClim* dataset. As described in the Section 4.3, a 7-month spin-up was selected and thus the simulations actually start on June 1st 1989, although only the results from January 1st 1990 are retained.

5.1.2   Description of the analysis

The eight model configurations are evaluated in terms of precipitation, Tmax and Tmin. The analysis is carried out at different time scales to assess the model capability to capture mean values and high-order statistics. Most of the comparisons are conducted region by region (Fig. 3.6) in order to overcome the aforementioned *representation error*, except for some parameters that were calculated station by station to examine their spatial distribution. Whenever the comparison is directly performed with site-specific measurements, the intention is not to draw conclusions at particular locations but to provide an overview of the broad spatial distribution of the model capabilities. This comparison provides very helpful information to physically interpret the error sources and identify possible spatial differences between the configurations, but it must be observed carefully because it is only a qualitative picture of the model performance.

The examination begins with analysis of the annual monthly cycle that is calculated at every region. Each station is represented in WRF by the nearest grid point and the grid points are grouped into the same regions that were obtained for the observations. The model outputs and observations are then spatially averaged over the regions to generate the annual cycle that corresponds to each region. The appropriate simulation of the annual cycle is essential because it is without doubt the prime characteristic that describes the local climate. The study of the annual cycle also makes possible to highlight the seasons when the largest differences between WRF and observations occurs and maybe clarify which processes are more troublesome to simulate.

Besides the annual cycle, the correlation, root-mean-squared error (RMSE) and mean absolute error (MAE) are computed between the model and the observational temperature time series at monthly scales. By contrast, the correlation,

relative RMSE and bias are analyzed for the precipitation ones. Different parameters are calculated for each variable in accordance with the values they take. A good agreement between simulated and observed monthly time series indicates that the model is able to capture inter-annual variability and the timing.

Coarse resolution models (GCMs) already provide an acceptable estimation of the monthly values when the large scale has a strong influence on them. Indeed, the major benefit of dynamical downscaling is the spatial resolution refinement, which has a noticeable impact on the distribution and magnitude of extremes (Bell et al., 2004; Frei et al., 2003; Giorgi, 2006b). The arise of regional climate models was precisely motivated by the necessity to reproduce the climate at higher detail and capture events that go unnoticed to GCMs. Therefore, it is crucial to evaluate the model ability in this respect. To this purpose different percentiles are calculated to ascertain whether WRF is able to represent the observed probability distribution function (PDF) of events. The evaluation in terms of the PDF completely disregards the timing of particular events, which is a great advantage if the model performance is to be assessed from a climate point of view. In climate studies, we are not interested in capturing the intensity and timing of a given event, but rather the frequency of particular events during a long period.

The parameters described above are also calculated for ERA-40 reanalysis to stress the improvement introduced by WRF with respect to the boundary-condition data.

A detailed description of how the statistical parameters used in this Thesis are calculated is provided in Appendix B.

5.2   Precipitation

Precipitation is known to be one of the most complicated variables to simulate because it is affected by several processes, of which many take place at subgrid scales. Therefore, it can be expected that precipitation results are highly dependent on the chosen parameterizations.

5.2.1   Monthly values of precipitation

Monthly time series

Accumulated monthly precipitation was calculated for every station and its nearest grid point, and then spatially averaged to obtain the monthly series for

each region. The correlation coefficient, relative RMSE and bias between WRF and observational series are shown in Figure 5.2. The same parameters are shown for ERA-40 so that the improvement associated with WRF can be evaluated. A clear distinction is evident between the eastern and the rest of Andalusia. In fact, all three parameters values are within a satisfactory range in all regions except for the E division. A remarkable monthly correlation is attained in most of the cases (0.90-1.00), but moderate values are obtained in the E region (0.65-0.76) and for some simulations that employed the KF cumulus scheme over regions N and S.
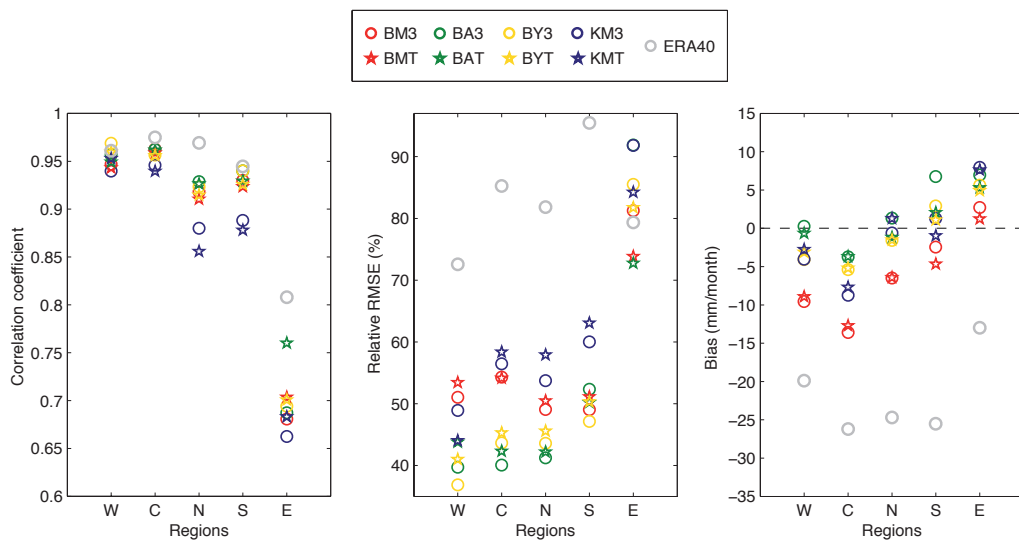
Figure 5.2: *Correlation coefficient, relative RMSE and bias calculated for WRF (colors) and ERA-40 (grey) monthly precipitation with respect to observations in the various regions.*

As the correlation, the relative RMSE is acceptable for every region, excluding the East, where it reaches values as large as 92% of the average monthly precipitation. On the other hand, the best combination for each of the other regions never exceeds 50% of the average monthly rainfall.

The differences between WRF and observed monthly mean precipitation displayed in terms of the bias manifest a tendency to underestimate total precipitation in the western regions (W and C) and overestimate in the east (regions E and S). This might be due to a misrepresentation of the orography because the narrow mountain ranges are flattened by the model resolution and thus the associated 'rain shadow' might be weakened. This results in a precipitation dis-

placement towards the East, with too many Atlantic fronts reaching the eastern areas creating a positive rainfall bias accompanied by negative biases in central Andalusia. Even though this seems to be the main factor that explains the biases distribution, the Mediterranean processes might not be accurately reproduced by the model and their influence should not be neglected.

Concerning WRF performance with respect to its boundary conditions, monthly ERA-40 time series are higher correlated with observations than WRF (except for W region) whereas both the bias and the RMSE are substantially worse. Actually, a clear improvement is attained with WRF, reducing by about half the error corresponding to ERA-40 in most of the regions. The E region embodies again the exception, where although the bias is evidently reduced in absolute value and has opposite sign, relative RMSE values are similar for both the model results and reanalysis. This feature, plus the low correlation, indicates that WRF might not be able to capture the timing as it would be desired, but it is able to noticeably refine reanalysis estimations of total precipitation over the E region.

The E region, and more generally the Mediterranean coast, is widely know for its singularity regarding precipitation since the marked convective nature of rain in semi-arid climates complicates the accurate description of total precipitation amount and location (Amengual et al., 2007). Indeed, not only WRF but also ERA40 shows a pronounced difference in correlation for the E region in comparison with other areas, which is reasonable bearing in mind that precipitation is a pure model result in ERA-40.

It might be surprising that ERA-40 is characterized by a systematic underestimation, whereas the WRF tendency is not so clear. However, it should be noted that the boundary conditions are specified only at the borders (except for the very large waves that are adjusted with spectral nudging). Hence, WRF is able to develop its own mesoscale dynamics which can produce precipitation regimes that vary from that prescribed by ERA-40, not only regarding distribution but the overall precipitation amounts as well. Therefore, it is here evidenced that even if the regional model is prone to partly inherit errors from the boundary conditions, it is also capable of reducing them and producing more accurate results in spite of the boundary data imperfections.

The analysis of the monthly time series led us to conclude that the simulations using BMJ cumulus scheme tend to perform generally better, particularly those with the ACM2 and YSU PBL schemes. The configurations that use MYJ PBL always generate drier conditions, whereas those using ACM2 provides wetter ones

in general. The WRF biases should be interpreted together with the ERA-40 biases because otherwise they might be misleading. For example, in the E region, it could seem that MYJ scheme produce better results but considering the ERA-40 bias with respect to other regions, this statement is not that obvious. Altogether, the explored parameters are not sufficient by themselves to single out an optimal parameterization and thus additional features must be regarded.

Annual cycle

The annual cycle with monthly means was also calculated for the ten-year period in order to examine the WRF performance in different seasons. The WRF model broadly captures the annual cycle (Fig. 5.3), including features that are not represented by the boundary conditions. For instance, the November relative minimum is missed in the ERA-40 annual cycle but reproduced by WRF to varying degrees. Andalusian precipitation is characterized by a summer minimum in August with basically no rain events and a maximum during December and January, which are also well represented by WRF.

Conversely, spring rainfall seems to be systematically exaggerated by WRF in regions N and S, whereas autumn precipitation is underestimated in most of the regions. Precipitation in the eastern region is remarkably overestimated, primarily in April May and to a lesser extent, in September; the latter can be attributed to an excess of soil moisture due to a positive deviation in August precipitation that might enhance evaporation and thus convective rainfall after the summer. In fact, summer deviations in precipitation only take place in the E region, where September deviations are especially marked. On the other hand, spring errors cannot be univocally attributed to a single source and different causes might contribute to these deviations (i.e., a misrepresentation of topography, an enhancement of land-surface thermal contrast or a deficient simulation of Mediterranean cyclogenesis that produce a large fraction of the East coast precipitation). This is actually not a WRF-exclusive feature but a common deficiency in RCMs over the IP (Herrera et al., 2010b).

Despite the high monthly correlations for ERA-40 precipitation, Figure 5.3 shows that the ERA-40 annual cycle is too flat and WRF actually provides a sharper depiction of it. This indicates that WRF is introducing interesting details in terms of monthly precipitation for climate studies. The combination BMJ-ACM2 (BA3 and BAT) appears to be the most accurate in reproducing the annual cycle, especially in regions C and W, where WRF estimates almost overlap
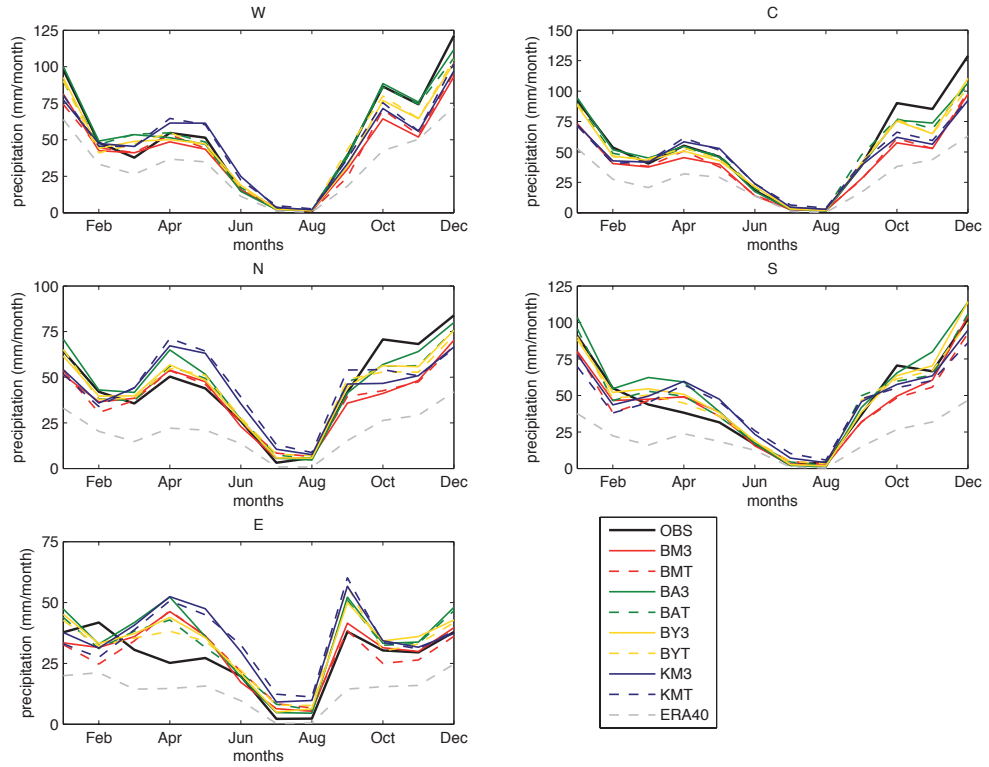
Figure 5.3: *Annual cycle of monthly precipitation for the different regions: observations (black), ERA-40 reanalysis data (grey dashed) and WRF simulations (colors).*

the observational curve. However, these configurations substantially overestimate precipitation in certain months over N and E regions.

5.2.2   Daily values of precipitation

The daily precipitation is examined through the percentiles (50th, 60th, 70th, 75th, 80th, 90th, 95th and 99th) of daily events that are computed taking only into account the rainy days defined by a 0.1mm/day threshold[1]. The daily percentiles are calculated considering all the events at all the stations within a region. To illustrate the WRF and ERA-40 percentiles with respect to the observed ones, a Q-Q plot is employed (Fig. 5.4), which allows for comparison of the PDF shapes.

---

[1]This threshold is adopted in accordance with observations that only register precipitation when it exceeds this value. Days when rain occurs and take values below this threshold are considered as dry days.

The Q-Q plot shows the simulated percentiles versus the observed ones with a line representing a perfect performance and delimiting over- and underestimation.
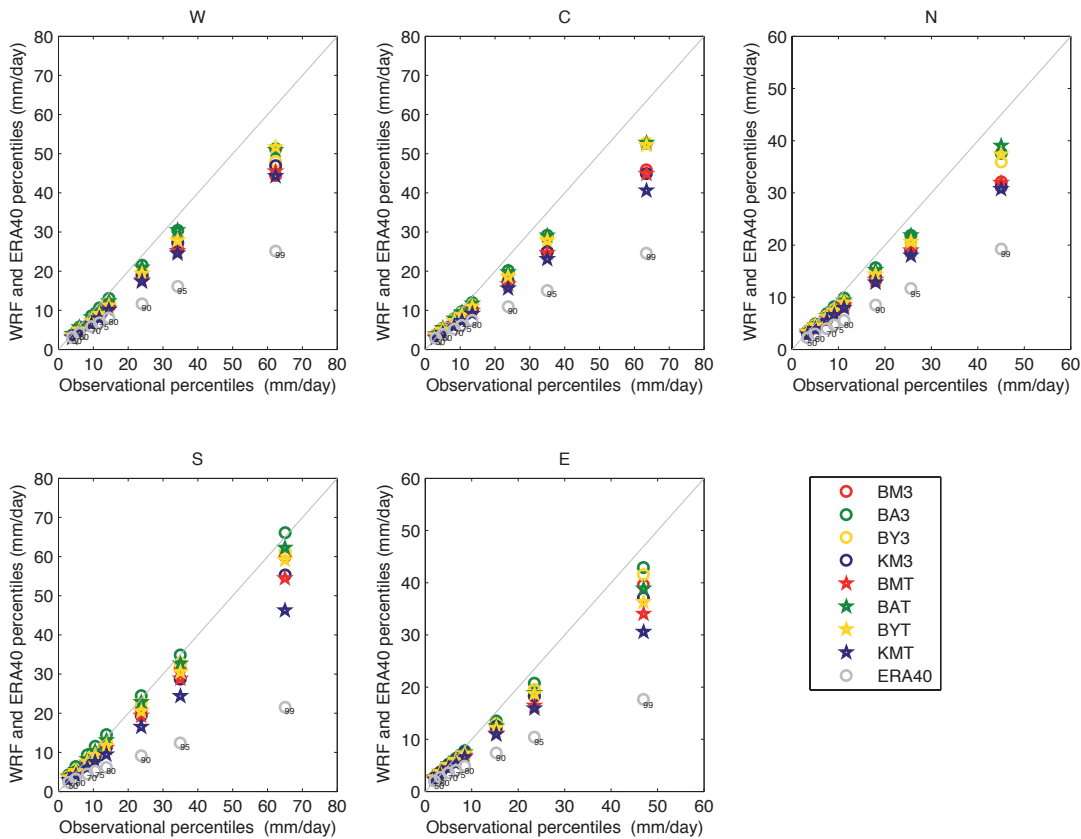
Figure 5.4: *Daily precipitation percentiles simulated by WRF (colors) and ERA40 reanalysis (grey) vs. observational percentiles for the different regions. The grey line indicates a perfect description of the Probability Distribution Function.*

In all five regions identified for precipitation, WRF tends to underestimate rainfall extremes, with the exception of the S region, where the BA3 combination captures remarkably well all the percentiles calculated, with a slight overestimation. Overall, this configuration provides the most accurate results yielding values within 10% of the magnitude of the observed events for even the most extreme conditions (99th percentile). Some other physics combinations (BY3, BAT and BYT) perform similarly or even slightly better for certain areas or thresholds.

It should be stressed that the cumulus parameterization seems to have a noticeable influence in describing the extremes, whereas microphysics appear to have

a minor impact on this climate feature with no superiority among the schemes, apart from WSM3 that produces slightly better results in S and E regions. This could be expected considering that most extreme events in this area have their origin in very strong vertical motions, and thus processes described by cumulus packages. Regarding PBL schemes, both the ACM2 and the YSU packages supply similar results, with minimal differences in favor of ACM2.

A clear enhancement in characterizing extremes has already been revealed as one of the main advantages of dynamical downscaling (Beniston et al., 2007; Fowler et al., 2005; Rosenberg et al., 2010; Sánchez et al., 2004) and indeed a notable improvement is achieved with WRF in terms of percentiles. Despite the undeniable effect of spatial resolution, the dependence of WRF results upon the different physics suggests that parameterizations also play an important role in reproducing precipitation extreme events.

5.2.3   Spatial distribution of precipitation

Besides WRF evaluation using regionalization, an analysis was also conducted station by station, even though it should be only interpreted qualitatively. By means of this analysis, orographic impacts and mesoscale dynamic effects on the modeled climate features can be explored. Rather than the WRF capabilities at individual stations, which might be affected by the *representation error*, the aim of this comparison is to depict the spatial patterns of the model accuracy. Figure 5.5 displays the spatial distribution of the correlation coefficient of monthly precipitation, the difference of total annual rainfall and the 95th percentile of daily precipitation for BA3 (a) and BY3 (b) simulations, and ERA40 (c). These two simulations were selected as a sample to illustrate the spatial distribution because the patterns were very similar for all the configurations. Additionally, the 95th percentile and the total annual precipitation obtained for the observations are also shown as a frame of reference (d).

Correlations show an evident zonal gradient with higher values in the western part (0.90-1.00) decreasing to the East with values of about 0.30-0.40 at certain stations. Annual differences in precipitation give an idea of the areas where rainfall is generally over- or underestimated. It is worth mentioning that most of the stations in the *Guadalquivir* river basin (regions W and C) presents deviations lower than 12% in the total annual precipitation (grey colors). Figure 5.5 evidences what was suggested before about the precipitation shift eastward as a consequence of unresolved topography features. A negative difference is thus

located in the western part because topography was smoothed and precipitation not induced sufficiently, whereas a positive deviation is found in the easternmost areas, where the highest mountains force the precipitation that did not fall before.

The spatial distribution of the 95th percentile for daily precipitation is clearly an improvement over ERA-40, which only resolves a broad gradient towards lower values in the east. In fact, WRF is able to largely capture topographic effects on extremes, particularly over mountainous regions (*Sierra de Grazalema* and *Sierra Nevada*, in the South), although their intensity is slightly diminished. This feature strongly emphasizes the convenience and benefit of using RCM models, primarily in terms of precipitation extremes, which is one of the main aspects to be surveyed in climate change studies.

5.3   Temperature

Surface temperature is not as sensitive as precipitation to parameterizations, but an analysis of the different simulations is desirable in order to assess the configurations validity and identify possible differences among them. In principle, the scheme that should impact more directly the temperature is the radiation scheme. Here, only the CAM3.0 package is used, however, preliminary results indicated that rather than the radiation schemes, which usually describe adequately the radiation processes, what most affects temperature is the use of an appropriate land surface model[1]. The PBL scheme might be expected to play a significant role too, especially for nighttime temperatures because the PBL is then stratified and stable, and thus more difficult to simulate.

Surface temperatures extremes (Tmax and Tmin) are obtained from WRF using the CLWRF version (see Sec 4.4) and stored on a daily basis. In order to refer grid-points and observations to common altitudes, the WRF outputs were adjusted using a standard environmental lapse rate (6.5 K/km) to account differences in elevation between the observations and the nearest grid-points. Nonetheless, in order to avoid the *representation error* the stations and grid-points are also grouped into regions to compare them, because a simple adjustment would not be enough. The standard environmental lapse rate was chosen according to a general consensus in regional climate modeling (Giorgi et al., 1998; Jacob et al., 2007; Mass et al., 2002; Vidale et al., 2003). It has also been proposed as an alternative to employ a model lapse rate, but Zhang et al. (2009) found

---

[1]All this preliminary tests were actually performed with 20 different configurations of MM5 (Argüeso et al., 2009).
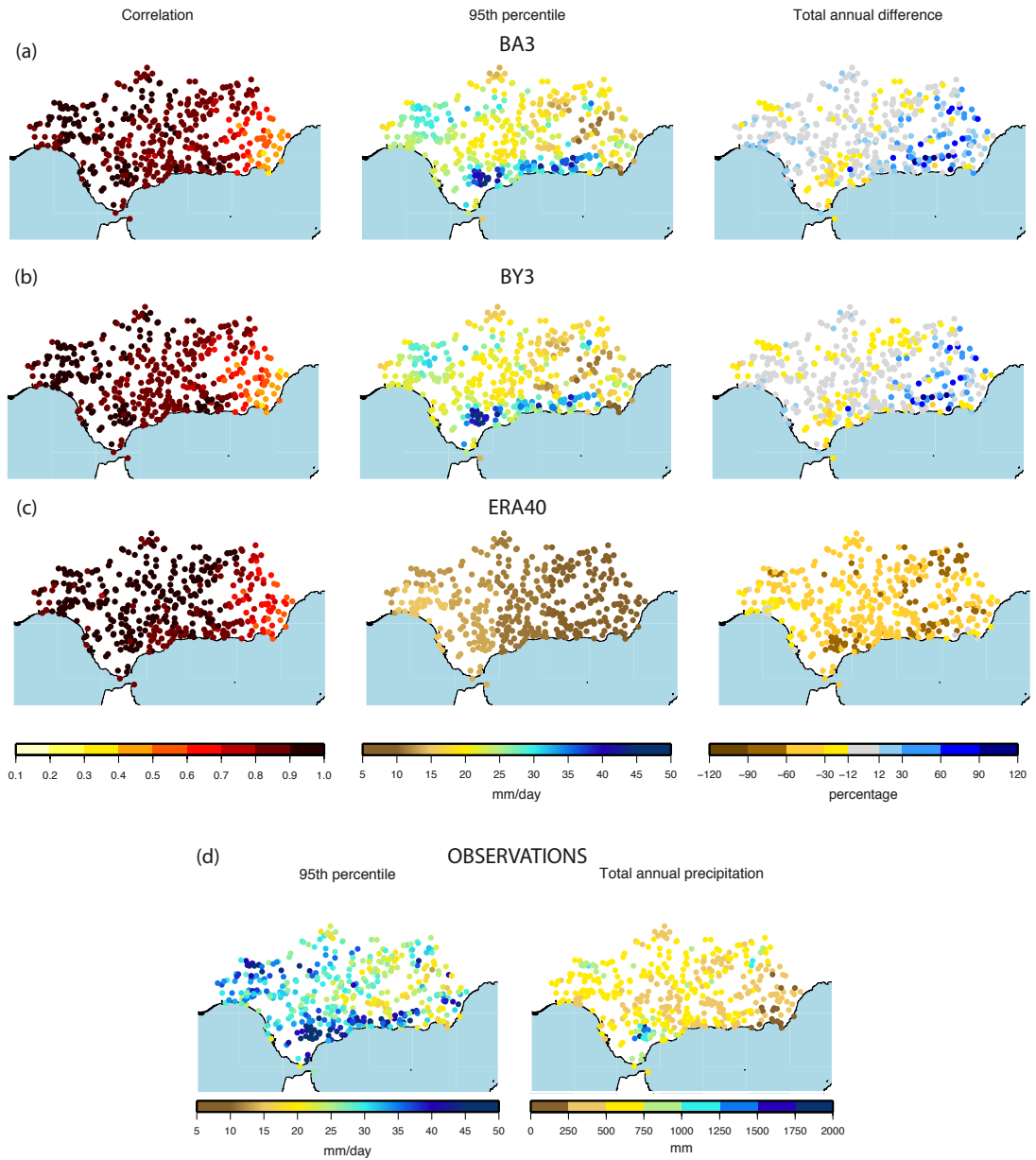
Figure 5.5: *Spatial distribution of monthly precipitation correlation, 95th daily precipitation percentile and the difference with respect to observed total annual precipitation, calculated station by station for BA3 (a), BY3 (b) and ERA-40 (c). Observed 95th daily precipitation percentile and total annual rainfall are shown in panel (d).*

that the differences between using model-derived lapse rates and the standard environmental one were almost negligible.

5.3.1   Monthly values of temperature

Monthly time series

By analogy with the precipitation treatment, the monthly mean values of daily Tmax and Tmin are calculated for each station and its nearest WRF grid-point (applying the standard environmental lapse rate), and then spatially averaged over the regions to compare them. Figures 5.6 and 5.7 show the correlation coefficients, the RMSE and the MAE between WRF and observational monthly means for both Tmax and Tmin, respectively. Results for ERA-40 monthly means are shown as well.
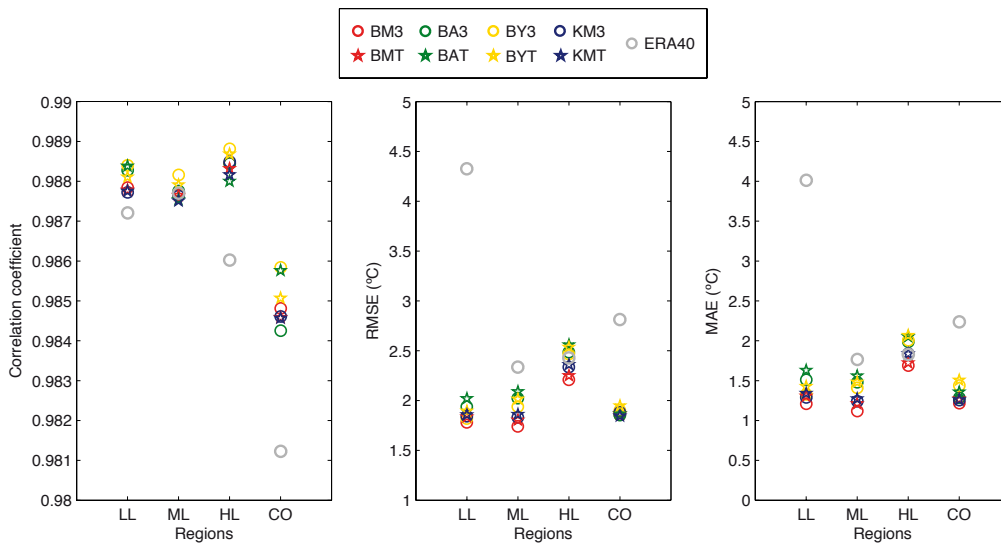
Figure 5.6: *Correlation coefficient, RMSE and MAE calculated for WRF (colors) and ERA-40 (grey) monthly mean maximum temperature with respect to observations in the different temperature regions.*

Although correlation coefficient values are almost indistinguishable for WRF and ERA-40 estimates (within the bounds 0.98-0.99 for Tmax and 0.97-0.99 for Tmin), both RMSE and MAE show a sharper distinction even among the WRF simulations. WRF outputs substantially improves the estimation of Tmax over LL and CO regions with respect to ERA-40 and likewise Tmin errors are clearly
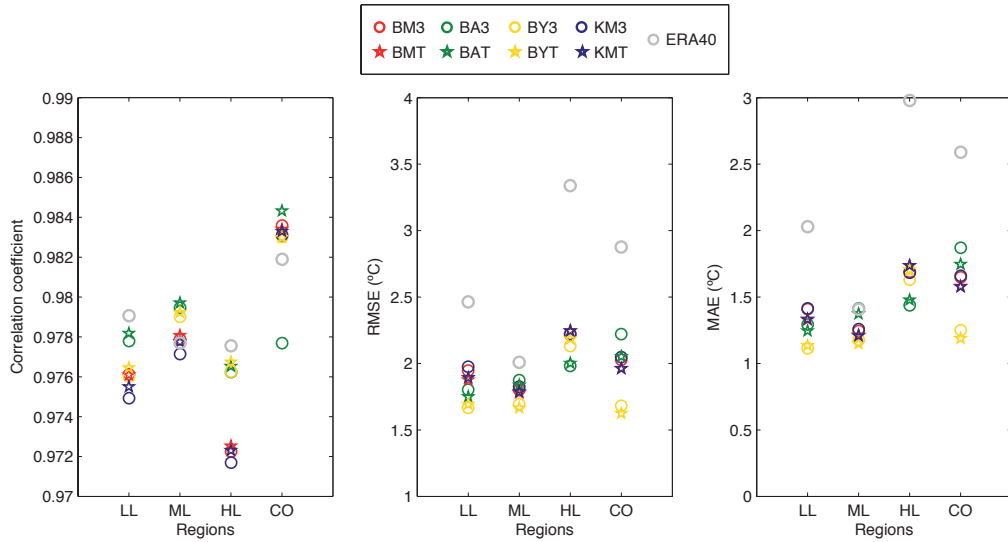
Figure 5.7: *As in Fig 5.6 but for monthly mean minimum temperature.*

reduced over LL, HL and CO. In the case of Tmax the RMSE is improved from about 4°C to about 2°C in LL region, and a similar WRF positive contribution is observed in terms of MAE. Concerning Tmin, HL is the most sensitive region to the model improvements and RMSE decreases from about 3°C to less than 2°C. In every region, most WRF results outperform ERA-40 monthly means of Tmax and Tmin with respect to observations.

As for the performance of individual WRF configurations, the combinations BMJ-YSU appears to be the most appropriate to describe monthly minimum temperature, whereas the BMJ-MYJ seems to better reproduce monthly mean maximum temperature. It is worth mentioning that PBL parameterization plays a significant role in describing surface variables, particularly at night, and thus it has an important impact on temperature, especially on the minimum values. In fact, those configurations that use the same PBL scheme usually perform very similarly (e.g. KF-MYJ and BMJ-MYJ), as can be seen in Figure 5.7. Conversely, the choice of microphysics has negligible repercussions on temperature estimations as occurred for precipitation, which is in agreement with conclusions drew by Fernández et al. (2007) for the IP in this respect.

Annual cycle

The temperature annual cycle is highly dependent on insolation and thus presents a smooth pattern with maximum values during the summer months and minimum during winter ones. The representation of this shape contributes to a large extent to the high correlation between the model and the observations and it is not directly associated with parameterizations. Therefore, the differences among the various simulations are very small as observed in Figure 5.8, which shows the annual cycle for both Tmin and Tmax monthly means in the different regions.
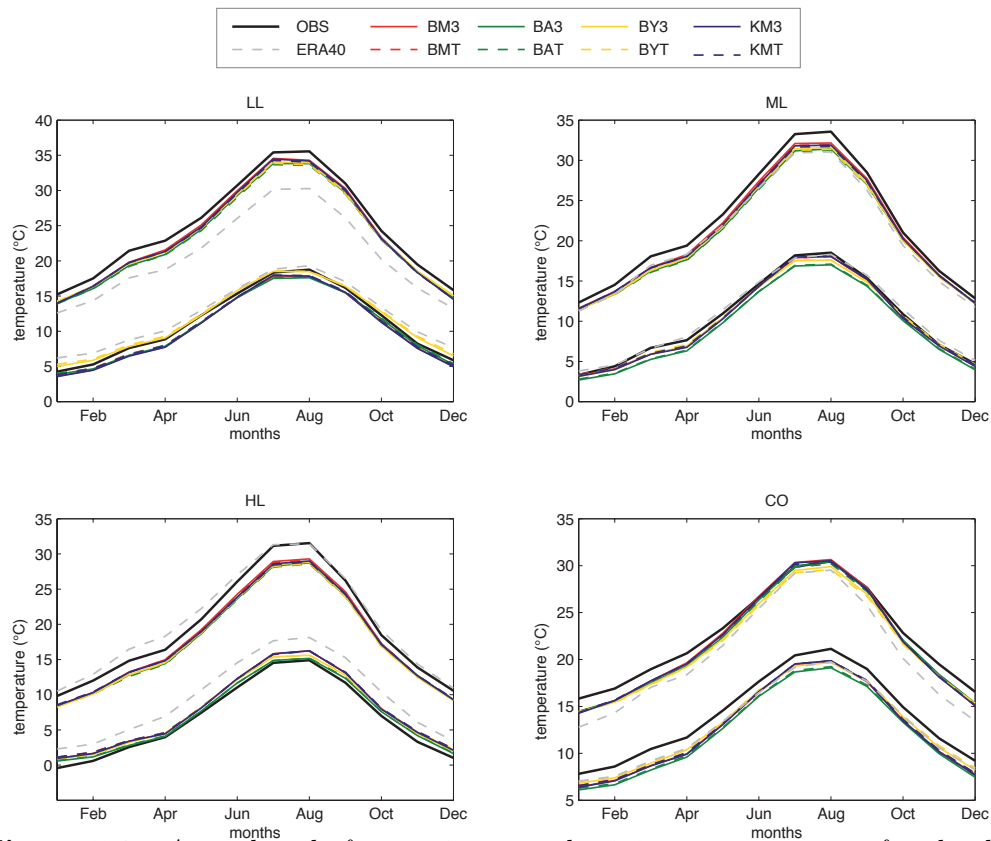
Figure 5.8: *Annual cycle for maximum and minimum temperature for the different temperature regions: observations (black), ERA40 (grey dashed) and WRF simulations (colors).*

In general, the WRF shape of the annual cycles show good agreement with the observations ones, although some deviations are evident in certain seasons. Maximum temperature is broadly underestimated, specifically during the summer. The HL region, where the stations are located higher in elevation, embodies

this tendency and indeed, the deviations reach about 4°C in July. The CO region is an exception since summer maximum temperature is very well captured with almost no errors. On the other hand, there is no clear propensity in the sign of the minimum temperature deviations, excluding once more CO where every WRF configuration presents a cold bias. In compliance with how similarly WRF configurations reproduce the annual cycle, no obvious decision can be made in relation to the most suitable physics combinations, although overall, BMJ-MYJ combination (BM3 and BMT) seems to perform slightly better for Tmax. In terms of Tmin, the most suitable configuration depends on the region and there is not a clear better option.

Regarding the comparison with the boundary data conditions, WRF contributes to improve the temperature annual cycle description in a few situations (e.g. Tmax in LL and CO, Tmin in HL and LL). Nevertheless, the annual cycle is reproduced similarly by ERA40 and WRF in other situations. As already mentioned, the monthly temperature is directly linked to insolation annual cycle and thus minor differences are observed among WRF simulations and ERA-40 estimates. An exception is found in places where the surface extremes play an decisive role, such as the maximum temperatures in the *Guadalquivir* river basin (LL), or minimum temperatures for stations at high altitudes (HL) that ERA-40 is unable to represent.

5.3.2 Daily values of temperature

All daily values from each region were considered to calculate eight percentiles of both maximum and minimum temperature (1st, 5th, 10th and 25th, 75th, 90th, 95th and 99th). Figures 5.9 and 5.10 are two Q-Q plots that represent the percentiles from different WRF runs (colors) versus observational percentiles for Tmax and Tmin respectively, with the grey line indicating a perfect description of the PDF. Percentiles from ERA-40 temperatures (grey) are shown too.

Minor differences are observed among the explored configurations since temperatures in RCMs mostly depend on the model elevation, the radiation schemes (that includes the aforementioned insolation) and the SST. All these factors are identical in all WRF simulations and therefore their temperature estimates even in terms of extremes, are very similar. Nonetheless, it is still important to analyze WRF temperature results because there might be differences between the configurations that should be determined.

Both Tmax and Tmin are in general accurately captured by WRF, with
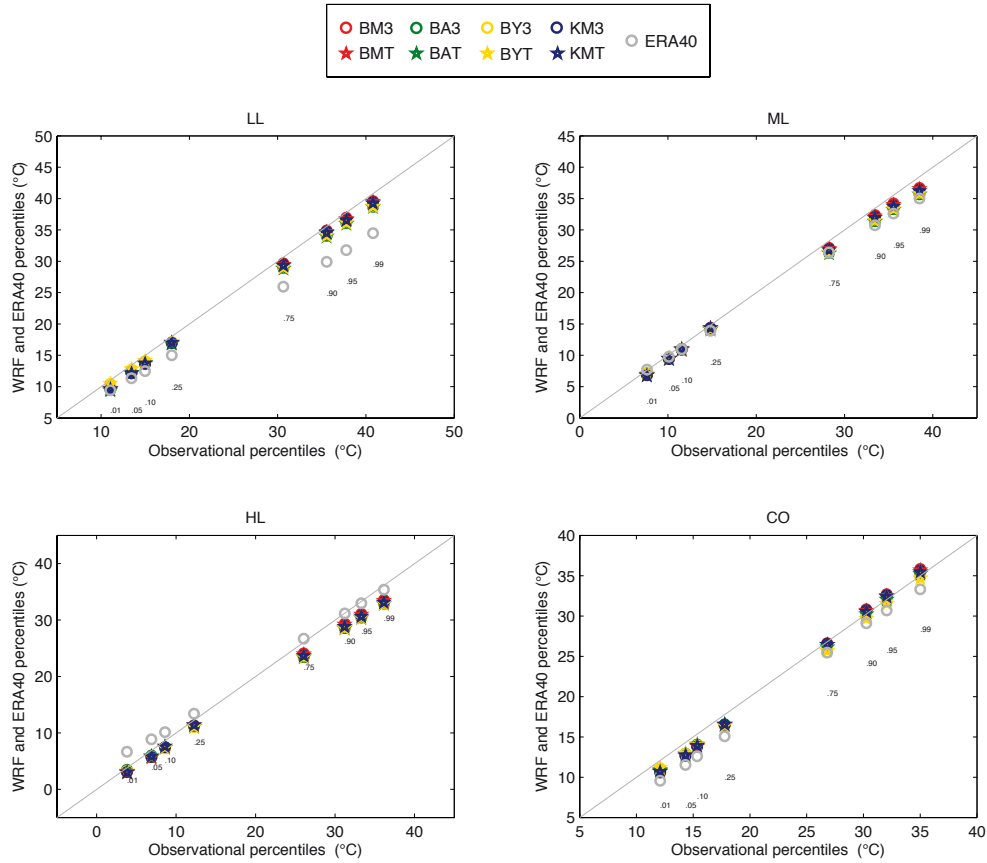
Figure 5.9: *Daily maximum temperature percentiles simulated by WRF (colors) and ERA40 reanalysis (grey) vs. observational percentiles for the different regions. The grey line indicates a perfect description of the Probability Distribution Function.*

slightly better results for the latter. Estimations of maximum temperature extremes tend to underestimate the observations, except for the CO region, where no clear tendency is observed. In fact, in the CO region, WRF produces higher summer temperature extremes (upper percentiles) probably due to an intensification of the land influence to the detriment of the sea influence. The spread of WRF esimates in minimum temperature is somewhat wider (lower percentiles in LL and upper percentiles in HL), however these differences are still not noteworthy. The reason that explains this spread might be found in the major impact of PBL schemes in nighttime processes (e.g. stratification and stable layers) and thus in minimum temperatures, although further analysis of particular days should be carried out to confirm this possible explanation.

In comparison with ERA-40, dynamical downscaling improves two impor-
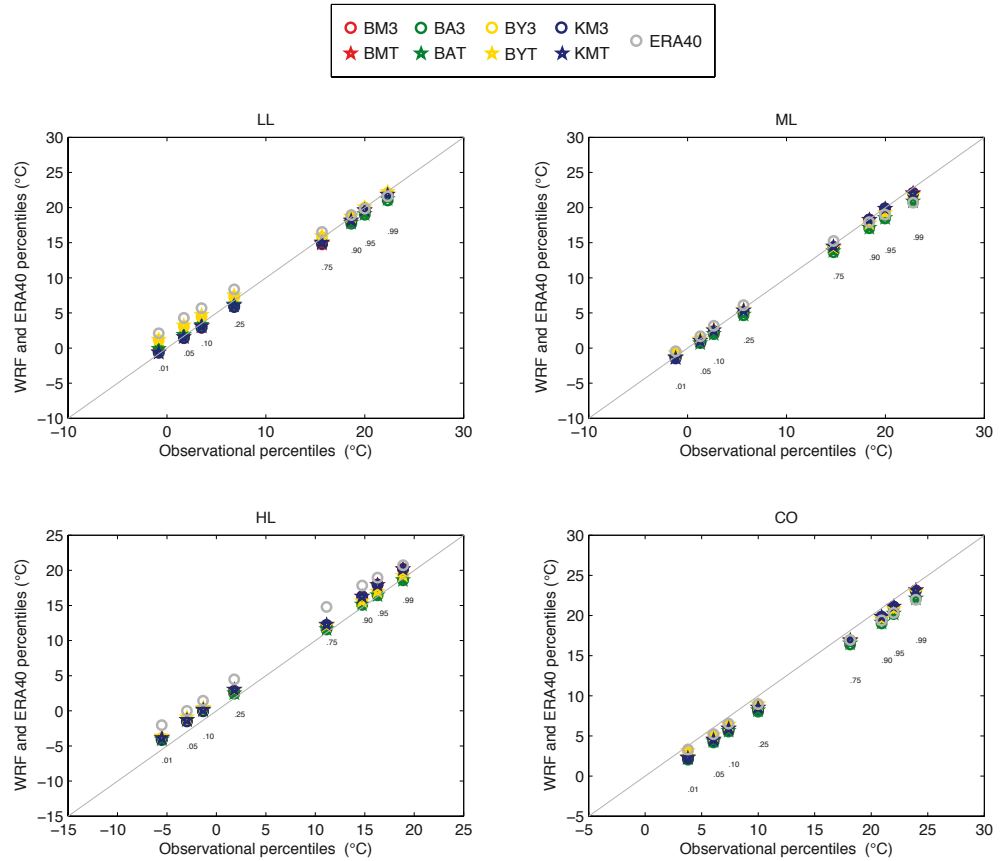
Figure 5.10: *As in Fig 5.9 but for daily minimum temperature.*

tant aspects that were already touched upon in the annual cycle examination. Firstly, higher extremes of maximum temperature are much better reproduced in LL region where the surface temperature attain the highest values in all Europe. Secondly, minimum percentiles are captured more accurately in HL, which basically comprises locations at high altitudes and thus where the absolute temperature minima are reached in southern Spain. On the other hand, maximum percentiles in HL are well described in ERA-40, whereas WRF seems to produce milder extremes. In ML and CO regions only slight improvements are achieved with WRF.

5.3.3   Spatial distribution of temperature

In line with the analysis conducted for precipitation, the spatial distribution of the correlation coefficient and the bias[1] for monthly values, together with the daily Tmax 95th percentile and the daily Tmin 5th percentile are explored for each WRF simulation. In order to illustrate the spatial distribution of these parameters, they are calculated station by station. It should be kept in mind that these examinations produce only qualitative information and their purpose is to provide a general overview of the model accuracy spatial patterns.

Figures 5.11 and 5.12 show the spatial distribution of the mentioned parameters for BA3 (a) and BY3 (b) WRF simulations, and ERA-40 (c) . Two different simulations have been selected among the eight configurations to represent the WRF capabilities. As in the case of precipitation, the spatial patterns of the different WRF runs were very similar and thus the maps for the rest of simulations are not shown here. In addition, the observed Tmax 95th percentile and the Tmin 5th percentile, and the means throughout the whole period are shown too as a means to put the results in context.

The temperature correlation spatial patterns are not as definite as they were for precipitation. Despite the lack of a clear pattern, Tmax inter-annual variability seems to be better captured in the *Guadalquivir* river basin and higher correlation values are observed in this area. Compared to Tmax, Tmin presents lower correlation values over the entire region. This feature is usually related to deficiencies in the simulation of the PBL during the night and it was also found by Zhang et al. (2009) in the US Pacific Northwest. At most stations, WRF Tmin is correlated over 0.95 with observations, although few stations show values below that threshold and are thus off the scale (grey), particularly for BA3 and ERA40. Nonetheless, these stations still present high correlations exceeding 0.90 for both Tmax and Tmin [2].

Although Figure 5.11 reveals that both WRF configurations are able to correctly distribute the maximum temperature 95th percentile, the model shows some limitations in reproducing its magnitude. In general, the percentile values over the mountains are somehow diminished by the model that substantially differs

---

[1]Here the bias is used instead of the MAE because it is calculated station by station and thus it is not prone to undesired compensation between stations of the same region, as it was in previous analysis. The bias also make possible to provide a picture of the areas where temperature tends to be under- or overestimated.

[2] *Marbella* in the central South is the only exception. However, it should be emphasized that these results are not intended to be analyzed station by station and they must be instead regarded as a whole
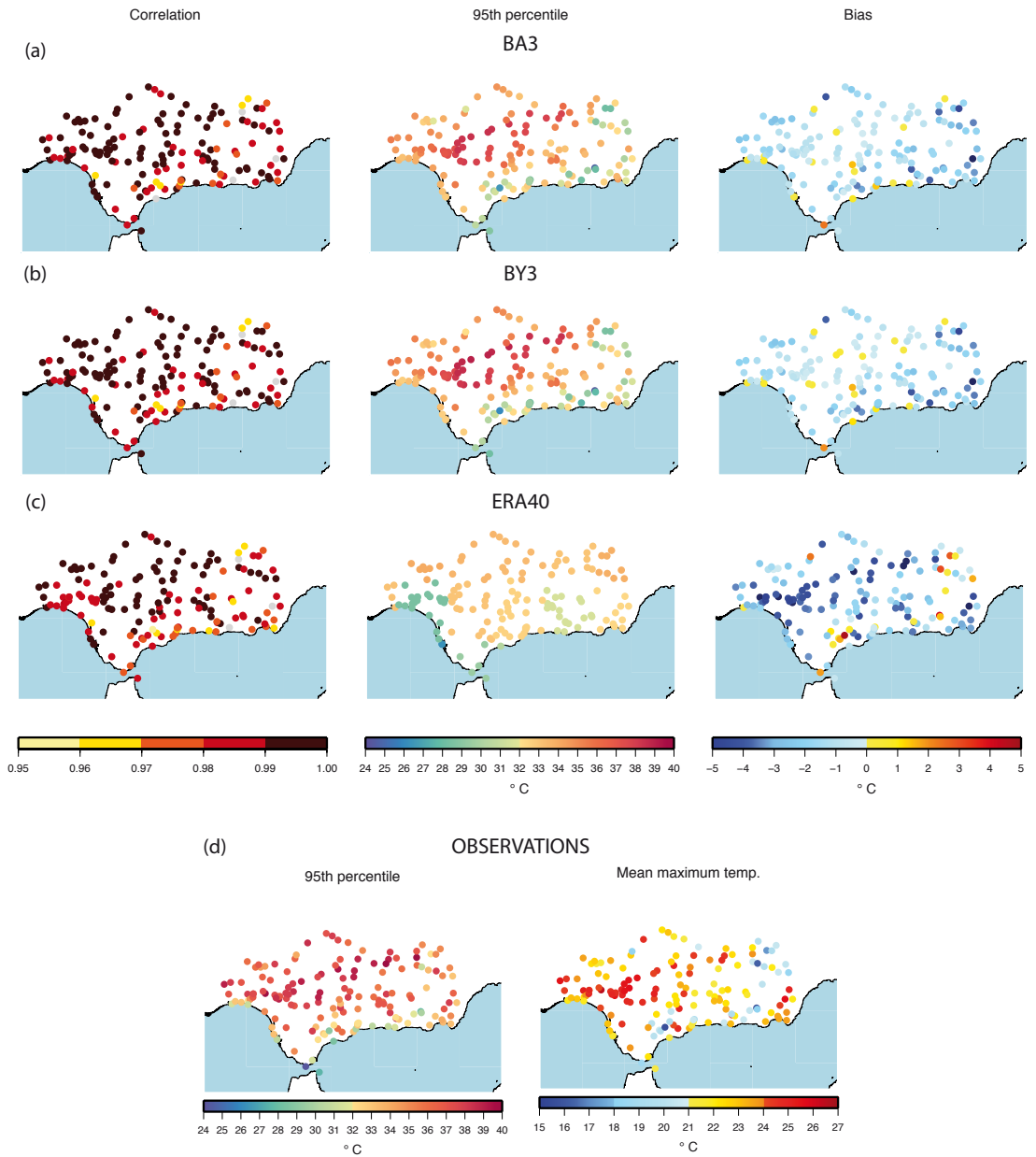
Figure 5.11: *Spatial distribution of monthly mean Tmax correlation coefficient, 95th daily Tmax percentile and the Tmax bias with respect to observations, calculated station by station for BA3 (a), BY3 (b) and ERA-40 (c). Observed 95th daily Tmax percentile and mean Tmax (d).*
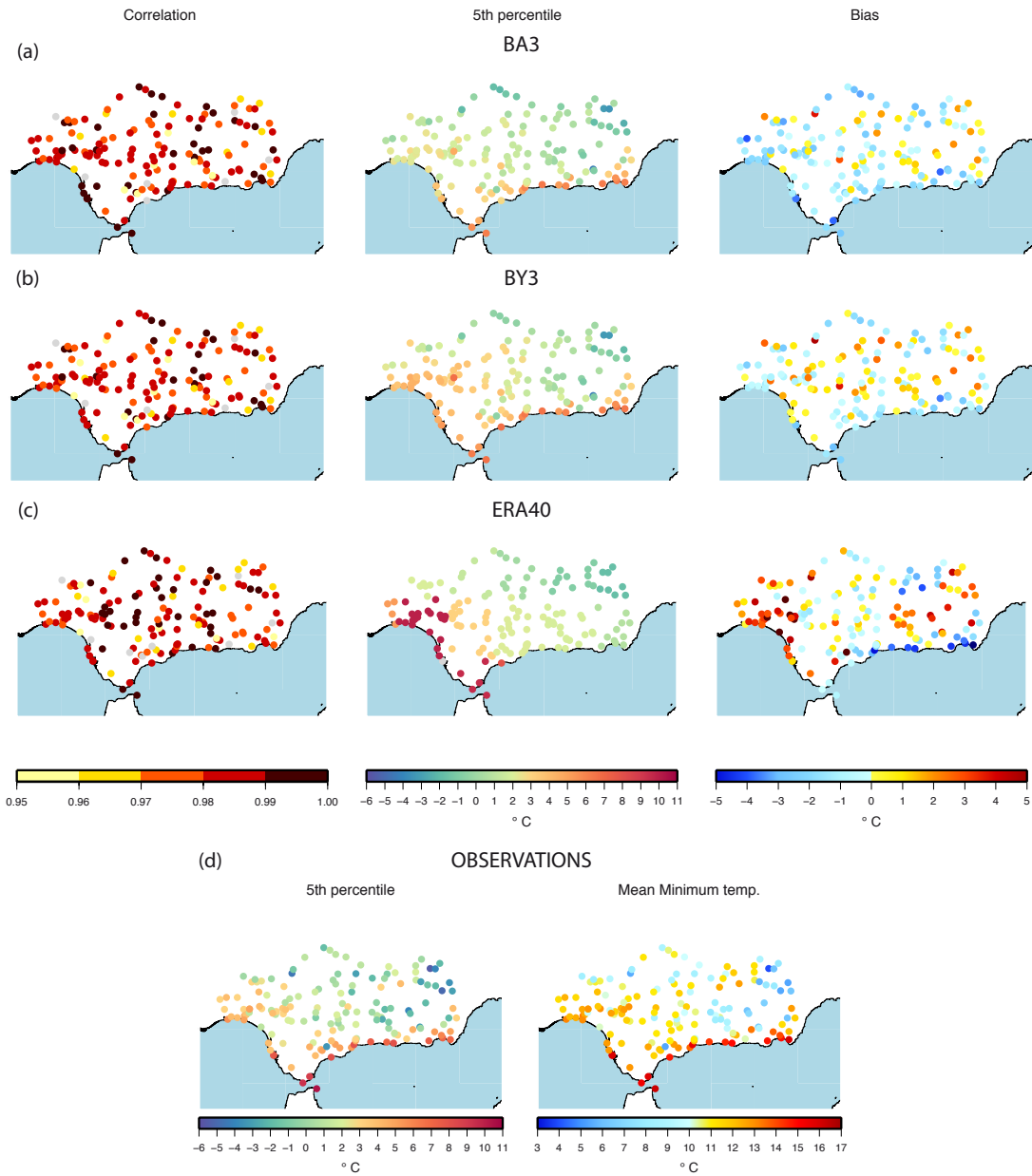
Figure 5.12: *Spatial distribution of monthly mean Tmin correlation coefficient, 5th daily Tmin percentile and the Tmin bias with respect to observations, calculated station by station for BA3 (a), BY3 (b) and ERA-40 (c). Observed 95th daily Tmin percentile and mean Tmin (d).*

from observations in the eastern areas. The extreme maximum temperatures are slightly overestimated in the coastal stations whereas WRF produces the best results in the *Guadalquivir* river basin. It should be noted that these spatial patterns observed for Tmax are almost identical in BA3 and BY3 simulations. Regarding Tmin, the WRF spatial distribution of the 5th percentile compares well with the observations but again some errors are noticed. For example, the BY3 tend to produce warmer Tmin extremes across the river basin, whereas BA3 yields colder values in the western areas. The minimum values obtained in the eastern mountains for the observations are captured by WRF but the magnitude is lessened. The 5th percentile of Tmin is correctly reproduced by WRF along the Mediterranean coast.

In terms of the Tmax bias, it does not show a clear spatial distribution pattern either, except for a marked underestimation over the eastern mountains, and an overall tendency to underestimate maximum temperatures is here confirmed. As for Tmin, there appear to be more significant differences among the WRF simulations, which stresses that the PBL scheme has certain influence on the minimum temperature under particular conditions. BY3 overestimates minimum temperature in many locations, whereas BA3 produces smaller deviations and does not show a clear tendency in the sign. BA3 is generally colder than BY3.

As could be expected from its coarse resolution, ERA-40 scarcely captures the spatial distribution of extremes. Indeed, WRF brings a remarkable improvement in their distribution and magnitude thanks to the finer resolution. In comparison with ERA-40, WRF reproduces better the maximum extremes in the lower elevations and minimum values over the mountains, as well as milder Tmin at the coast and lower Tmax at high altitudes. ERA-40 provides Tmax and Tmin estimates that are highly correlated with observations, but the percentiles and the biases indicate that ERA-40 magnitudes are completely inadequate. For example, the biases for both Tmax and Tmin exceed 3°C in absolute terms in a large number of locations.

5.4   The appropriate combination of parameterizations

The question that arises out of a sensitivity test to parameterizations is whether there is an optimal configuration for every region and all through the year. Seldom a configuration outperforms the others for all the locations, for all the variables and at every timescale. Instead, a configuration that overall produce satisfactory results should be selected. Because of the large number of

factors in play, the identification of the most appropriate combination of schemes is not straightforward and we must prioritize certain aspects. For example, the differences between WRF simulations in terms of precipitation are more pronounced than for temperature, hence the configuration suggested for precipitation should prevail over those for temperature. Furthermore, the complete spectrum of physics options has not been examined and thus it cannot be affirmed that the most suitable configuration is among the explored ones. Nonetheless, the analyses presented in this chapter make possible to choose an appropriate configuration and shed light on the importance of certain parameterizations. For instance, cumulus and PBL schemes have been revealed as chief components in the description of precipitation in southern Spain whereas the microphysics choice seemed to be of minor importance. Overall, the combinations BMJ-ACM2 (BA3 and BAT) and BMJ-YSU (BY3 and BYT) compared best with observations. Schemes that have less impact on results are then chosen using different criteria. For example, the simplest microphysics scheme (WSM3) is recommended bearing in mind the computational costs.

Regarding temperature, almost no differences could be noticed between the varying configurations and only PBL scheme seems to modestly affect Tmin due to its direct relation to the nocturnal boundary layer simulation. The MYJ scheme appear to provide slightly better results. However, the BA3 also provides fairly good results.

Altogether, BA3 seems to be a suitable configuration that describes both temperature and precipitation with satisfactory confidence and thus it is here selected to perform the upcoming WRF simulations.

In addition to an appropriate configuration choice, a first approach to ascertain the WRF improvement with respect to the boundary conditions has been completed here. However, the examination of WRF capabilities over longer periods is required to assess the added-value information gained with dynamical downscaling for climate studies. This is further studied in the next chapter, where 30-year simulations are analyzed to provide an insight of the model performance over a climate period of reference[1].

---

[1]According to the World Meteorological Organization (WMO) a period of at least 30 years must be considered to study the climate.

Chapter 6

Present climate (1970-1999): the model evaluation

> Climate is what we expect, weather is what we get.
>
> ————————————————————————————
>
> Mark Twain

The configuration of WRF suited to adequately simulate the processes that define the Iberian climate has been addressed so far. This chapter tackles the evaluation of the model in order to assess its capabilities to correctly resolve temperature and precipitation over climate periods. The model evaluation will help to identify the uncertainties with respect to observations and it will then be possible to establish whether the model is adequate for future climate simulations over Spain. Not only the performance of the model driven by 'perfect boundary conditions' is analyzed, but also the model outputs when GCMs information is downscaled. The model evaluation focuses on precipitation and temperature at varying timescales, although SLP is tangentially studied as well to supply with additional physical interpretation of possible model errors[1].

6.1 The present climate evaluation

6.1.1 Why should the model be validated?

In principle, the answer to this question might be regarded as a truism, but in truth the model validation has been traditionally omitted in climate change studies and its importance must be emphasized.

---

[1]Some of the results presented in this chapter are part of a study submitted to *Journal of Climate* (Argüeso et al., -).

Let us look at the concept behind the future climate projections. Dynamical downscaling and climate change studies in general rely on the assumption that an appropriate representation of present climate implies a correct description of future climate as well. This statement is founded on the idea that GCMs should represent present and future climate similarly, which is a fairly restrictive assumption. Unfortunately, present climate is the only available backdrop to validate our model estimates and verify our hypotheses. The model evaluation with present climate is not a guarantee that future projections are accurate, but the future projections will be unquestionably much more trustworthy than if the model is not validated at all. In fact, how could a future projection be reliable if we do not even know the model ability to reproduce present climate?

Despite being crucial to produce reliable climate change projections, the validation process has too often been conducted carelessly, or even omitted. A rigorous validation requires at least 30-year runs (climate runs) to ensure that the model represents the local climate. Shorter periods have been usually used to evaluate the model, but they might characterize very particular conditions instead of the actual climate of the region. In the last few years, computational resources have enabled the model evaluation over longer periods and it is now a requisite to generate future projections. Other aspects such as the timescales of the validation have been usually disregarded which resulted in incomplete evaluations. Both mean values and high-frequencies are important factors that define the climate and should be equally considered in the assessment of the model potentials.

6.1.2   Description of present climate simulations

Three different 30-year simulations were completed to evaluate the model capabilities to reproduce present climate characteristics. All three simulations are identical in their configuration except for the boundary conditions. The simulations were driven by ERA-40, ECHAM5 and CCSM, and they will be referred from now on as WRFERA, WRFEH5 and WRFCCSM, respectively. The model has been configured as described in Chapter 4 and the physics schemes combination was set to BA3 (see Table 5.1) according to results obtained in Chapter 5. To make the most of the computational resources, the 30 years are split into three decadal simulations, each of them including a 7-month spin-up that is discarded afterwards (see Sec. 4.3).

6.1.3   Description of the analysis

The present climate runs are evaluated in terms of both precipitation and temperature using Spain02 version 2.1 dataset. The WRF outputs (land grid-points only) have been degraded using bilinear interpolation to the regular 0.2° Spain02 grid to make them comparable. Several parameters are analyzed by directly comparing grid-points. They are then grouped into regions to explore some additional aspects of climate that cannot be easily studied grid by grid (e.g. annual cycle, percentiles distribution). In Sec. 3.2.2 it was mentioned that Spain02 v2.1 presents some problems over the Balearic Islands for Tmin and consequently, this dataset could not be used to evaluate the model over this region in terms of temperature. Actually, the model temperature evaluation is confined to the peninsular territory.

The model evaluation must be performed not only studying long-term means but also high-order statistics, as already emphasized by some authors (IPCC, 2007; Leung et al., 2003). In fact, several studies have focused on RCMs performance addressing the issue at different timescales (Caldwell et al., 2009; Evans and McCabe, 2010; Herrera et al., 2010a; Jacob et al., 2007; Kostopoulou et al., 2009; Rosenberg et al., 2010). The assessment of the model capabilities from a multi-temporal approach stems from two main reasons:

1. If only the long-term means are analyzed it might occur that the model outputs are apparently correct due to incorrect reasons as a results of error compensation. The analysis of the model at different timescales is hence preferable to bring to light the errors that might be cancelled out by averaging.

2. Under global warming conditions, not only changes in means have impact on ecosystems and population, but extreme events do also play a crucial role. For example, in terms of precipitation, the long-term means directly affect water availability and slow hydrological processes. However, the occurrence and intensity of extreme events are directly associated to flood risk and thus have major impacts in sectors such as agriculture.

The model is then evaluated comparing from annual to daily values with Spain02 and using a number of statistical parameters (see Appendix B) that characterize different precipitation and temperature timescales.

6.2   Precipitation

Precipitation in the IP can be roughly classified in three main regions: the eastern coast, the northern Cantabrian Coast and the south and interior of the Iberian Peninsula (Esteban-Parra et al., 1998). In the case of summer precipitation, the latter can be further divided in two regions (northern and southern interior). A broad northwest to southeast decreasing gradient in precipitation can be observed, basically due to a combination of topography and the storm track placement.

The nature of precipitation varies considerably across the region. The east coast rainfall has a marked convective component that produces few but intense events that in general result in low annual precipitation (<150 mm/yr in the southeast). On the other hand, the northwestern region presents a precipitation regime that is linked to the presence of Atlantic fronts and thus characterized by more regular precipitation events and high climatological values (exceeding 2000 mm/yr). Furthermore, some localized centers of high precipitation induced by topography take place in the interior and south, over the mountain systems.

An additional feature of Spanish rainfall is related to its pronounced seasonal variability, a consequence of the Azores high pressure center seasonal shift. It induces precipitation maxima during the cold season (from october to march depending on the different subregions) and a marked minimum during the central warm months (July-August) with almost no rain events in most of the IP.

These two characteristics, the high spatial diversity and temporal variability, are here explored.

6.2.1   Annual precipitation

Firstly, the total annual precipitation has been calculated for Spain02 and the three WRF simulations over the entire 30-year period and a climatological yearly value is obtained for every grid point. The model capacity to adequately distribute the precipitation throughout Spain can be determined from the total annual rainfall and the areas with larger deviations in the total precipitiation can be identified. The pattern correlation (Walsh and McGregor, 1997), which is basically a standard Pearson's correlation over the space, is also computed to evaluate the similarity of the WRF annual precipitation spatial patterns with respect to the Spain02.

Figure 6.1 illustrates the climatological annual precipitation for the period 1970-1999. The pattern correlation coefficients are shown in brackets. All three

simulation present high spatial correlations with Spain02 (0.80-0.83), which suggests that the model is largely able to describe the broad southeast to northwest gradient and recreate the influence of topographical features on precipitation.
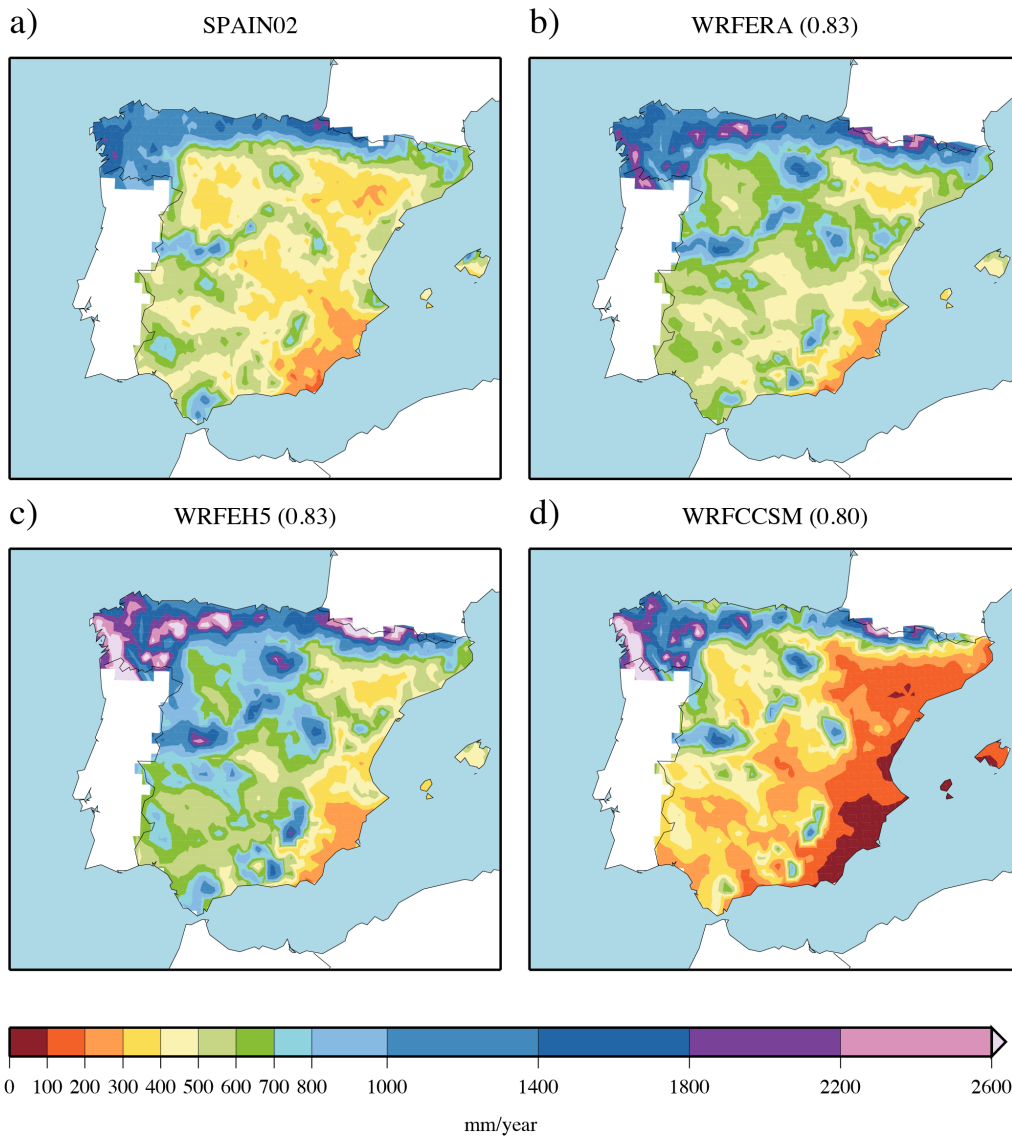
Figure 6.1: *Climatological annual precipitation (1970-1999) for the Spain02 dataset (a) and the WRF simulations nested with ERA40 (b), ECHAM5 (c) and CCSM (d). In brackets the pattern correlation between the WRF simulations and the observational dataset Spain02. White areas indicate values above the scale.*

Nonetheless, it should be noted that the pattern correlation is insensitive to

biases and thus it only explains the spatial similarity of the various maps. Indeed, substantial differences are noted between WRF total amounts of precipitation despite the the fact that the correlations are very similar among them.

The WRF model compares generally well with observations when driven by 'perfect boundary conditions', namely the ERA-40 reanalysis. Some exceptions can be observed at particular areas such as the northwestern quarter of the IP, where WRFERA produces moderate overestimations, or the driest region in the southeast that is clearly reduced by WRF. In line with these two factors, the river basins and the plateaus that are usually dry in Spain02, are somehow wetter in WRFERA. Very few regions tend to be drier in the model, but they do exist too (e.g. southwestern mountains).

Conversely, the GCM-nested simulations generates annual precipitation rates that significantly differ form observations over specific regions, even though they are highly correlated (pattern correlation) with observations. On average, WRFEH5 tends to produce an excess of rainfall with particularly noticeable deviations in the northwest, although along the eastern coast the model shows a good agreement with observations. The pattern correlation is as high as for WRFERA and the major topographical features of precipitation can be easily identified in WRFEH5 estimates. The WRFCCSM simulation does not show systematic differences across the IP but instead it seems to enhance the broad precipitation gradient (from southeast to northwest). For instance, WRFCCSM produces less precipitation over the east and south, and too much rainfall over the northwest, where values are similar to WRFEH5.

To provide further details in these features of the WRF simulations and single out possible error sources, the seasonal and monthly values are analyzed.

6.2.2   Seasonal precipitation

As a means to examine differences between WRF runs and Spain02 the seasonal and annual relative biases[1]are calculated. Figure 6.2 depicts the WRF relative bias with respect to observations at seasonal and annual timescales. The relative biases stress the differences between the WRF simulations that were already pointed before, but adds supplementary details on how the model performs at different moments of the year.

---

[1]The relative bias is the difference in the total seasonal/annual precipitation amount divided by the observed seasonal/annual precipitation and thus the values are given in percentage. See Appendix B.
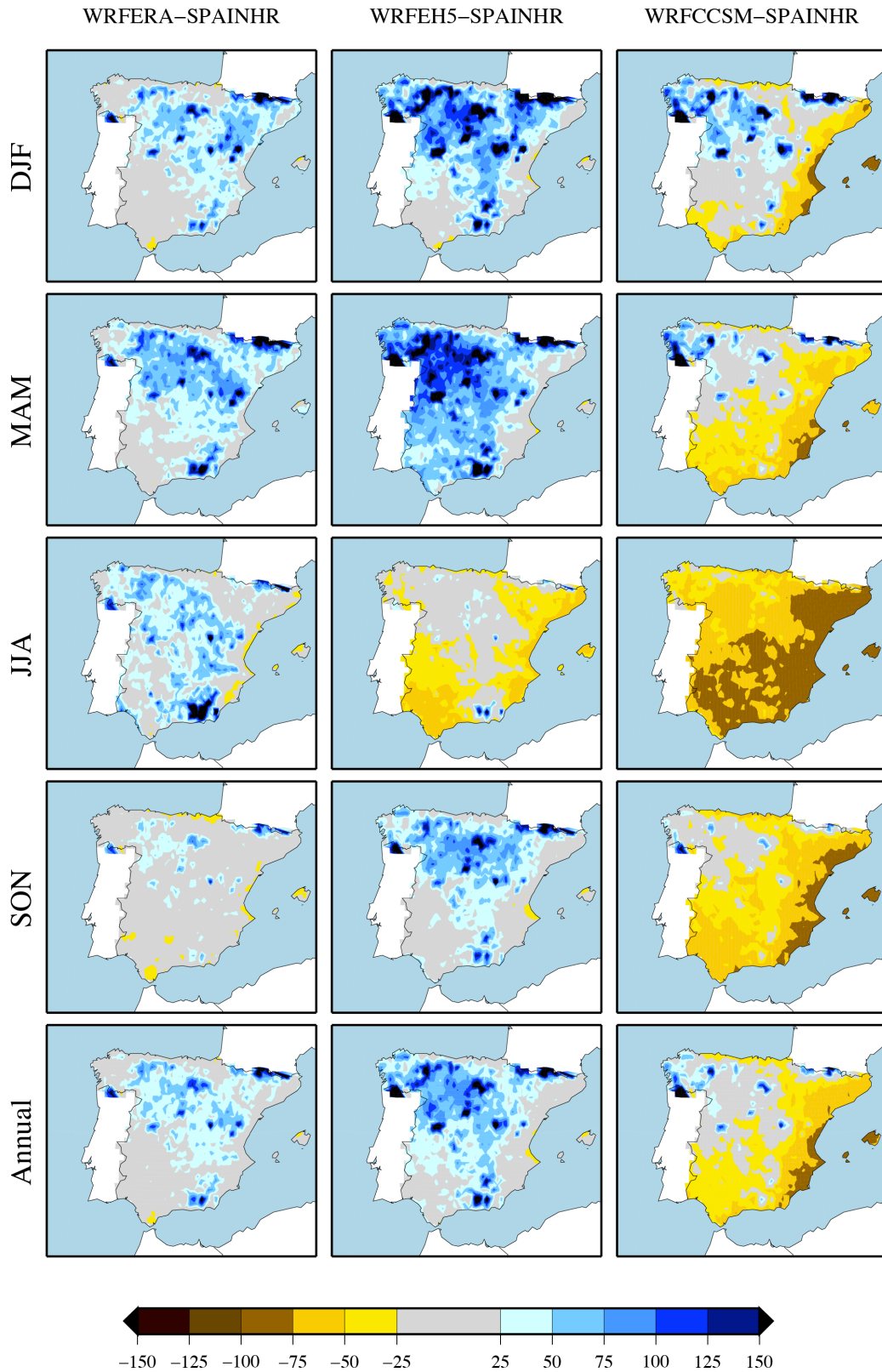
Figure 6.2: *WRF seasonal and annual precipitation relative bias (%) with respect to Spain02. In columns, the WRFERA, WRFEH5 and WRFCCSM runs. In rows, the seasonal (DJF, MAM, JJA and SON) and the annual biases.*

The WRFERA simulation produces remarkable results in most of Spain in yearly terms. The total annual deviations stay below 25% of the total precipitation in many areas, and only very few locations show biases over the 50% threshold. This is valid for both positive and negative biases, although the latter are rare for this WRF simulation (only in the very south). Since the annual deviations might mask possible errors by compensation, the seasonal biases are slightly larger than the annual ones. However, the model still produces noteworthy results at seasonal timescales. Some positive biases, that become more relevant during the spring, are observed in the northern interior of the peninsula. Specific areas of localized an intense positive biases are also noticed during the summer over some mountain ranges, such as *Sierra Nevada* in the southeast. The WRFERA performance during autumn is especially outstanding, since the bias remains below 25% practically over the entire region. Autumn rainfall accounts for a large part of the total annual precipitation in many places over Spain and indeed, the low bias obtained for this season together with the aforementioned compensation are reflected in the annual bias.

Regarding the simulations driven by GCMs, they yield very contrasting results with respect to the precipitation bias. The WRFEH5 run generally overpredicts precipitation whereas WRFCCSM tends to underestimate it. Despite the differences in the deviation sign, it is worth mentioning that the spatial patterns of the biases are very similar. For instance, both tend to produce positive to neutral deviations over the northwest and negative to neutral biases along the east and south coast. The equivalence in these spatial patterns might be interpreted as the regional model effect on the precipitation distribution according to topography (Atlantic fronts are usually blocked in their pass through the IP), beyond the large scale biases introduced by the boundary conditions.

For WRFEH5, the largest deviations are found during the winter and spring, and are systematically positive. During the summer, negative biases take place in the south and east. Summer rainfall in these areas has a minor contribution to total annual precipitation and the errors are not as critical as those corresponding to the cold season. Autumn differences are broadly low but reach considerable values in the northern interior.

As for the WRFCCSM, the most noticeable errors arise during summer and autumn in the form of negative biases. In the winter and spring months, WRFCCSM does not show a clear tendency in the deviations and the enhancement of the precipitation gradient that was suggested before is evidenced here too. As stated for WRFEH5, summer errors do not have a decisive impact on annual

precipitation because very little precipitation take place during these months. Nonetheless, it must also be admitted that a proper representation of summer rainfall is important in terms of describing hydrological stress and droughts, especially along the east coast. Furthermore, in this area, extreme events sometimes take place in the late summer due to high Mediterranean temperatures that enhance convective processes, which should also be captured accurately. This is examined further on when analyzing the extreme events occurrence.

The three WRF simulations are identical in their configuration and they only differ in the boundary data conditions. Therefore it might be interesting to examine the large scale to look for possible reasons that explain, at least partially, the differences between the WRF runs. For example, a particular GCM might not be able to reproduce Atlantic pressure fields adequately and thus the storm tracks are not distributed correctly.

For this reason, the modeled and observed SLP fields were also compared through a PCA. Namely, the EOFs corresponding to the principal components that explained more variability were examined. The spatial patterns obtained for all WRF simulations were very similar to the observed ones. However, despite the fact that this procedure is largely used to validate the GCMs (Casado and Pastor, 2011), it is not fully appropriate and further analyses are advisable, as in Errasti et al. (2010). The EOFs identify areas with similar SLP variability, but misses the magnitude and therefore only characterizes the SLP partially. So, the seasonal and annual mean Sea Level Pressure (SLP) from the coarser WRF domain have been calculated and are displayed in Figure 6.3 to provide supplementary information that might help to identify some error sources.

Prior to analyzing the SLP fields, it must be kept in mind that the SLP is largely prescribed by the boundary data conditions, specially when spectral nudging is switched on. Therefore, the pressure patterns are mostly inherited from the reanalysis and the GCMs. Overall, the GCMs induce SLP patterns that show very good agreement with WRFERA, describing strikingly well the different phases along the year. For instance, the distinct zonal distribution during the winter with higher SLP in the southern areas that evolves into a high-pressure center located in front of the Portuguese coast during the summer is represented by all simulations. The large scale dynamics than can be inferred from SLP are thus reproduced by the GCMs and the main characteristics of mean SLP in the zone are discernible, such as the summer blocking due to the high-pressure system in the Atlantic. The winter mean values of SLP over the IP are usually larger than the summer ones (Ahrens, 1998; Lutgens and Tarbuck, 1998), which is also

captured by all three simulations.

Although the shape of these configurations are accurately captured by both GCMs and transferred to WRF, the magnitude of the pressure centers are not always represented adequately. The WRFEH5 yields mean seasonal SLP fields that are very similar to those provided by WRFERA, but differences with WRFCCSM are noteworthy. CCSM tends to create too zonal configurations as observed in the winter mean SLP. The WRF model driven by CCSM strengthens the SLP gradient from north to south and thus channels the fronts above the IP. An exaggerated high SLP system is located in northern Africa which prevents many fronts from reaching the south of the peninsula. During the summer, WRFCCSM intensifies the Azores high-pressure system that enhances the blocking and results in very low precipitation rates during this season too.

Not being the only error source, the seasonal mean SLPs explain several features of precipitation biases that were observed in Figure 6.2. For example, the WRFCCSM strengthening of the SLP gradients is accompanied by intensification of the southeast-northwest gradient in precipitation over the IP. Likewise, the WRFCCSM presents significant negative biases during the summer because the high-pressure center is stronger and extends further to the north.

In the WRFEH5 simulation, it seems that areas with higher SLP values expand less to the north during winter and spring, but these differences are not significant enough to explain rainfall deviations by themselves. Although the pressure gradient are also strengthen by ECHAM5, the correspondence between SLP and precipitation biases in WRFEH5 is not as clear as for WRFCCSM and hence there must be other mechanisms in play that might be at the origin of the precipitation differences with respect to observations.

An additional observation that can be made out of this analysis is that spectral nudging might be advisable when the large scale is correctly represented by the boundary conditions, but it might force the simulations towards wrong values when the boundary data are imperfect, as in the case of CCSM. Regarding the WRFEH5, its ability to generate accurate large scale features has been proven and thus the use of spectral nudging can only be beneficial. Since all simulations must be identical in their configuration, the nudging was also adopted in the WRFCCSM run for the sake of homogeneity among the experiments. In any case, the spectral nudging employed in these simulations is very weak and should not excessively affect the results. However, it still reduces the impact of the domain design and maintains the consistency between the boundary conditions and WRF. Nevertheless, an in-depth analysis of the spectral nudging effect on
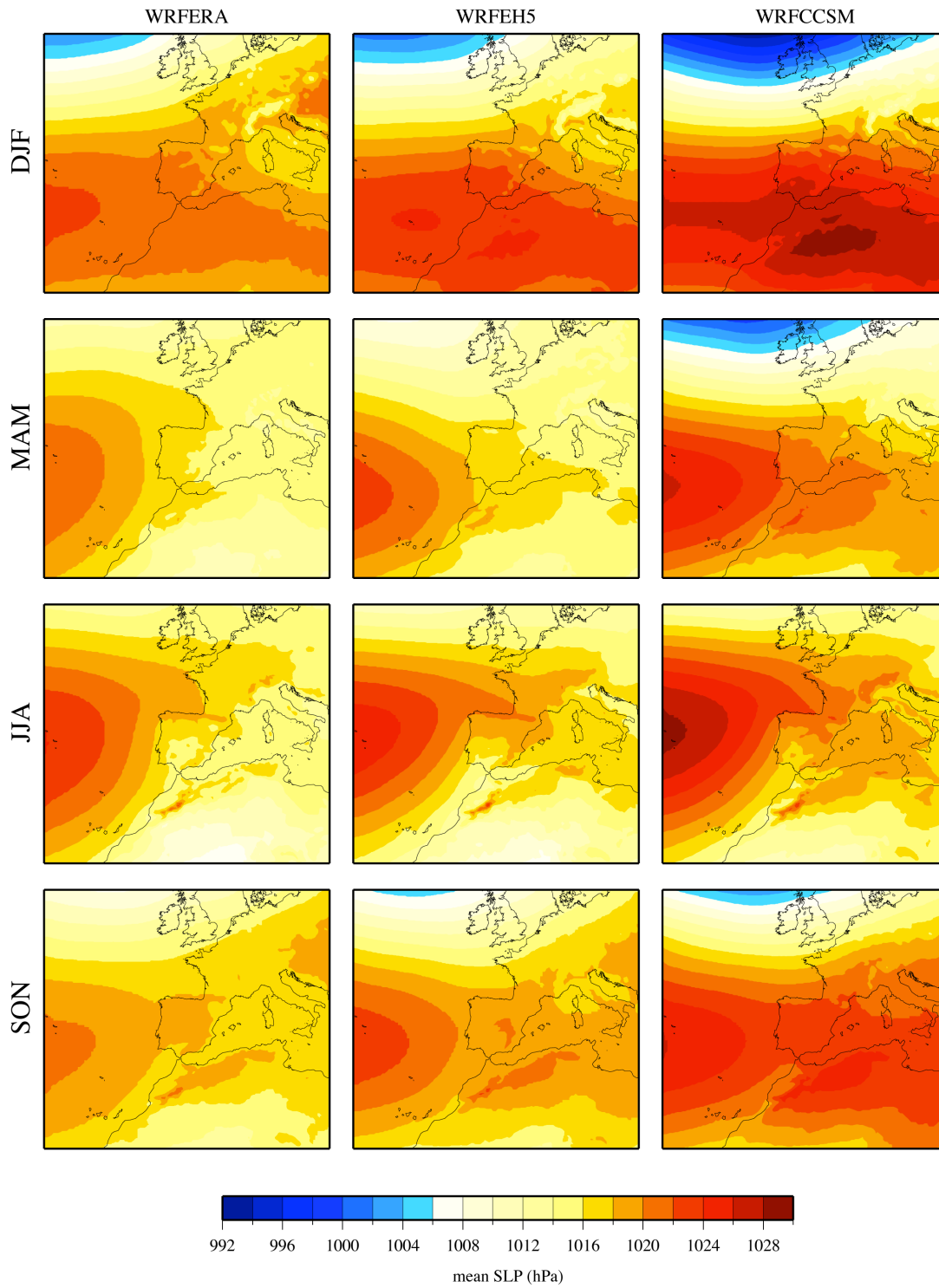
Figure 6.3: *Mean seasonal SLP fields for WRFERA, WRFEH5 and WRFCCSM calculated over the period 1970-1999.*

the results would be very interesting, but it remains open to future research due to obvious computational limitations.

6.2.3   Monthly precipitation

Precipitation in the mid-latitudes is often very variable in time and space, and therefore the maximum and minimum values can be attained at very different moments of the year in relatively close locations. Monthly precipitation is here analyzed to supply with additional information about the model performance in these terms. The annual cycle for all the Spain02 regions (Fig. 3.7) is explored to ascertain whether the model is able to reproduce this feature of climate.

The shape of the annual cycle is in general reproduced by the model (Fig 6.4, although it is worth mentioning that substantial errors are also evident mainly during the spring.

The WRFCCSM run tends to flatten the annual cycle at most of the regions and the relative maxima are usually removed. This is particularly marked in the eastern regions (SE, EC, IS) and results in significative negative biases all through the year. Overall, precipitation is systematically underestimated in the last months of the year, whereas no clear tendency is observed during the first ones. An exception is found for NW and IN, where overestimation is predominant all through the cold season (October-April). These results are consistent with seasonal rainfall biases that where pointed out before.

On the other hand, the WRFEH5 is able to reproduce further details of the precipitation annual cycle, despite the fact that some large deviations are still observed. Specifically, from December to April, WRFEH5 broadly overestimates precipitation and there are regions where these deviations are particularly worthy of attention, such as in regions SW, IN or NE. Conversely, the monthly rainfall is accurate from May to September in almost all regions. During the last third of the year, WRFEH5 produces slight overestimations too, but the biases are not as large as winter and spring ones. In fact, there are regions such as the SE or SW where autumn and early winter precipitation is correctly simulated by WRFEH5. This WRF simulation performs singularly well for the IS regions regarding the annual cycle and indeed deviations are basically negligible in all months. An interesting feature of WRFEH5 annual cycle is that the spring maximum is produced in advance and it is brought one month forward.

In contrast to GCM-driven simulations, the WRFERA run provides excellent results. The shape of the annual cycle is reproduced in most of its details over
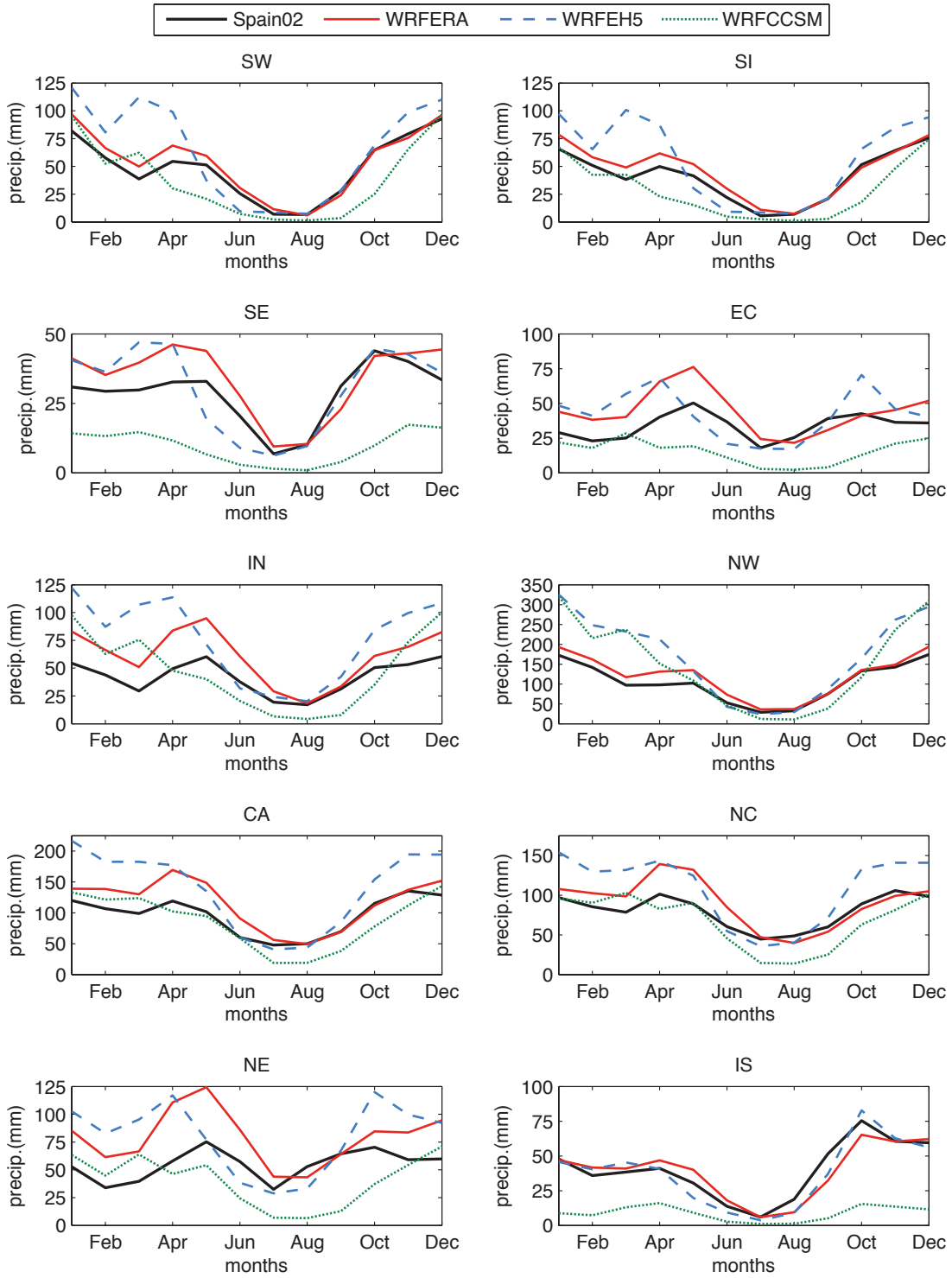
Figure 6.4: *Precipitation annual cycle for the period 1970-1999 for the three WRF simulations (color) and Spain02 (black).*

nearly all Spain. The rainfall from January to May tends to be overestimated, but from June to December, the WRF model performance is strikingly accurate and in many regions the WRFERA annual cycle almost overlap with the Spain02 curve. This is a good indicator of the regional model ability to generate precipitation correctly because it is precisely during the summer and the early autumn that precipitation is mainly controlled by local factors and thus the model parameterization has a larger impact on precipitation processes. However, during the rest of the year, precipitation is strongly driven by large scale (i.e. the boundary data) and thus the RCM physics, still being important, are not as decisive.

6.2.4   Daily precipitation

Different aspects of daily precipitation are explored. Firstly, the contribution of daily events of different intensity to total precipitation and the frequency of occurrence in terms of the percentiles are analyzed. Then, various extreme indices for both the WRF simulations and the Spain02 dataset are calculated to assess the model potentials in this respect.

Frequency of events

The standard procedure to determine the probability of a particular event consists in the analysis of the probability density function (PDF). Precipitation PDF is skewed towards low-intensity events and heavy rainfall are unlikely. Despite the probability disparity between heavy and light precipitation events, their contribution is equally determinant. Small errors in the simulation of upper-percentile precipitation events might affect total annual rainfall significantly. Therefore, if a linear-scale plot is used to represent the PDF of a certain region, errors in the tail of the distribution might not be noticeable in spite of their importance. An alternative is that of using logarithmic-scale plots to highlight the heavy events. Nonetheless, in that case, large errors in light precipitation events are masked which might led to wrong conclusions because they also have an important contribution to total rainfall.

A plot that takes into consideration these caveats is here proposed and consists in representing the accumulated precipitation caused by events of different intensity. As a result, a sort of PDF is obtained, but precipitation amounts replace the events probability (herein referred as pseudo-PDF). This enable the analysis of the entire spectrum of events at once, instead of focusing on heavy or light precipitation separately.

Figure 6.5 illustrates the amount of annual precipitation grouped by events. Therefore, each value represents how much precipitation within a year is caused by events of particular intensity. The last bin accommodates all events exceeding 80 mm/day. These values have been calculated over the entire period (1970-1999) and comprise all grid-points within a region. The results are then divided by the number of years (30) and the number of stations included in each region. Events of intensity below 0.1 mm/day are not considered because observations only record precipitation over this threshold.

A common deficiency of climate models is that they tend to produce too much light precipitation and underestimate heavy events (Bukovsky and Karoly, 2011; DeMott et al., 2007; Gutowski Jr et al., 2003). The first statement is here confirmed, but the second one is not clearly evidenced in our simulations (except for the high-order statistics that are explored later on).

The overall shape of the pseudo-PDF is well captured by WRF, except in the eastern regions (SE, EC and IS), where WRF misplaces the maxima. All simulations assign the maximum contribution to events between 1-5 mm/day, whereas the observations locate the maximum between 5-10 mm.

The WRF model generally produces too many rainfall events from 0.1 to 15 mm/day, apart from WRFCCSM that only overestimates the contribution of events below 5 mm/day. Actually, errors in the occurrence of events within the bins 1-5 mm/day and 5-10 mm/day amount to an important bias contribution, over 100 mm/year in regions such as IN or NC. Along the east coast this errors might be especially important in relative terms because the annual rainfall rates are smaller (SE, EC or IS regions).

The frequency of events that exceed 20 mm/day are accurately described by WRFERA in the majority of regions with minor underestimations, except in the NE that are overestimated and in the IS where they are markedly underestimated. The other two simulations present dissimilar performance. WRFCCSM tend to underestimate extreme events (except for NW region, where all WRF runs present a clearly distinct behavior), whereas WRFEH5 generally return satisfactory results with moderate overestimation. As for the very extreme events (>80 mm/day) two features are remarkable: (1) a clear underestimation in the SE and IS regions and, (2) too many of them in northern regions, particularly for NW and NE.

These characteristics of simulated precipitation regimes are in accordance with previous results. Indeed, areas where both WRFERA and WRFEH5 led to positive seasonal biases show systematic overestimation of almost all types of events.
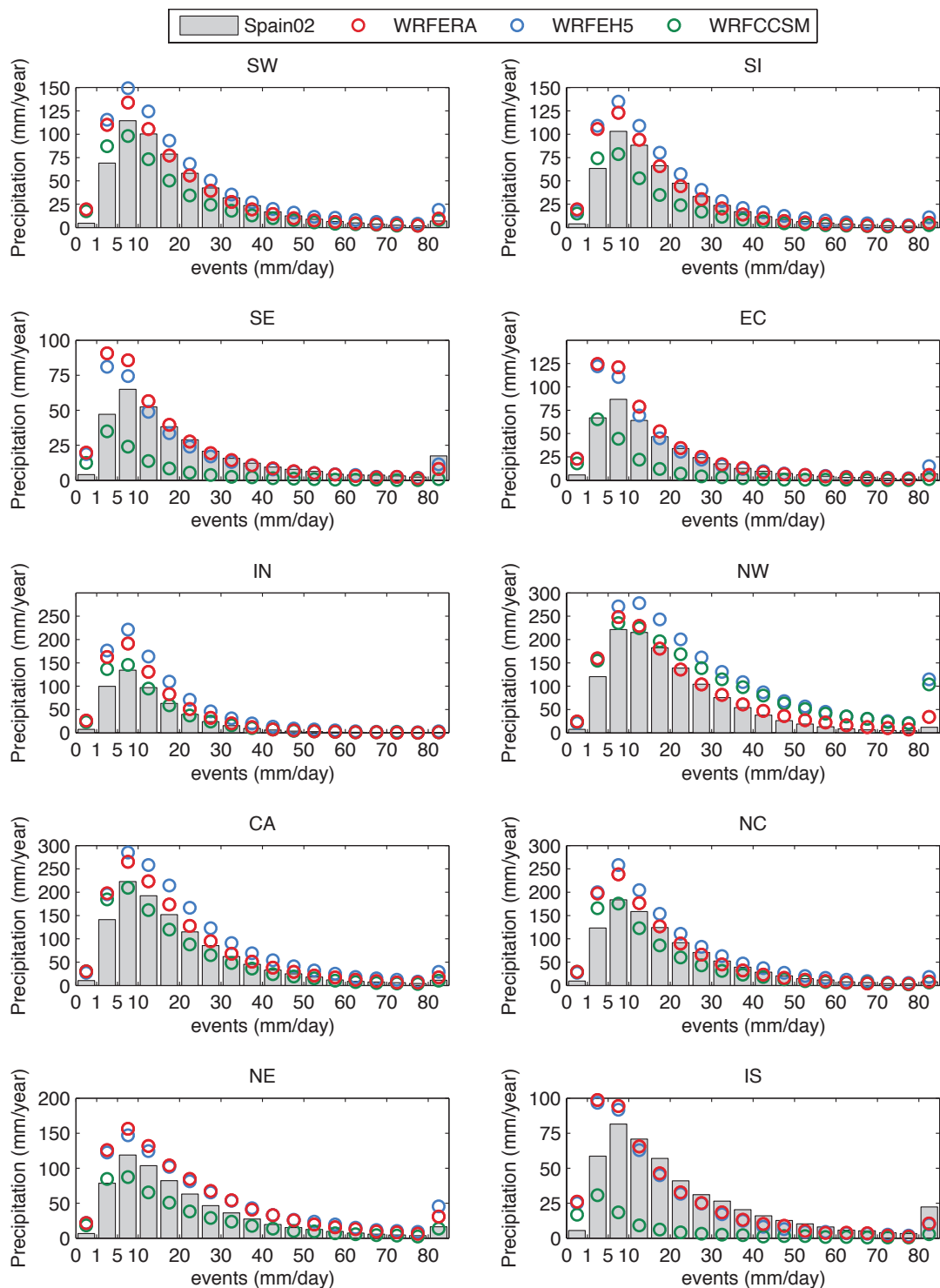
Figure 6.5: *Annual precipitation amounts explained by events of different intensity in the 10 Spain02 regions. The amounts have been calculated over the entire period (1970-1999) and comprising all stations within a region, and divided by the number of years and the number of stations that constitute each region.*

On the other hand, basically the complete range of events are underestimated by WRFCCSM over the Mediterranean regions (SE, EC, NE and IS).

This analysis supports the idea that the problem of the precipitation PDF simulation might not be directly related to WRF deficiencies, but to boundary data conditions instead. In most of the regions, the WRF simulation that was nested in 'perfect boundary conditions' provided fairly good results in terms of the precipitation events intensity. However, in the case of WRFCCSM, rainfall in general is strongly reduced over a large portion of the IP and thus the number of all kind of events is diminished.

In addition to the pseudo-PDF, the standard probability density function is calculated using 1 mm/day bins[1] and ranging from 0-120 mm/day to compute the Perkins Skill Score (SS, Perkins et al., 2007)[2]. Kjellström et al. (2010) found that the bin size might affect the SS values, particularly when events below 1 mm/day are considered. The SS accounts for the percentage of PDF that is shared between the observations and the model runs at each grid point. Hence, the SS ranges from the poorest skill at 0% to a perfect one that would produce a 100% SS. Figure 6.6 illustrates its spatial distribution over the IP for all three WRF simulations.
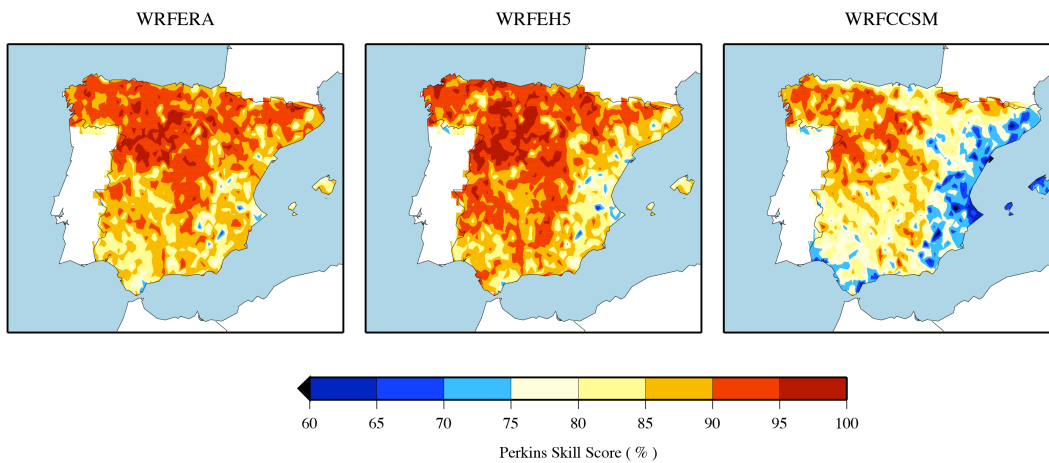
Figure 6.6: *Spatial distribution of the precipitation Perkins Skill Score (%) with respect to Spain02 for WRFERA, WRFEH5 and WRFCCSM simulations.*

The PDF area shared by Spain02 and WRF simulations exceeds 80% in most

---

[1]Smaller (0.5 mm/day bins) where also employed for the 0-1 mm/day range with no significant differences in the SS results.

[2]See Appendix B for a detailed description.

of the cases, except for WRFCCSM that attain more modest values. Precipitation in the southern and eastern regions appear to be the most difficult to model in terms of capturing the PDF, since the lowest values are obtained over these areas. Conversely, higher values are obtained at the northern regions. It should be noted that SS results for WRFEH5 are higher than those of WRFERA in many situations. which represents a noteworthy feature of WRFEH5 simulation, since ERA-40 is largely based on observations and thus should constitute better boundary conditions.

Percentiles of precipitation

Finally, the WRF performance regarding daily precipitation is addressed from the viewpoint of the percentiles. Several percentiles (5th, 50th, 55th, 60th, 65th, 70th, 75th, 80th, 85th, 90th, 95th and 99th) are calculated for each simulation and they are shown in a Q-Q plot. A Q-Q plot displays the modeled percentiles versus the observed ones and thus the line with slope 1 represents a perfect skill. This kind of plot is very helpful to characterize very extreme events because emphasize differences on upper percentiles.

Figure 6.7 comprises 10 different Q-Q plot that represent each of the Spain02 regions. Once again, the largest deviations are found for the Mediterranean regions (SE, EC and IS). The case of the islands is particularly interesting because although the annual cycle was extraordinarily well reproduced by WRFERA and WRFEH5, the regional model fails to capture extreme events. This is an illustrating example of accurate long-term values due to incorrect reasons as a consequence of errors compensation because light events (0-10 mm/day) over this area are markedly overestimated (see Fig. 6.5). The peculiarities of the region, a small area surrounded by the sea, might be one of the causes of these deviations. The west Mediterranean is characterized by strong convective processes that are particularly localized. Since the Balearic Islands are relatively small, it is very likely that the confined downpours are misplaced and thus do not fall over the islands in the model. Furthermore, it is also probable that errors in the SST together with deficiencies in the cumulus scheme lessen the convective processes and prevent the model from capturing these events with all their strength.

Over regions where extreme events are rather generated by large scale, the Q-Q plots show a good agreement between modeled and observed precipitation percentiles (IN, CA and NC), which is due to the fact that large-scale systems carrying significant amounts of water vapor are easier to simulate than localized

and vertical processes. The results obtained for the NE cannot be attributed to a good representation of the large scale because rainfall here has a strong convective component. The adequate simulations of precipitation high percentiles might be explained by other factors that have not been identified.

The magnitude of the WRF percentiles are consistent with the seasonal and annual biases and WRF results range from the lightest extreme events produced by WRFCCSM to the those of higher intensity generated by WRFEH5. Nonetheless, in accordance with what was affirmed before about the common deficiencies in climate models with respect to the PDF, the very extreme events are generally underestimated.

It must be stressed that these events are particularly difficult to simulate for regional models, because they are usually produced under very singular or unstable conditions that the model must capture in detail to produce similar precipitation rates.

Therefore, the results here presented constitute an important point in favor of WRF because despite the errors, it makes possible to approach the study of extreme events, which cannot be addressed with GCMs due to their coarse resolution, not even from a qualitative point of view.

Precipitation extreme indices

Besides the characterization of precipitation extremes in terms of their intensity, it is also interesting to attend to extreme events from an alternative perspective. For example, the fraction of total precipitation that is originated by very extreme events might provide an interesting picture of the rainfall regimes but cannot be characterized by just analyzing percentiles and probability distributions. The Expert Team on Climate Change Detection and Indices (ETCCDI) has defined a set of extreme indices that approaches the subject of extremes from a wider point of view. For instance, the ETCCDI proposes 11 different indices for precipitation that are described in their webpage[1]. Five indices are actually selected from those suggested by ETCCDI. The indices that were singled out are listed in Table 6.1 together with a brief description of them.

The last two indices, CWD* and CDD*, are actually modified versions of the original ETCCDI indices, CWD and CDD, that compute the maximum length of a wet/dry spell over the entire period of study. The modified versions calculate the annual mean of the maximum number of consecutive wet/dry days and computes

---

[1]http://cccma.seos.uvic.ca/ETCCDI/

Figure 6.7: *Precipitation percentiles simulated by three WRF runs vs. Spain02 precipitation percentiles. The grey line indicates a perfect skill and delimits over- and underestimation of the different percentiles. The vertical lines determine the 50th, 75th, 90th and 95th percentiles as reference. The plot extends to the 99th percentile.*

Table 6.1: *Selection of ETCCDI extreme precipitation indices.*

Identifier	Description	Units
R5xday	Maximum 5-day (consecutive) precipitation amount	mm
R10	Number of days when precipitation exceeds 10 mm	days/year
R95T	Percentage of total precipitation above the 95th daily percentile	%
CWD*	Annual mean maximum number of consecutive wet days (> 1 mm)	days/year
CDD*	Annual mean maximum number of consecutive dry days (< 1 mm)	days/year

an annual mean. Although the very extreme character of the original indices is missed in these new indices, they describe the attributes of the local rainfall much better and are much more stable. CWD and CDD are too sensitive to small errors that can split the largest spell in the period. For example, CDD might be dramatically affected by few light events and might show very large variability among similar simulations. By contrast, CWD* and CDD* are calculated every year and thus are more resistant.

Other indices, such as the maximum 1-day precipitation (Rx1day), the number of days that precipitation exceeds 20 mm (R20) or the simple daily intensity index (SDII) were also calculated but results are not shown because they do not add any information to that provide by the previous ones.

The persistence of a certain situation, such as extremely dry conditions, might have the same or even greater impact on the environment than individual events and might be as important as the occurrence of heavy rainfall. This is particularly true in areas within the Iberian Peninsula where precipitation is often concentrated in very few rain events. The 5 indices that have been chosen can be divided into two different classes that describe the high-order statistics (Rx5day, R10 and R95T) and the persistence of both wet and dry periods (CWD* and CDD*). Figure 6.8 illustrates these extreme indices for the Spain02 observational dataset as well as for the three WRF simulations.

The indices that refer to heavy rainfall are in general well represented by WRFERA in both magnitude and spatial distribution. The GCM-driven simulations also capture the spatial distribution correctly, but they fail to reproduce the intensity indices with accuracy.

The Rx5day spatial pattern is defined by low values in the interior plateau
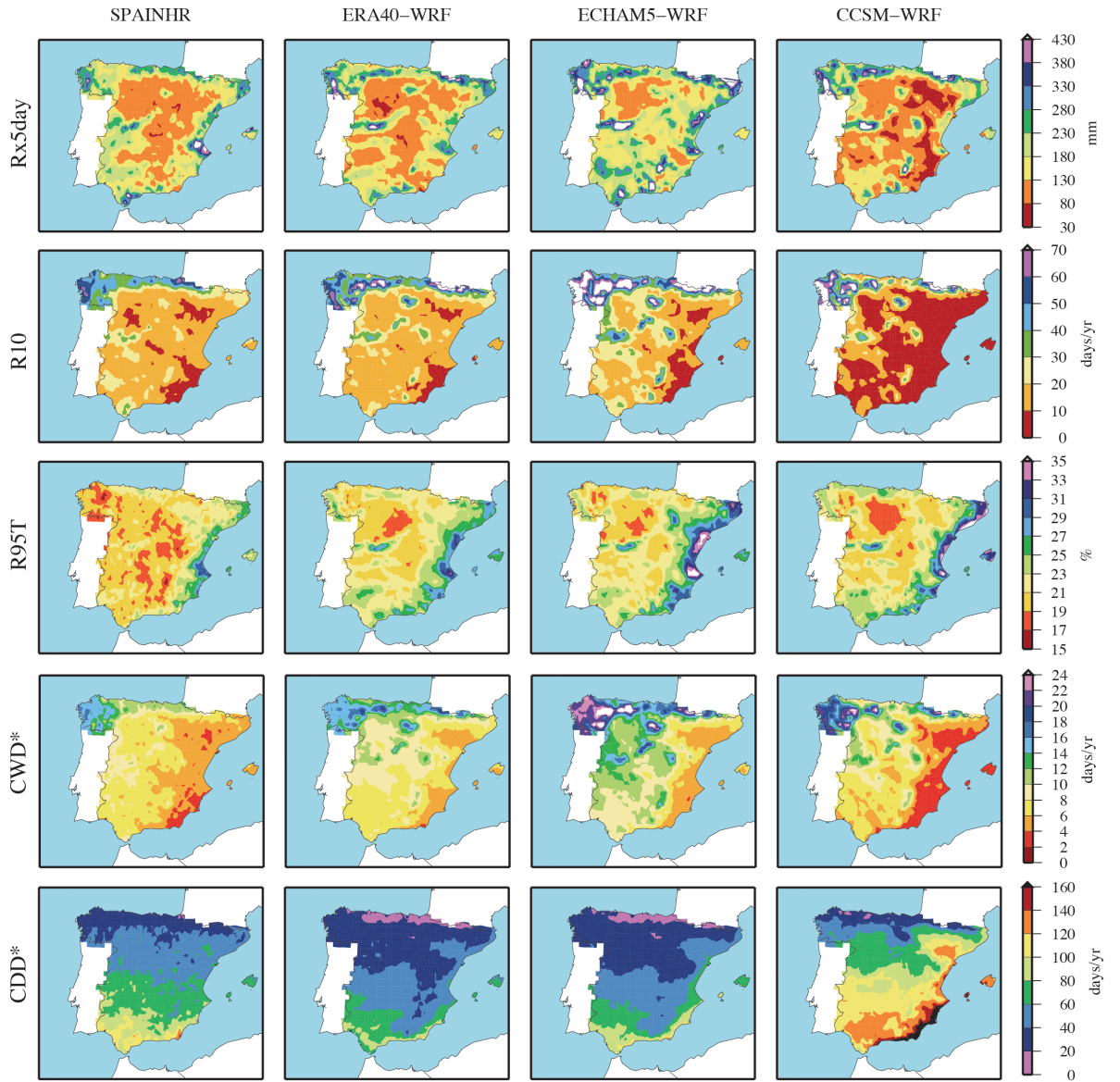
Figure 6.8: *Extreme indices proposed by ETCCDI for Spain02, WRFERA, WRFEH5 and WRFCCSM. The different extremes are displayed by rows (Rx5day, R10, R95T, CWD* and CDD*). White areas indicate off-the-scale values.*

(80-130 mm) and higher ones in the rest of the IP, that are particularly large for mountainous areas, the northwest and the east coast, where the 5-day maximum precipitation reaches 544 mm (out of the scale). WRFERA generates a very similar spatial distribution of Rx5day, but it generally tends to lessen the magnitude of 5-day accumulated precipitation, particularly in areas along the east coast where differences rise up to 100 mm. Some exceptions are observed in the mountains located in the northwest half of the IP, where WRFERA intensifies the index value. The WRFEH5 run tends to enhance the maxima located over mountain systems whereas WRFCCSM is distinguished by underestimation of Rx5day in most of Spain, except for the Central System and Galician Massif.

Regarding the days when precipitation exceeds 10 mm (R10), the broad gradient from the southeast to the northwest is adequately reproduced by WRFERA, with some local overestimations in the northwest mountains. Both WRFEH5 and WRFCCSM simulations compare very well with the observations in terms of the spatial pattern but again does not succeed to produce accurate values in certain areas. For instance, number of days with moderate precipitation is clearly overestimated in the north, where WRFEH5 produces R10 values that reach 122 days/year. WRFCCSM tends to generate lower R10 than the observations over a wide area in the east, which is probably caused by the general underprediction of precipitation, as found in the analysis of the seasonal and annual biases. On the other hand, except for the aforementioned overestimation in the north, WRFEH5 is able to adequately reproduce the R10 index in nearly all Spanish regions and the errors in relation to Spain02 seldom exceed 10 days/yr.

In accordance with the description of Spanish precipitation regimes made at the beginning of section 6.2, heavy rainfall accounts for a large portion of total precipitation in certain region. For example, the percentage of rainfall explained by events over the 95th percentile reaches a maximum over the east coast, where very extreme events explain as much as 30% of total precipitation. All three simulations recreate this feature of climate, but all of them tend to intensify the magnitude of this index in almost the entire region. However, apart from positive deviations in the east coast and the Central System, the three simulations yield values that fall within an error of 2% with respect to Spain02.

Concerning the indices that refer to persistence (CWD* and CDD*), the spread among WRF simulations estimates is more perceptible. The most remarkable difference between WRF and Spain02 is found for the CCSM-driven simulation in terms of the yearly maximum number of consecutive dry days. The WRFCCSM produces more than double CDD* in some locations, such as the

east coast, where it estimates a mean maximum number of consecutive dry days of 227 days/year versus the 110 days/year observed in Spain02. Nevertheless, differences in the CWD* are not as dramatic, and WRFCCSM is able to recreate the values obtained for Spain02, except for slight overestimations in the northwest and underestimations in the east. The WRFEH5 yields similar results to WRFCCSM for CWD*, although the overestimation in the northwest is more pronounced. But it provides much better estimates of CDD*, since the errors barely exceed 20 days/year. The WRFERA simulation produces acceptable results in terms of persistence, in spite of slight underestimations of both CDD* and CWD*. The broad patterns of these two indices adequately captured by all WRF simulations, although the CDD* gradient from north to south is clearly smoothed, whereas the opposite happens with the CWD* gradient from northwest to south east that is intensified. Bearing in mind that RCMs tend to create too much drizzle events and the peculiarity of CWD* and CDD* that measure the persistence of particular conditions, the results obtained with WRF are certainly satisfactory.

6.3   Temperature

The IP is distinguished by a wide range of temperature regimes that are mainly associated to latitude, elevation and distance to the sea. The four large masses that surround the IP exert a strong influence on temperature values. Lowest values are usually linked to continental winds coming form the northeast, whereas the highest ones are mostly caused by air coming from the Sahara desert in the south. The Atlantic Ocean and the Mediterranean Sea also modulates and make temperatures much milder, particularly along the coast.

In fact, large differences are observed in the IP depending on the location with respect to the sea. Mediterranean coast and to a lesser extent the Atlantic coast, tend to be temperate during the winter and temperature variability is relatively small throughout the year. Conversely, most of the IP is dominated by a continental character that induces large annual and daily variability.

Besides the temporal variability, complex topography in the IP generates an intricate distribution of temperature regimes with marked differences between river basins and mountain ridges, not only due to elevation but to orographic cloudiness as well.

The procedure to assess WRF performance in terms of temperature is analogous to that employed for precipitation and annual, seasonal, monthly and daily

values are analyzed. The annual and seasonal values of temperature define aspects of climate that directly affects the species and the crops of the region, because they broadly describe ranges of temperature. The monthly means of temperature help to describe the annual cycle. Finally, daily records are useful to delimit extreme events and possibly identify heat waves and cold spells that have an important impact on the population, the energy consumption or the environment (e.g fire risk).

6.3.1   Annual temperature

A first approach to examine temperature results is performed using the annual mean of both Tmax and Tmin. Annual means for Spain02 temperatures are calculated over the 30-year period to visualize their general distribution across the IP and provide a frame of reference. To compare with observations, WRF annual values are also calculated and the pattern correlation coefficients between maps are computed to measure the similarity in the spatial distribution. It must be emphasized once again that pattern correlation do not take into account biases and only provides information on the spatial variability equivalence between WRF and Spain02.

Figure 6.9 and 6.10 illustrate the mean over the period 1970-1999 for both temperature extremes. The pattern correlation are expressed in brackets.

All three simulations show a remarkable agreement with the observations in terms of the spatial distribution as indicated by the pattern correlation values and minor differences are observed among the WRF runs. Correlation coefficients are slightly higher for Tmax (0.94-0.95) than for Tmin (0.89-0.90).

Overall, WRF seems to accurately capture the broad north-south gradient and the main topographical features that affect temperature. Indeed, the most important basins and mountain ranges are visible in the spatial distribution of the annual means. It seems that WRF provides information at higher detail than Spain02, which might be explained by the finer original resolution of WRF and the methodology used to generate Spain02 that might produce more homogeneous fields. Nonetheless, this remains only a qualitative appreciation because no evaluation of Spain02 is performed in this study.

Looking closer at annual mean maps, it can be observed that WRF generally underestimates both Tmax and Tmin all over the IP. Despite the fact that the temperature spatial patterns are well reproduced, significant errors are manifest in certain areas. The regional model recreates the maximum temperatures in the
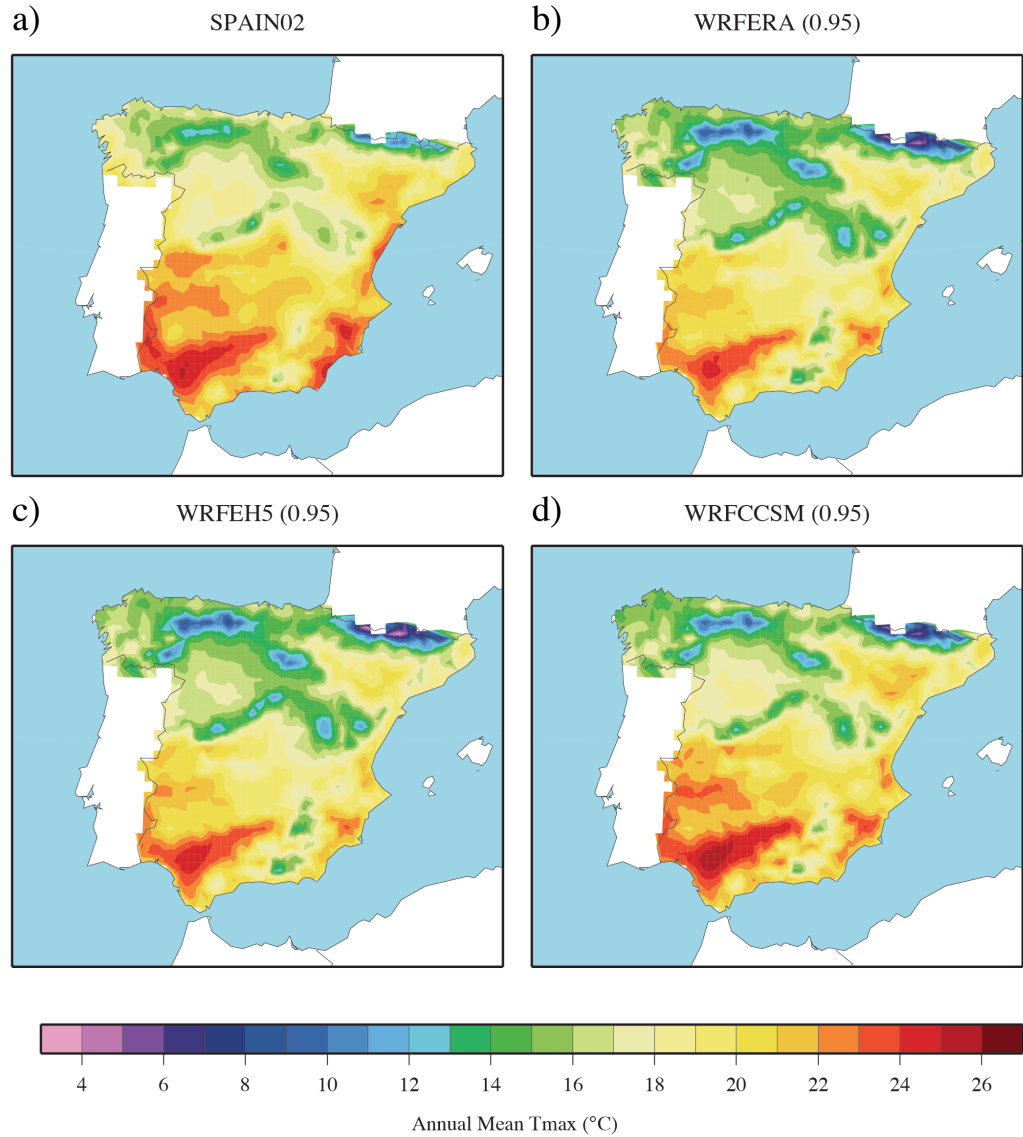
Figure 6.9: *Climatological Tmax annual mean (1970-1999) for the Spain02 dataset (a) and the WRF simulations nested with ERA40 (b), ECHAM5 (c) and CCSM (d). In brackets the pattern correlation between the WRF simulations and the observational dataset Spain02.*

Guadalquivir Basin and the minimum values in the most elevated areas in the north. It also reproduces the mildest temperatures along the Mediterranean coast. Nonetheless, both temperature extremes are smaller for WRF than for Spain02 in most cases. Deviations between the model and observations are analyzed next
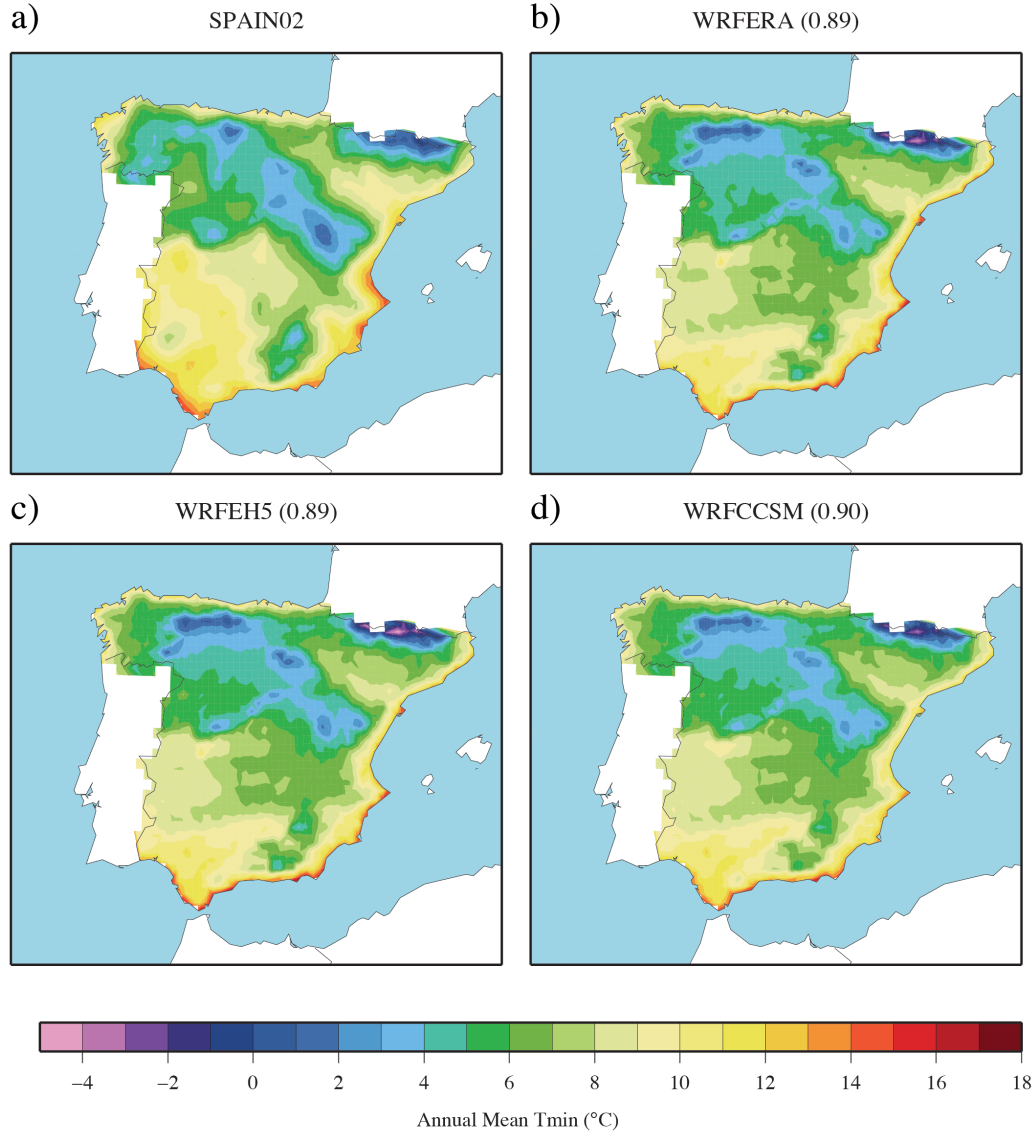
Figure 6.10: *As Figure 6.9 but for Tmin.*

on a seasonal scale.

6.3.2 Seasonal temperature

Differences between WRF and Spain02 long-term means of temperatures are studied with the seasonal bias. Figures 6.11 and 6.12 show the seasonal and annual bias of WRF simulations with respect to gridded observations.

Seasonal Tmax means (Fig. 6.11) tend to be systematically underestimated by WRF when using ERA-40 as boundary conditions. A very similar behavior is observed for WRFEH5, with deviations that range from -2.0°C to -1.0°C in most of the locations. The WRFCCSM leads to slightly different results and biases range from -1.0°C to 1.0°C over a large portion of the IP. It provides the largest coverage with bias between -0.5°C and 0.5 °C. Indeed, WRFCCSM does not show a clear tendency in the seasonal Tmax deviations as the other two simulations do, and positive and negative bias occur simultaneously.

There is no evident spatial pattern of biases in none of the simulations, although it seems that WRF estimates tend to be better in the valleys whereas the most negative deviations are found in the mountains. In particular, all simulations produce very significant deviations over some mountainous areas, specially in the highest ones (Pyrenees and *Sierra Nevada*, in the Baetic System). Biases are more pronounced during the spring and summer for WRFERA and WRFEH5. WRFCCSM embodies the exception once again because there is no season when biases are clearly more prominent.

Concerning minimum temperature (Fig. 6.11), spatial patterns of biases are even more heterogeneous and none of the simulations show a plain tendency. Centers of substantial overestimation alternate with areas of underestimation. However, there does not seem to be a clear reason that explains their location. The land-use category assigned to each grid point and differences in elevation between Spain02 and WRF (degraded to 0.2°) have been analyzed and they do not provide any clue with respect to the Tmin biases spatial distribution. In general, most intense overestimations are placed in mountainous regions whereas negative deviations mainly occur over the flat areas such as the river basins or the internal plateaus. Nonetheless, there are a number of exceptions such as the eastern Galician Massif or the western Pyrenees, where Tmin is underestimated on average. Except for the summer and for certain localized areas where biases are larger, the Tmin biases fall in the range from -2.0°C to 2.0°C, which is certainly not negligible.

In contrast to Tmax, there seem to be larger differences among seasons for Tmin, particularly in the case of WRFCCSM, for which winter Tmin are broadly overestimated and summer Tmin are overall underestimated. On the other hand, differences between WRF simulations are almost negligible and indeed, annual biases are nearly identical for all three runs. The effect of the selected PBL, that was the same for all simulations, is probably playing an important role, since Tmin is often reached during the nighttime when the lower atmosphere is
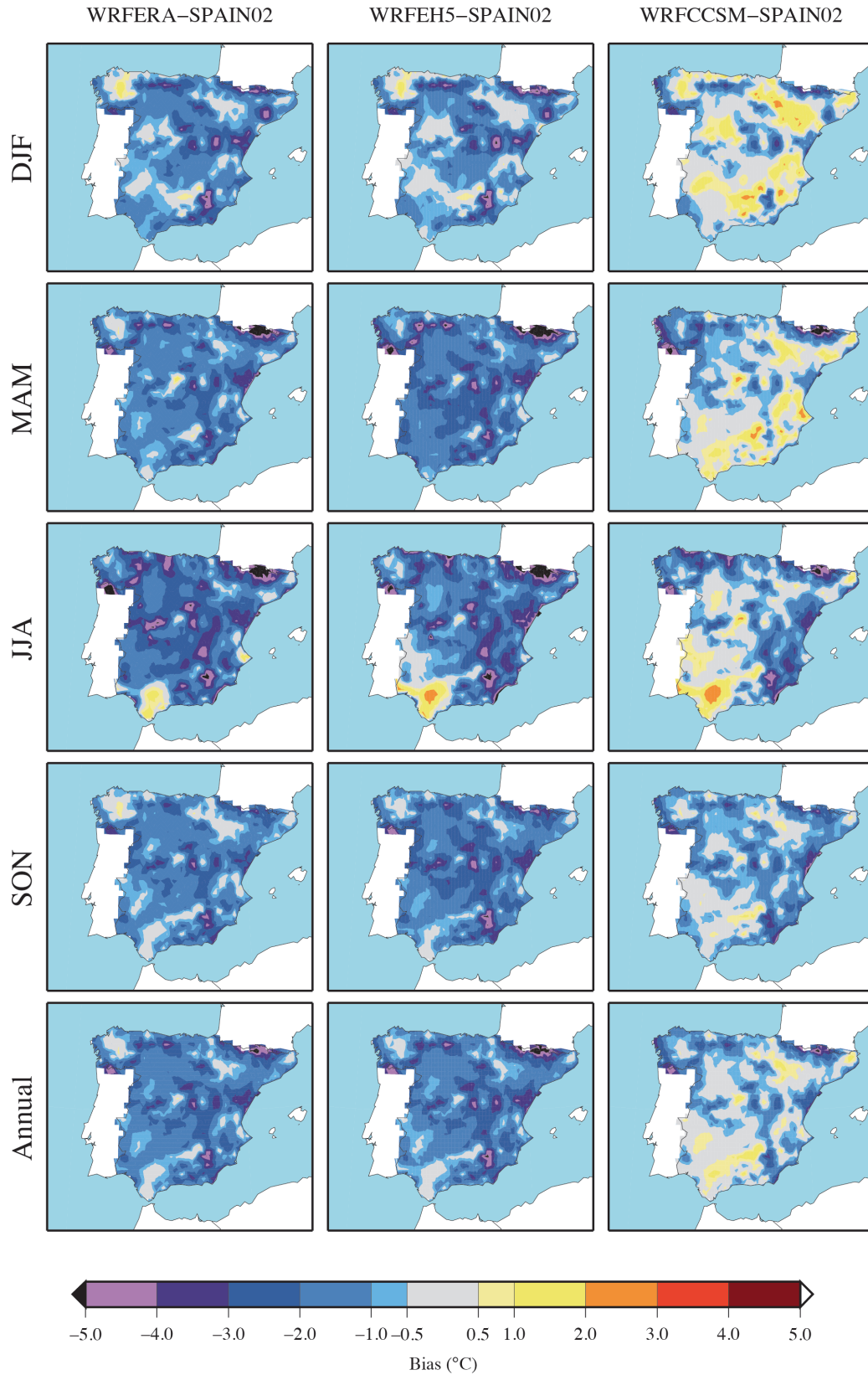
Figure 6.11: *WRF seasonal and annual Tmax bias with respect to Spain02. In columns, the WRFERA, WRFEH5 and WRFCCSM runs. In rows, the seasonal (DJF, MAM, JJA and SON) and the annual biases.*

strongly stratified.

As mentioned above, both Tmax and Tmin seasonal biases are far from being negligible and they must be considered carefully. Nevertheless, temperature errors in a particular grid-point are mainly affected by bias, which is probably the least troublesome error since it is potentially correctable. Despite the fact that Spain02 is a gridded daily dataset and thus more comparable to WRF outputs than *in situ* observations, it does not yet represent the exactly same scale as WRF (20-km Spain02 resolution vs. 10-km WRF original resolution). In other words, although the *representation error* is considerably reduced by comparing WRF with Spain02, there are still scale differences between them and the biases cannot only be attributed to model deficiencies. In addition, Spain02 might be subjected to interpolation errors because the temperature network was not as dense as for precipitation, which give rise to areas with very few data.

Assuming that biases are inherent to the WRF, whatever their source is, they should be constant through the years, and thus a comparison of future and present estimates would cancel them. As a consequence, projected changes for future would be unaffected by biases up to a large extent.

6.3.3   Monthly temperature

The temperature at monthly scales is examined through the annual cycle. The annual cycle is one of the most important features that characterizes the climate in a region. For precipitation, the location of the maxima and minima monthly rainfall along the year was analyzed, but in the case of temperature this is somehow meaningless. Owing to temperature dependency upon the Earth inclination, the evolution of temperature in the course of the year follows a similar pattern in the entire northern hemisphere, with a maximum during the summer and a minimum during the winter. Even a fairly simple model is able to simulate these variations and here the magnitude of monthly Tmax and Tmin is addressed instead.

The annual cycle cannot be displayed for all the grid points and the generation of averaged cycles for the different climate divisions provides a comprehensive picture of the model performance over the entire region. Accordingly, Figure 6.13 shows the annual cycle for monthly means of Tmax and Tmin over the 8 temperature regions obtained for Spain02 (Fig. 3.8).

The spread of WRF simulations in terms of the annual cycle is almost insignificant and only in particular regions the differences are slightly appreciable.
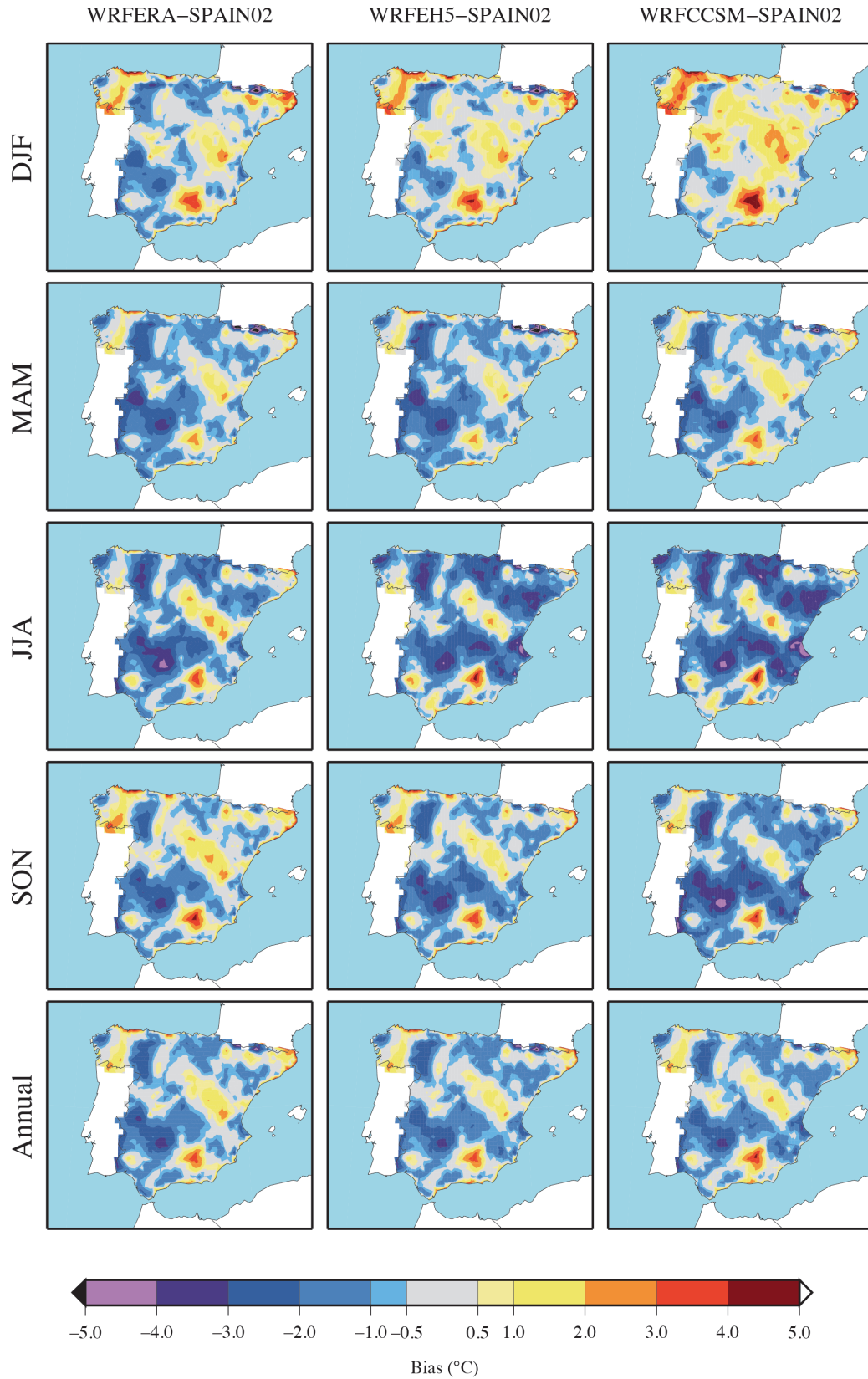
Figure 6.12: *As Figure 6.11 but for Tmin.*
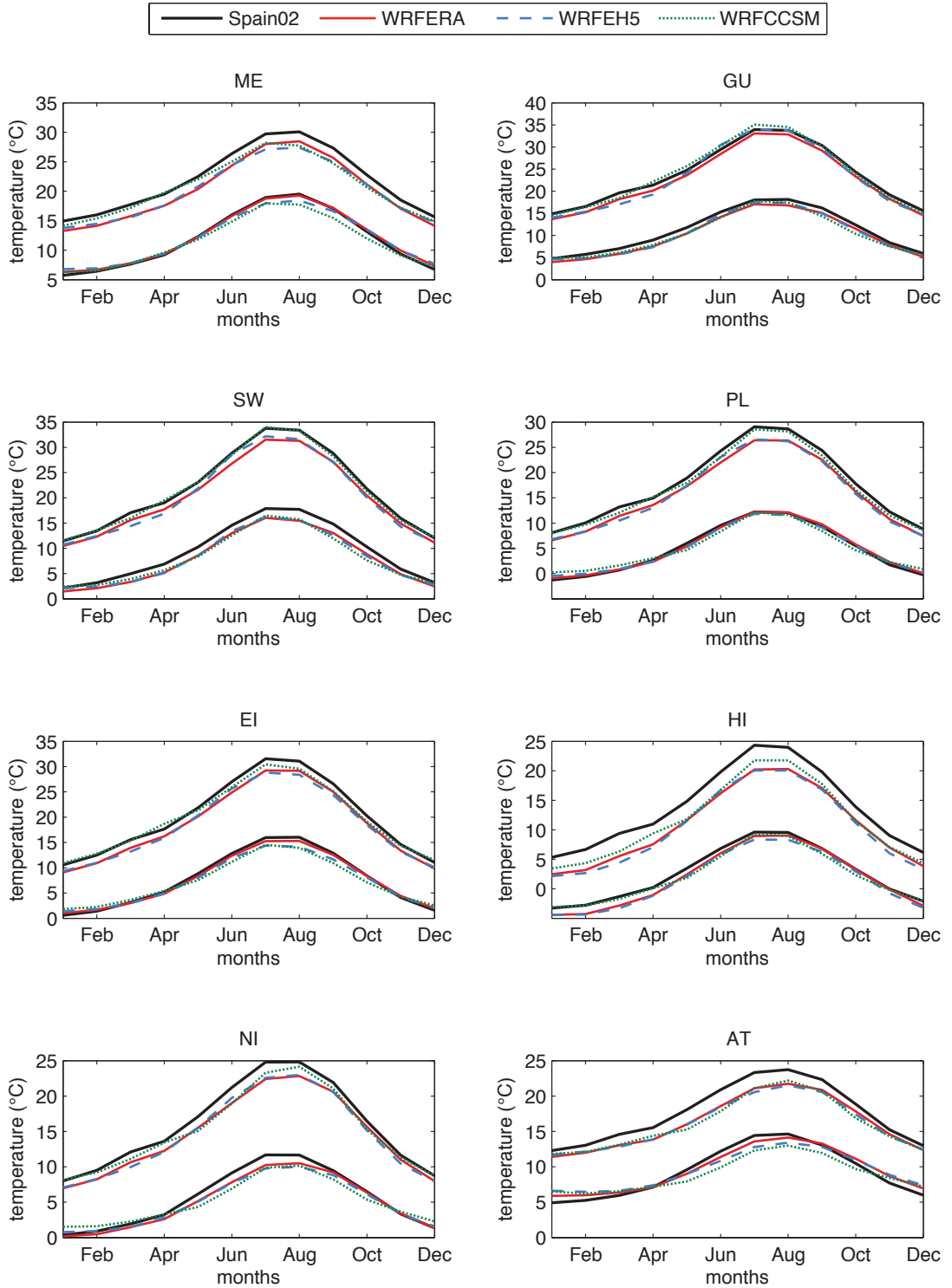
Figure 6.13: *Tmax and Tmin annual cycle for the period 1970-1999 for the three WRF simulations (color) and Spain02 (black).*

In general, the Tmin yearly evolution is better captured than the Tmax one. For instance, WRF produces Tmin monthly means that are vey close to Spain02 values in the majority of regions, whereas deviations of WRF Tmax monthly means with respect to observations are much more evident.

In particular, the HI region that encompasses high-altitude areas shows the largest errors for Tmax annual cycle, which is consistent with the results obtained for seasonal biases. The deviation in this region is nearly constant during the year, which indicates that the error source might not be related to atmospheric processes but to elevation deficiencies. In fact, just as the seasonal biases were not found to be related to elevation or land-use category factors, the elevation differences between the model and the Spain02 topography were noticeable for the HI region and might be a cause of these errors.

The coastal regions (ME and AT) are also affected by significant biases in Tmax. In the AT regions the biases are larger during the spring and summer and almost no deviations are found for the autumn and winter. In the case of ME region, differences between WRF and Spain02 are stable for almost all months, except for WRFCCSM that appear to perform better during the first half of the year. Errors in the coastal regions could be partially explained by the fact that conversion from 10-km resolution to 20-km resolution could include sea points in the interpolation and enhance the SST contribution to coastal temperatures. In fact, the influence of the sea is observed in the flattening of the annual cycles and the diminution of monthly temperature range (difference between Tmax and Tmin).

By contrast, in two of the major river basins, the Guadalquivir and Ebro valleys, included in the GU and EI regions respectively, the model shows the best agreement with observations. This supports the idea that differences in the elevation of the model and Spain02 might be important, because the river basins are mostly flat and homogeneous.

6.3.4   Daily temperature

Daily values of Tmax and Tmin are examined by comparing the PDFs and certain percentiles calculated for WRF simulations and Spain02.

Tmax and Tmin PDFs

Unlike precipitation, daily events of temperature equally contribute to long-term values and it is possible to analyze the complete spectrum without the

risk of weighting particular events in excess. Therefore, no consideration on the magnitude of the events is made and only the probability of an event to occur is computed.

Figure 6.14 illustrates the PDF for daily Tmax over the 8 temperature regions. All temperature events corresponding to grid points within a region have been computed together to calculate the PDF. The negative deviations in the seasonal means observed before are manifest here too. For instance, in most of the region, the PDF is displaced towards lower values. Although the shift of the curve, the shape is overall well reproduced. This is particularly evident for the HI region, where despite the prominent deviation of the curve, the PDF pattern obtained for WRFERA is very similar to observations.

In the case of minimum temperature there is also a slight displacement towards lower values in the southern regions (SW, GU, ME) but no clear tendency for the rest (Fig. 6.15). Errors are more significant in the central part of the distribution than for Tmax. The Tmin PDFs are actually somehow straightened and probabilities are diminished for the extremes in most of the regions, whereas central values probabilities are largely overestimated, particularly for the GCM-driven simulations. Besides the Tmin variability reduction, the distribution seems to be somehow skewed towards lower values as observed in regions EI, SW, NI and especially in PL, which essentially are the regions situated in the central IP.

In theory, temperature probability is distributed according to a gaussian distribution. However, these two figures show that both Tmax and Tmin tend to have a bimodal distribution instead. This behavior is generalized for Tmax and appears to be more marked in the certain regions (ME, GU, SW, PL and EI). As for Tmin, the bimodal shape also exists but not for all the regions. For instance, NI, HI and AT PDFs are very close to a gaussian. The bimodal distribution is associated to marked seasonality with rapid transitions from cold to warm periods embodied in the two modes. This feature of Iberian temperature is broadly captured by WRF but tends to be exaggerated (e.g. Tmax in AT and ME, and Tmin in ME, SW and GU).

Despite the mentioned deviations, both Tmax and Tmin PDFs are fairly reproduced by WRF, which represents a major advantage with respect to current climate change information. It is already well-known that global warming signal will not only be reflected in the means but also in the standard deviations. Bearing in mind typical GCMs resolution, this is an aspect of climate change that could not be explored with global models. Nonetheless, this analysis evidences that WRF is able to supply with valuable and reliable information in this respect.

Regarding differences among WRF simulations, it is worth mentioning that GCM-driven simulations tend to generate less Tmin variability than WRFERA as inferred from the PDF spread. They also seem to be slightly further skewed to lower values. Nevertheless, these differences are not substantial and GCM-driven runs also provide satisfactory results in terms of the PDF.

The similarity of two PDFs can be measured using the Perkins Skill Score (SS). The SS is computed here at each grid point and using 1°C bins to generate the PDF (from -25°C to 50°C). The SS represents the probability shared by observed and simulated PDFs (see Appendix B) by specifying the area shared by both distributions. Figure 6.16 and 6.17 illustrate the SS values all over the IP calculated for Tmax and Tmin respectively. The SS reach high values for the entire region ($> 75\%$), except for very limited areas where it drops to values ranging from 65% to 75% (e.g. northwest).

In general, WRFERA and WRFEH5 produce very similar values in terms of both Tmax and Tmin, although their spatial distributions are different. Coversely, WRFCCSM temperature probability distribution is much closer to observations for Tmax. Over a large portion of the IP, WRFCCSM and Spain02 Tmax SS takes values over the 90% of the total probability, whereas in the case of Tmin, SS barely exceeds that threshold.

The spatial patterns of SS do not seem to be directly affected by factors such as topography or distance to the sea and there must be other elements that might have an important effect on the simulated temperature PDF (e.g. land-use, soil properties).

Temperature percentiles

An additional way of examining the distribution of the PDF is that of focusing on the percentiles, and more specifically on the uppermost and lowest quantiles to explore the distribution tails. A comprehensive analysis of the percentiles can be performed using the Q-Q plots, where the WRF temperature percentiles are plotted versus the observations percentiles.

Figures 6.18 and 6.19 contain the Q-Q plots in the different regions for Tmax and Tmin, respectively. The plot covers nearly entire spectrum of events from the 0.1^{st} to the 99.9^{th} percentiles. Several percentiles (0.1^{st}, 1st, 5th, 10th, 25th, 50th, 75th, 90th, 95th, 99th and 99.9^{th}) have been calculated to create this plot for each region.

The model shows an outstanding ability to reproduce the Tmax percentiles.
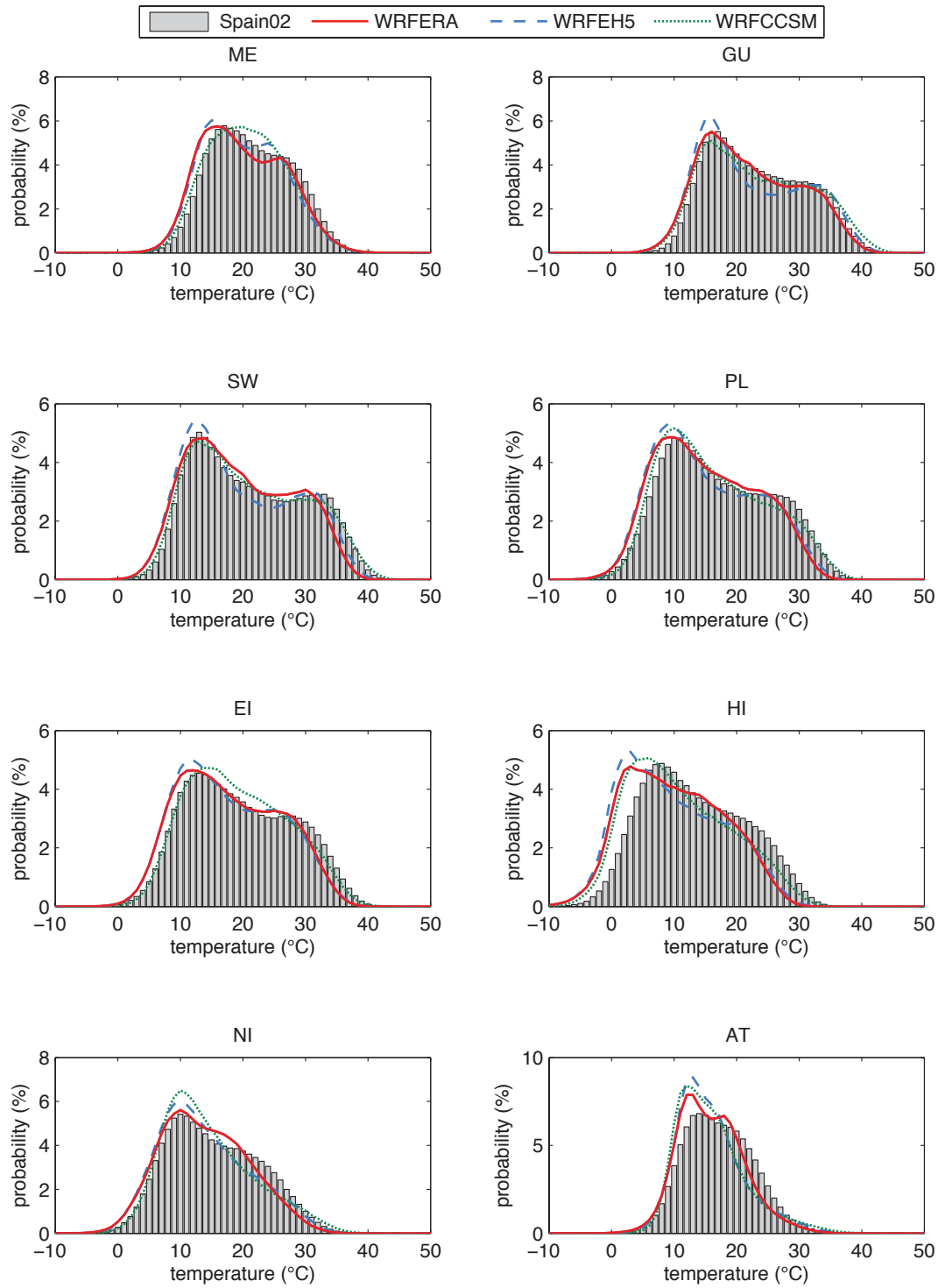
Figure 6.14: *Probability Distribution Function for daily Tmax calculated over the entire period (1970-1999) displayed by regions for WRF simulations (color) and Spain02 (black).*
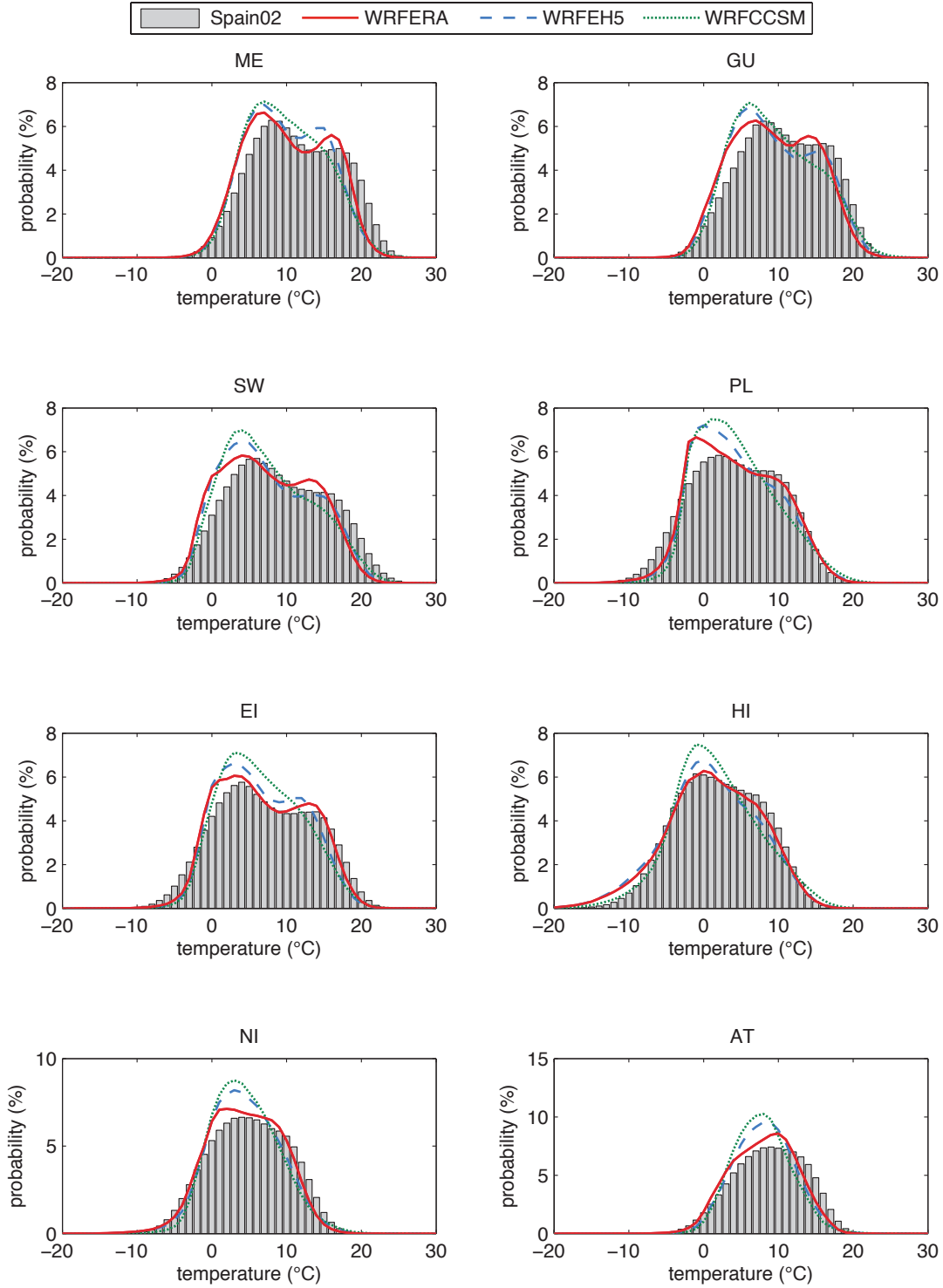
Figure 6.15: *As Fig. 6.14 but for Tmin.*
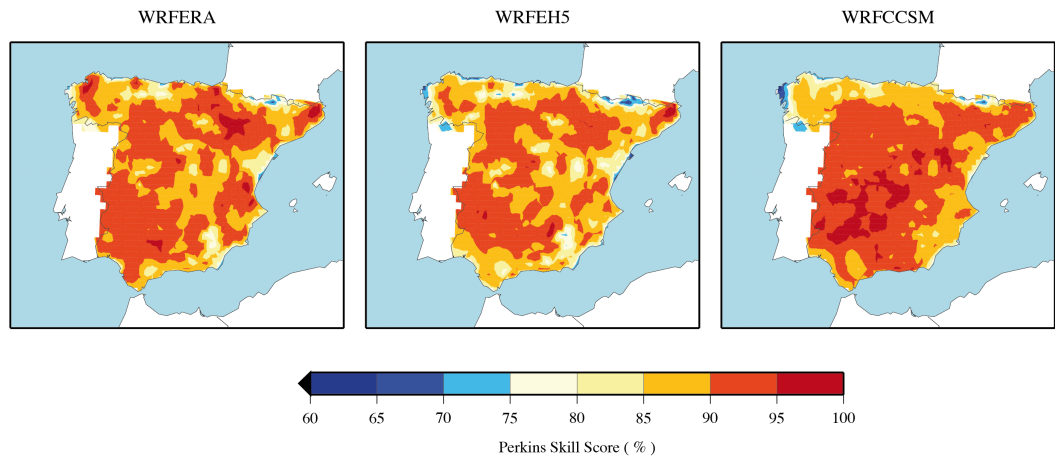
Figure 6.16: *Spatial distribution of the Tmax Perkins Skill Score (%) with respect to Spain02 for WRFERA, WRFEH5 and WRFCCSM simulations.*
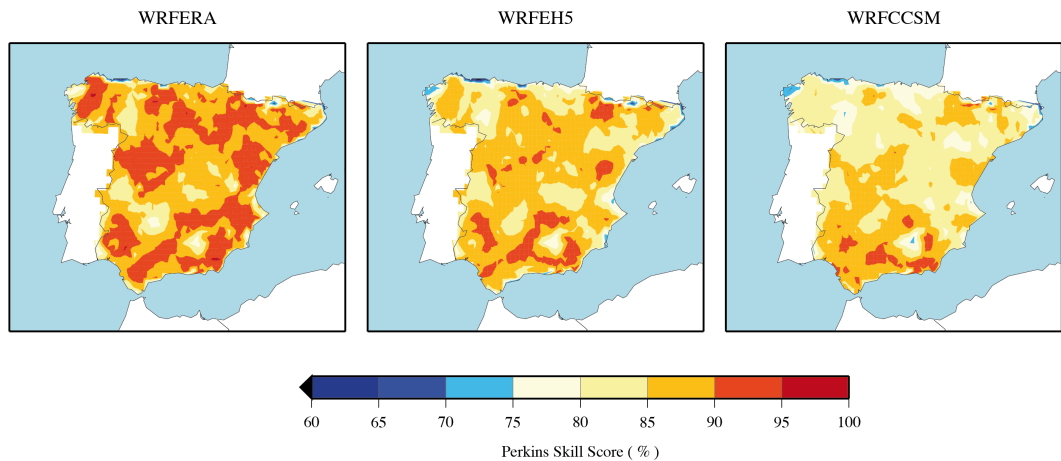
Figure 6.17: *As Fig. 6.16 but for Tmin.*

For instance, the WRF curves are very close to the perfect-skill grey line in most of the climate divisions. Even the most extreme events are accurately described in many regions (e.g. GU, EI, NI or SW). Nevertheless, some noticeable deviations are also obtained for other regions such as HI, where Tmax percentiles are systematically underestimated, or AT, PL and NI, where the upper percentiles are not accurately captured by WRFERA. By contrast, the WRFCCSM provides very good results even in the aforementioned areas and reproduces very well the percentiles at most of the regions, even those events beyond the 99th
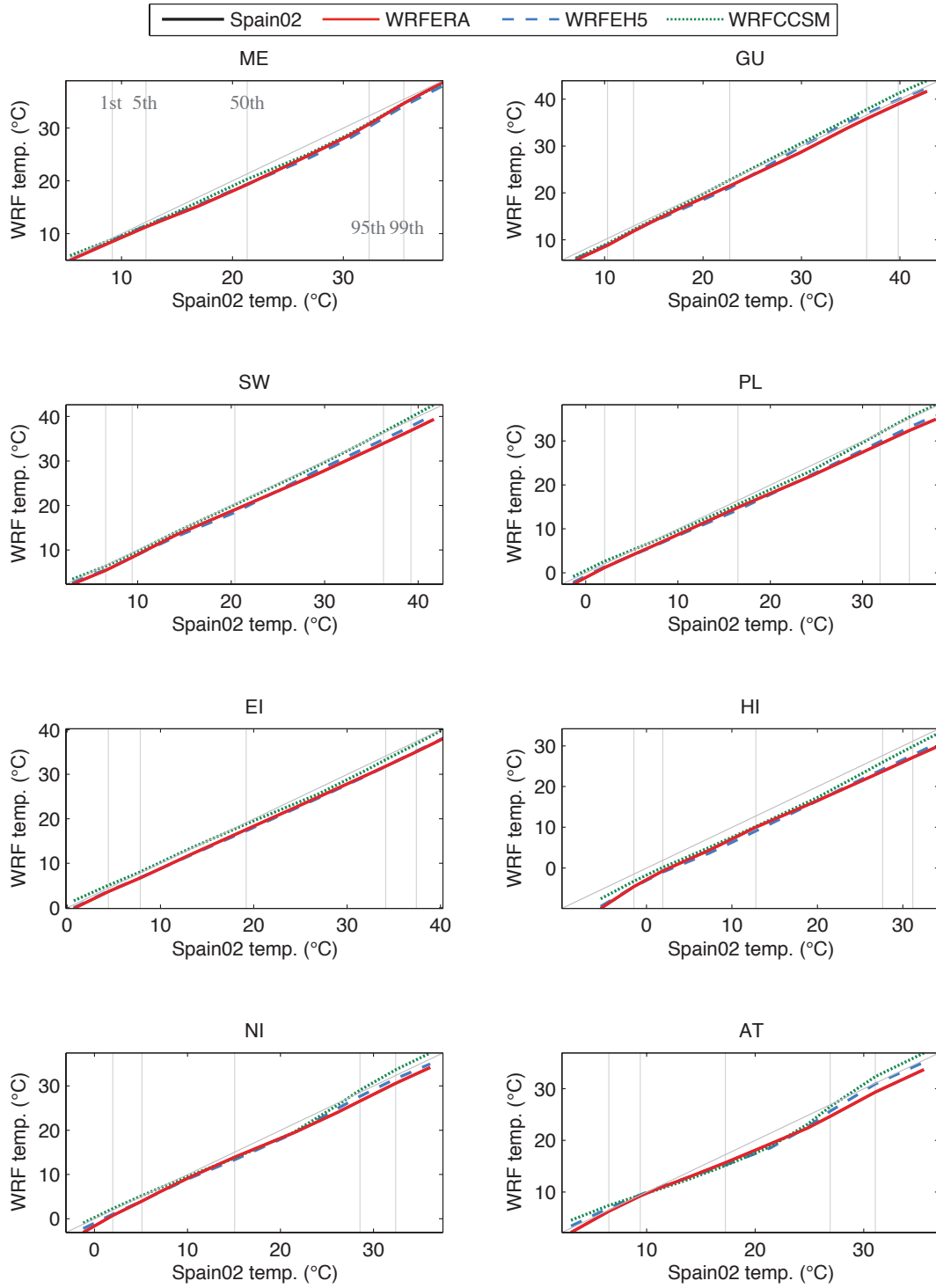
Figure 6.18: *Tmax percentiles simulated by three WRF runs versus Spain02 Tmax percentiles. The grey line indicates a perfect skill and delimits over- and underestimation of the different percentiles. The vertical lines determine the 1st, 5st, 50th, 95th and 99th percentiles as reference. The plot extends from the 0.1st to the 99.9th percentile.*
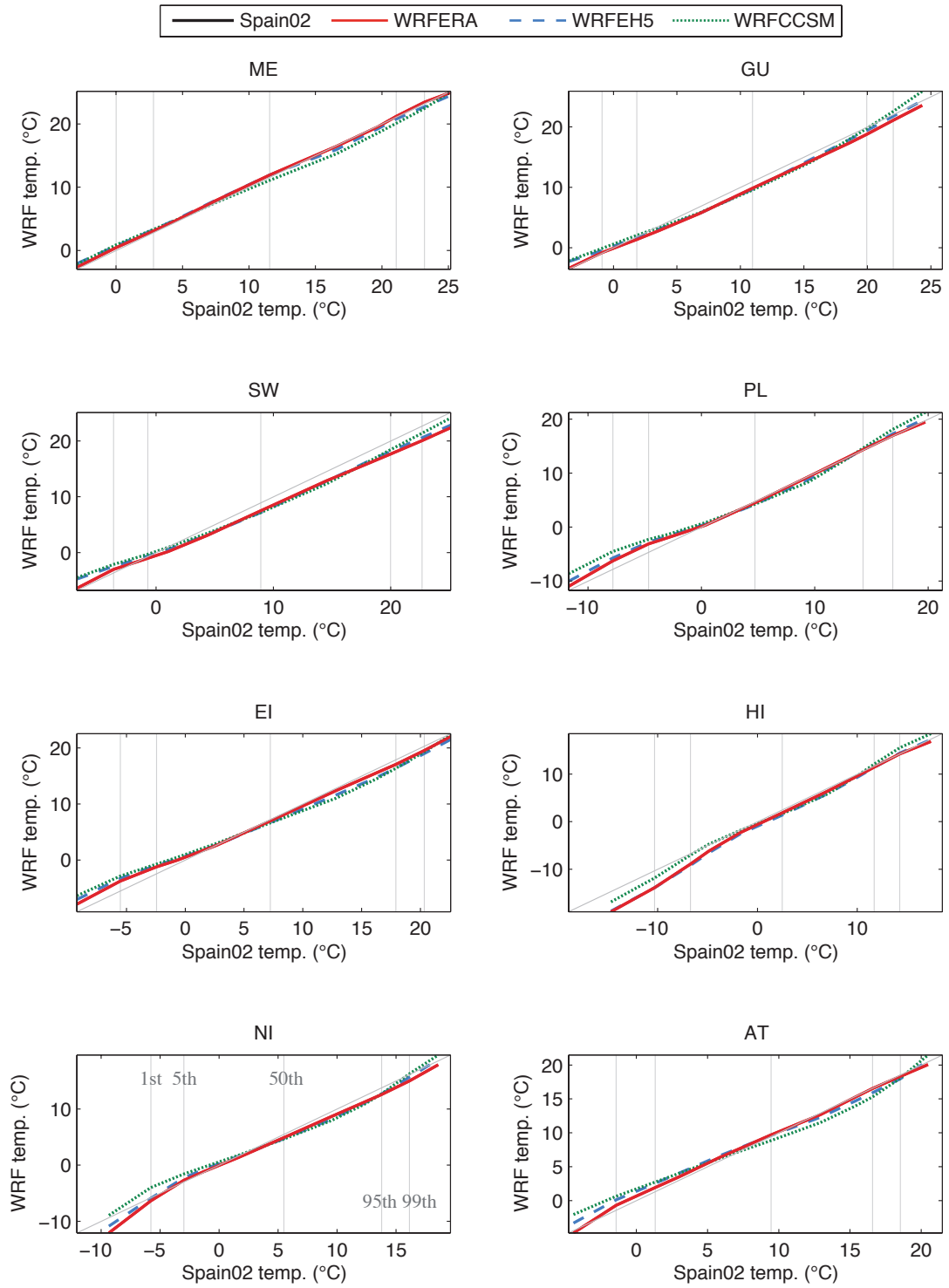
Figure 6.19: *As Fig. 6.18 but for Tmin.*

percentile. Actually, most of the differences between WRFCCSM and Spain02 are smaller than 1.0°C in absolute terms, except for the HI and AT regions where the deviations are larger (up to 2.7°C).

Regarding Tmin, WRF also provides good results, but differences with respect to Spain02 are more significant. In the regions that include highest locations (HI and NI), the very low Tmin values are exaggerated by WRF, although the percentiles are correctly captured from the 5th percentile upwards. For the rest of the regions, the WRF lowest percentiles are closed to the observed ones and if anything, WRF tends to overestimate them. Nonetheless, these differences are insignificant in most cases. In fact, the lowest percentiles (0.1^{st}, 1st and 5th) fall within a exceptionally good range in many regions (1.0°C), although some substantial errors are found in other areas (EI, NI and especially HI). Particularly accurate are the WRF percentiles over the ME and GU regions, where the curve nearly follows the perfect-skill line (grey).

With respect to the different WRF simulations, the spread among them for Tmin percentiles is very small and no run seems to generally provide better results. WRFERA might capture better very low values at some regions (SW, PL, EI or AT) but the other percentiles are almost reproduced identically by all WRF simulations.

Overall, the differences between simulated and observed percentiles are of the same order of the deviations in the mean values (biases), which speaks very well of the WRF potentials in describing the upper-percentiles. The ability of WRF to correctly simulate temperature percentiles is of major importance and represents one of its most relevant strengths because it enables the study of future climate from a point of view that could hardly be approached otherwise.

Temperature extreme indices

To further examine the WRF ability to simulate the extreme events, an excerpt of the set of extreme indices proposed by ETCCDI has been used. The ETCCDI defines 16 indices that characterize Tmax and Tmin extremes occurrence and persistence. Other aspects of temperature extremes are also described by these indices such as the daily range of temperatures or the length of the growing season.

The WRF evaluation is limited to a few key indices that can be divided into two groups: (1) threshold extreme indices that measure the number of days when temperature is above or below a certain value and (2) those do not rely on prefixed

thresholds. They are succinctly described in Table 6.2. Additional details on the indices can be found in the ETCCDI webpage.

Bearing in mind the mean values of maximum temperature in the region, a supplementary threshold index, hot days (HD), has been included and consists in the average number of days per year when Tmax exceeds 35°C, which characterizes the extreme warm conditions during the southern-Iberian summer much better that the standard summer days (SU, 25°C), which rather embodies moderate conditions.

In the table below, two indices are defined using percentiles (WSDI and CSDI). The percentiles are calculated for each calendar day (e.g. June 6th) and using a 9-day window centered in each calendar day (e.g. June 2th-10th). As a result, a sort of annual cycle is obtained for the percentiles at each grid point. These thresholds are calculated for observations over the reference period (1970-1999)[1] and used to evaluate the model.

Table 6.2: *Selection of ETCCDI temperature extreme indices.*

Identifier	Description	Units
FD	Number of frost days (Tmin<0°C)	days/year
ID	Number of icing days (Tmax<0°C)	days/year
SU	Number of summer days (Tmax>25°C)	days/year
TR	Number of tropical nights (Tmin>20°C)	days/year
HD	Number of hot days (Tmax>35°C)	days/year
WSDI	Warm spell duration index. Annual count of days with at least 6 consecutive days when Tmax > 90th percentile of the corresponding calendar day	days
CSDI	Cold spell duration index. Annual count of days with at least 6 consecutive days when Tmin < 10th percentile of the corresponding calendar day	days

Temperature extremes, and particularly the percentile-based ones, are very sensitive to biases. The analysis of temperature extreme events without considering the biases would yield useless information because the occurrence and persistence of anomalous conditions would be masked by systematic errors. Namely, whenever the WRF estimate is biased the number of days that exceed both the

---

[1]It should be noted that ETCCDI uses the reference period 1961-1990 and 5-day windows whereas the reference period here is 1970-1999 and the windows span 9 days. Changes in future extreme indices will be referred to this new reference period too.

10th and the 90th will be strongly affected, and the number of consecutive warm or cold days will change dramatically. These differences are not related to the model ability to reproduce situations that are particularly exceptional, but a simple displacement towards colder or warmer conditions.

Therefore, in order to study the model ability to simulate the temperature extremes a bias-correction strategy has been adopted, using the annual Tmax and Tmin biases at each grid point (Figs. 6.11 and 6.12). It must be admitted that not all temperatures are equally affected by the same error (annual bias), but categorizing the errors depending on the temperature magnitude or other considerations on the model mean deviation with respect to observations would not be acceptable because the WRF time series would be too much altered. Namely, further adjustments of the model outputs would fake the WRF ability to represent extremes and the evaluation could be distorted in favor of the model. The bias-correction strategy is certainly the least intrusive approach that enables the generation of meaningful information with respect to extremes.

Moreover, the future projections are compared with the present simulations to determine possible changes. Namely, the biases are assumed to be constant in time and thus will be implicitly removed in the analysis of changes.

The ETCCDI extreme indices obtained for Spain02 and WRF simulations are illustrated in Figures 6.20 and 6.21. The former displays the parameters that are based on standard thresholds (FD, ID, SU, TR and HD) whereas the latter includes the rest of indices (WSDI and CSDI).

The bias-corrected results from WRF provide excellent results in terms of threshold temperature extremes indices. In fact, the model-obtained indices show an exceptional agreement with those from Spain02 (Fig. 6.20). Not only the spatial pattern is accurately captured by WRF, but the magnitude of these indices are very close to the observed values.

The number of both ID and TR is very low over a large portion of the IP. In the southern and coastal areas the ID index does not go beyond 0.2 days/year, whereas only in the southwest, the Ebro valley and along the Mediterranean coast the TR index is over 10.0 days/year. Conversely, the spatial variety of FD and SU indices is much wider. The HD index reach as much as 57.0 days/year at points in the Guadalquivir river basin. In general, the number of very hot days is considerably high over significant areas in the southwest. These features of temperature extreme indices are remarkably reproduced by all WRF simulations and none of them seems to outperform the others.

The outstanding performance of WRF in terms of temperature extremes once
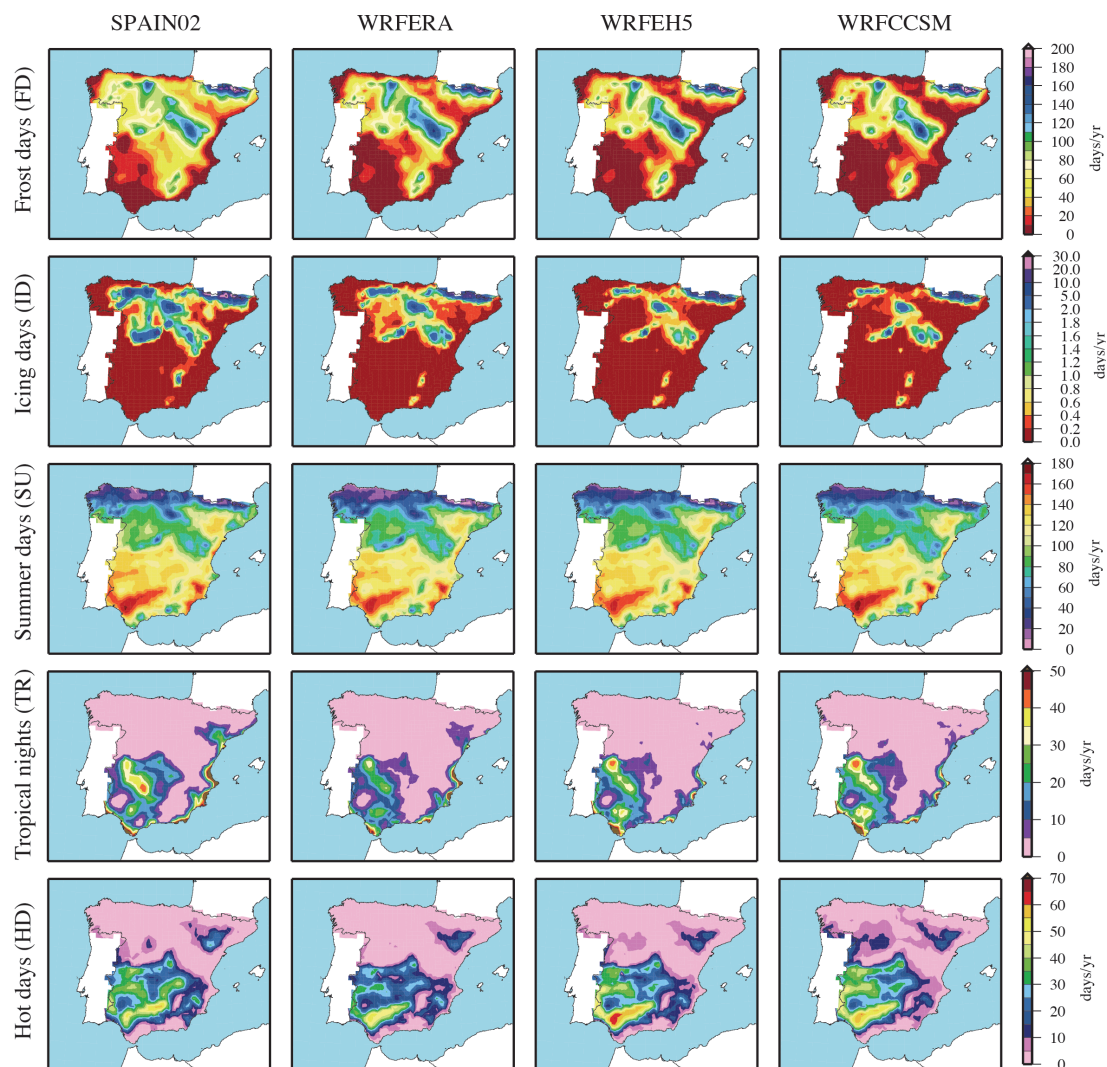
Figure 6.20: *ETCCDI temperature extreme indices (in rows) based on thresholds for Spain02 and WRF simulations (in columns) for present climate (1970-1999). The customized Hot days (HD) index is also shown. All indices refer to the average number of days per year that exceed a threshold.*

the outputs are bias-corrected manifest that although the WRF estimates are prone to errors with respect to observations, they are often caused by a simple shift of the series towards colder or warmer values, which means that they are potentially correctable to obtain very accurate simulations.

Nonetheless, there are other extreme indices, especially those referring to persistence that are not represented as adequately as the threshold extreme indices.
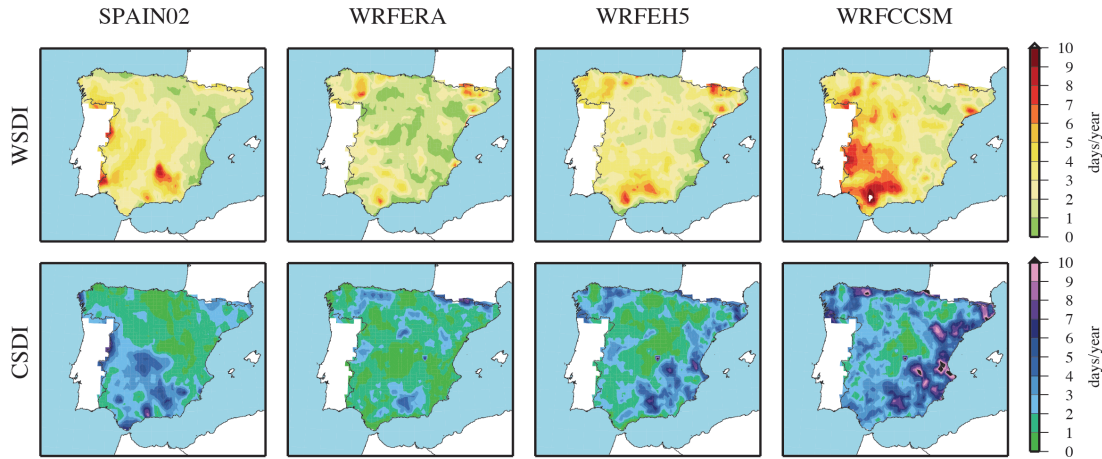
Figure 6.21: *Persistence (WSDI and CSDI) ETCCDI extreme indices for Spain02 and WRF simulations for present climate (1970-1999). White and Black areas represent out of the scale values.*

Figure 6.21 displays the two indices that measure the frequency of cold and warm spells (CSDI and WSDI, respectively) . Although the spatial patterns for WRF and Spain02 do not match, the magnitude of CSDI and WSDI are of the same order in all maps. It should be noted that both CSDI and WSDI do not refer to extreme absolute values. In other words, warm spells do not necessary take place during the summer and anomalous warm conditions in the winter might count as warms spells too. The same occurs for CSDI. Therefore, these indices do not say anything about the season when the spells take place. Instead, they characterize particularly warm or cold periods with respect to the temperature percentiles at that moment of the year. The persistence indices are a sort of cumulative extreme conditions and thus are extremely difficult to simulate because they are highly affected by deficiencies in the model timing with respect to observations (which is clearly a minor problem from a climate point of view), since the percentiles are calculated using Spain02, and also because frequent small errors might cause great deviations in their estimation. This was already observed for precipitation and is here confirmed for temperature.

6.4   Estimation of errors and correction

In principle, the climate change projections provide information about the changes that might be expected. Namely, the future climate simulations are compared with the present ones and only the differences are analyzed. This

approach is usually called the 'delta-change' method and is basically based on the assumption that the biases in the present and future simulations will cancel each other (Räisänen, 2007; Rummukainen, 2010), because the GCMs are assumed to more reliably simulate relative changes rather than absolute values (Hay et al., 2000). The 'delta-changes' normally ends by adding these changes to the observed variables.

However, the studies concerned about the impact of climate change are usually carried out using impact models, which cannot be run with the information contained in the observations. They normally require a large set of variables that has to be available over the entire domain. In that case, the outputs of the models are employed to feed the models and thus they must be corrected (Dosio and Paruolo, 2011; Piani et al., 2010; Rosenberg et al., 2010).

It is not the purpose of this Thesis to evaluate the impact of climate change, but rather to provide information at fine scales of the projected changes. Nonetheless, the climate change projections here presented might be used in the assessment of the impact and therefore the caveats and issues related to the outputs correction must be reviewed.

The estimation of the model errors and their projection into the future is certainly not a trivial task. Besides the model deviations with respect to the present climate, the future projections are prone to a number of uncertainties, as detailed in Sec. 2.1.2. The model evaluation should enable the determination of margins of confidence by calculating the errors between simulated an actual present climate conditions. It would make possible to correct the model outputs, but it would not be enough to ensure that the corrected future outputs are valid. To be rigorous, even the observations that are used to validate the model are subjected to errors that should also be accounted.

In any case, different approaches to the correction of biases have been proposed (Ainslie and Jackson, 2010; Boé et al., 2007; Terink et al., 2010) aimed at different applications. In fact, the procedure to correct the model outputs also depends on the variable (e.g., temperature, precipitation, wind) and the studied impact (e.g., river flows, crops, fire and flood risk). The methodologies range from a simple bias correction to adjustments of the PDF.

Temperature tends to be distributed normally, although not exactly, and hence the correction is easier to perform. Actually, a straightforward bias correction based on differences in the mean values was applied to Tmax and Tmin in the analysis of extreme events (Sec. 6.3.4) with satisfactory results. Such a correction was adopted because of its simplicity and its reasonably good results. However,

precipitation distribution is much more complex and the bias correction must be more elaborate. Common approaches use a correction factor that varies depending on the parts of the distribution that are explored (Ines and Hansen, 2006) or adjusting the PDF to a theoretical distribution (Piani et al., 2010). Nonetheless, they are fairly complex and impose additional assumptions that might be too restrictive within the climate change framework. For that reason and bearing in mind the objectives of this Thesis, precipitation was not corrected here.

However, along these pages, a number of uncertainties have been identified and the errors of the model have been highlighted. Therefore, the information required to perform the model outputs corrections is supplied and future research on the field of climate change impact could take advantage of the validation here conducted.

6.5   Conclusions from WRF evaluation

The results obtained from the model evaluation are summarized in this section. A number of temporal scales have been analyzed to determine whether WRF is able to reproduce present climate over the Iberian Peninsula.

A primary benefit of using RCMs to produce climate change information is that their resolution should allow a good simulation of variability and high-order statistics. Even though the boundary data have not been evaluated in this chapter, considering their very coarse resolution and results for the limited region of southern Spain (see Chapter 5), it cannot be expected that GCMs capture events that are usually very localized and short, especially in the case of precipitation.

By all means, the major advantage of using WRF is the possibility to study the climate at scales that GCMs were not design to. The WRF model provides information at such degree of detail that it is possible to assess not only possible future changes in the means but in the distribution tails as well. Despite the fact that WRF estimates produce non-negligible errors with respect to observations over certain regions or time scales, it is overall able to generate features of climate that are missed in global models and thus represent an extremely valuable tool to study the regional implications of climate change.

Precipitation is fairly well captured at all timescales with the exception of some seasonal biases found over particular regions principally during the spring. The analysis of the outer domain SLP revealed that these deficiencies are largely induced by boundary data misrepresentation of large-scale circulation as a result

of a wrong location and intensity of the main pressure centers. Nonetheless, the regional model also contributes to seasonal deviations since the spatial patterns of the biases are very similar between the GCM-driven simulation in spite of their differences in the SLP. As already noticed for other models, WRF tends to produce too much light-to-moderate precipitation whereas the heavy rainfall events are slightly underestimated. The most remarkable features of WRF performance are its ability to correctly distribute precipitation all over the IP and the good skill shown with respect to the extreme indices. The former indicates that WRF is efficient at differentiating the climate regimes within the region and incorporate the effect of small topographical features that GCMs are unable to capture. The latter is a sign of the model ability to reproduce events that are usually short and localized.

Regarding temperature, the model errors with respect observations are mostly characterized by systematic deviations, as observed in the seasonal analysis. The biases in temperature are potentially correctable and are the less troublesome errors to deal with. Leaving aside these biases, temperature is accurately simulated at all timescales. The factors that determine the temperature distribution across the IP do affect WRF temperature spatial distribution too. Indeed, coastal areas, mountains and river valleys are evidently distinguished in the model temperature outputs. WRF simulates the temperature PDF very well and produces most of the distribution features, such as the bimodality at certain regions. But undoubtedly, the most striking aspect of the model performance in relation to temperature refers to the percentiles and the extreme indices. They are exceptionally well reproduced by WRF in nearly all situations considering that these are the very furthest part of the distribution tail. This is a crucial benefit with respect GCMs because it allows the study of the extreme events, a facet of climate that has been barely explored and still remains to be carefully addressed.

The spread between WRF simulations is generally larger for precipitation than for temperature, for which all runs perform almost equally. Precipitation is much more sensible to the model configuration and thus minor differences in the boundary data might bring about significant divergence in precipitation amounts. The WRFERA run provides remarkably good estimates for both variables which suggests that WRF is able to reproduce the Iberian climate if it is driven by the appropriate boundary data. For the other two cases, WRFEH5 and WRFCCSM, despite the fact that the boundary conditions are far from being perfect, the model performance is acceptable for long-term means and noteworthy with regard to upper-percentiles.

Despite the limitations documented in this chapter, the WRF adequacy to simulate climate over the IP has been addressed and it has been proven that it is a remarkably useful tool to create high-resolution climate change projections over this area.

Chapter 7

Future climate (2070-2099): the projected changes

> The scientist does not study nature because it is useful; he studies it because he delights in it, and he delights in it because it is beautiful. If nature were not beautiful, it would not be worth knowing, and if nature were not worth knowing, life would not be worth living.

> J. H. Poincaré

This Chapter is devoted to analyze and discuss the high-resolution WRF projections of climate change scenarios over the IP. The changes resulting from the increase of GHGs concentration in the atmosphere are here examined at regional scales in terms of precipitation and temperature. The procedure is analogous to that followed for the present climate evaluation in Chapter 6.

To put WRF results in context, an introductory section describes the IPCC projected changes for the Mediterranean area. Some details about the WRF future climate simulations and a description of the analysis conducted to determine the changes are included in this preliminary section. Afterwards, precipitation and temperature changes projected by WRF are presented to thoroughly address the global warming impact on Iberian climate.

7.1   Introduction to projected changes for the IP

7.1.1   Overview of IPCC projections for the Mediterranean Area

Before analyzing the WRF outputs for future Iberian climate, let us summarize the IPCC AR4 (Christensen et al., 2007a) projections for the Mediterranean area to set a backdrop to compare with. As stated in the IPCC AR4, warming in Europe is projected to continue at a rate somewhat greater that its global mean. In the Mediterranean, warming is expected to be larger during the summer, when variability –from seasonal to daily– is also *likely* to increase due to reduced soil moisture and increased land-sea temperature contrast. Highest maximum temperatures seem to increase more than the median daily maximum temperature. Conversely, a more moderate warming is projected over south-western Europe during the winter. Regarding extreme events, heat waves are *very likely* to increase in frequency, intensity and duration, and the number of frost days is *very likely* to decrease.

The Mediterranean area will be *very likely* affected by significant decreases in precipitation. The most consistent and largest decreases (in percentage) occur in summer. Nonetheless most models project decreases in precipitation for the rest of the seasons as well. The decrease in precipitation together with enhanced evaporation during the spring and early summer is very likely to lead to reduced summer soil moisture in the Mediterranean region (Douville et al., 2002; Wang, 2005), which might constitute a positive feedback for summer warming.

The projected changes with regard to precipitation extremes over the Mediterranean region do not seem to show a clear tendency. Extreme short-term events may either increase due to the increased water vapor content in the atmosphere or decrease due to a decrease number of precipitation days which could make heavy precipitation less common. Long-term extreme events, which includes anomalous months or years, are expected to follow the changes in mean precipitation more closely than are those in short-term extremes.

However, the IPCC also asserts that there are still significant quantitative uncertainties with regard to the projected changes over this region, particularly for precipitation. The high-resolution WRF simulations might help to provide further insight to this respect and quantify the changes at finer scales over the IP.

7.1.2   Description of the future climate simulations

A set of high-resolution 30-year simulations have been completed with WRF to characterize future climate (2070-2099). A range of possible scenarios is here covered to include different possible pathways in the evolution of the climate system. In particular, three different SRES scenarios (B1, A1B and A2) with different rates of GHGs emissions are considered. In addition, two GCMs (ECHAM5 and CCSM) have been selected to drive the regional model to explore changes with different boundary conditions in order to take into consideration their associated uncertainties.

Although WRF configuration has already been described in Chapter 4, a brief summary of model setup is presented to recall the most relevant parameters:

- Two one-way nested domains are employed to describe the region under survey. The finer domain covers a region that extends 1350 km by 1350 km at a spatial resolution of 10 km with the purpose of generating high-resolution climate change information.

- The vertical is divided in 35 levels distributed in such a way that resolution is higher near the surface and decreases towards the top of the atmosphere, located at 50 hPa.

- A weak spectral nudging is switched on in the outer domain and only for the scales larger than 1300 km (wavenumber 3). All input variables are nudged above the PBL except for relative humidity that was not nudged at all.

- The parameterization configuration BA3 (BMJ for the cumulus, ACM2 for the PBL and WSM3 for the microphysics, see Table 5.1 for the full list of explored combinations) with Noah LSM and CAM3.0 radiation schemes was adopted.

The set of future simulations is composed of 6 different runs (3 SRES scenarios x 2 GCMs). The nomenclature to refer each of the simulations used in this chapter is shown in Table 7.1

7.1.3   Description of the analysis

Just like for the present climate simulations, the future climate is examined through precipitation, Tmin and Tmax estimates from WRF. The strategy to

Table 7.1: *Acronyms of the GCM-driven simulations*

Driving Data	ECHAM5	CCSM
20th Century	WRFEH5	WRFCCSM
B1 Scenario	WEB1	WCB1
A1B Scenario	WEA1B	WCA1B
A2 Scenario	WEA2	WCA2

assess the changes in these variables consists in comparing each of the GCM-driven future simulations with the corresponding present climate run, using the so-called 'delta-change' method. As detailed before, the delta-change method is based on the assumption that biases in present and future simulations should cancel each other, giving rise to smaller error in the relative changes than in the present climate simulations (Hay et al., 2000; Räisänen, 2007).

As in previous analysis of WRF outputs, it is much more practical to group the outputs by regions to show certain results such as the changes in the annual cycle. Grouping the outputs by regions facilitates readability and makes possible to supply with an overall picture of the results. The regions used in this chapter are identical to those used in the model evaluation that were generated with the Spain02 dataset. A nearest-neighbor interpolation from Spain02 grid to WRF grid (land grid points only) is applied to define the regions over the latter .

A number of parameters are calculated to study potential changes in both long-term means and daily values. It should be noted that these parameters have been computed for the entire IP, including Portugal, and the Balearic Islands. Bearing in mind that due to data availability the evaluation of the model was limited to Peninsular Spain (and the Balearic Islands for precipitation), results for the rest of the region should be interpreted with caution because the model ability to represent climate features of these areas has not been determined. Nonetheless, the model performance is likely to be similar over Spanish IP and Portugal, and hence it has been decided to show WRF projected changes over the whole IP to enable, at least, a qualitative analysis. In any case, WRF results are only discussed over those areas where it has been evaluated even if WRF estimates are shown over a larger region.

7.2   Precipitation Changes

Precipitation plays a paramount role in the development and preservation of the natural environment in a region. Furthermore, there is basically no facet of human activity that is immune to changes in precipitation and water availability. Potential changes in rainfall frequency and intensity would be particularly dramatic over regions where the economy is strongly based on agriculture and tourism such as the IP.

It is thus evident that among the effects of global warming, the quantification of precipitation changes is a priority to estimate the impact of climate change over the IP. The IP is already under an intense hydrological stress and indeed, water management is one of the main sticking points in national politics. Therefore, an exhaustive study of future precipitation changes is crucial to design efficient mitigation and adaptation measures.

7.2.1   Changes in annual mean precipitation

All simulations project a substantial decrease in annual mean precipitation for the period 2070-2099 with respect to 1970-1999 over nearly the entire IP under all three scenarios (Fig. 7.1). Very few exceptions are found in the central Mediterranean coast, where slight increases that barely exceed 10% are projected by WEB1 and WCA1B. Figure 7.1 also shows the areas where these changes are significative using a two-sided Student's t-test (see Wilks, 2006 for details) with margin of confidence of 95%. Contrary to the usual criterion of indicating significative areas with black dots, it has been here chosen the opposite to enhance clarity and a black dot flags a grid-point where the null hypothesis (means are equal) cannot be rejected, and thus the projected change is not statistically significative.

Simulations driven by both GCMs show a similar response to GHGs atmospheric concentration and precipitation presents a progressively larger decrease as the GHGs concentration increases. The ECHAM5-driven simulations yield -18% for the B1, -20% for the A1B and -27% for the A2 on average over the IP. Whereas simulations constrained by CCSM indicates that precipitation diminishes -23% for B1, -31% for A1B and -42% for A2 on average over the IP. Therefore, annual mean precipitation decrease is projected to change within a range of -18% to -42% from the most moderate WEB1 to the most severe WCA2.

Focusing on the regional scales of the changes, there are noticeable differences

Figure 7.1: *Projected changes for annual mean precipitation over the IP. In rows are displayed the three different SRES scenarios (B1, A1B and A2). In columns, the simulations driven by ECHAM5 and CCSM. The changes are expressed in percentage: difference between future and present annual mean precipitation with respect to the present annual mean. Areas with black dots indicate that changes are not significative according to a two-sided Student's t-test with a 95% of confidence. Please note that, contrary to what is usual, black dots indicate non-significative changes instead of significative ones.*

within the IP. The most affected regions by a decrease in precipitation are the mountain areas and more specifically, the Baetic System in the south, where rainfall decrease is expected to range from about -30% to about -65%. This region is systematically (all 6 simulations) projected to be the most affected by climate change in terms of precipitation. For the rest of the mountainous areas (Cantabrian Range, Central System, Iberian System and Sierra Morena) precipitation decrease is also noteworthy (over -30% in most of the runs).

On the other hand, minor decreases or even a slight increase is found for the east coast in all simulations, although the extension of these areas varies from run to run. It should be also noted that according to the Student's t-test, most of these projected changes over the Mediterranean coast are not statistically significative (black dots). Other areas where changes are not significative are found in the Northern Central Plateau and at the south of the Central System for ECHAM5-driven simulations (WEB1 and WEA1B) and regions in the southwest and central IP for simulations constrained by CCSM (WCB1).

There are also regions where dissimilarities between different scenarios or driving data are almost negligible, such as the Ebro Valley, the Balearic Islands or the Atlantic coast. In fact, some projections over these areas are not significative in many simulations (western Atlantic coast in WEB1 and WEA1B; Ebro Valley in WCB1 and WCA1B; and the Balearic Islands in all simulations nested in CCSM)

The annual mean projected changes provide an interesting overview of the future climate, but further detail is desirable. The seasonal changes are analyzed to examine the behavior of precipitation in different moments of the year. It is also important to address seasonal changes bearing in mind that the region is subject to strong variability along the year and precipitation in different seasons are likely to evolve diversely under climate change conditions.

7.2.2   Changes in seasonal precipitation

Precipitation changes have been calculated individually for all four seasons. Figures 7.2 and 7.3 illustrate precipitation changes at seasonal timescales. A contrasting behavior is manifest among the different seasons for all simulations. In line with the IPCC projections for the Mediterranean area (Sec. 7.1.1), precipitation decreases are generally more pronounced during the summer, whereas in winter both minor decreases and marked increases exist. In particular, all simulations predict increases during the winter in areas along the east coast that even exceed 100% (out the scale) in very localized regions: northeast (WCB1) and

central east coast (WCA1B). ECHAM5-driven simulations also project positive changes during this season in large areas over the IP, although these increases exceed 10% only in certain regions. Specifically, in the Mediterranean coast for all three simulations constrained by ECHAM5 and in the Northern Central Plateau for WEA1B and WEA2. On the other hand, WRF simulations systematically project decreases during the winter for the southeastern and northern mountains. They are particularly prominent in the Cantabrian Range for the simulations driven by ECHAM5 (up to −30%) and over the Baetic System for those nested in CCSM (between −40% and −60%).

In Figures 7.2 and 7.3 the statistical significance of the changes is also illustrated. Black dots delimit areas where the changes have been found to be non-significative by means of a Student's t-test (95% confidence). The most striking feature of the test results is that during the winter, very few simulations yield significative changes over a considerable area. Indeed, a large portion of the changes projected for the winter by all simulations are not significative, except for WCA1B and WCA2 that produce significative decreases of winter rainfall over the southern half of the IP and over the Cantabrian Range. In the case of ECHAM5-driven simulations changes in winter precipitation are significative only in certain mountainous areas (Cantabrian Range, confined spots in the Iberian, Central and Baetic Systems, and also in the Northern Central Plateau for WEA1B).

For the rest of the seasons, decreases in precipitation are generalized over the entire IP, apart from some slight increases certain regions in the Mediterranean coast (WEB1, WEA1B, WCB1 and WCA1B) and in the Guadalquivir valley during the summer (WEA1B).

On average over the IP, precipitation changes during the spring range from −24% (WEB1) to −58% (WCA2). Downscaled information from ECHAM5 yields a clear gradient from south to north in the spring rainfall changes, although in the western Atlantic coast, in the Northern Central Plateau and in the Mediterranean coast, the changes are not always significative. In the case of CCMS-driven simulations, major decreases are expected along the east coast, particularly in the northern half. The t-test applied at seasonal scales suggests that these changes are partly significative and partly not. In the very northern Mediterranean coast, the projections are significative, whereas in the central and southern part, the t-test indicates that they are not. In the remaining areas, spring changes are mostly significative according t-test for all WRF simulations.

Projected changes in the summer vary from −32% (WEA1B) to −71% (WCA2) on average. Nonetheless, in the southmost half of the IP, the t-test suggests that
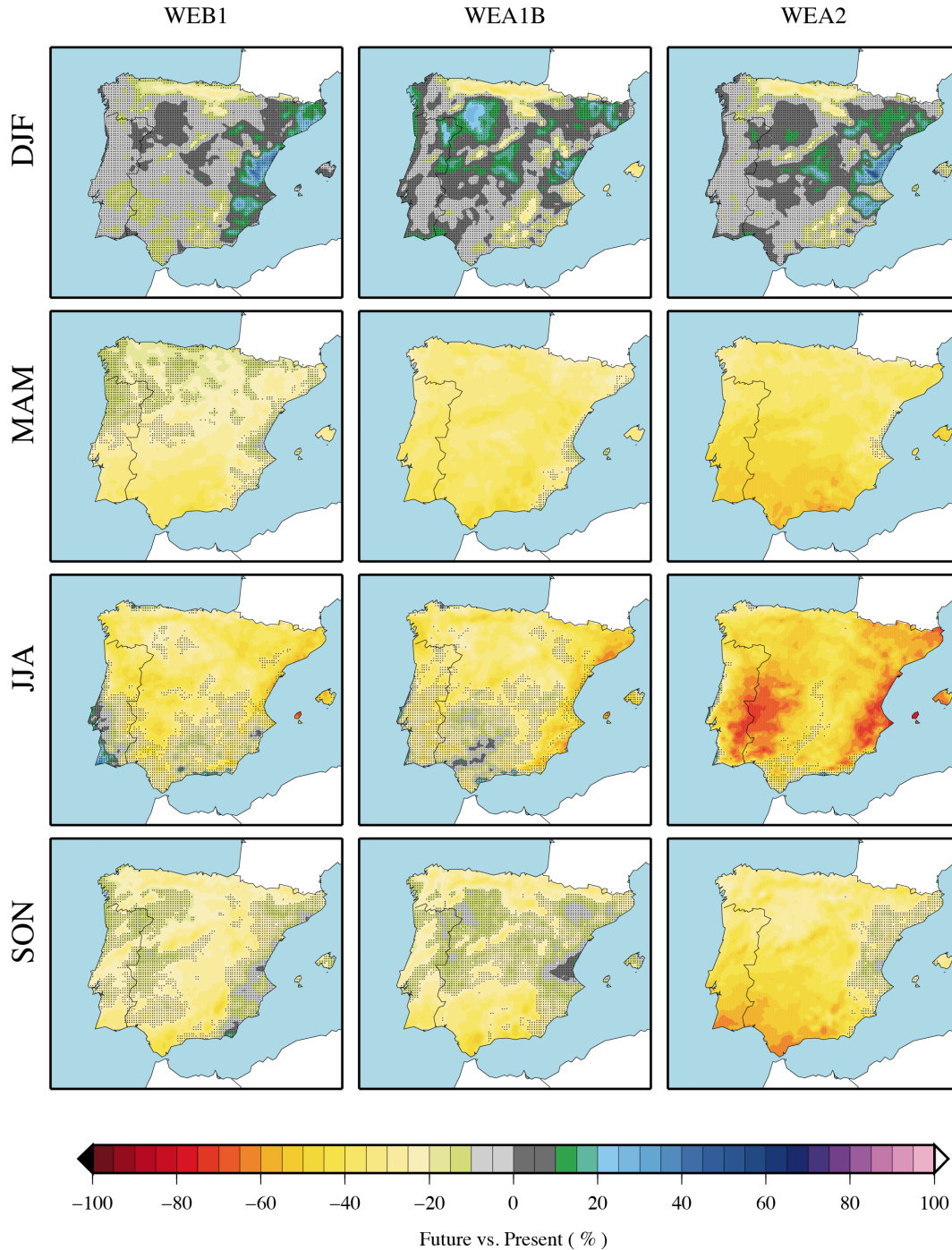
Figure 7.2: *Projected changes for seasonal mean precipitation over the IP for simulations nested in ECHAM5. In rows are displayed the seasons, whereas in columns, the different scenarios. The changes are expressed in percentage: difference between future and present seasonal means precipitation with respect to the present seasonal means. Black dots indicate that changes are not significant according to a Student's t-test at 95% of confidence.*
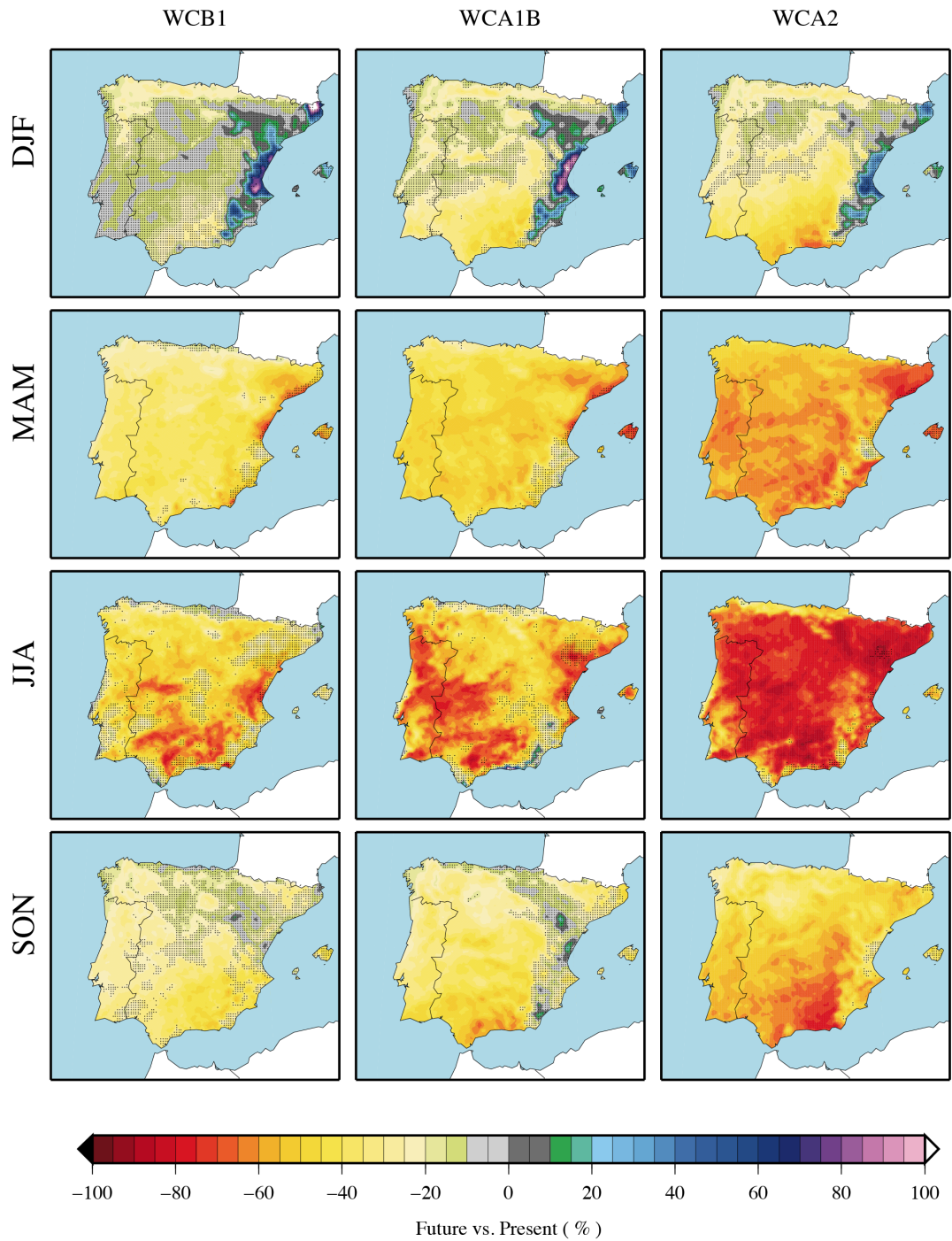
Figure 7.3: *As Fig. 7.2 but for simulations nested in CCSM.*

many of the changes are not significative, especially in the case of simulations nested in ECHAM5. In any case, projections over this region are not consistent among the 6 simulations and both small increases and decreases are projected. Furthermore, summer precipitation in the south of the IP is often very low and comes from very short thunderstorms. Small errors o changes in the number of precipitation events result in large percentage differences for summer rainfall. Possible changes in short events will be further address in the analysis of daily precipitation. Diminution in summer precipitation is particularly marked for CCSM-driven simulations and even under the B1 scenario changes larger than -60% are projected in certain regions in the south. Over the northern half, changes are significative and are greater than 30% in most of the cases.

In autumn, spatially averaged changes are between -23% (WEA1B) and -50% (WCA2). All changes are generally significative under the A2 scenario (WEA2 and WCA2), except for small regions in the east coast. Under the other two scenarios, the are large areas with non-significant changes mainly located along the east coast, in the Ebro valley and over some western mountains. The ECHAM5-driven runs project larger changes over the mountainous areas (Baetic System, Central System and Cantabrian Range). In particular, over the southern mountains, changes range from about -40% for the B1 scenario to more than -60% for the A2 scenario. The CCSM-driven simulations predict decreases even larger for the Baetic System, reaching up to -75% in the A2 scenario. Changes that barely exceed -20% are expected for the rest of the IP according to most of the WRF simulations (except WCA2).

Although summer decreases are more substantial in percentage terms, changes in spring and autumn rainfall have a larger impact on the annual mean due to their contribution to total precipitation. In fact, the spatial pattern of annual mean changes are very similar to those obtained for spring and autumn. Nonetheless, summer changes should not be disregarded because substantial decrease in summer precipitation might have remarkable impacts on natural environment, particularly in terms of fire risk and plants hydrological stress, and also on humans due to urban atmosphere pollution.

7.2.3 Changes in monthly precipitation

In order to ascertain possible changes in the future precipitation annual cycle, rainfall is analyzed on a monthly timescale. Figures 7.4 and 7.5 illustrate the annual cycle of monthly precipitation changes for the different regions ac-

cording to WRF future simulations. A Student's t-test at 95% of confidence has been adopted to determine if changes are statistically significative. Months when changes for a particular simulation are significative are flagged with a square in the plots.

The broad pattern of monthly changes suggest that the annual cycle shape is not expected to change substantially. If anything, monthly changes will enhance the contrast in precipitation rates between warm and cold months, increasing intra-annual variability. However, precipitation is expected to decrease in all months for most of the regions and most of the simulations.

In accordance with results from the previous section, summer months are expected to suffer from larger precipitation decreases (in percentage terms) in most of the regions. More generally, rainfall during the period from April to September tend to decrease more than for the rest of the months, despite some exceptions. Indeed, winter precipitation changes are not expected to be significative in most regions, apart from CA and NC for some ECHAM5-driven simulations, and SI, CA and NC for some CCSM-driven simulations. Winter changes seldom exceed 30% (with both positive and negative sign), except for the SI and IS regions. For instance, in the islands, positive changes in January range from 36% to 60% (non-significative) for the CCSM-driven runs, although it must be noted that precipitation annual cycle was poorly captured by WRFCCSM in this region. In fact, WRFCCSM dramatically underestimated precipitation in the islands and thus CCSM-drive simulation results in this region should be interpreted with caution.

In general, in the regions where both large and local scale have an important contribution to total precipitation (NE, SE, EC and IS) the changes are more variable through the year and indeed, consecutive months might be subject to completely different behavior of precipitation evolution. On the other hand, in areas where precipitation mainly comes from the large scale (NW, CA and NC) monthly variability of the changes is not that prominent, although differences among months are still noticeable.

A remarkable feature of the annual cycle of precipitation changes is the systematic drop in precipitation changes from April to May in the CCSM-drive simulations, and from March to April in the ECHAM5 driven simulations. Bearing in mind that WRFEH5 showed a tendency to bring the maximum of precipitation on month forward during the spring (Fig. 6.4), and considering that the spring maximum is attained in May (April in WRFEH5), this suggest that the spring maximum is projected to clearly diminish in all WRF simulations. For instance,
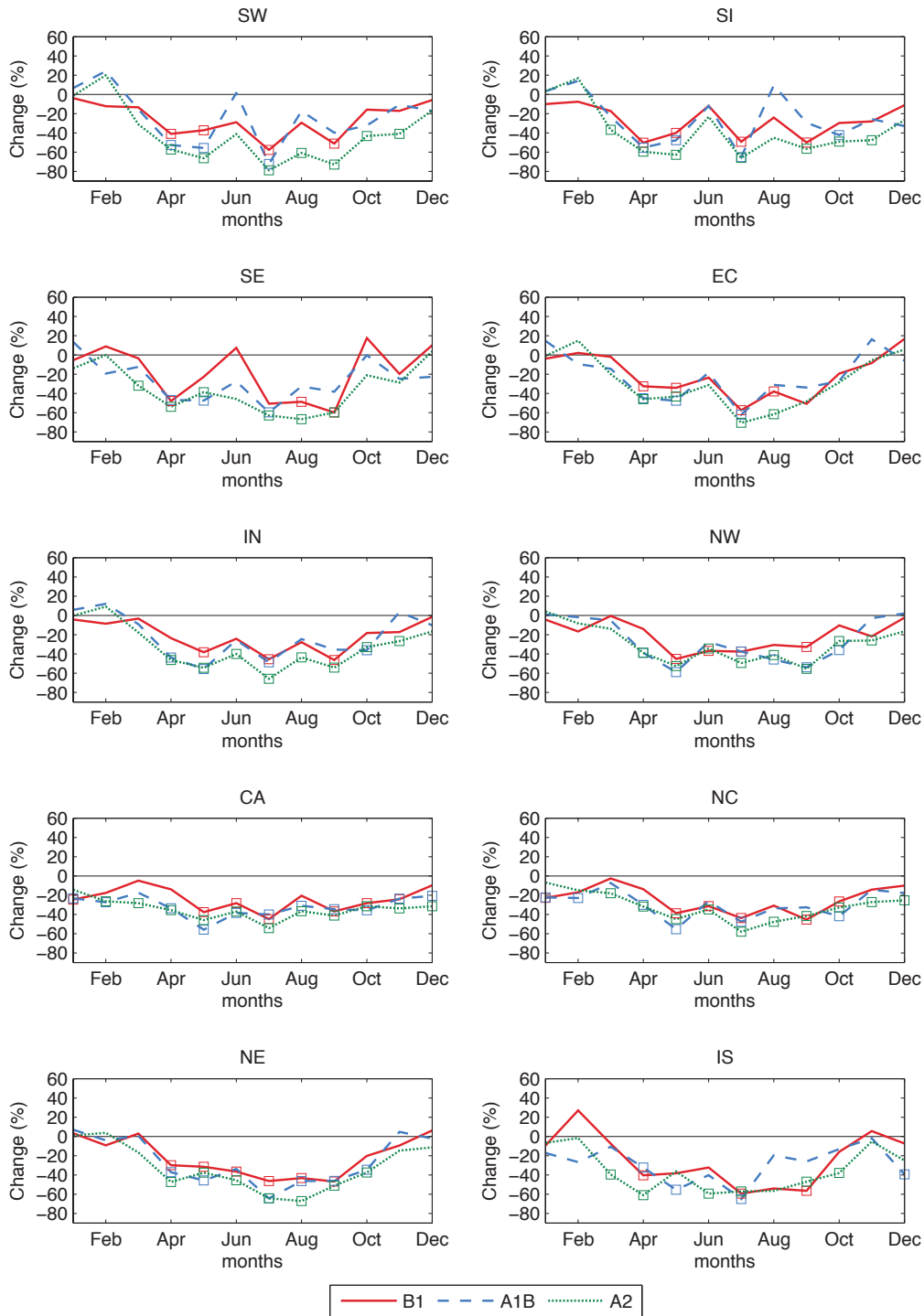
Figure 7.4: *Projected changes in the precipitation annual cycle from the ECHAM5-driven simulations. The changes are expressed as percentage with respect to present climate simulation WRFEH5 and are referred to Spain02 regions. For the period 2070-2099 vs. 1970-1999. Squares indicate months when changes are significative according to a Student's t-test (95% confidence).*
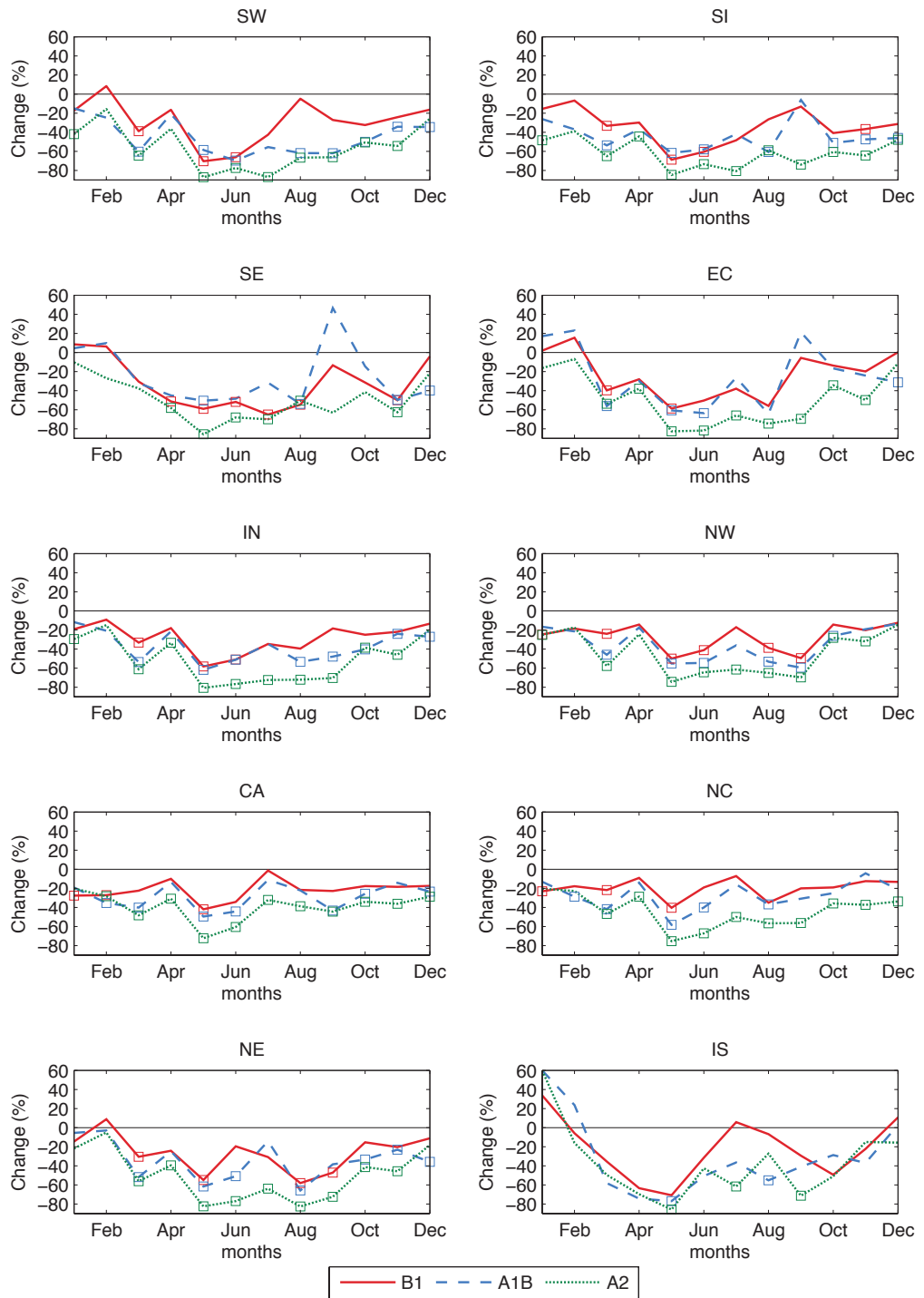
Figure 7.5: *As Fig. 7.4 but for simulations nested in CCSM.*

largest decreases are projected for May (up to -80% under the A2 scenario in the southern regions) in the runs forced by CCSM. Conversely, this behavior does not apply for the autumn maximum in October.

Results obtained from the changes in monthly precipitation through the year emphasize that, despite some isolated increases, precipitation is projected to decrease in all the regions and almost for all the months (exceptions found primarily in December, January and February). The largest decreases are broadly projected under the A2 scenario, whereas only slight differences can be observed between B1 and A1B scenarios.

7.2.4   Changes in daily precipitation

Besides the projected changes in precipitation long-term means (annual, seasonal and monthly), the distribution in daily events is also explored. Different approaches are adopted to characterize daily precipitation. The probability distribution is assessed using pseudo-PDF plots, the changes in percentiles are examined through the Q-Q plots and finally a number of extreme indices are calculated to determine differences between the periods 2070-2099 and 1970-1999.

Frequency of events

Figures 7.6 and 7.7 are the pseudo-PDF plots for future simulations and shows the total annual precipitation accumulated in events of different intensity for ECHAM5- and CCSM-driven simulations respectively. The problem of the scale when representing precipitation PDF is solved with the pseudo-PDF and the analysis of the complete spectrum of events can be performed at once (see Sec. 6.2.4). The pseudo-PDF makes possible to study which are the events that are more likely to change in the future and characterize the future daily rainfall.

The pseudo-PDFs calculated for all WRF simulations suggest that most of the annual decreases are a result of less medium-intensity events. According to WRF projections, an important decrease in precipitation events from 1 to 30 mm should be expected (up to approximately 50% in SW for WCA2). On the other hand, the total precipitation that extremes events account for is not projected to substantially change in absolute terms (mm/year), but due to the generalized reduction in annual precipitation, their probability is likely to increase significantly. Namely, the total precipitation is projected to decrease, but the same number of extreme evens will occur, which results in a displacement of the probability distribution towards heavier precipitation.
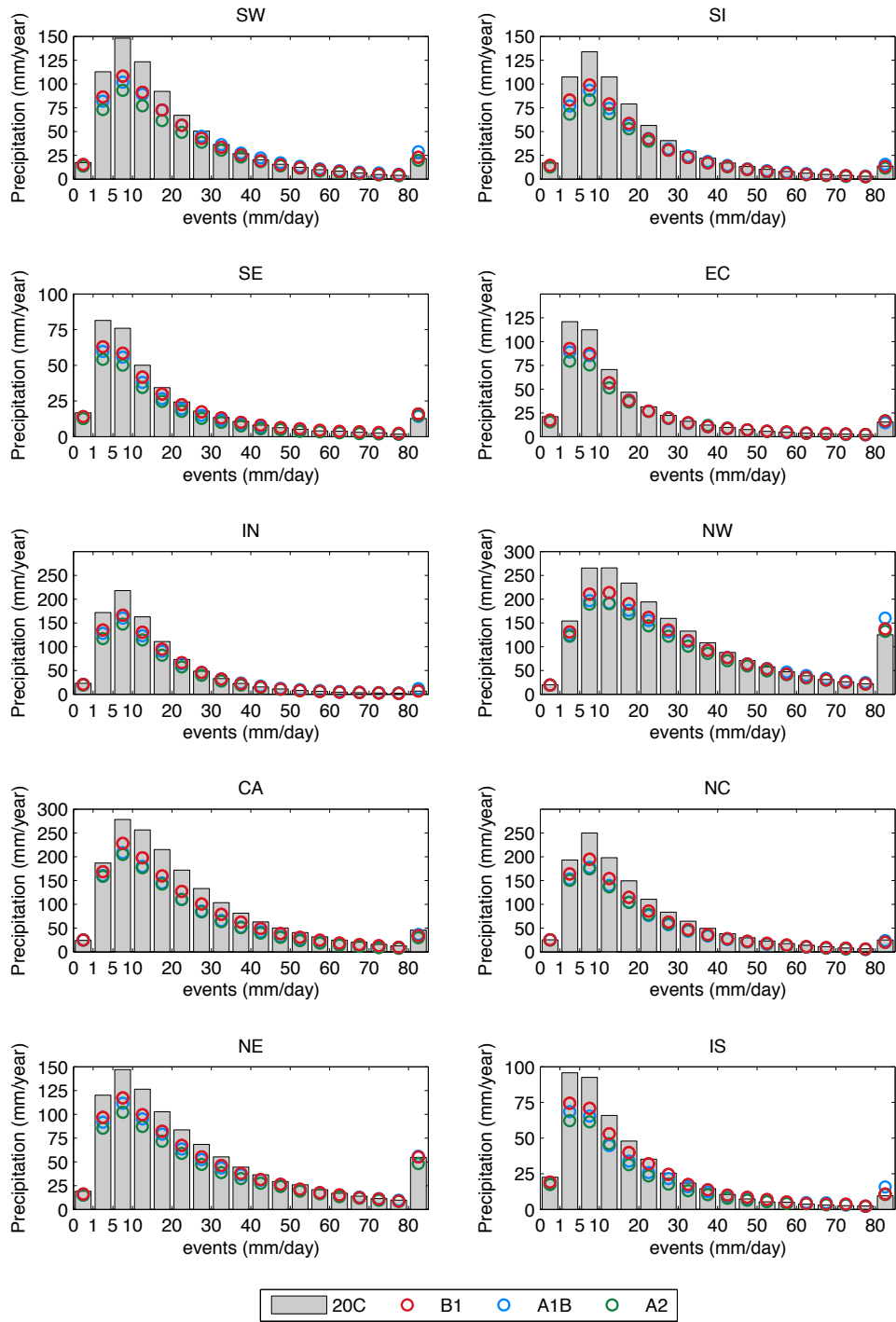
Figure 7.6: *Pseudo-PDF shows the Annual precipitation amounts explained by events of different intensity displayed by Spain02 regions. Grey histogram express the present climate simulation (1970-1999) and the circles represent future simulations (2070-2099).*
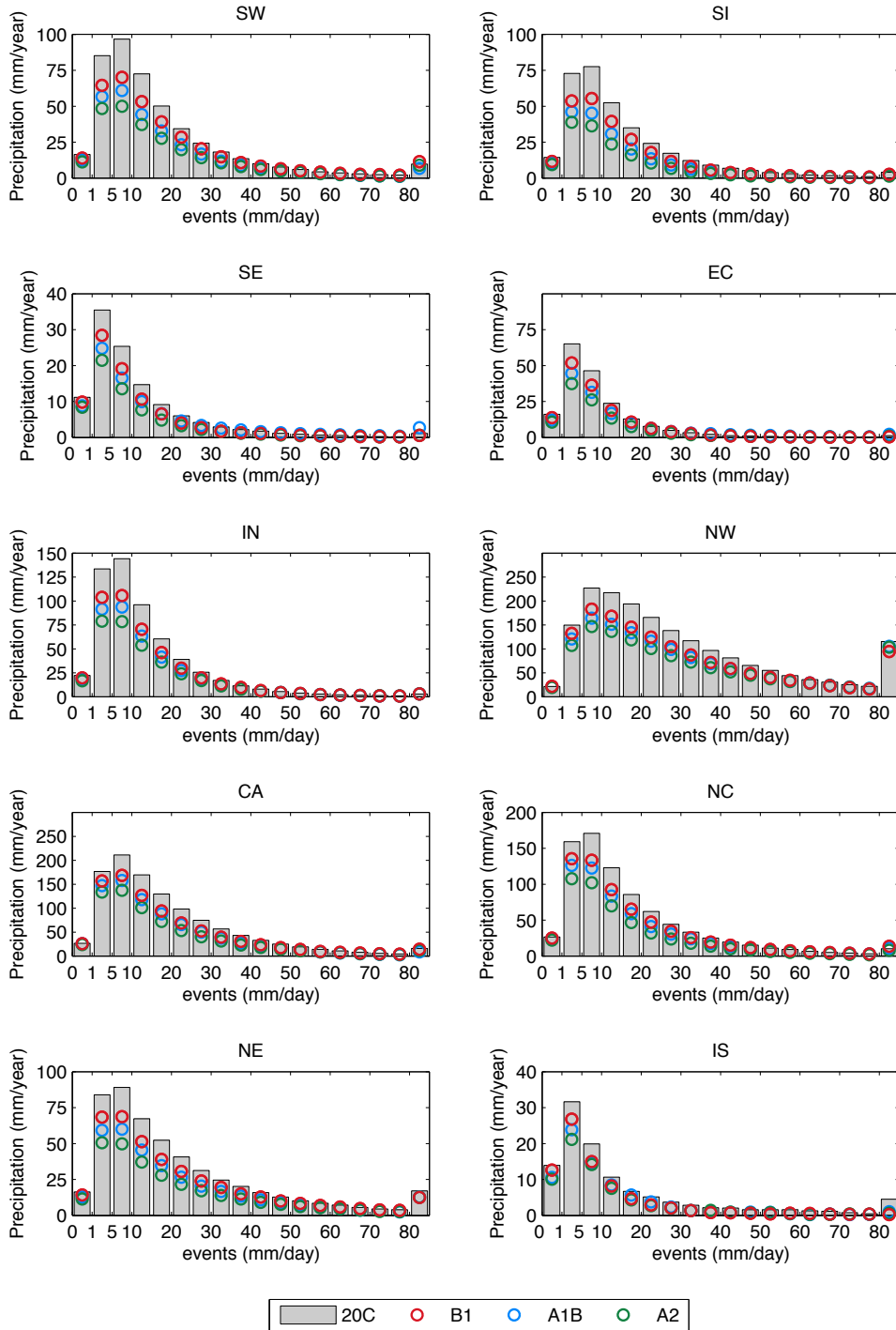
Figure 7.7: *As Fig. 7.6 but for simulations driven by CCSM*

The rainfall regimes are thus projected to be characterized by less precipitation produced in fewer number of events but with higher probability for the downpours. This behavior is common to all regions with differences only in the decrease of occurrence for medium-intensity events.

An interesting feature of changes in the events probability is that despite the fact that WRFCCSM and WRFEH5 produced different probability distributions, the projected changes are fairly similar in relative terms (with respect to the corresponding present climate simulations). These similarities stress the consistency in the decrease of certain precipitation events (from 1 to 30 mm) and the robustness of the displacement of probability distribution towards heavy rainfall in the future. Nonetheless, CCSM- and ECHAM5-driven simulations differ in some aspects, such as the changes in the very extreme events. Future projections forced by ECHAM5 produced an increase in the very extreme events (>80 mm) over certain regions, whereas those constrained by CCSM systematically show a decreasing tendency.

The pseudo-PDF plot is useful to examine the distribution of precipitation in different rainfall events, but changes in the magnitude of the extreme events cannot be addressed with this approach. To study extreme events, the upper percentiles must be explored.

Percentiles of precipitation

In addition to the study of extreme precipitation in terms of their contribution to total annual precipitation, changes in the magnitude of the upper percentiles must also be analyzed. Different percentiles (5th, 50th,55th, 60th, 65th, 70th, 75th, 80th, 85th, 90th, 95th and 99th) have been calculated for both future and present simulations. They are compared in a Q-Q plot to determine changes in the future precipitation percentiles.

The Q-Q plots for precipitation regions are shown in Figures 7.8 and 7.9 for the simulations forced by the two different GCMs, respectively.

In the model evaluation, it was obtained that the WRFEH5 simulation produced the best results in terms of precipitation percentiles in all the regions (Fig. 6.7), even better than the simulation driven by 'perfect boundary conditions' (WRFERA) in many regions, and thus the results from ECHAM5-driven simulations should be given more consideration.

An increase in the most extreme events of daily precipitation is projected by simulations nested in ECHAM5 in most regions, except for CA and NC, where
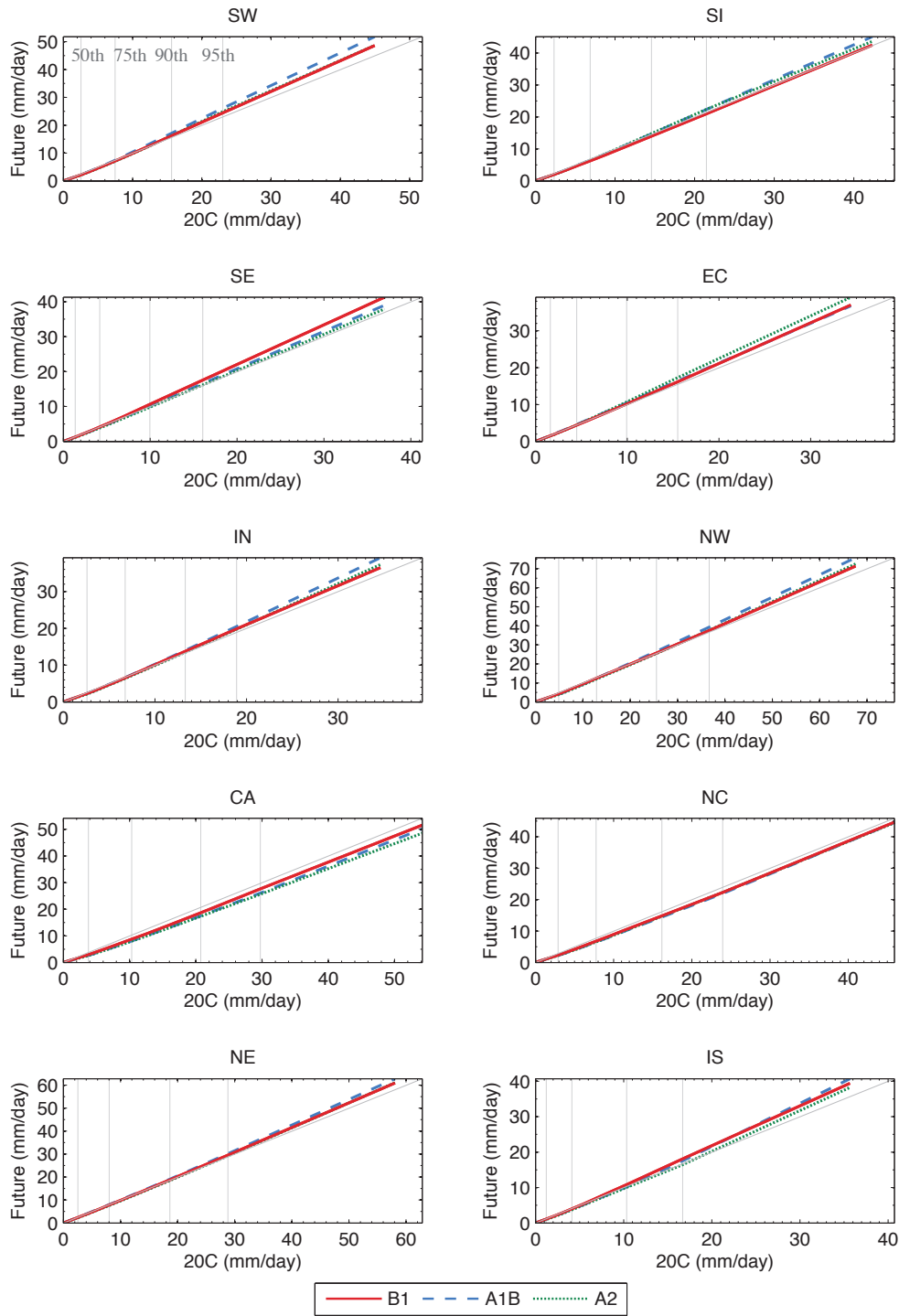
Figure 7.8: *Precipitation percentiles simulated by three ECHAM5-driven WRF future runs (2070-2099) vs. WRFEH5 (1970-1999) precipitation percentiles. The grey line indicates a perfect skill and delimits over- and underestimation of the different percentiles. The vertical lines determine the 50th, 75th, 90th and 95th percentiles as reference. The plot extends to the 99th percentile.*
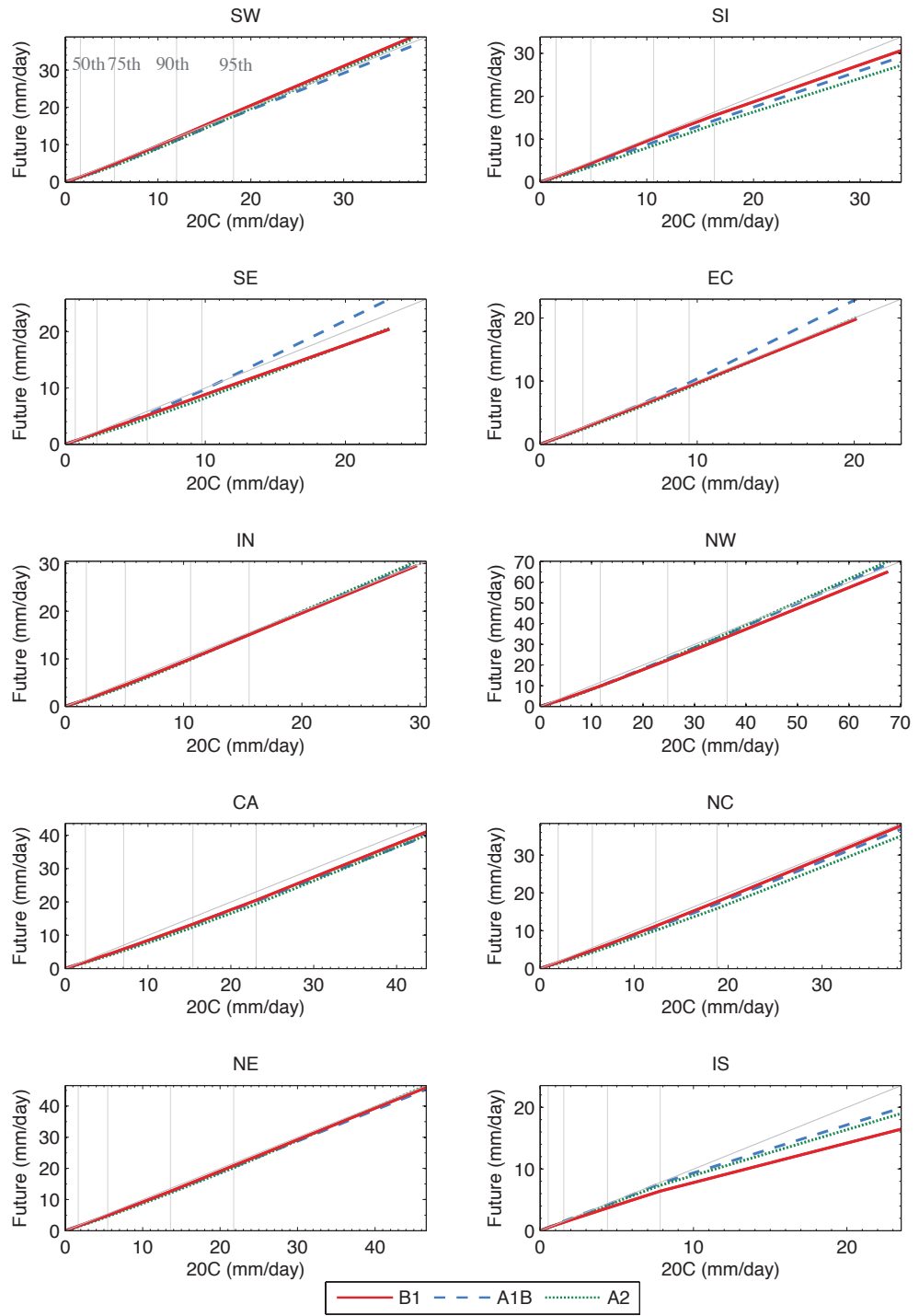
Figure 7.9: *As Fig. 7.8 but for CCSM.*

a slight decreases might be expected. Substantial changes are only projected for events above the 95th percentile, since below that threshold only minor differences that barely exceed 5 mm are obtained between future and present simulations. Heaviest events (up to the 99th percentile) are subject to larger changes but still within a range of 10 mm with respect to the present simulation. Regarding the different scenarios, the projections using ECHAM5 as boundary conditions do not differ considerably and indeed, the largest changes in each region can be attributed to different scenarios (WEB1 in SE, WEA1B in SW, IN, NW, or WEA2 in EC).

In the case of the simulations forced by CCSM, differences among scenarios are larger in some regions (SI, SE and IS), but again they are generally quite similar and there do not seem to be a clear relation between scenarios and changes in the percentiles. By contrast with the ECHAM5-driven simulations, these runs project almost no changes or a slight tendency to lighter heavy events (SI, CA, NC and IS). In fact, only in certain regions the changes exceed 5 mm in the 95th percentile, whereas in the rest of the IP, changes are negligible up to the 99th percentile. It should also be stressed that owing to the severe underestimation of precipitation percentiles by WRFCSSM along the Mediterranean and the southern regions, the information downscaled from CCSM in this areas and with regard to precipitation percentiles should be regarded with caution.

Everything considered, projections of changes in the magnitude of upper percentiles of daily precipitation are not overall important and critical changes in the extremes might be rather related to the intensity of several-day events. Additional facets of extreme precipitation that include the duration of dry and wet periods might be also affected. To address the issue of extreme events from a different point of view, some extreme indices are calculated for the future and compared with present simulations.

Changes in precipitation extreme indices

The changes in the extremes of precipitation are studied using a selection of the ETCCDI extremes indices just like in the model evaluation (sec. 6.2.4). The excerpt of the ETCCDI extreme indices that was chosen to characterize high-order statistics of precipitation in the present climate (see Table 6.1) has been adopted here in an extended version[1]. Namely, the indices that describe the

---

[1]Note that the modified CDD* and CWD* indices are also employed here instead of the original CDD and CWD.

precipitation events above 20 mm/day (R20) and the average intensity of events (SDII) have been added to explore future projections of extreme events (Table 7.2). These indices were calculated for the present climate, but were omitted in the evaluation of the model because they did not provide additional information. However, in the case of future climate projections they help to determine the future regimes of precipitation with respect to present climate and have thus been included here.

Table 7.2: *Selection of ETCCDI extreme precipitation indices for future projections.*

ID	Description	Units
Rx5day	Maximum 5-day precipitation amount	mm
R10	Number of days when precipitation exceeds 10 mm	days
R20	Number of days when precipitation exceeds 20 mm	days
SDII	Simple daily intensity index. Total precipitation divided by number of rain events	mm/day
R95T	Percentage of total precipitation above the 95th daily percentile	%
CWD*	Annual mean maximum number of consecutive wet days (>1 mm)	days
CDD*	Annual mean maximum number of consecutive dry days (< 1 mm)	days

The most remarkable feature of changes in the extreme events is related to their spatial distribution, which tends to be fairly heterogeneous within the IP. This emphasizes the necessity to study this facet of climate from a region point of view. Differences between relatively closed areas are substantial and usually governed by both large scale and topographical features.

The changes in the heaviest events during the period 2070-2099 with respect to 1970-1999 represented by changes in the Rx5day index are shown in Figure 7.10[1]. The 5-day maximum precipitation is projected to both increase and decrease depending on the region, the boundary data and to a lesser extent, the emission scenario. The central part of the Mediterranean coast is expected to be subject to a significant increase in the maximum precipitation accumulated in 5 consecutive days. Indeed, all simulations project changes that reach up to 150% near *Cabo de la Nao*, except for WCB1 that project smaller changes in this area.

---

[1]Note that the scale extends below −100% to preserve its symmetry, even though the maximum possible decrease is −100%
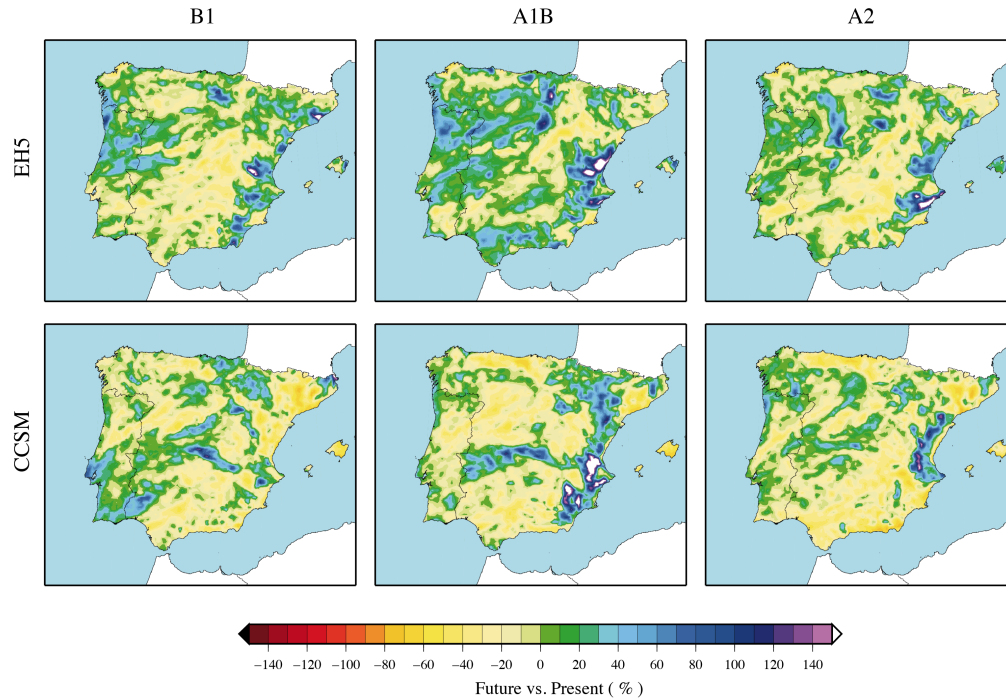
Figure 7.10: *Changes in the Rx5day index in percentage terms (2070-2099 vs. 1970-1999). The simulations using different boundary data are placed in rows and the emission scenarios are placed in columns.*

Overall, the ECHAM5-driven simulations project a decrease in the Southern Central Plateau and areas of the Iberian System. Decreases of the Rx5day index are also projected in certain areas across the IP (southwest, southeast coast, and parts of the Iberian System and the Cantabrian Range), but they often alternate with notable increases. In fact, the spatial distribution changes for the different scenarios and only broad characteristics are common to all three. For example, there seem that in areas of the Northern Central Plateau and the northwest coast, the 5-day maximum precipitation is likely to increase up to 60%, although the areas change in location and extension among the WEB1, WEA1B and WEA2 simulations. Largest positive changes are found for the A1B scenario, whereas under B1 and A2 the projections are generally negative in most of the IP, except for the aforementioned regions in the Mediterranean coast and the Northern Central Plateau.

The projections from the simulations forced by CCSM are slightly different, apart from the tendency in the east coast that still appear in the CCSM-driven

simulations, particularly for the WCA1B. The spatial patterns of Rx5day projections are somehow more consistent among these simulations. Indeed, certain areas are systematically projected to be subject to a decrease in the Rx5day index. For instance, the very extreme precipitation in the Cantabrian coast, the south of the IP, the northeast coast and the Balearic Islands are expected to be less severe than in the present, according to CCSM-downscaled information. Under the A2 scenario, the lessen of the index is particularly marked in the north and south extremes of the Mediterranean coast, with reductions that reach -70%. In addition to the increases in the central east coast, the area limited by the Central System and Sierra Morena seems to be affected by larger 5-day maximum precipitation in the future. This result can also be inferred from the ECHAM5-driven simulations to a degree.

Regarding the moderate rainfall, all WRF simulations project a diminution in the number of days with precipitation above 10 mm as deduced from the changes in the R10 index (Fig. 7.11), although some simulations yield slight increases in certain regions. In the south, the Galician Massif and the Cantabrian Coast all runs project decreases that vary in magnitude depending on the boundary conditions and the scenario. For example, all simulations project decreases that exceed -40% (except WEB1). Over the Baetic System, the Southern Central Plateau and the northernmost Mediterranean coast changes are particularly remarkable, since the decreases in the R10 index arrive at -70% for the WCA2 simulation. The number of days with precipitation over the 10m threshold are likely to decrease over the mountainous areas as well. Very few regions are expected to suffer from increases in R10 and are mainly located in the central Mediterranean coast, the Northern Central Plateau and the Ebro valley.

By contrast with the changes in R10, projections in the number of day with precipitation above 20 mm suggest both substantial positive and negative changes (Fig. 7.12). This results are in line with the analyses of the pseudo-PDF that indicate displacement towards heavier rainfall in some areas. In particular, a consistent projection of positive changes in the R20 index is obtained from all simulations over the Northern Central Plateau ($>30\%$). On the other hand, WRF outputs systematically point in the direction of decreases over the Cantabrian Range and the south, particularly in the case of CCSM-driven runs (up to -70%, WCA2). In fact, most of the mountainous regions are affected by decrease in the R20 index. ECHAM5-driven simulations also project an increase in heavy precipitation over the Southern Central Plateau and parts of the Mediterranean coast, where CCSM-driven project severe increases too. In addition, simulations
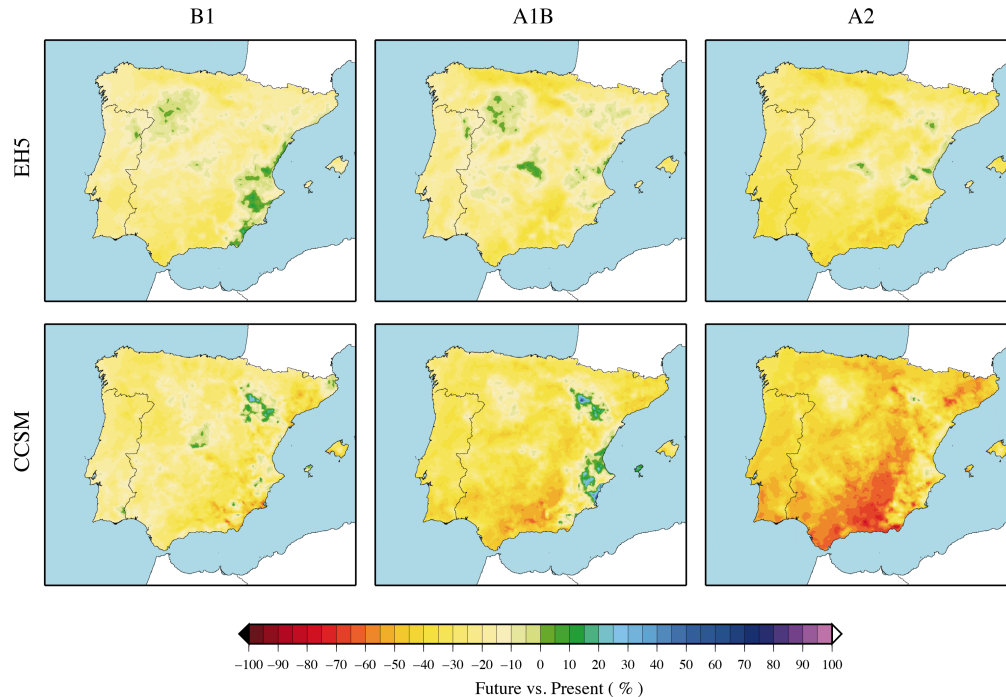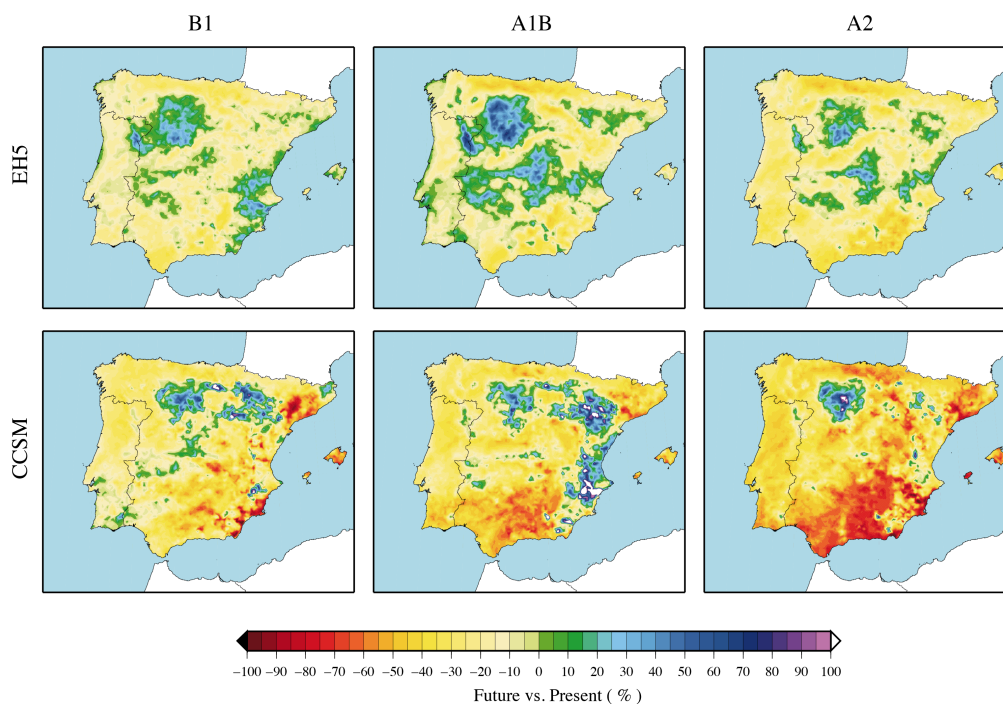
Figure 7.11: *As Fig. 7.10 but for R10.*

forced by CCSM denote important decreases in the number of days with teeming rain over the northeast and the islands.

A picture of the displacement towards heavy precipitation is provided by the magnitude of the R95T. Changes in the total amount of precipitation explained by events above the 95th percentile manifest the probability rise of extreme events to occur. Figure 7.13 shows the changes in this index and illustrates the tendency towards larger amounts of rainfall produced by downpours[1].

Most changes fall in the range between 0 and 2 percentage units, but in many regions the changes are projected to be about 4 percentage units. Bearing in mind the R95T values obtained for the present (Fig. 6.8), changes projected by WCA1B and WCA2 in the central Mediterranean coast would lead to R95T values over the 35%. Other significative changes shared by most simulations are found in areas of the Baetic System, the northwest and the Northern Central Plateau, although the spatial distributions within this areas are not common to all simulations.

---

[1]Note that unlike the rest of indices, R95T values are given in percentage and thus changes are provided as differences instead of relative changes to present climate.

Figure 7.12: *As Fig. 7.10 but for R20.*

The ECHAM5-driven simulations project positive changes all over the IP, except for some limited regions (Ebro valley and parts of the very southeast). On the other hand, CCSM-driven simulations project negative changes over large areas in the south and in the northeast. Some isolated regions in the Mediterranean, such as the north coast and the Balearic islands, are expected to suffer from decreases that exceed 8 percentage units.

All in all, there are evidences of an overall tendency towards larger percentages of precipitation accumulated in the furthest part of the distribution function. The projections of the R95T index are similar among simulations and they are quite consistent consistent over certain areas (positive in central Mediterranean coast, northwest quarter of the IP, Baetic System and Pyrenees; and negative in the south and northeast).

To provide further insight on the rainfall intensity, the changes in the simple daily intensity index are plotted in Figure 7.14. In accordance with changes in the previous indices explored, all simulations project positive changes in the average intensity of rain events over the Northern Central Plateau, the Ebro valley and below the Central System. Furthermore, most simulations suggest positive
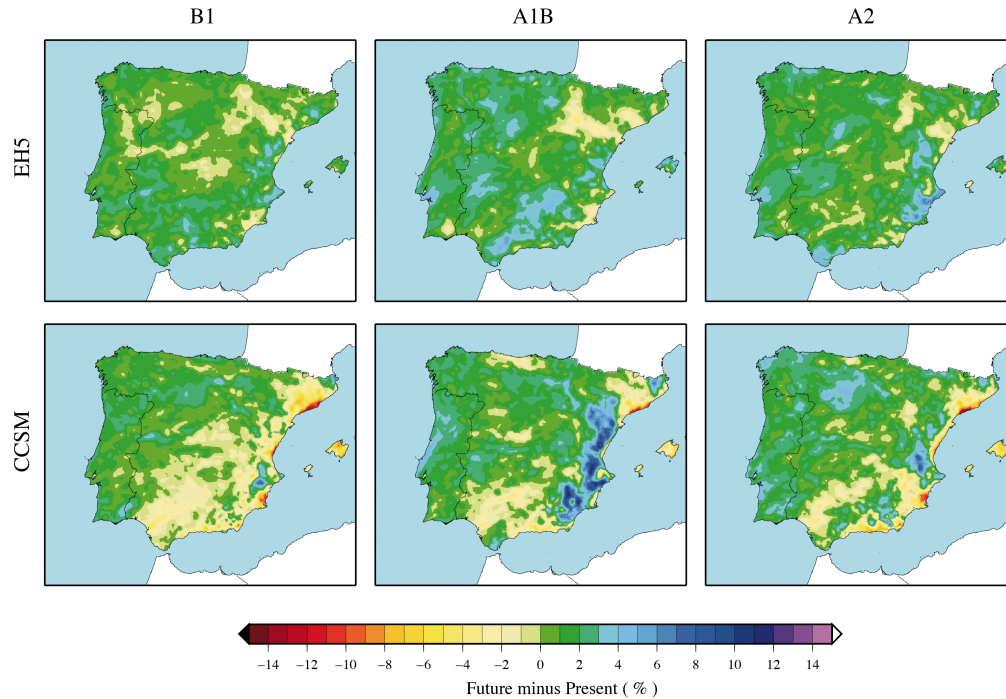
Figure 7.13: *Difference of the percentage of precipitation accumulated in events above the 95th percentile (R95T) between future and present simulations. Changes express increments or decreases in these percentages and not relative changes to present climate.*

changes in the central Mediterranean coast and the Balearic Islands. In addition, ECHAM5-driven simulations also project positive changes in the southwest. The magnitude of these changes varies from run to run, but most of them exceed the 10% threshold. In the case of the Mediterranean coast, the increases often arrive at 30%. In general, the ECHAM5-driven simulations show higher spatial coherence, whereas those constrained buy

On the other hand, negative changes are very likely to occur in the Cantabrian coast. Decreases in the SDII over this region seem to be rather consistent since all simulations agree with projections between -20% and -10%. Simulations nested in CCSM also project decreases in the south of the IP and in the northern Mediterranean coast, and are of the same magnitude as those projected in the north. In general, the ECHAM5-driven simulations show higher spatial coherence than CCSM-driven ones.

Besides the intensity of precipitation events, it is interesting to address the persistence of dry and wet periods. In areas where precipitation is not very fre-
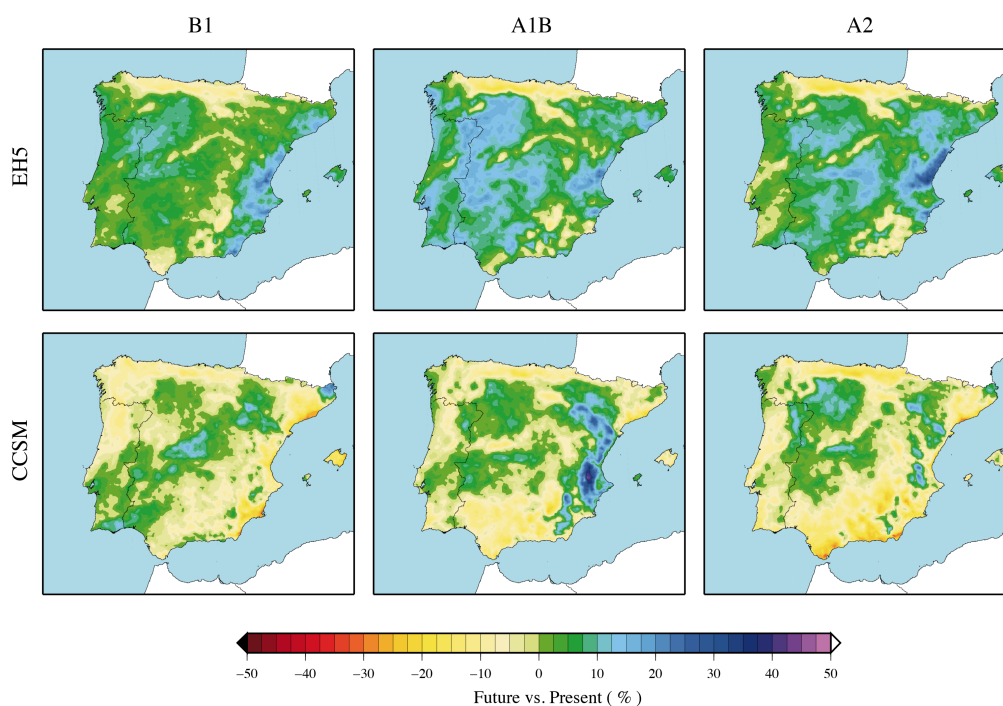
Figure 7.14: *Changes in the average rainfall intensity (SDII) in percentage terms (2070-2099 vs. 1970-1999). Simulations with different boundary data conditions are arranged in rows and the emissions scenarios are placed in columns.*

quent, the duration of dry spells might be of paramount importance. Two indices describe the persistence of dry and wet conditions, the annual mean maximum length of dry spell (CDD*) and the annual mean maximum length of wet spell (CWD*).

Figure 7.15 illustrates the changes projected for the annual mean maximum number of consecutive dry days. The spatial pattern of the changes from the different simulations are rather consistent and all project a general increase in the CDD* index.

Only very isolated areas are likely to have shorter dry spells, of which the most noticeable is the area located near the French border in the northern coast. Even under the A2 scenario that lead to most severe increases in CDD*, very few places might also be expected to experience slight increases (WEA2, very confined in the northwest). In the WCA2, values are positive but there is a clear distinction between the Cantabrian coast and the rest of the northern IP. Largest increases are projected in the surroundings of the Galician Massif, to the south
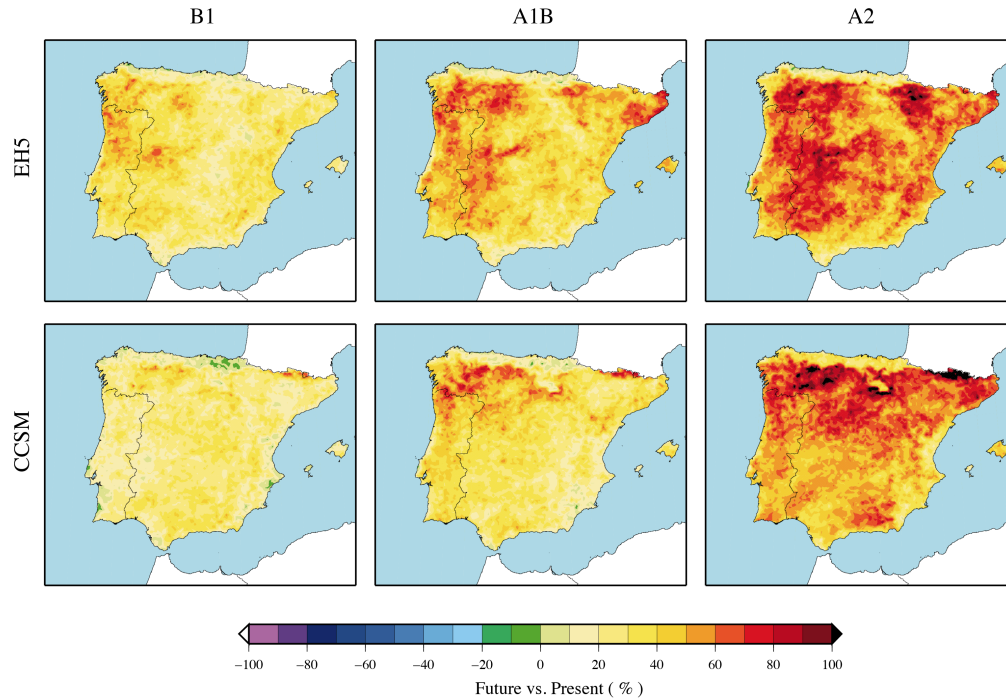
Figure 7.15: *As Fig. 7.14 but for CDD*.*

of the Cantabrian Range and in the Pyrenees. In the WCB1 simulation, which projects the more moderate changes, the CDD* might increase by up to a 60%, whereas the rest of the IP changes remain in about a 20%. As the emission scenario changes from B1 to A2, the changes are more acute. Actually, both WEA2 and WCA2 projects changes that reach the 80% in a large portion of the IP, being the north half part the most affected. Other areas that are likely to suffer from important changes is the west (WEA1B and WEA2) and the Baetic System (WCA2). On the other hand, there are regions that do not seem to be as affected as the other by changes in the scenario, and the projections are similar for all of them, such as the south ($\sim$ 20-40%) .

The change in the annual mean maximum number of consecutive wet days is shown in Figure 7.16. The spatial distribution of the changes is again fairly similar among simulations. Despite the differences in the scale with respect to the previous index, there seem to be more variability within the IP for the CWD* since areas with considerable positive and negative values coexist.

By contrast with the CDD* index, the Cantabrian coast is one of the regions that is likely to experience largest changes in the CWD*, reaching -50% in certain
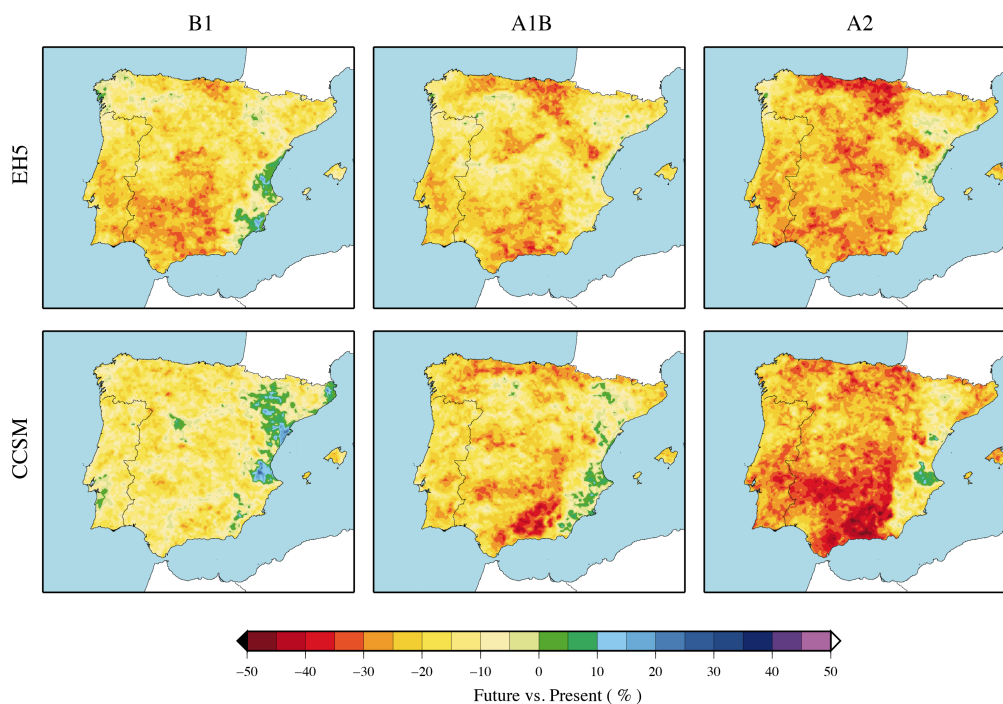
Figure 7.16: *As Fig. 7.14 but for CWD*.*

locations. In addition, the Baetic System and Sierra Morena, in the south, are also projected to undergo important changes by all simulations (except WCB1), particularly in the case of WCA1B and WCA2. Some areas in the Iberian System and Central System might also be affected by changes that exceed −30%.

On the opposite side, the duration of the wet spells is projected to be larger in areas of the Mediterranean coast (that vary depending on the simulation) and to a lesser extent in the Ebro valley. The CWD* might also be expected to be slightly higher in some areas in the interior and the northwest, but only according to certain simulations. Changes in the Mediterranean coast are particularly significant, and the increasing might reach values over 20% over specific locations (WEB1 and WCB1). Nonetheless, as the projection in the GHG emissions increases, these areas might reduced and the magnitude of the changes might be more limited.

On average, the WRF simulations project larger dry spells and shorter wet periods nearly almost the entire IP, with very few regions that are likely to behave the contrary.

7.3   Temperature changes

Changes in temperature is the most direct effect of the radiative forcing due to the GHGs atmospheric concentration increase. Nonetheless, the magnitude of the changes is likely to vary from region to region depending, for example, on the distance to the sea. Moreover, not only a displacement of the temperature means might be expected, but also changes in the distribution tails. Therefore, the changes in both maximum and minimum temperatures are here address studying both long-term means and high-order statistics. In fact, changes in the extremes might have greater impact on human activities and natural environment than mean climatic changes (Kunkel et al., 1999), leading to pollution episodes, altering the biological cycle of plants, causing health problems or giving rise to high energy demands.

7.3.1   Changes in annual mean temperature

According to all WRF simulations, the entire IP is likely to suffer from increases in both Tmax and Tmin (Figs. 7.17 and 7.18) by the end of this century (2070-2099) with respect to the period 1970-1999. Changes near the coast are projected to be more moderate than in the interior of the IP due to the sea thermal inertia. In the mountains temperature changes are projected to be particularly severe. Regarding differences between the two temperature extremes, Tmax is likely to increase more than Tmin in all cases. The significance of the changes obtained from a Student's t-test at 95% of confidence is also illustrated in Figures 7.17 and 7.18. To be specific, the locations where the changes are non-significative are flagged with black dot. Nevertheless, the changes are significative practically over the entire IP and thus the very few black dots are hardly noticed. It must be stressed that the traditional criterion is to flag significative changes, but the contrary is chosen here to enhance readability.

Changes in maximum temperature range on average over the IP from 2.0°C (WCB1) to 4.6°C (WCA2). The WCA1B projects an average increase of 3.3°C. With respect to the ECHAM5-driven simulations, they yield increases of 2.9°C (WEB1), 4.2°C (WEA1B) and 4.3°C (WEA2).

Except for the WCB1 simulation that projects an homogeneous change between 1.0°C to 2.0°C in most of the IP, the rest of simulations suggest changes that exceed 3.0°C in large areas of the Peninsula. The largest changes are found in the mountains, particularly in the Pyrenees and in Sierra Nevada (Baetic System), where Tmax might raise up to 6.1°C (WEA2). According to most of the
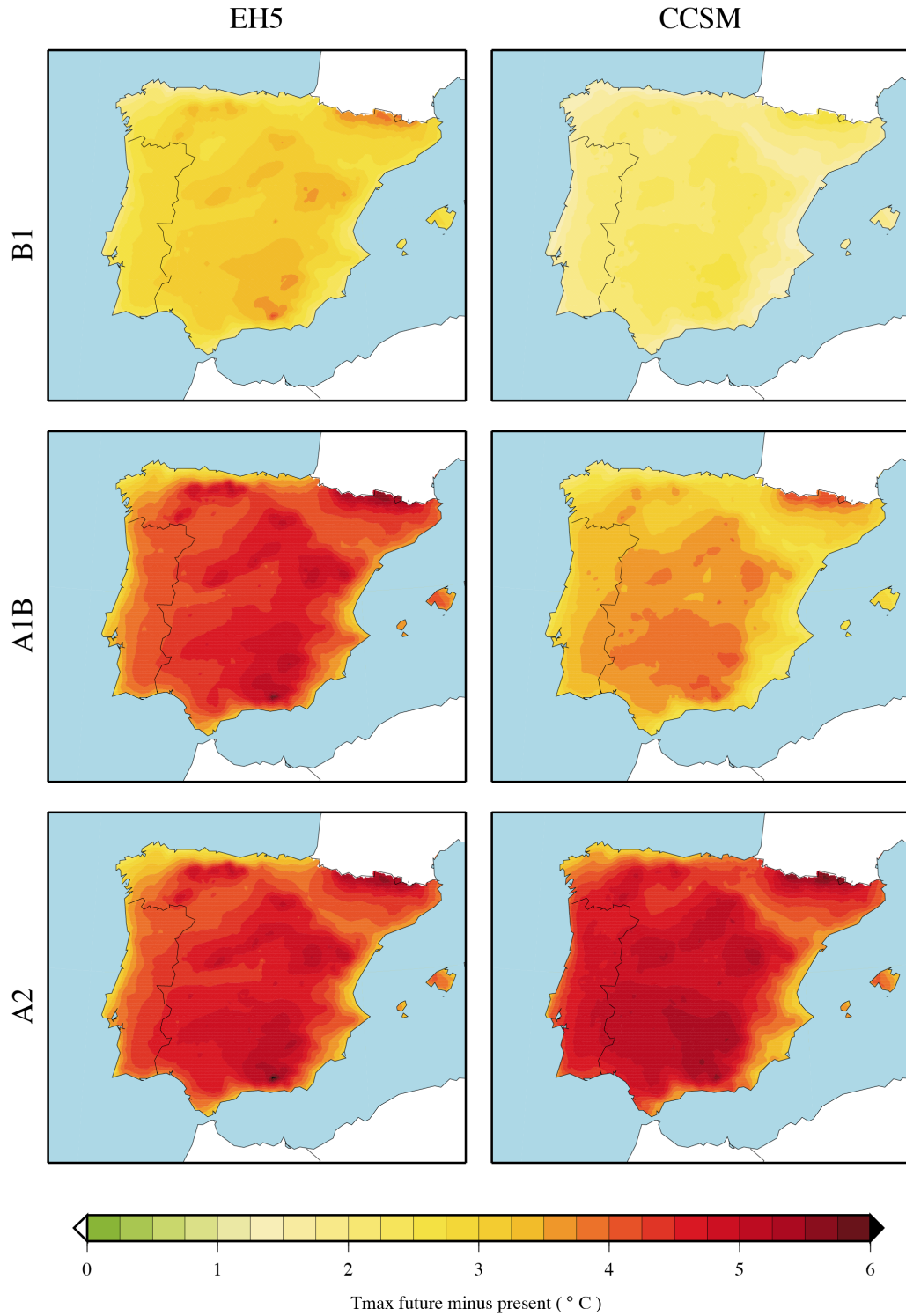
Figure 7.17: *Projected changes for annual mean Tmax over the IP. The difference between the annual mean for the period 2070-2099 and 1970-1999 are expressed in degrees Celsius. The simulations using different boundary conditions are arranged in columns, whereas the different scenarios are placed in rows. Black dots indicate points where changes are not significicatve acceding to a two-sided Student's t-test with a 95% of confidence. Please note that, contrary to what is usual, black dotes indicate non-significicative changes instead of significative ones.*

simulations (apart from WCB1), the mountainous areas are likely to be exposed to Tmax increases larger than 3.5°C. More generally, the interior of the IP might be subject to the largest increases in temperature, whereas in the coasts and the Ebro valley the changes are projected to be more moderate, but still significant (up to 2.5°C in WEA2 and 3.0°C in WCA2).

Concerning the minimum temperature, the increases are not as large as for for Tmax, and indeed the largest projected changes barely exceed 4.0°C. On average, the changes range from 1.4°C (WCB1) to 3.4 °(WEA1B)[1]. The rest of simulations project 2.2°C (WEB1), 3.2°C (WEA2), 2.4°C (WCA1B) and 3.2°C (WCA2).

In accordance with results for Tmax, the most affected regions are the mountains, where all simulation project the greatest changes. In particular, the Pyrenees, the Baetic System, the Central System, the Iberian System and the northwest mountains comprise the areas with the most significant increases. Both WEA1B and WEA2 reveal increments that might exceed 4.0°C, whereas only the WCA2 project changes of such magnitude. Nevertheless, the area covered by these changes is certainly limited to few locations. Changes over 3.0°C are much wider and cover a large portion of the IP for the simulations WEA1B, WEA2 and WCA2.

Conversely, the areas where changes are not as pronounced are the Northern Central Plateau and the northern Atlantic coast. Indeed, the two simulations under the B1 scenario and the WCA1B project changes below 2.0°C in these regions. Actually, according to WCB1 run most of the IP might be subject to changes that hardly exceed 1.5°C. Unlike what was found for Tmax, the Tmin changes in the Mediterranean coast might be expected to be of the same magnitude as in the interior.

---

[1]The fact that the largest change is found under the A1B scenario for the ECHAM5-driven simulations might seem contradictory when considering the global projections of surface mean temperature shown in Figure 4.9b. However, the mean surface global temperature directly retrieved from ECHAM5 actually attains higher values in the period 2070-2099 for A1B than for A2. This behavior might be explained by a largest inertia in the ECHAM5 model than in the rest of GCMs, since the radiative forcing for the A1B scenario is larger than for the A2 until approximately 2065 (Fig. 4.9a). In fact, for the period 2070-2079, the ECHAM5 model projects an increase in the global surface mean temperature of 3.3°C under the A1B scenario and 3.2°C under the A2, whereas for the period 2090-2099 the changes are 4.0°C under the A1B and 4.5°C under the A2.
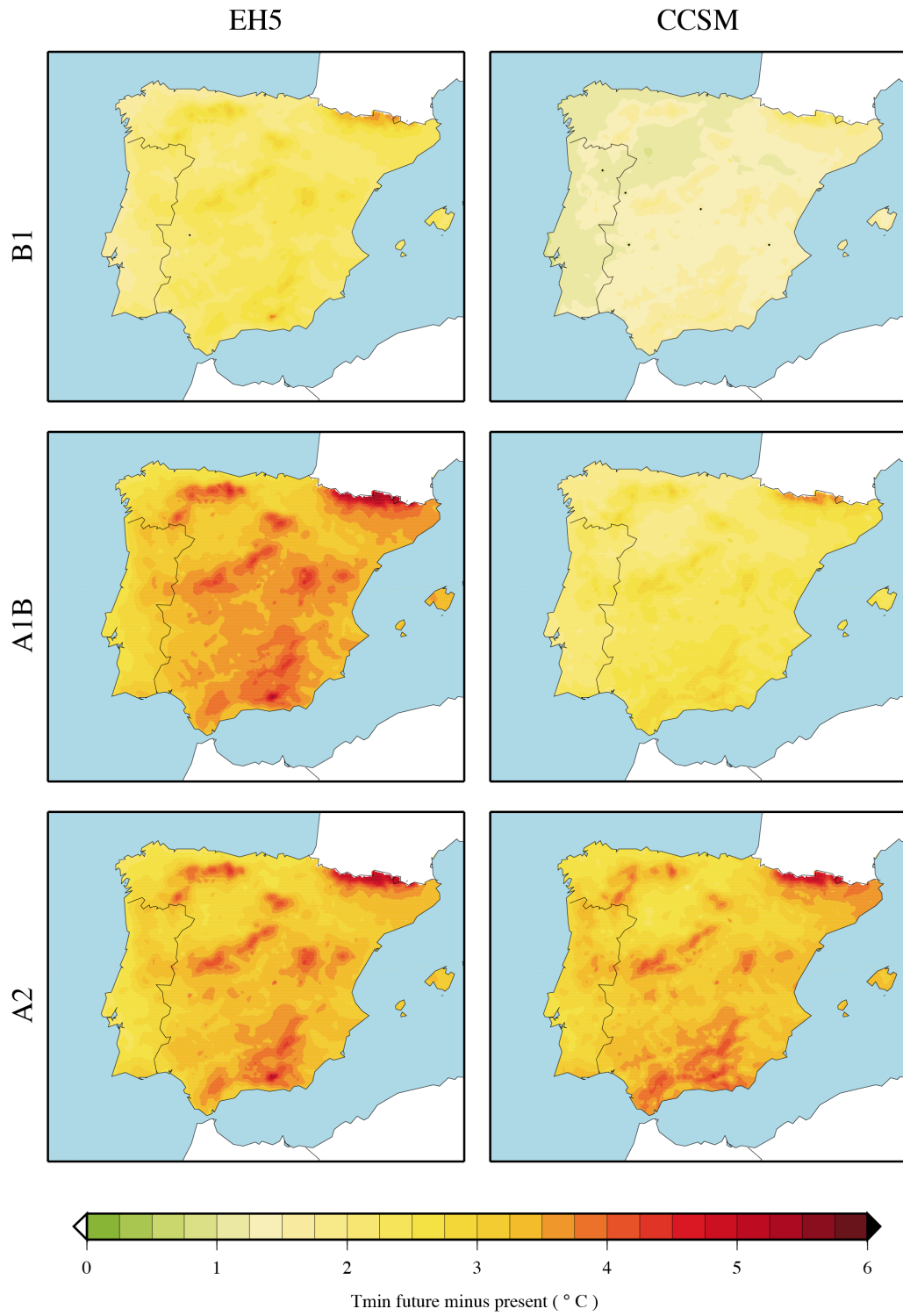
Figure 7.18: *As Fig. 7.17 but for Tmin.*

7.3.2   Changes in seasonal temperature

The analysis of the Tmax projected changes at seasonal scales (Figs. 7.19 and 7.20) reveals that largest increases might be expected in the summer, except for the WCB1, where differences with autumn and spring changes are negligible. During the summer, the increase exceed 4.0°C over large areas in the interior of the IP and under the A2 scenario changes above 5°C are projected over nearly the entire IP. Similar changes are also projected by WEA1B for this season.

In the winter, the Tmax might experience changes considerably smaller than for the rest of the seasons. In fact, according to WCB1, winter Tmax changes are improbable to exceed the 1.5°C threshold. In the east coast, WCB1 actually project changes below 1.0°C that in some cases are even non-significative. The WEB1 also project more moderate changes, within the range 1.5-2.0°C that slightly rises to 2.0-2.5°C in the elevated regions. Indeed, the mountainous areas are the most likely to be exposed to the largest changes that might reach up to 4.5°C (WEA1B, WEA2 and WCA2) during the cold season.

Most substantial changes in Tmax during the spring might be found in the half south of the peninsula. The information obtained from all simulations clearly distinguish the south form the remaining IP. For example, the projections under the A1B and A2 scenarios suggest changes above the 4.0°C threshold in most of the southwest quarter of the IP and over 4.5°C in the Baetic System and Sierra Morena. The Pyrenees and the northwestern mountains are also likely to experience large changes in spring Tmax. On the other hand, the north Atlantic and the Mediterranean coasts, the North Central Plateau and the Ebro valley might be exposed to less severe changes. In particular, the coast changes are likely to remain below 3.0°C, whereas for the rest of the regions they might be slightly higher. The projected changes from the WCA2 are somehow more pronounced, and the Ebro valley and the Northern Central Plateau might undergo changes above 4.0°C.

During the autumn, most of the simulations project changes that are more moderate than for the summer, especially in the CCSM-driven simulations. In the WCB1, projected changes are in line with the rest of seasons and barely exceed 2.5°C. However, for the rest of the runs, large areas are covered by projections of increases above 3.5°C, even exceeding 4.5°C in WCA2, WEA1B and WEA2. In the latter, a significant portion of the IP might be expected to suffer from autumn Tmax increases over 5.0°C.

The magnitude of Tmin changes at seasonal scales is significantly smaller than
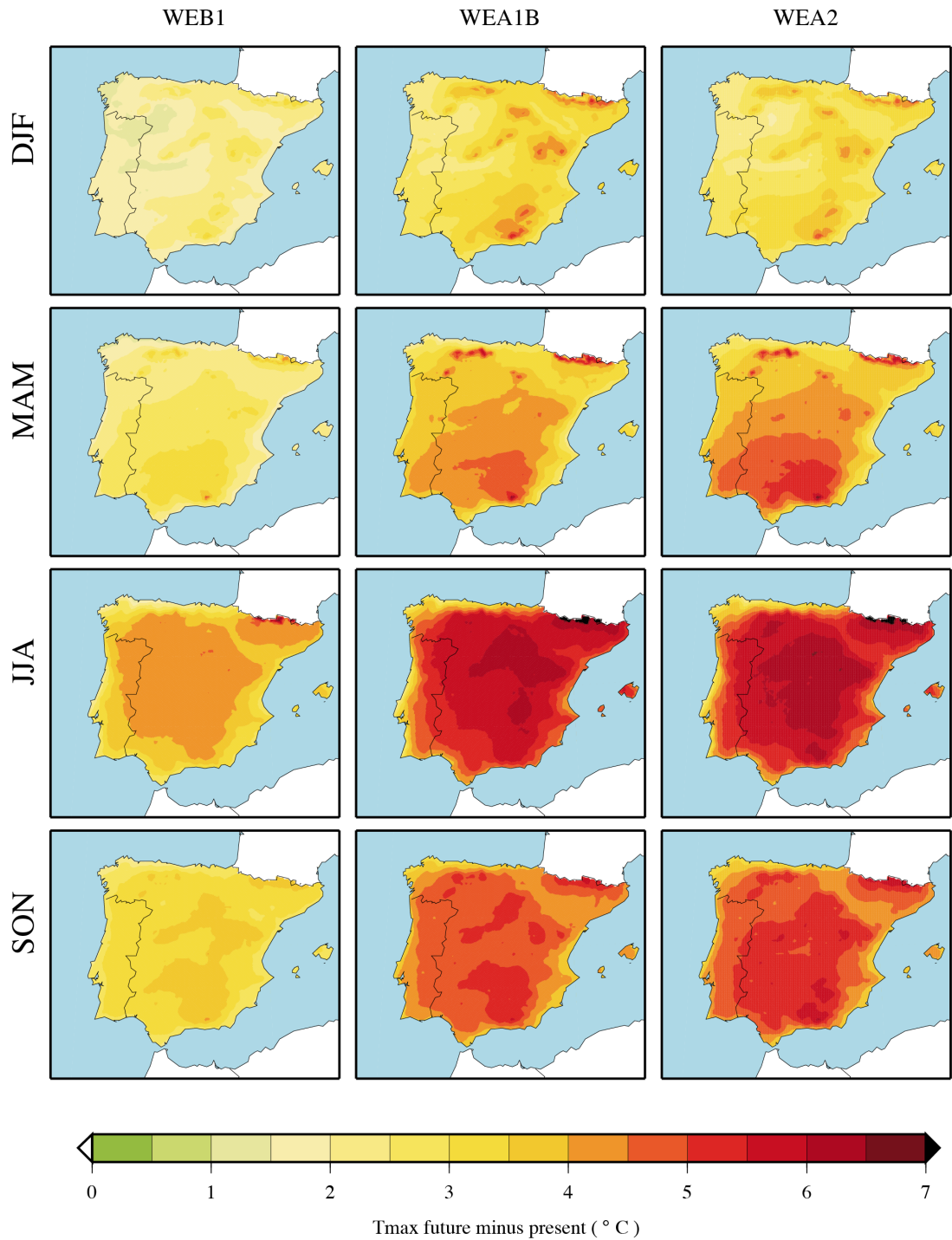
Figure 7.19: *Projected changes for seasonal mean Tmax over the IP for simulations nested in ECHAM5. In rows are displayed the seasons, whereas in columns, the different scenarios. Differences between 2070-2099 and 1970-1999 seasonal means. Black dots indicate non-significative changes at 95% of confidence (t-test).*

Figure 7.20: *As Fig. 7.19 but for CCSM*

those projected for the Tmax in all WRF simulations (Figs 7.21 and 7.22). All changes are significative except at some locations in the WCB1 for the winter. Similarly to Tmax, largest changes are again projected for the summer and over the mountainous areas.

Winter Tmin changes are projected to range from the most moderate increases in the WCB1 simulation (0.5-1.5°C) to the largest simulated changes in the WEA1B (over 2.5°C in the entire IP). Differences among regions are still associated to elevation, but distance to the sea does not seem to be as determinant as for Tmax. Apart from the Pyrenees and some isolated locations in the mountains, where Tmin increases might be expected to be larger than 4.0°C (WEA1B, WEA2 and WCA2), the changes are quite homogeneous in the peninsula. The northwest, the Northern Central Plateau and the western river basins are subject the smallest changes (<2.0°C in the CCSM-driven simulations and < 3.0°C in the ECHAM5-driven runs).

The Tmin changes during the spring are fairly similar to winter ones in the simulations forced by ECHAM5 and slightly larger in the CCSM-driven runs. Indeed, in the WCA1B, increases between 1.5-2.5°C are projected, and in the WCA2, the range raises up to 2.5-3.5°C. Overall, the southeastern area is likely to suffer from large rises in temperature (>3.5°C in WEA1B, WEA2 and WCA2). Once more, the most severe changes are projected in the Pyrenees, the Central System and the Baetic System.

Concerning the summer Tmin, the interior of the IP is likely to experience changes in temperature over 4.0°C in both simulations under the A2 scenario, and changes over 4.5°C might be expected over considerable extensive areas according to the WEA1B simulation. On the opposite side, WCB1 project changes between 1.5°C and 2.0°C over nearly the entire IP. The other two runs (WEB1 and WCA1B) indicate slightly larger increases for summer Tmin (2.5-3.5°C in most of the regions). The areas with most significant changes are limited to the north by the Central System and the Iberian System, and extend down to the Mediterranean coast, especially towards the east. The Galician Massif and the Pyrenees are also among most affected regions. On the other hand, the northern coast, the Northern Central Plateau and the main river basins are subject to smaller increases.

Autumn Tmin changes are spatially very homogeneous for both WCB1 (1.5-2.0°C), WCA1B (~2.5°C in most cases) and WEB1 (~2.5°C). The rest of simulations project larger changes in the Central System, the Pyrenees and the Baetic System, except for WEA1B that extends these changes to the southern half of

Figure 7.21: *Projected changes for seasonal mean Tmin over the IP for simulations nested in ECHAM5. In rows are displayed the seasons, whereas in columns, the different scenarios. Differences between 2070-2099 and 1970-1999 seasonal means. Black dots indicate non-significative changes at 95% of confidence (t-test).*
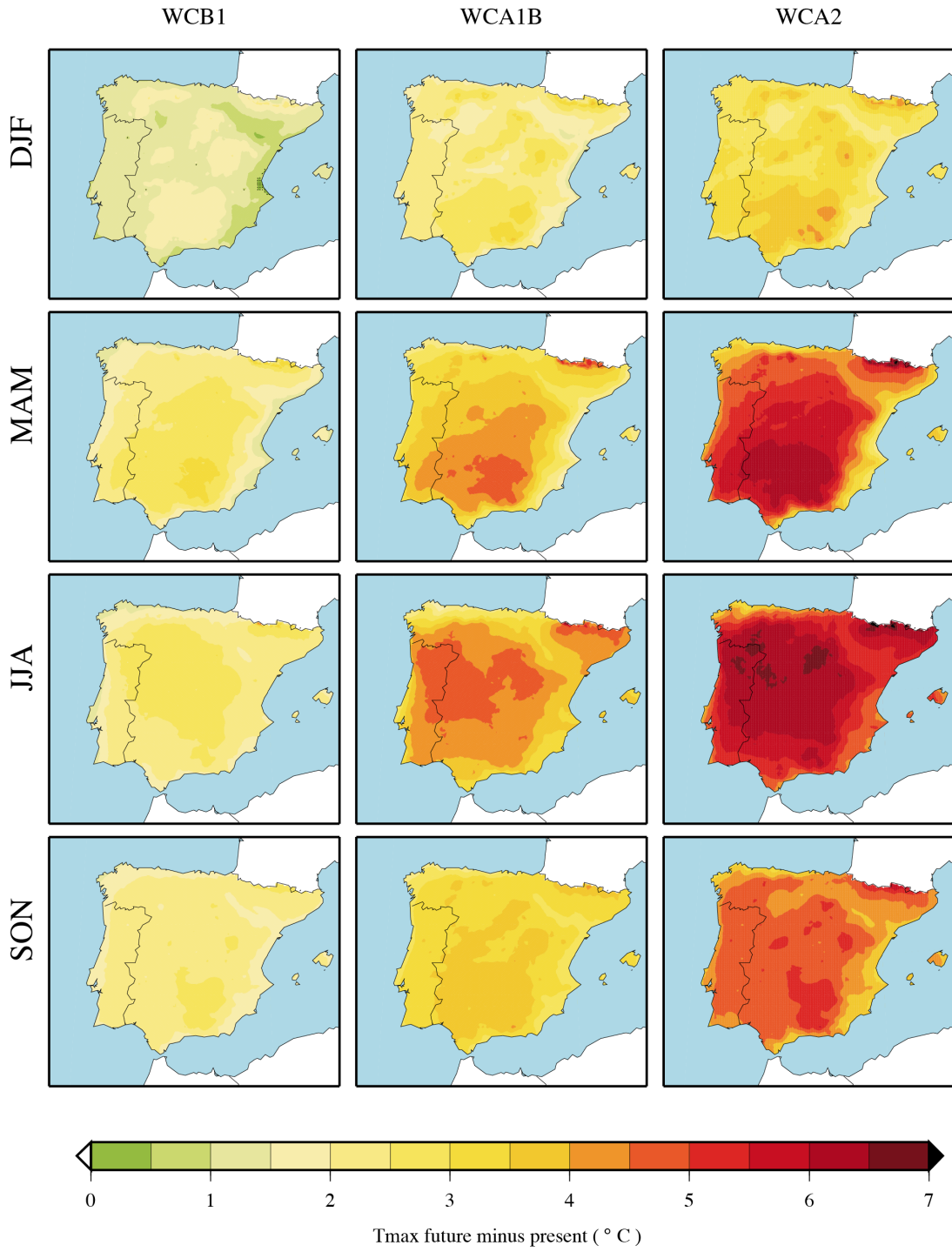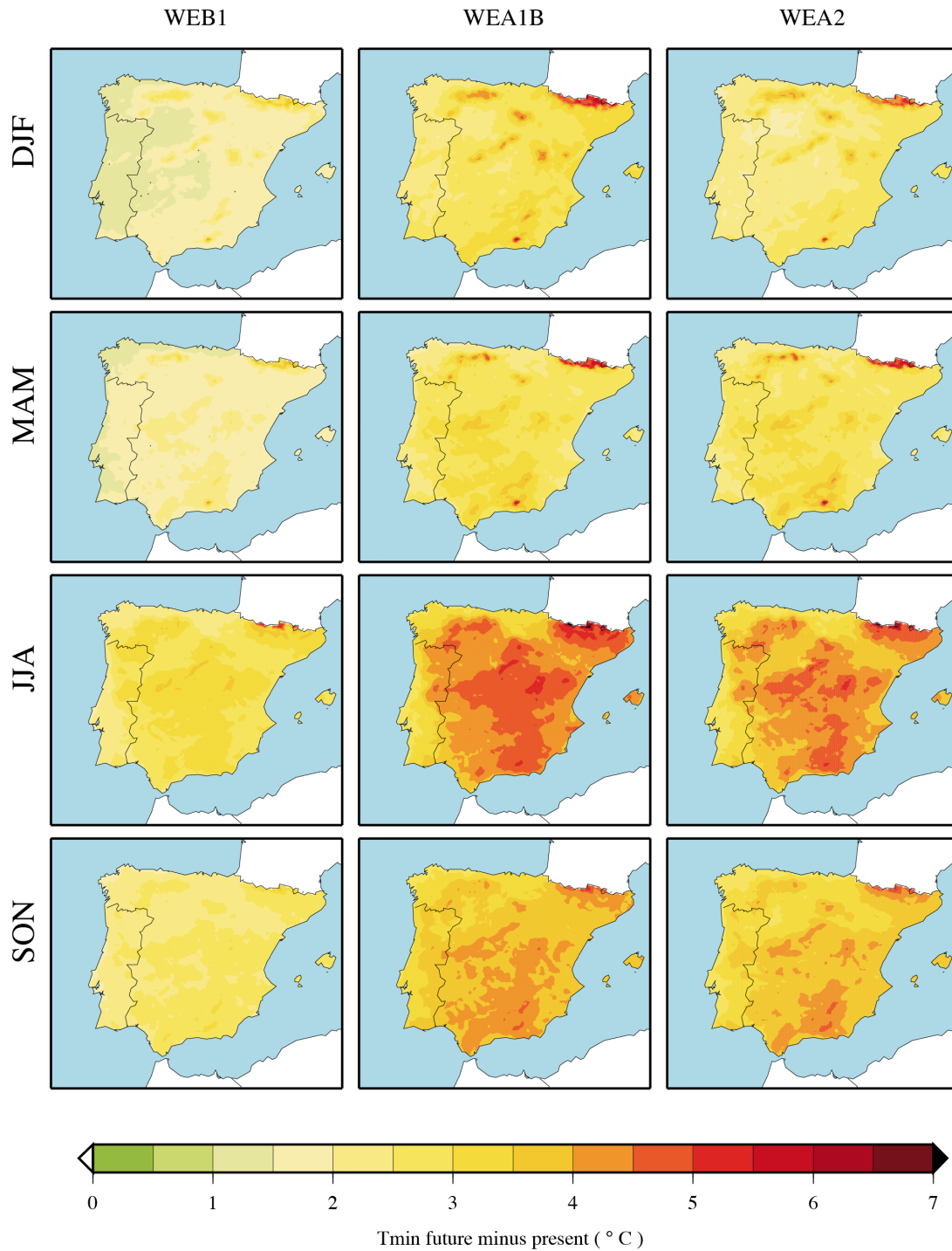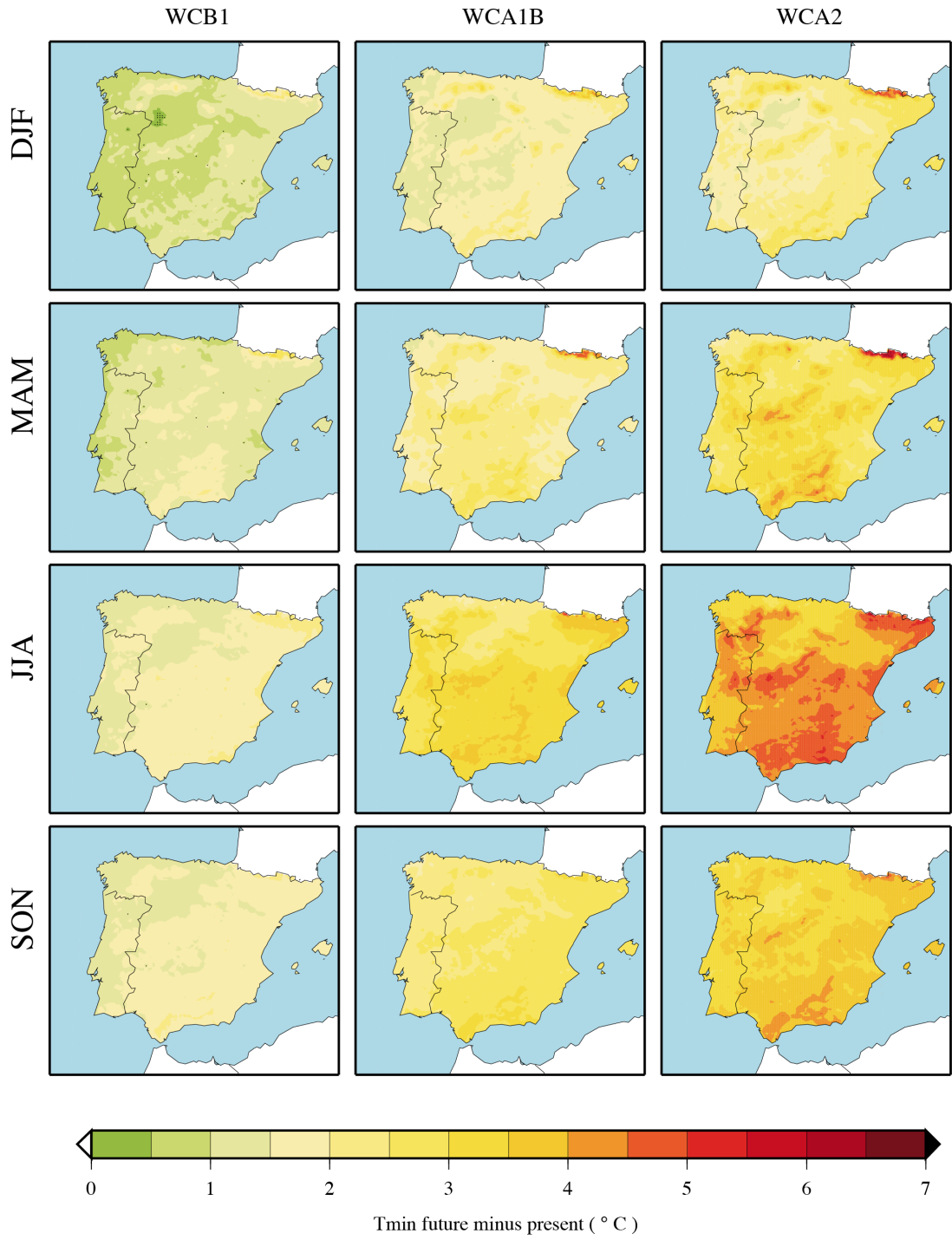
Figure 7.22: *As Fig. 7.21 but for CCSM*

the IP. Most of the increases for these simulations are within the range 3.5-4.0°C, with areas that might raise up to 4.0-4.5°C. The Baetic System is systematically projected to suffer from severe changes in all simulations, although the magnitude varies among scenarios.

In general, the behavior of seasonal Tmax and Tmin is similar to annual mean changes in terms of the spatial distribution, although there might be expected a disparity between different seasons. Winter is season when changes might be more moderate, whereas during the summer the Tmax and Tmin changes attain their maximum. The river basins, the Northern Central Plateau and the coasts for Tmax, are the regions where temperature changes might be milder, whereas the mountainous and internal areas are overall those most exposed to substantial temperature changes. Nevertheless, it should be kept in mind that it was precisely over high-elevated regions where the largest errors were found in the model evaluation, and thus the projections over these areas should be taken with caution.

7.3.3   Changes in monthly temperature

The changes in temperature might be different at different moments of the year. To explore how these changes might vary through the year, the changes in monthly mean Tmax and Tmin are calculated. Figures 7.23 and 7.24 illustrate the changes of monthly Tmax for the period 2070-2099 with respect to 1970-1999 over the eight temperature regions according to ECHAM5- and CCSM-driven simulations, respectively.

In accordance with previous results, Tmax changes are projected to be especially large during the central months of the year (May-October), although in the simulations constrained by CCSM the changes are more pronounced in May and September. In fact, the most prominent feature of Tmax changes in the annual cycle is the generalized increase in May. In all the regions and under all the scenarios, a peak in the Tmax monthly changes is observed during this month. There are regions where this feature is particularly marked (GU, SW, PL, EI and HI) and might be associated with earlier summer conditions. Less cloudiness might be at the origin of this Tmax increases, which is supported by a negative peak in monthly precipitation changes (Fig. 7.5).

On the other side, the most remarkable characteristic of the changes in the Tmax annual cycle from the ECHAM5-driven simulations is the almost undistinguishable projections obtained for the A1B and A2 scenarios. This is in agreement

with the discussion presented before about the evolution of radiative forcing for different scenarios and the GCM inertia (Sec. 7.3.1). For these two scenarios, the increases in temperature during the warmest months (July-September) often exceed 5.0°C. Under the B1 scenario, the changes exceed 3.0°C in most of the regions, except for the coastal AT. Smallest changes are systematically observed in February-March, even though they still exceed 1.0°C in all regions under the B1 scenario. In the other two scenarios, changes during these months are slightly below the 3.0°C threshold.

As for the largest changes in the CCSM-driven runs, May Tmax changes reach up to 7°C in many regions under the most severe conditions of A2 scenario. Differences between A2 and A1B scenarios are more marked in these runs and in fact, under the A1B scenario, the projected increases are more moderate. Nonetheless, the changes still go beyond the 4.0°C during the warmest months. Smallest changes are projected in December-February, where monthly mean Tmax might be expected to increase between 1.0°C and 2.0°C (except for ME region).

The annual cycle of monthly Tmin changes are also calculated. Figures 7.25 and 7.26 show the evolution of monthly Tmin changes through the year for simulations driven by ECHAM5 and CCSM, respectively.

The shape of the annual cycle for Tmin changes is quite similar to that obtained for Tmax, although the projected changes for Tmin are considerably smaller (note that the scale in the plots is different: 0-8°C for Tmax and 0-5°C for Tmin). The maximum values are attained during the central months (May-October) whereas the minimum are obtained for the coldest ones (December-April).

Under the B1 scenario, the ECHAM5-driven simulation projects changes that remain below 3.0°C for monthly Tmin, except in the high-elevation areas. However, it should be mentioned once again that the errors were particularly large for this region in the model evaluation and thus the projections should be regarded with caution. Under the other two scenario, projected changes are vey similar, as occurred for Tmax and range from about 2.0°C in February to almost 5.0°C in August over certain regions (SW, PL, EI, and HI).

Regarding the information downscaled from CCSM, the changes are significantly smaller for the B1 scenario (between 1.0°C and 2.0°C in most of the situations) and the A1B scenario (between 1.5°C and 3.5°C), whereas under the A2 scenario, the projected changes are similar in magnitude to those yield by the ECHAM5-driven simulation. Just like for Tmax, the most remarkable feature in the annual cycle of Tmin changes is the maximum attained in May, which is
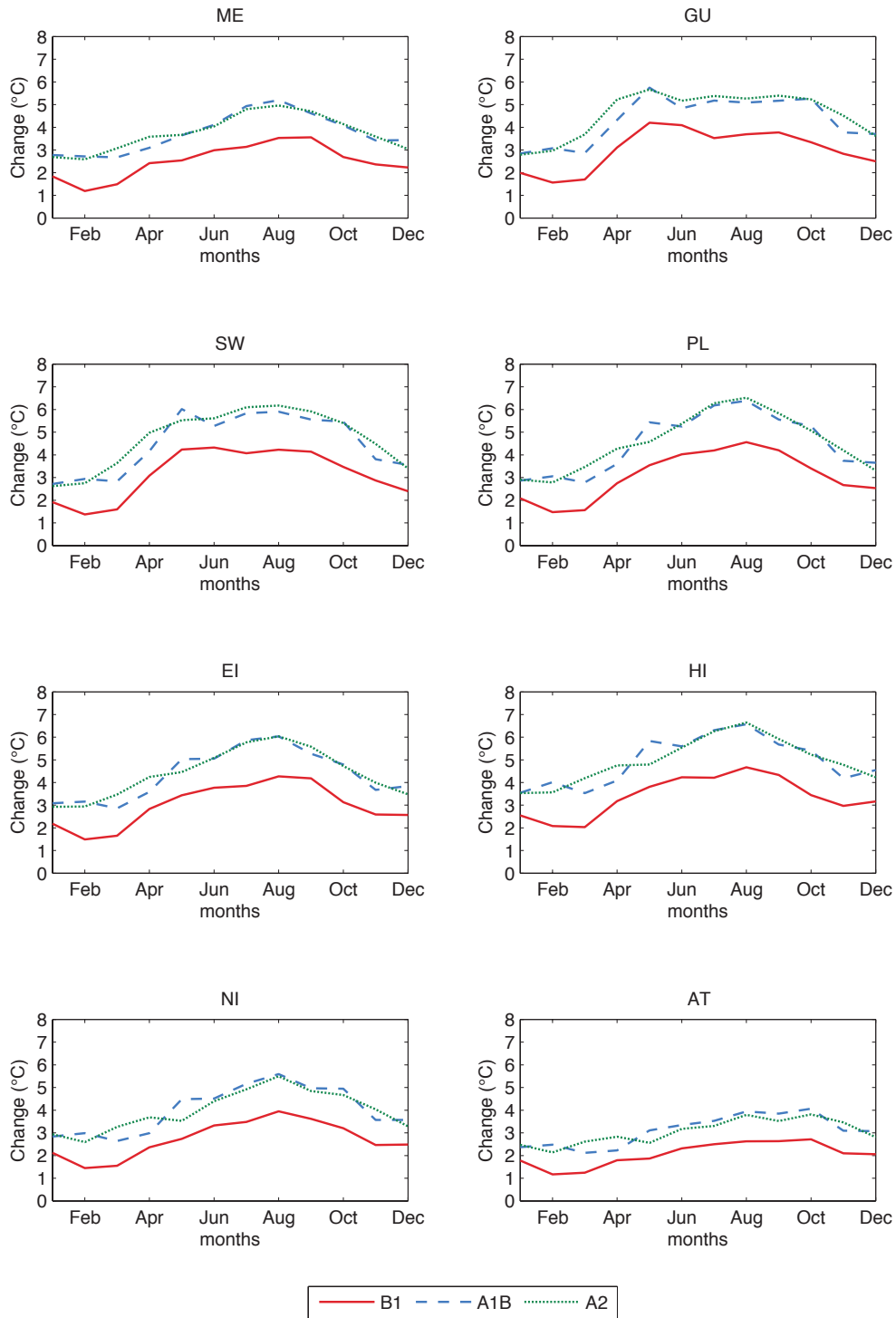
Figure 7.23: *Projected changes in the monthly mean Tmax annual cycle from the ECHAM5-driven simulations. The changes are the differences between monthly climatologies for the periods 2070-2099 and 1970-1999, and over the eight temperatures Spain02 regions. All changes are significative (Student's t-test, 95% confidence).*

Figure 7.24: *As Fig. 7.23 but for CCSM.*

Figure 7.25: *Projected changes in the monthly mean Tmin annual cycle from the ECHAM5-driven simulations. The changes are the differences between monthly climatologies for the periods 2070-2099 and 1970-1999, and over the eight temperatures Spain02 regions. All changes are significative (Student's t-test, 95% confidence).*
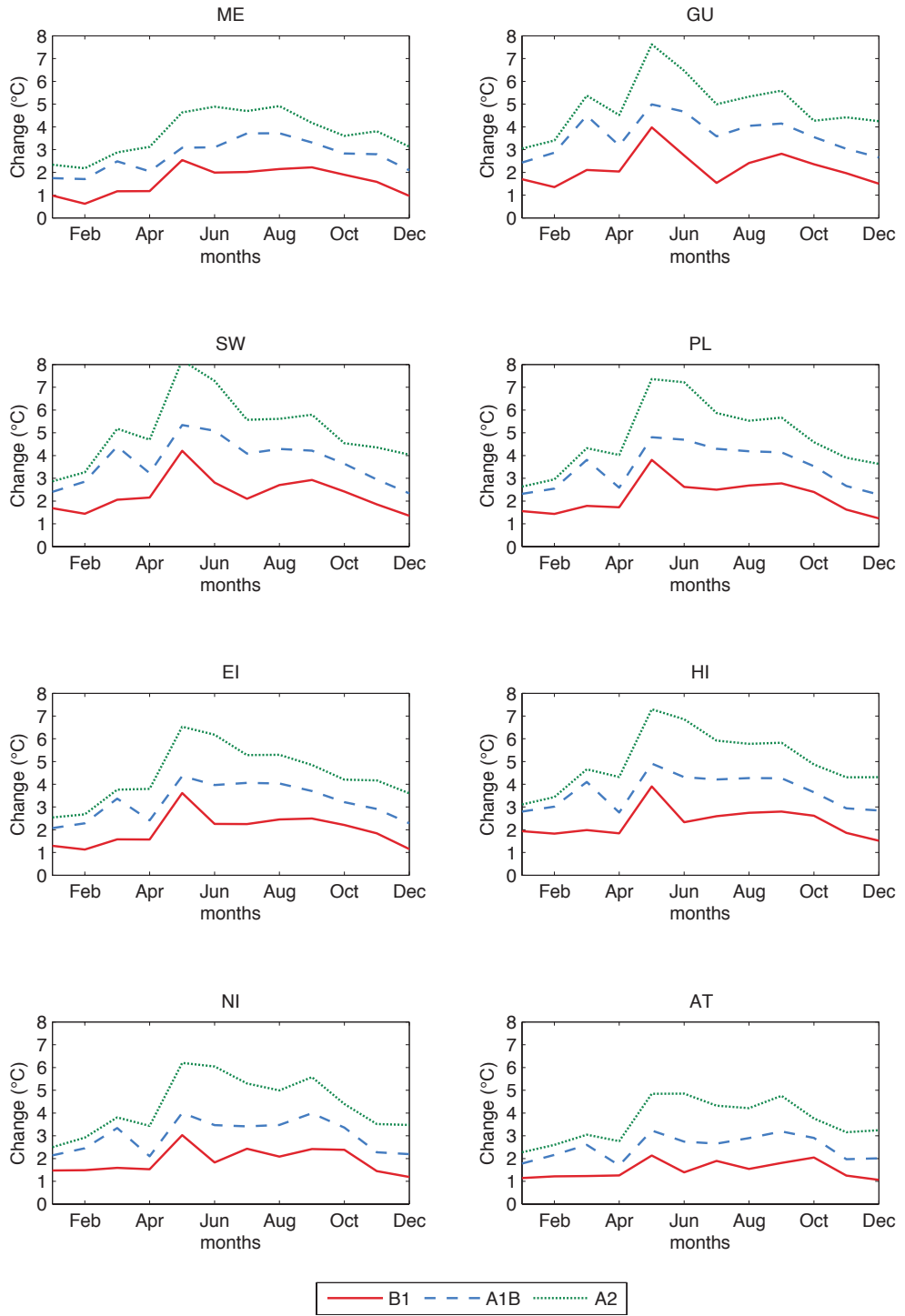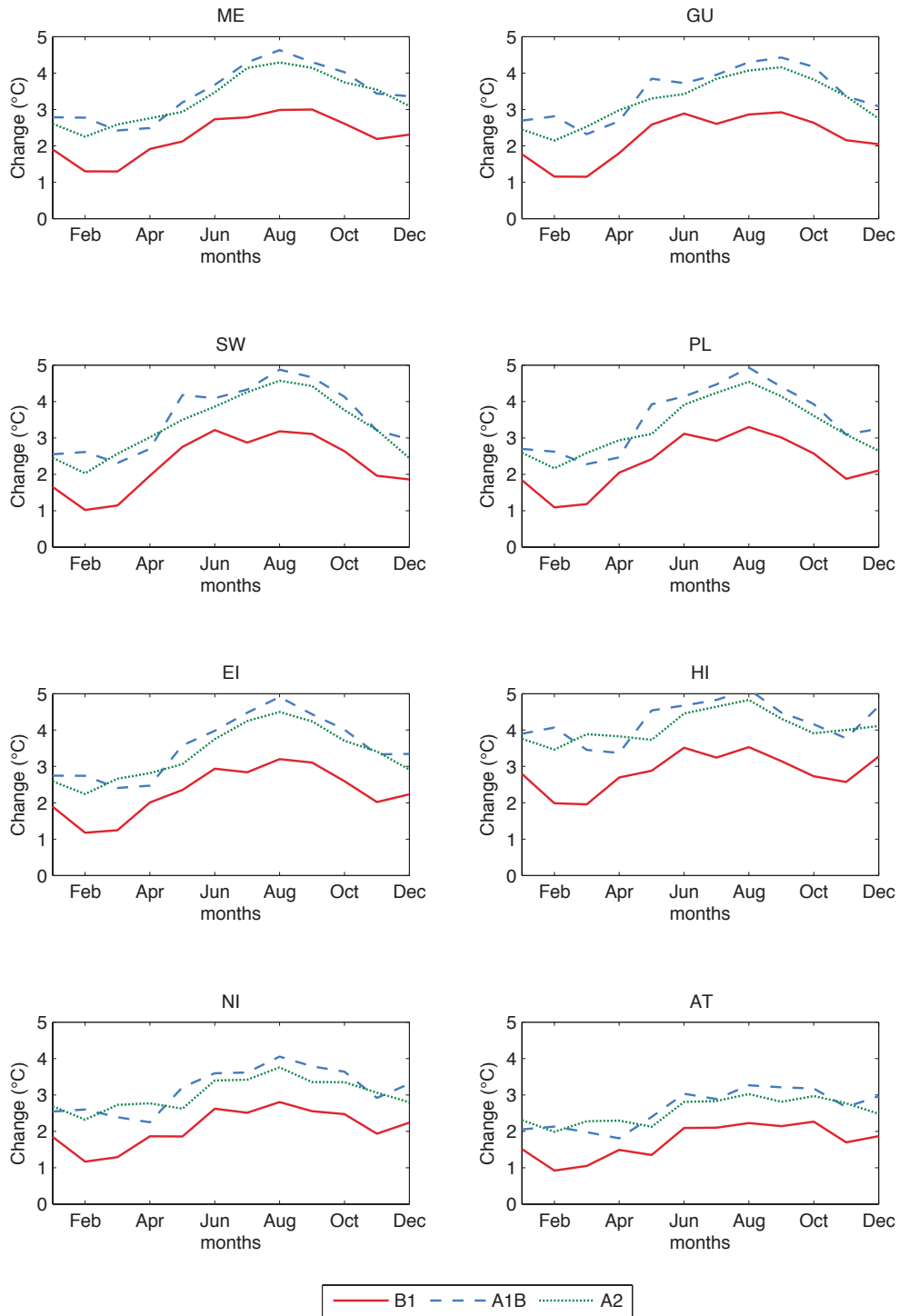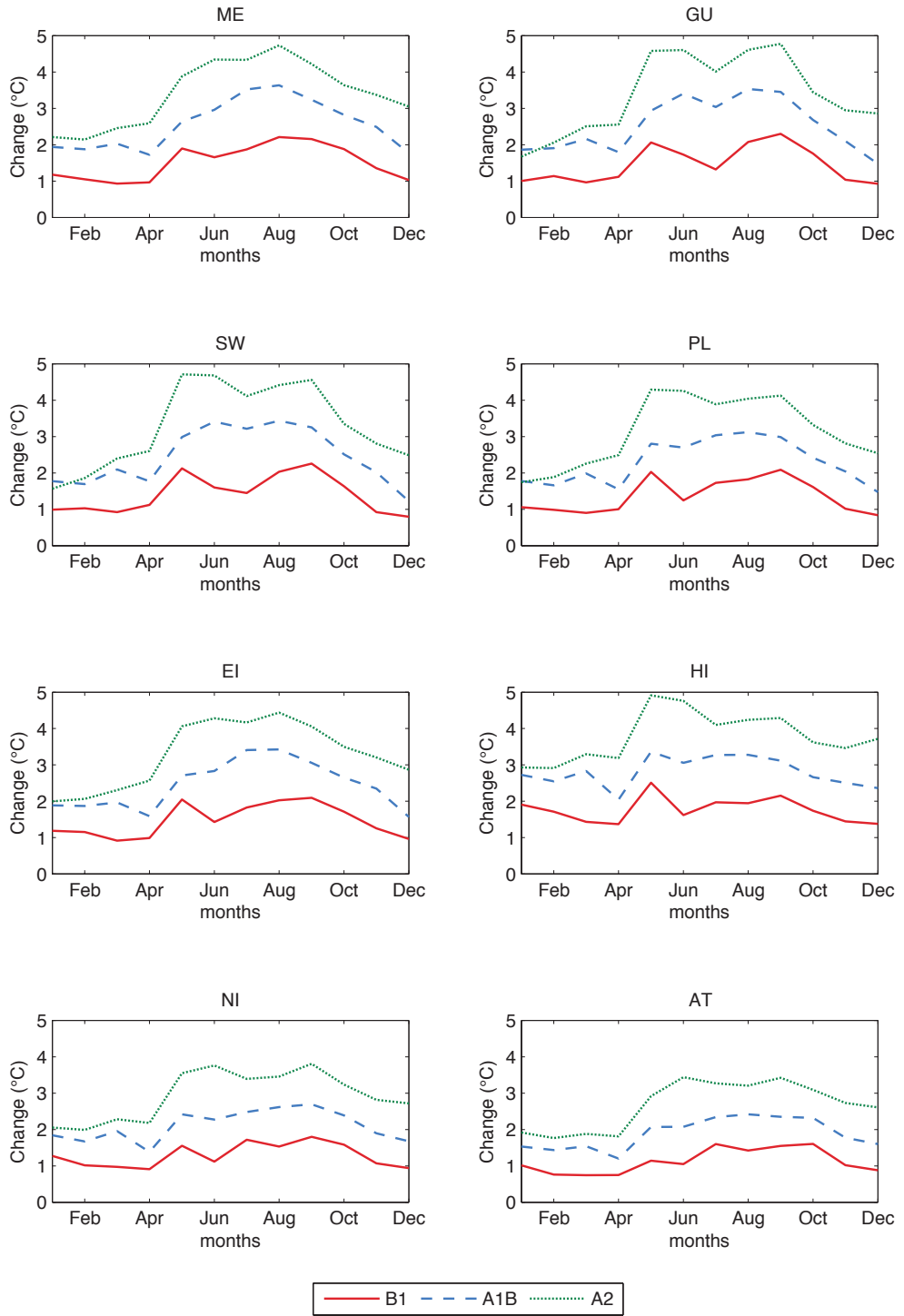
Figure 7.26: *As Fig. 7.25 but for CCSM.*

clearly differentiated from the rest of the months in most of the regions.

The analysis of the projected changes for both Tmax and Tmin along the year emphasizes the results obtained for seasonal changes and provide further detail in the timescale. The warmest months are likely to be affected by largest changes. Besides differences in radiation through the year, other aspects might be at the source of these results. For example, an important decrease in precipitation during spring and early summer might cause depletion of soil water during the summer, changes of the surface heat flux partition and thus an enhanced increase in temperature during these months.

In addition, the distance to the sea also plays an important role. In particular, the distance to the Atlantic Ocean, which is expected to warm less than the Mediterranean Sea due to thermal inertia. The effect of the Atlantic Ocean is observed in the AT, where changes tend to be milder than for the rest of the IP.

7.3.4 Changes in daily temperature

The long-term means projected changes for both Tmax and Tmin have been addressed so far. The picture of future changes is here completed through the analysis and discussion of projected changes in daily temperature. The examination of future temperature PDFs, the study of percentiles using Q-Q plots and the assessment of changes in extreme events will help to provide information to describe future climate in terms of temperature.

Tmax and Tmin PDFs

The analysis of the temperature PDFs makes possible to project future changes beyond the simple study of the means. The daily Tmax and Tmin PDFs are here calculated for both present and future in order to to explore changes in the full spectrum of events. Figures 7.27 and 7.28 illustrate the PDFs for Tmax calculated over the periods 1970-1999 and 2070-2099 to ascertain displacements of the distribution or changes in their shape.

It should be stressed that these figures show absolute values of temperature instead of changes with respect to present conditions. However, the deviations between WRF estimates and observations described in Chapter 6 prevent from drawing any conclusion about the probability of a particular event to occur. In fact, the aim of these plots is not to determine the distribution of future temperature, but compare between present and future distributions.
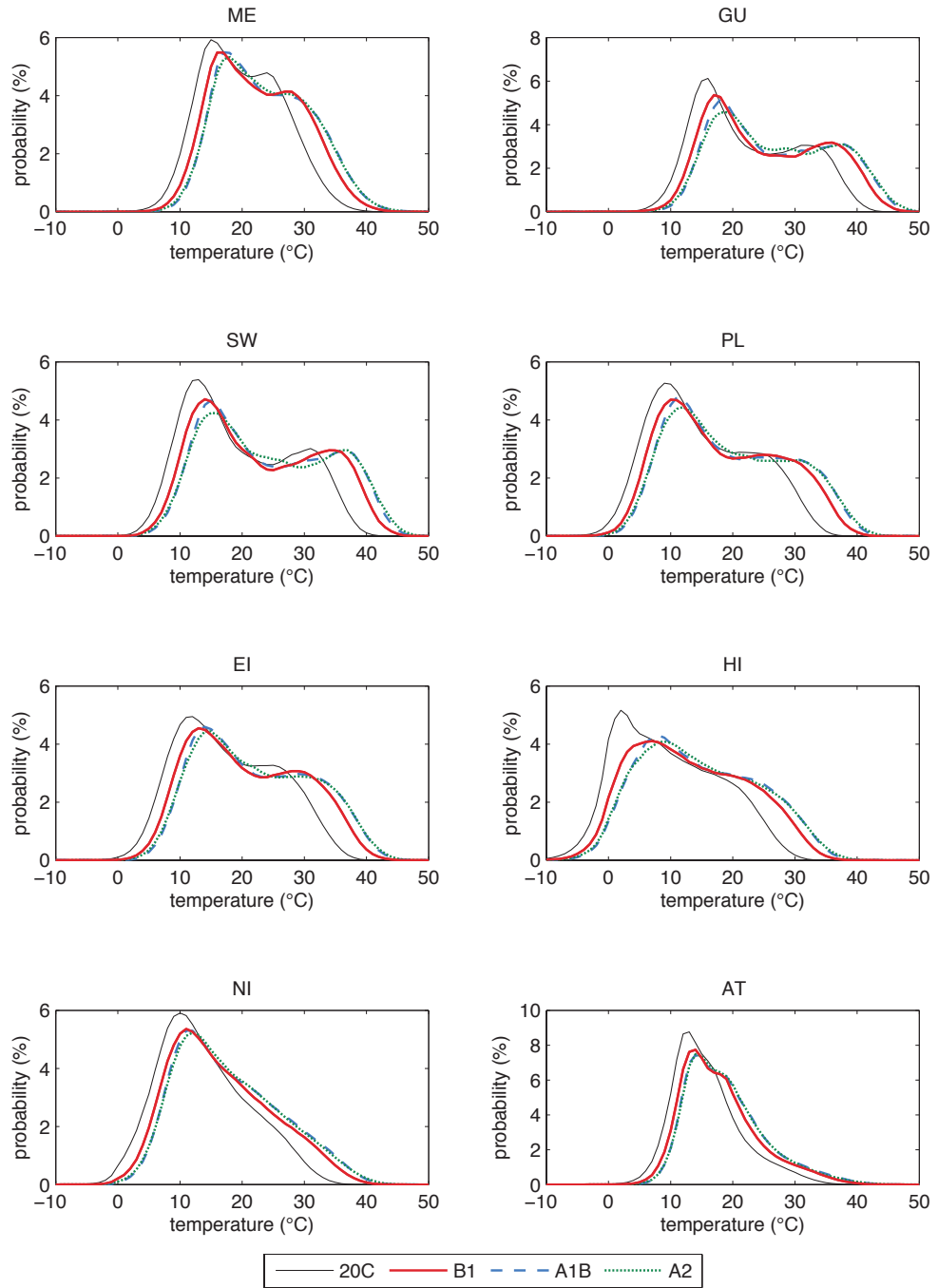
Figure 7.27: *Present (1970-1999) and future (2070-2099) daily Tmax PDFs from ECHAM5-driven simulations over the eight temperature regions. The X-axis values are only shown for guidance and the probability of particular events cannot be addressed with this plot. The relative position and shape between present and future distribution should be regarded instead.*

Figure 7.28: *As Fig. 7.27 but for CCSM.*

At first sight, the most noteworthy differences between present and future distributions for daily Tmax are the shift towards higher values and the largest Tmax variability embodied in the flattening of the curves. All values of the distribution are not equally shifted and highest values tend to be subject to largest increases. Namely, not only the means are displaced, but also the distribution expands towards higher temperatures. This behavior is observed for all WRF simulations and over the entire IP.

The bimodal shape that characterizes temperature in certain regions of the IP (Ch. 6) is likely to be enhanced in the future in some regions (GU, SW, PL and EI), which reveals that transitions between warm and cold seasons might be faster in the future.

This two features (the largest variability and the enhanced bimodality) seems to be more intense as we move from the B1 to the A2 scenario in the CCSM-driven simulations. Indeed, the differences between the scenarios for the lower tails of the distribution are smaller than for the upper percentiles. And also the two differentiated modes are more evident in the A2 scenario than in the B1. In the case of ECHAM5-driven simulations, differences among scenarios are not as significant, particularly between A1B and A2, for which the differences are almost negligible.

The projected changes of the daily Tmin PDFs are characterized by the same features that affect Tmax PDFs. Figure 7.29 and 7.30 show the present and future Tmin PDFs obtained from the different WRF simulations (ECHAM5- and CCSM-driven, respectively) over the eight temperature regions.

The main features that define the projected changes for Tmin PDFs are the displacement of the entire distribution towards higher temperatures and the increase of daily Tmin variability. The latter is evidenced in the flattening of the curve, that results in a wider distribution and hence in a higher standard deviation. This is particularly true for the upper tail of the distribution, which means that higher values of Tmin might be subject to larger changes in the future. Indeed, the lower values are projected to change significantly less than the higher values in all regions and for all simulations.

Another feature observed for Tmax that is also observed in the Tmin PDF projected changes is the enhancement of the bimodality, although it was more noticeable in Tmax distributions. Nevertheless, for the CCSM-driven simulations, the two modes are clearly identifiable over certain regions, particularly in the south and east of the IP (ME, GU, SW and EI).

It is interesting to note that differences between A1B and A2 scenarios in the
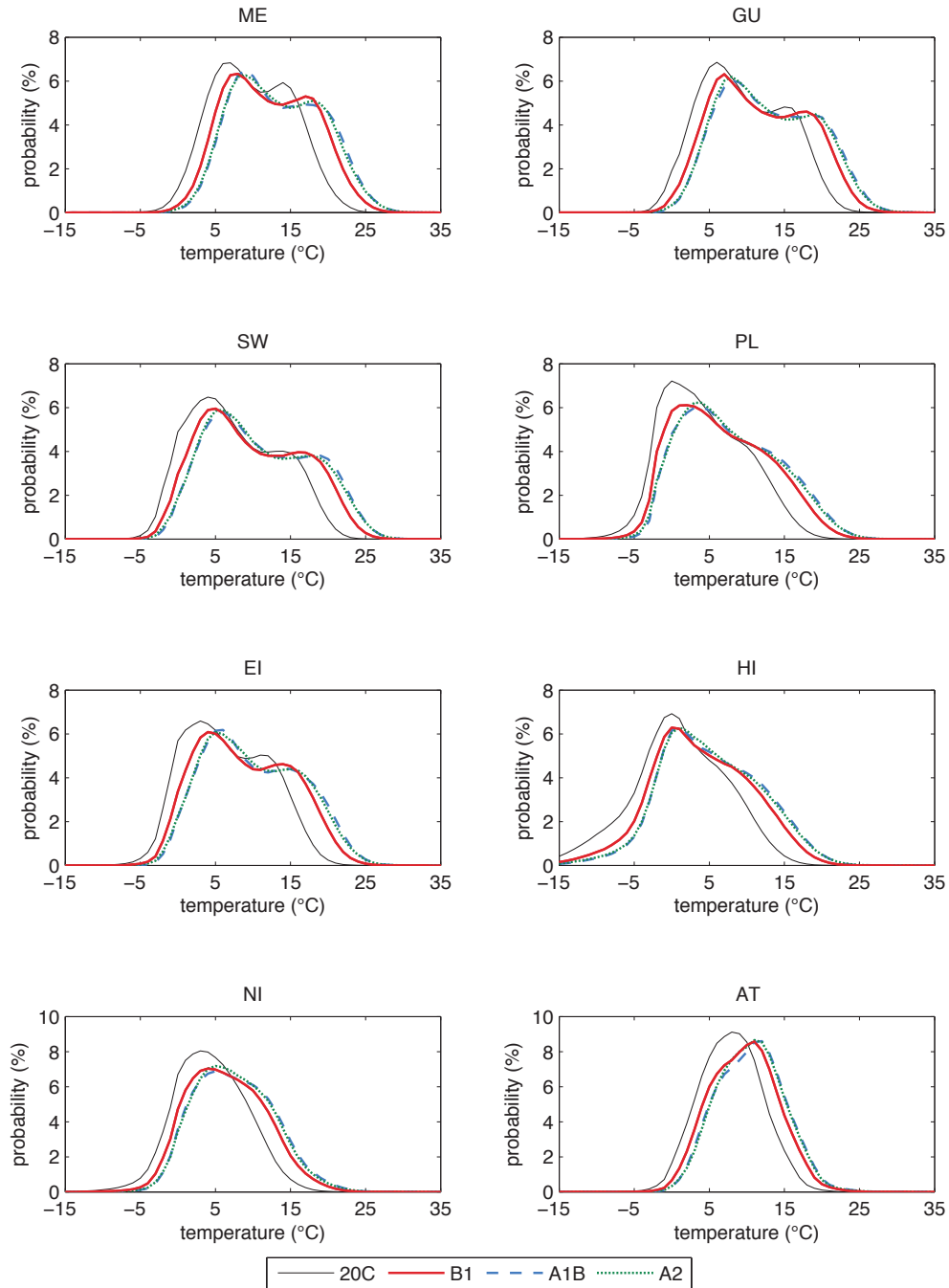
Figure 7.29: *Present (1970-1999) and future (2070-2099) daily Tmin PDFs from ECHAM5-driven simulations over the eight temperature regions. The X-axis values are only shown for guidance and the probability of particular events cannot be addressed with this plot. The relative position and shape between present and future distribution should be regarded instead.*
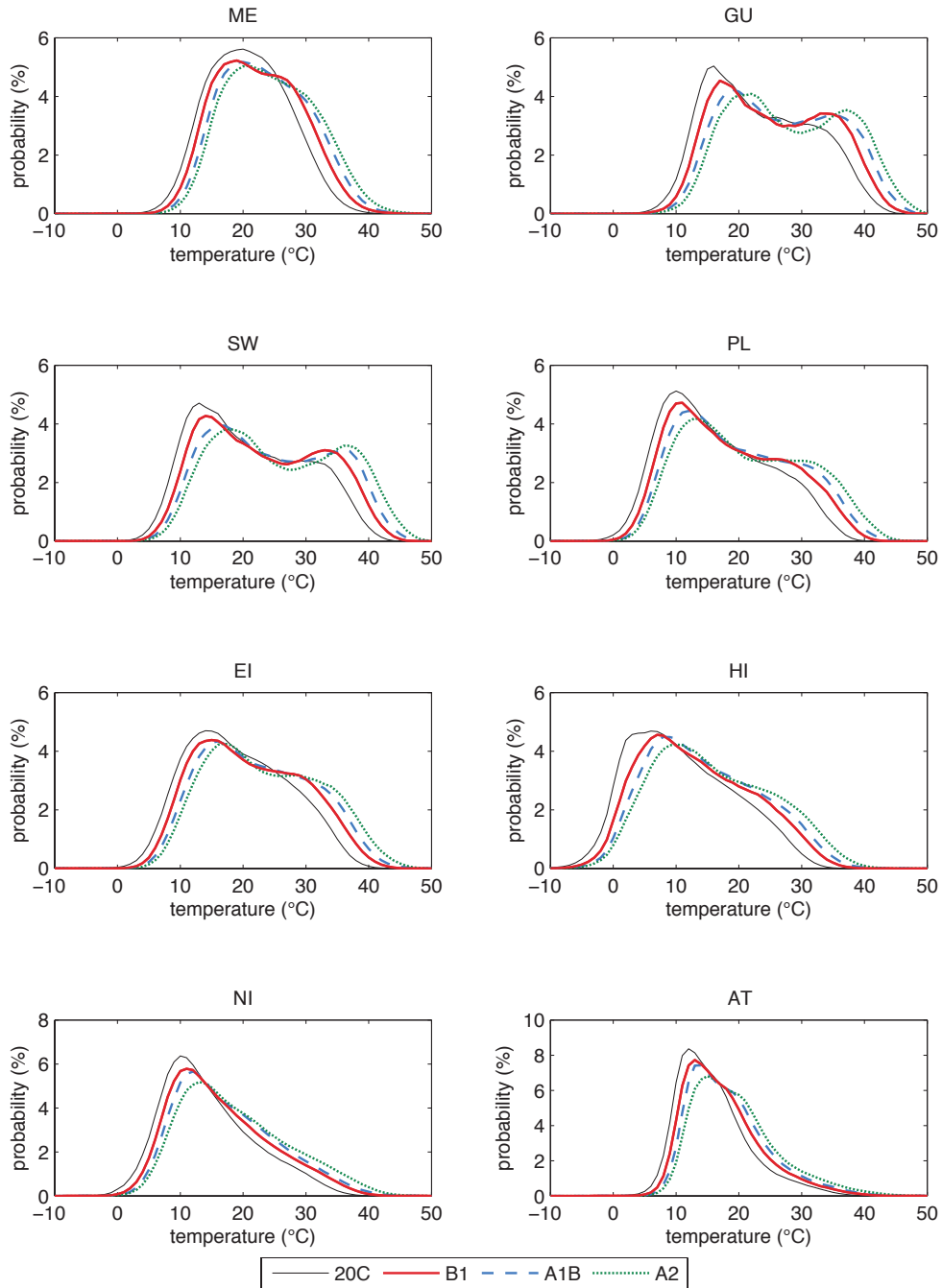
Figure 7.30: *As Fig. 7.29 but for CCSM.*

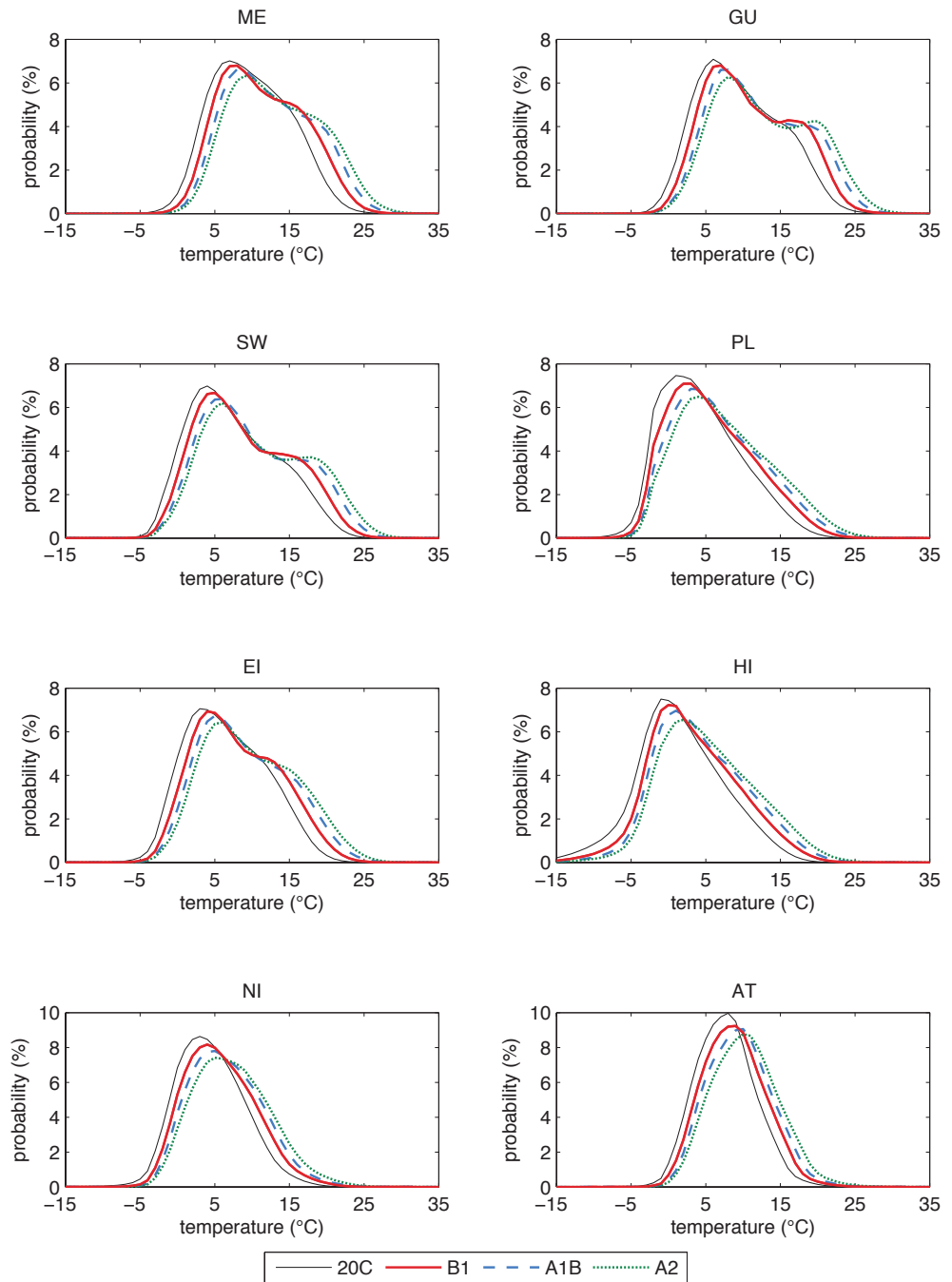runs forced by ECHAM5 are nearly negligible in all regions. Conversely, the Tmin distributions obtained from CCSM-downscaled information are dissimilar under the different scenarios, and the two main features mentioned above (displacement and increased variability) are more intense as we move from the B1 to the A2 scenarios. However, even under the B1, all simulations point to a clear increase in the high Tmax and Tmin values.

Temperature percentiles

The previous section analyzes the changes in the distribution through the PDF. Here a different approach is proposed and the percentiles of both Tmax and Tmin are examined. To be specific a number of percentiles (0.1^{th}, 1st, 5th, 10th, 25th, 50th, 75th, 90th, 95th, 99th and 99.9^{th}) have been calculated and the projected changes are depicted using a Q-Q plot that compares the future and present percentiles.

Figures 7.31 and 7.32 illustrate the Tmax percentiles for future simulations under the three different scenarios versus the percentiles obtained from the present simulations for ECHAM5- and CCSM-driven simulations, respectively. The displacement towards higher temperatures observed in the PDF analysis is here confirmed since all the curves remain above the grey line that indicates no projected changes. The increased variability is also noticeable in these plots and in most of the cases the lowest and highest percentiles are further from the grey line than the central percentiles, which indicates that the distribution tails are subject to more significant changes, especially the upper ones.

Indeed, the most extreme Tmax events (99.9^{th} percentile) are likely to increase in up to 7.0°C under the A2 scenario for both ECHAM5- and CCSM- driven WRF simulations under certain regions (PL, HI, NI and AT). Under the B1 scenario the changes for the uppermost percentile are projected to be more moderate, although they still reach about 5.0°C in HI and 4.9°C in NI, according to ECHAM5-driven simulation and about 3.0°C in the WRF simulations nested in CCSM over all regions except GU and SW, where changes are projected to be about 2.0°C.

The upper percentiles (90th, 95th and 99th) changes might be expected to be of approximately the same magnitude as the uppermost one. At some locations (GU, SW and PL) the WRF simulations constrained by CCSM project the largest changes for the 75th. In general, the changes for the different percentiles in the ECHAM5-driven simulations have the following pattern: moderate changes for the lowest percentiles (0.1^{st} and 1st percentiles), then they reach a minimum for
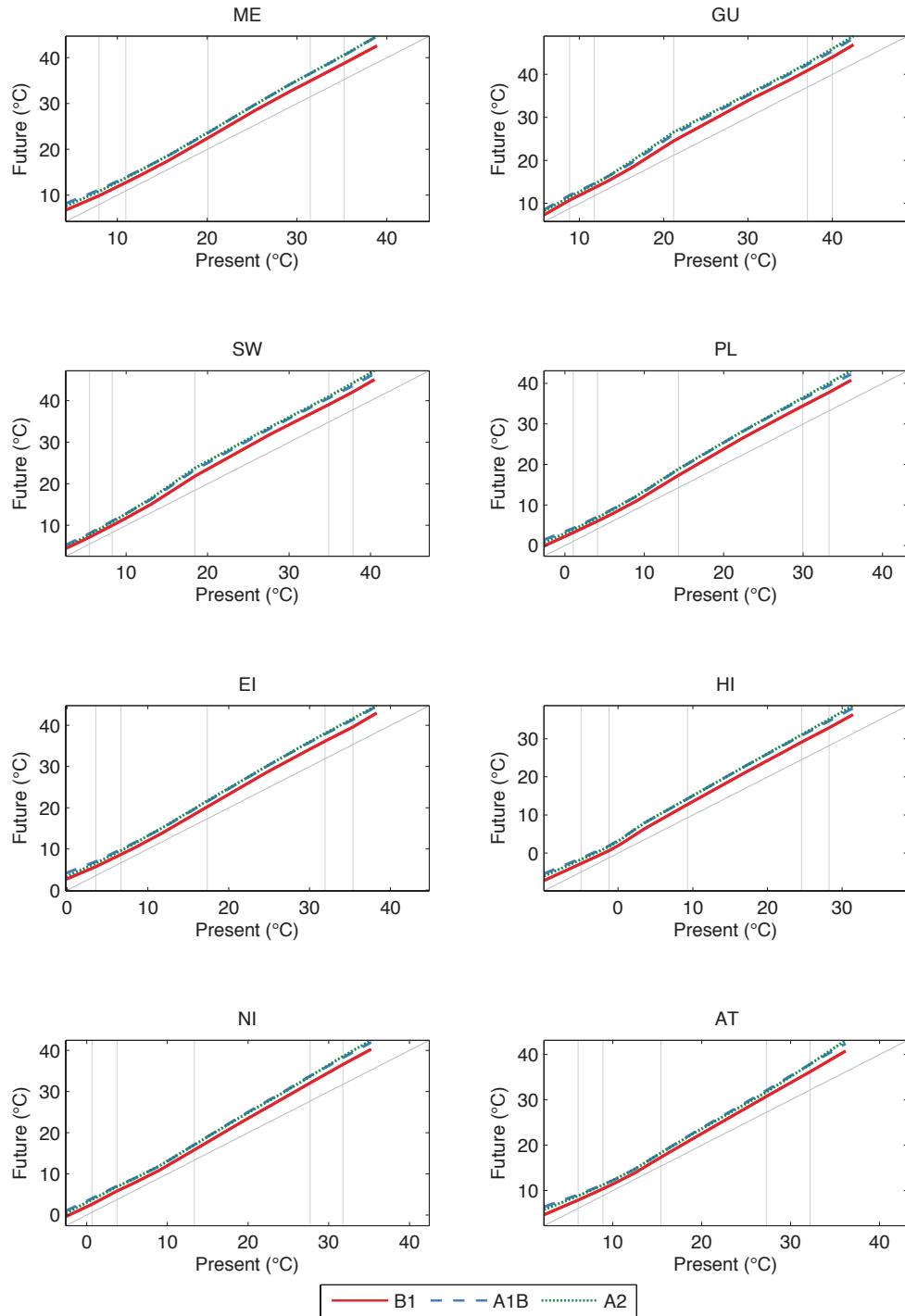
Figure 7.31: *Tmax percentiles from ECHAM5-driven future (2070-2099) simulations versus WRFEH5 present (1970-1999) WRFEH5 percentiles. The grey line indicates no projected changes and delimits increase and decrease in the projected percentiles. The vertical lines determine the 1st, 5st, 50th, 95th and 99th percentiles as reference. The plot extends from the 0.1st to the 99.9th percentile.*
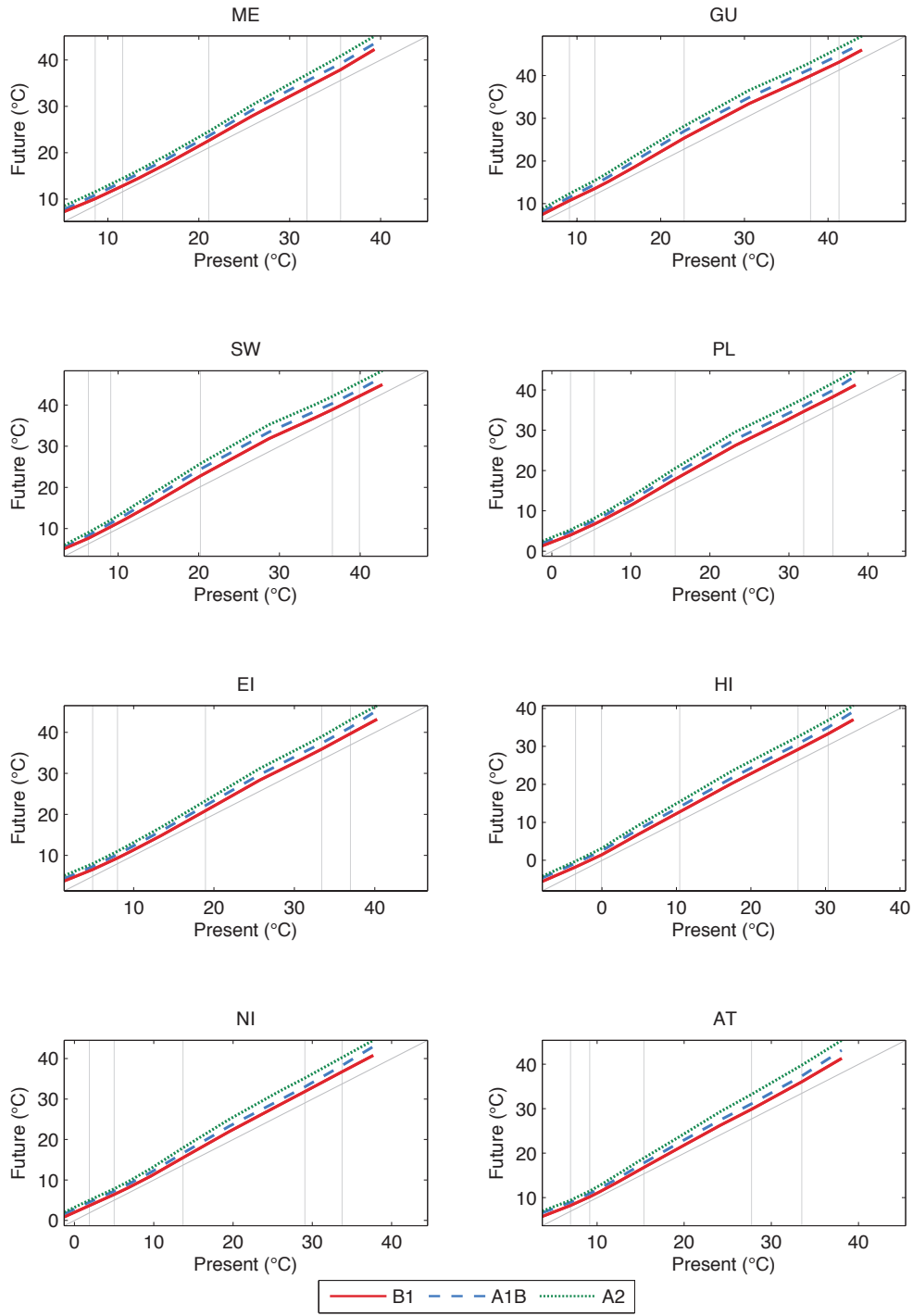
Figure 7.32: *As Fig. 7.31 but for CCSM.*

the next percentiles (5th, 10th and 25th) and start rising up to the maximum attained in the 99th percentile (Fig. 7.33a). On the other hand, the percentile projected changes for the CCSM-driven simulations are slightly different: a moderate change in the lowest percentiles that again reach a minimum in the middle ones (5th, 10th and 25th), but they increase up to the 75th percentile and then stabilize. In fact, in some regions (GU, SW and PL) the maximum changes are reached in this percentile and slightly smaller changes are projected for the highest percentiles (Fig. 7.33b).

According to WRF constrained by ECHAM5 and with regard to Tmin percentiles, the changes in the lowest percentiles, which are actually the extreme minimum temperatures, are projected to be as large as the higher percentiles or even larger in all regions, except the ME, GU and SW, where the upper percentiles are likely to suffer from more significant changes (Fig. 7.34). All the Tmin percentiles are projected to be higher in the future (2070-2099).

The overall shape of the Q-Q plot indicates that the lowest Tmin values (0.1^{st} percentile) might increase considerably, then the smallest changes might occur in the 5th and then they remain quite constant until the 25th percentile, to finally continue growing

Figure 7.33: *Typical changes projected for different Tmax percentiles as simulated by ECHAM5-driven simulations over ME region (a) and by CCSM-driven simulations over PL region (b).*

until the 99.9^{th} percentile. Exceptions are found for the HI region, where the changes are very pronounced until the 25th percentile or the GU and ME regions, where the changes continuously increase from the 0.1^{st} to the 99.9^{th} percentile.

The lowest extremes of temperature (0.1^{st} percentile) might be expected to rise up in even 6.5°C under the A1B scenario in the NI region. Indeed, the largest changes are systematically projected under this scenario, being the projections for the A2 scenario more modest, although very similar. For the rest of the regions, the largest changes in the lowest Tmin percentile are projected occur in the PL (5.9°C, A1B) and in the EI (4.7°C, A1B). The southern regions (ME, GU and

Figure 7.34: *Tmin percentiles from ECHAM5-driven future (2070-2099) simulations versus WRFEH5 present (1970-1999) WRFEH5 percentiles. The grey line indicates no projected changes and delimits increase and decrease in the projected percentiles. The vertical lines determine the 1st, 5st, 50th, 95th and 99th percentiles as reference. The plot extends from the 0.1^{st} to the 99.9^{th} percentile.*

SW) might be subject to less substantial changes, ranging from 2.4°C in the GU to 3.1°in the ME, both for the A1B. On the other hand, the projected changes under the B1 scenario are much less severe for the lowest temperatures and are between 1.0°C for the GU region to 3.6°C in the PL.

The warmest values of Tmin (99.9^{th}) are also projected to vary considerably in the future. In fact, the changes are within the range 4.9-5.6°under the A2 scenario and 3.4-3.9°C under the B1 scenario, in all regions except AT, where changes are slightly smaller. Changes under the A1B scenario are very similar to those obtained for the A2. For the rest of the upper percentiles (75th, 90th, 95th and 99th), the changes progressively decrease but a very slow rate and actually remain very similar to the changes of the uppermost percentile.

Regarding the CCSM-driven simulations, the projected changes for Tmin percentiles (Fig. 7.35) follow a similar pattern to that obtained for the ECHAM5-driven simulations with some differences. The lowest Tmin values (0.1^{st} percentile) are expected to be warmer in the future in up to 5.9°C over the most elevated areas (HI region) and about 1.9°C in the GU region, both under the A2 scenario. Conversely, under the B1 scenario, changes are expected to be less important: from 1.2°C in the GU and SW regions to 2.4°C in the EI, with the outlier regions of PL (3.3°C) and HI (4.2°C).

Most of the regions show minor changes for the next percentiles (1st, 5th, 10th and 25th) and large changes in the upper percentiles of Tmin. Indeed, the changes in the 1st percentile, which represent remarkably cold temperatures, remain below 2.5°C in all regions except in HI (5.5°C) and in ME (2.6°C). Under the B1 scenario none of the regions are expected to be subject to changes in the 1st percentile that are larger than 1.5°, excluding once again two regions: the HI (2.6°C) and NI (1.7°C). For the warmest Tmin values, the changes exceed 4.0°C under the A2 scenario in all regions and reach up to 5.8°C in the HI region. Under the B1 scenario the changes are projected to be from 1.3°C (GU) to 2.6°C (HI).

It must be stressed that although the mountains are expected to suffer from changes in temperature that might be above the average (Christensen et al., 2007a), the results obtained here for the HI region might be hampered by the substantial errors found in the model validation for this region, and thus they must be regarded with caution.
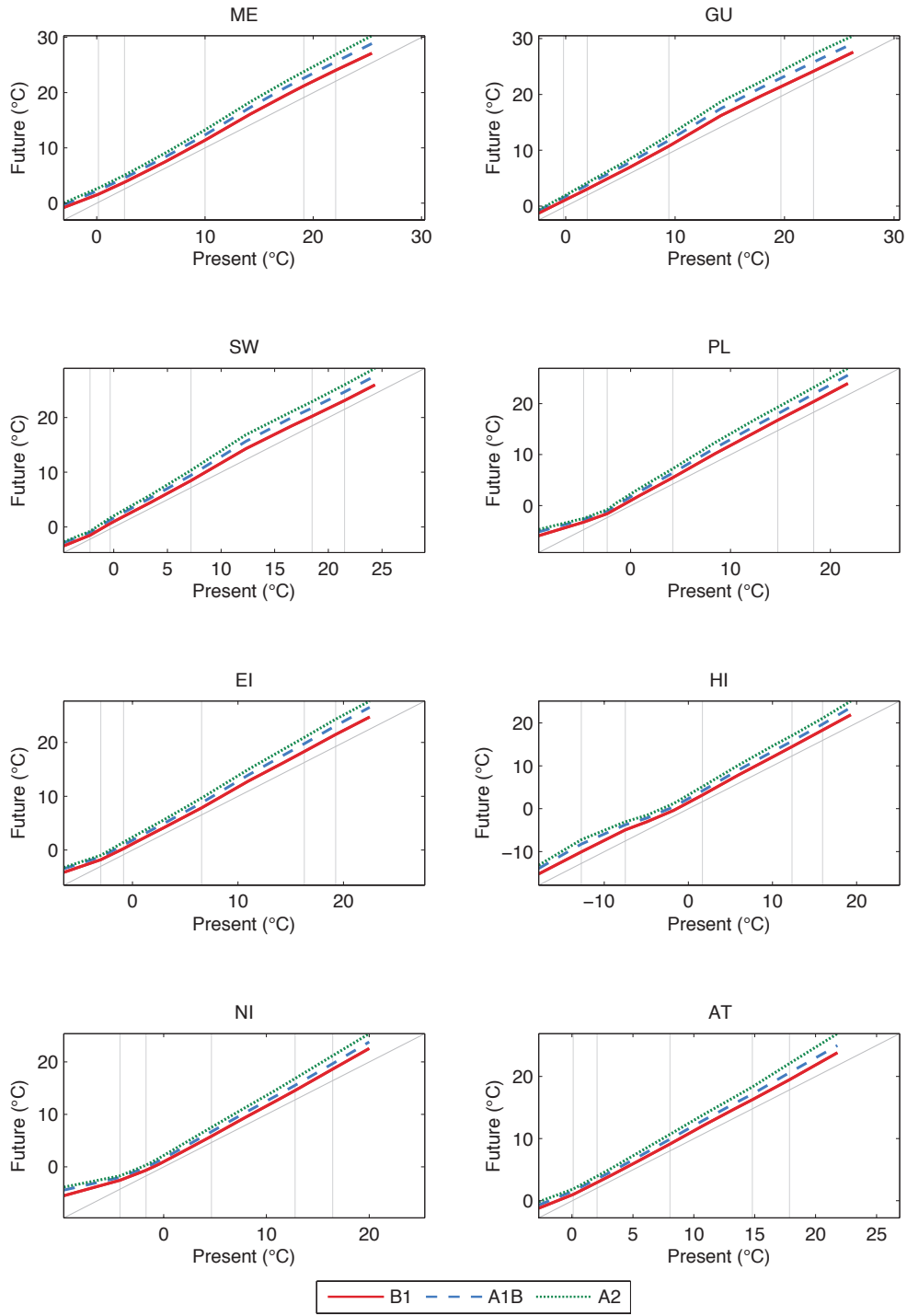
Figure 7.35: *As Fig. 7.34 but for CCSM.*

Changes in temperature extreme indices

To provide a further insight into the issue of future temperature extreme events, changes in a number of extreme indices are analyzed. A selection of the ETCCDI indices has been adopted as done in the model evaluation (Ch. 6). To be specific the FD, ID, SU, TR, WSDI and CSDI are here examined. In addition, the Diurnal Temperature Range (DTR) is calculated and its changes are shown too. The DTR is the mean difference between the daily Tmax and Tmin. Finally, the specifically defined HD index is also employed to characterize very hot days (see Table 6.2 for further details).

Since some of the indices are defined as the number of days that exceed a certain value, and thus employ directly the values of temperature, they must be bias-corrected as done in Sec. 6.3.4. Bearing in mind that the biases are calculated using the Spain02 dataset, the WRF outputs must be degraded to the Spain02 grid using a bilinear interpolation and then bias-corrected. Therefore the maps created to show changes in the extreme indices have a 0.2° spatial resolution instead of the 10 km original one[1]. In addition, the nature of such indices makes difficult to interpret maps that directly show changes (either in terms of days/year or in percentage). For example, over large areas of the IP, the number of icing days (ID) might not change in the future, however, Tmax always remains above the freezing point in these areas even in the present climate (Fig. 6.20) and thus the difference between future and present ID is zero. Hence it has been decided to plot the absolute values of the indices calculated from the bias-corrected WRF outputs and infer the changes from them.

As a consequence of the generalized increases in temperature, the aforementioned indices show a systematic tendency towards warmer extreme conditions. For instance the number of days with Tmin below 0°C is projected to decrease over the entire IP (Fig. 7.36).

Areas with a significant number of frost days in the present will be likely to suffer from severe reduction in this index, such as the northern mountains (Pyrenees, Galician Massif, Cantabrian Range, and Iberian and Central Systems). Indeed, the regions where FD exceeds 100 days/year are remarkably reduced under the B1 scenario (WEB1 and WCB1) and they completely disappear under the A1B and A2 scenarios (except for two tiny areas in the Iberian System and in the Pyrenees under the A1B). Actually, under the most severe projected changes,

---

[1]Although not all indices are threshold-based, they are all represented over the Spain02 grid for the sake of homogeneity.

the mountain regions where the frozen days might be expected to come more than 40 days/year are considerably reduced. Furthermore, even under the B1 scenario, the areas where Tmin drops down to 0°C less than 10 days/year are projected to widen markedly and cover most of the IP.
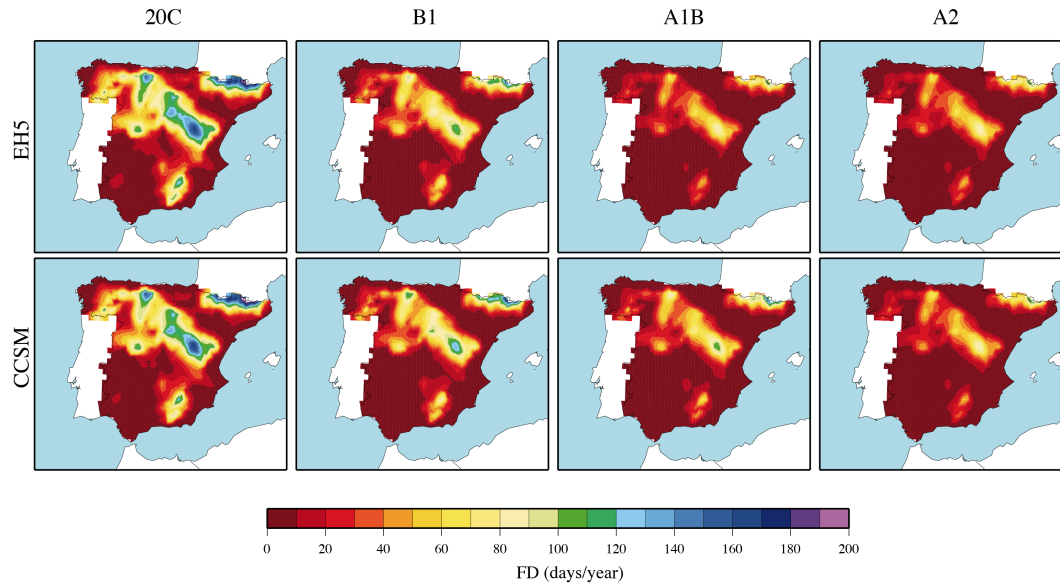
Figure 7.36: *Number of days with Tmin<0°C (FD). FD for present climate simulations (1970-1999) are displayed in the first column (WRFEH5 and WRFCCSM) and FD for future climate simulations (2070-2099) are arranged in the next three columns.*

Regarding the number of days when temperature remains below the freezing point (ID, Tmax<0°C), nearly no region might be expected to exceed 0.2 days/year, no matter which scenario or simulation is considered (see Fig. 7.37). The exception are the Pyrenees, where even under the warmest conditions there are projected to be a number of days with Tmax<0°C, although the ID index is clearly reduced with respect to the present (note that the scale is not linear). Areas located at high altitudes such as the Central System, the Iberian System and the Cantabrian Range are projected to experience important decreases in the ID index even under the B1 scenario. To be specific, locations where ID range between 1.8 and 5 days/year in the present, the number of icing days might barely reach 0.6 days/year in the future.

As for the indices that characterize the warm extremes, the SU index significantly increases all over the IP (Fig. 7.38). In the Guadalquivir river basin and over the southeast, it might be expected Tmax exceeds 25°C more than 220 days/year (out of the scale), which contrast with present simulated SU values
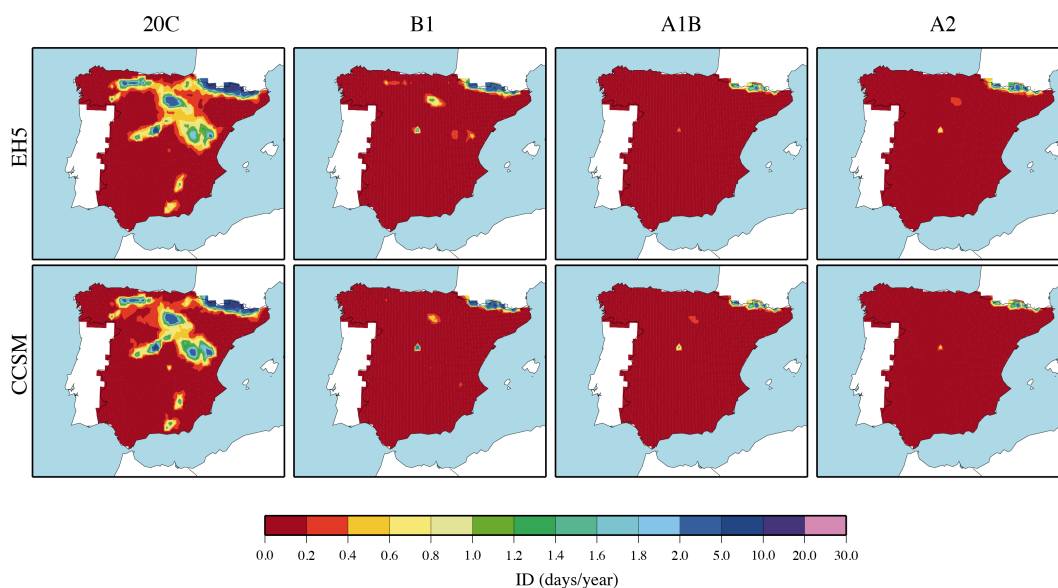
Figure 7.37: *As Fig. 7.36 but for ID (number of days with Tmax<0° C).*

over these regions (140-170 days/year). In Sierra Morena and just to the north of it, the SU values are projected to increase from the current ~120 days/year to about 180 days/year under the A1B and A2 scenarios. A large area in the north presents SU values below 50 days/year for the 1970-1999 period, but it is progressively reduced as we move from the B1 to the A2 scenario. Indeed, in the WEA2 and WCA2 this area is confined to a very reduced region in the Atlantic coast.

The TR index represents the number of days when Tmin exceeds 20°C. Present climate simulations yield TR values within the range 0-5 days/year in most of the IP, with the only exception of the southwest and the Mediterranean coast (Fig. 7.39). Future projections indicate that areas with values within this range will be significantly smaller even under the B1 scenario, particularly in the case of WEB1. Indeed, the number of tropical nights are likely to double in southwest and at certain locations of the Mediterranean coast, reaching as much as 75-80 days/year.

Under the A1B and A2 scenarios, these changes are likely to be much more prominent and significant areas of the peninsula might be expected to experience more than 80 days/year with Tmin above the 20°C threshold. In the southern extreme of the IP, the TR index could even exceed 120 days/year.

The Ebro valley and the interior might be subject to substantial increases in
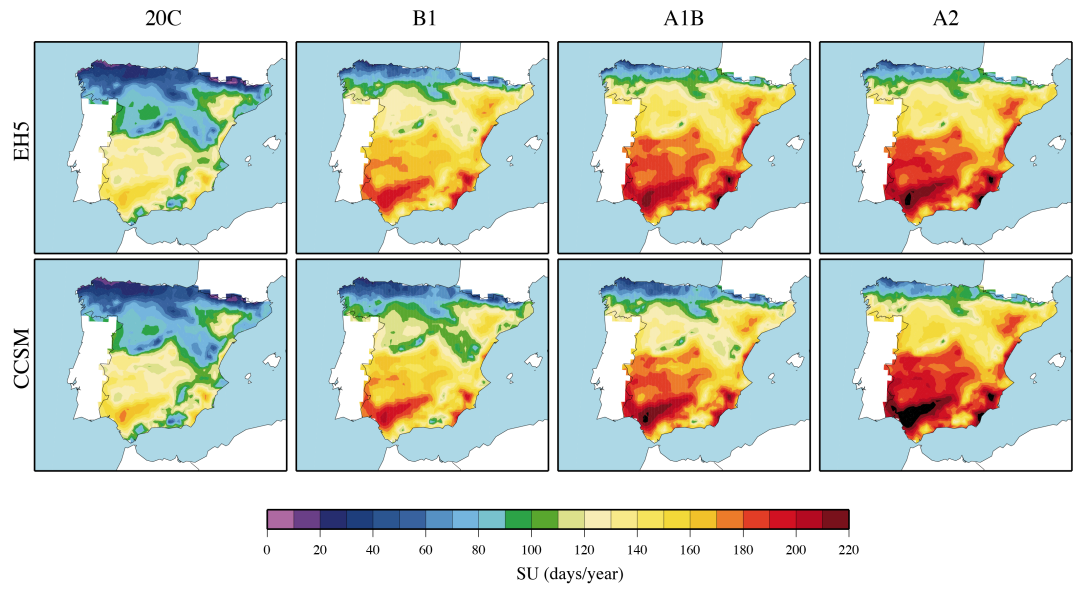
Figure 7.38: *As Fig. 7.36 but for SU (number of days with Tmax>25° C).*

TR too. In these regions, the TR index hardly reach 10 days/year, whereas in the future projections it might be expected to attain values of about 50 days/year. The coldest regions in the north and over the Iberian System are likely to remain in the level 0-5 days/year even under the warmest conditions.
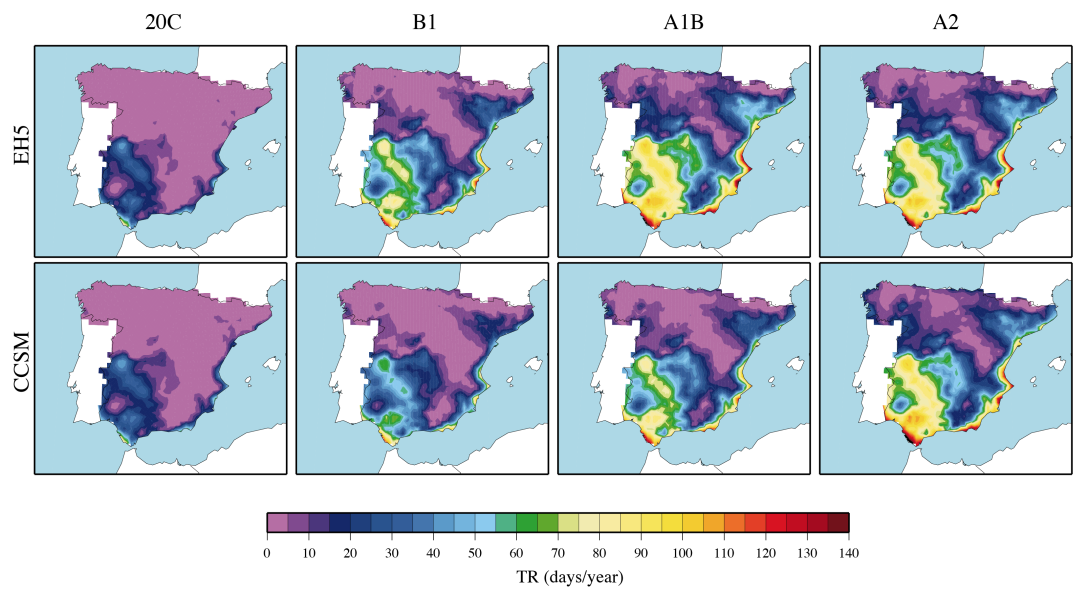
Figure 7.39: *As Fig. 7.36 but for TR (number of days with Tmin>20° C).*

Taking into account the particular features of the IP in terms of Tmax extremes, an additional index was included in the model evaluation (Ch. 6) and is here analyzed as well. The HD index represents the number of days when Tmax exceeds the 35°C threshold. In the present climate, only the southwest quarter of the IP and the Ebro valley reach significant HD values. Very few regions sparse all over the IP are projected to maintain low HD values (0-5 days/year), such as the northern coast, the Pyrenees and the Baetic, the Iberian and the Central Systems. In the rest of the regions, the number of days with temperature above 35°C are likely to significantly increase (Fig. 7.40).

In the future B1 scenario, almost the entire IP be subjected to more than 30 days/year with Tmax larger than 35°C according to WRF simulations. In addition, in most of the future simulations (apart from WCB1), the Guadalquivir valley is likely to undergo Tmax>35°C more than 100 days/year. More generally, the region bounded by the Central, the Iberian and the Baetic Systems might be expected to exceed HD values of 80 days/year as simulated by all WRF runs, except for WCB1 that yield slightly smaller values. The Ebro valley is likely to be subjected to similar changes. Furthermore, the Northern Central Plateau is also projected to suffer from remarkable increases in HD, changing from 0-15 days/year to even more than 60 days/year at certain locations (WEA1B, WEA2 and WCA2).
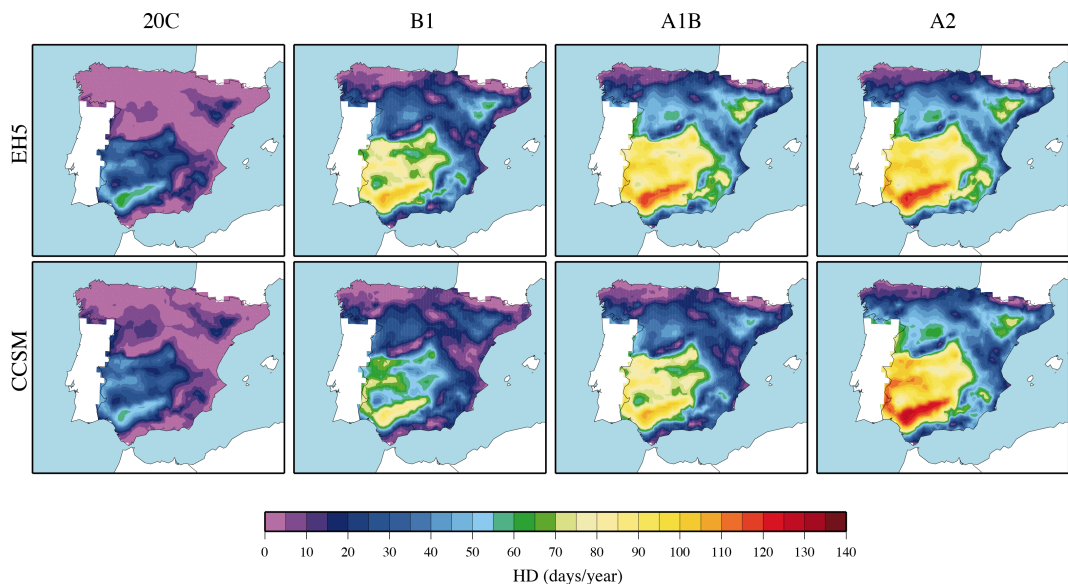
Figure 7.40: *As Fig. 7.36 but for HD (number of days with Tmax>35°C).*

Besides the so-called 'threshold indices' analyzed above, changes in three other indices are also examined: DTR, WSDI and CSDI. Since they are not defined using thresholds they do not require to be bias-corrected. Furthermore, the changes in DTR are easily interpreted directly using difference between future and present values, because they are expressed in°C. Therefore, their changes are explored through the differences between future projections and present climate simulations.

Figure 7.41 illustrate changes in the daily temperature range. Overall, the variability of temperature within a day is projected to increase by all WRF simulations. An exception is found for the Mediterranean coast, where slight decreases in DTR might be expected (between 0°C and −0.5°C). In general, coastal regions are likely to experience the smallest changes in DTR due to the thermal inertia of the large water masses. On the other hand, the regions in the interior might be subjected to changes in DTR of even 2.5°C (WCA2). WEA2 also project substantial increases in the daily temperature range (∼ 1.5°C in the interior), but smaller than WCA2. The WCA1B run suggests that DTR changes might reach the 1.5°C threshold only over limited areas and changes between 1.0°C and 1.5°are more likely to occur in most of the IP. In the eastern part, DTR projected changes barely exceed 1.0°C for this simulation. Under the B1 scenario, both ECHAM5- and CCSM-driven simulations project increases in DTR that range 0.5-1.0°C in the interior and 0-0.5°C in the peripheral areas.

To characterize changes in the warm spells, the WSDI is calculated using a calendar day percentile at each grid point (see Sec. 6.3.4), over the 1970-1999 reference period and using the present climate simulations (WRFEH5 and WRFCCSM). Future WSDI are calculated using the same percentiles to determine possible changes.

The WSDI changes indicate an systematic increase in the number of consecutive warm days (Fig. 7.42). Under the B1 scenario, some areas are projected to experience approximately the same WSDI (0-5 days/year, WCB1). However, the rest of the regions are projected to suffer from very important increases in the warm spells (>30 days/year for WEB1, and 10-20 days/year for WCB1). The largest changes are expected to occur under the A2 scenario, with WSDI reaching up to 80 days/year in many parts of the IP, particularly in the southwest and the Pyrenees that seem to be the most affected regions. In line with previous results, the WEA1B yields similar results to WEA2 in terms of WSDI changes, whereas the WCA1B project WSDI changes that remain below 40 days/year in most of the locations.
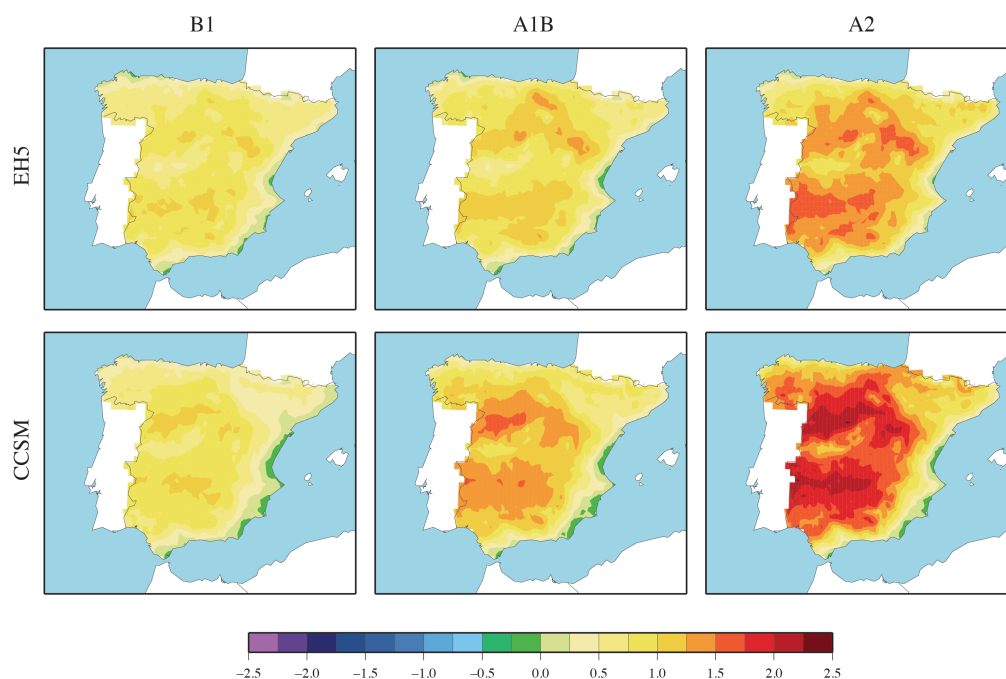
Figure 7.41: *Changes in the mean difference Tmax-Tmin (DTR): 2070-2099 minus 1970-1999 (in° C). The simulations using different boundary data are placed in rows and the emission scenarios are placed in columns.*

Likewise, the cold spells are calculated using a calendar day percentile. The comparison of future and present CSDI reveals that practically over the whole IP the number of consecutive cold days are likely to decrease down to almost zero (Fig. 7.43). Owing to the CSDI sensitivity to small changes in Tmin, even under the most moderate changes (B1 scenario), it might be expected that no cold spells will take place. Actually, all simulations project changes in CSDI that would cancel present values and nearly the entire IP might be exposed to very low CSDI values. It means that the cold spells (characterized using present climate percentiles) are very unlikely to occur in the future in this region (<0.5 days/year).

7.4   Discusion

The results here presented helped to elucidate how might global warming affect Iberian precipitation and temperature in the future. They indicate that
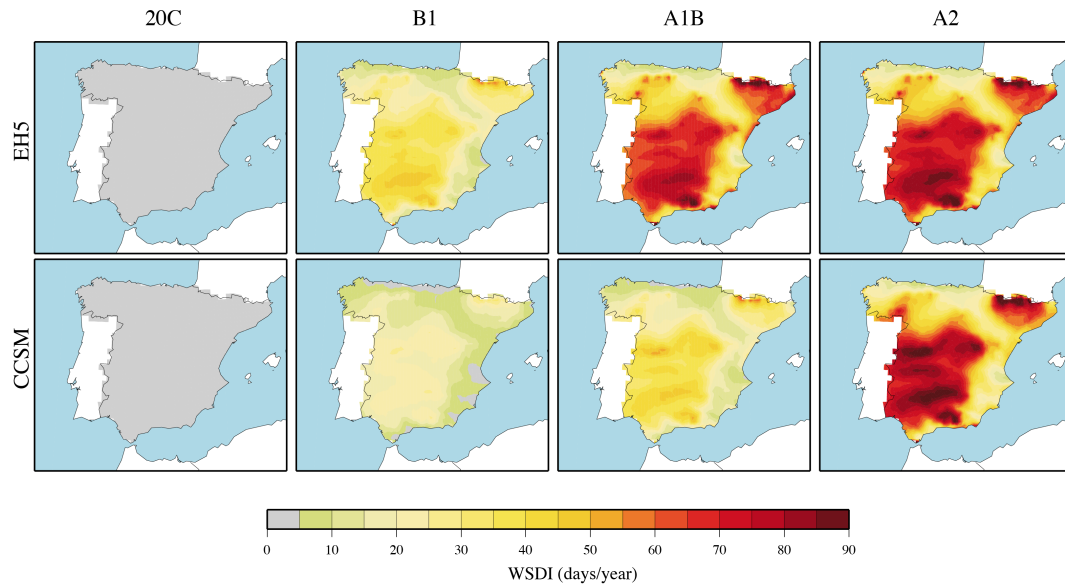
Figure 7.42: *The number of consecutive warm days (WSDI). WSDI for present climate simulations (1970-1999) are displayed in the first column (WRFEH5 and WRFCCSM) and WSDI for future climate simulations (2070-2099) are arranged in the next three columns.*
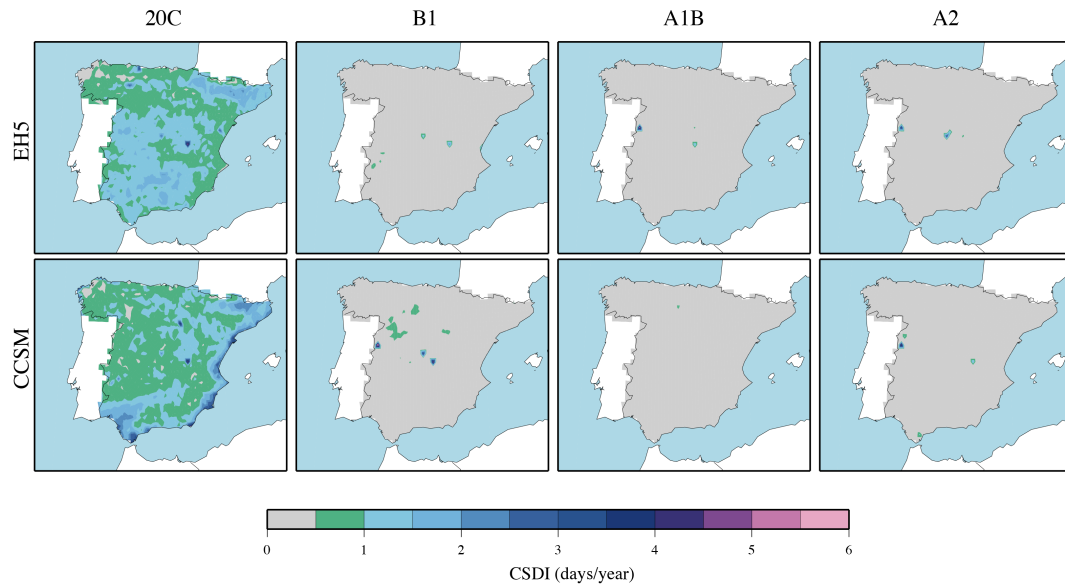
Figure 7.43: *As Fig. 7.42 but for CSDI.*

the changes in that substantial changes might be expected over the IP by the end of this century. For instance, even under the B1 scenario, the changes in the

mean Tmax and Tmin are for the period 2070-2099 are projected to be larger than those observed for the last century (Brunet et al., 2007).

The changes in the means for both temperature and precipitation are fairly consistent among the WRF simulations and agree with previous studies. For example, (Christensen et al., 2007a) projected decreases of annual mean precipitation over the entire IP that ranged between −15% and −30% for the A1B scenario, which are similar to the results obtained here with WRF. Other studies also projected similar diminutions of precipitation over the region (Gao et al., 2006; Sánchez et al., 2009; Tapiador et al., 2009). However, the projections generated in this Thesis are able to provide much more spatial detail thanks to the high resolution that suggested larger changes over certain mountainous areas (Baetic, Central and Iberian Systems). In terms of temperature, the IP has already been identified as one of the regions within Europe that might be more affected by temperature increases, with warmings that might reach 6°C in the interior of the IP(Christensen et al., 2007c). Previous studies (Gallardo et al., 2001; Schär et al., 2004) also found that interior areas might experience more severe warnings, whereas in the coastal regions the changes might be milder. The WRF runs provided a similar spatial pattern and made possible to go further and determine that the mountainous areas might be particularly exposed to future warming.

Regarding the seasonal changes, the WRF simulations revealed that precipitation tends to suffer from the largest decreases during the summer, accompanied by more moderate decreases during the transition seasons. However, the winter is projected to be wetter over some ares in the IP. Trigo and Palutikof (2001) found a similar behavior which would concentrate precipitation in a shorter rainfall season, although they extend it to the entire IP . As for temperature, the changes are systematically projected to be larger during the summer and lower during the winter, which is in agreement with most of the other works (Giorgi and Lionello, 2008; van der Linden and Mithchell, 2009). Once again, the WRF simulations describe these changes at much higher detail and shed light on the differences among the Iberian regions.

Although a significative decrease of annual precipitation is projected by most regional climate simulations, the changes in the extreme events are not so clear. Indeed both slight increases and decreases are observed across the IP. According to WRF, the very extreme events are likely to be approximately the same in the future, although their relative probability with respect to total rainy days might increase because light-to-moderate events are projected to significantly decrease. In previous studies, the extreme events are projected to decrease in

the IP overall (Beniston et al., 2007; Christensen et al., 2007a), but during the summer they might increase (Sánchez et al., 2004). The disparity among WRF simulations generates uncertainty in terms of the extreme for the IP, a feature that has already been emphasized by other authors (Frei et al., 2006).

With respect to the persistence of dry conditions, some authors have projected very small changes over the Cantabrian coast (Beniston et al., 2007; Sánchez et al., 2011) and longer dry spells over the south in the future. According to other authors (Gao et al., 2006) the spatial distribution of the dry spell changes is not that obvious and it varies substantially for the different seasons.despite the fact that the dry spell indices are defined very differently in these studies, it should be emphasized that they all agree in the smaller changes over the Cantabrian coast. The WRF simulations show similar results with respect to this feature, but at higher spatial detail, and there is a clear division between the northern coast and the areas to the south of the Cantabrian Range.

The projections of temperature changes were provided separately for Tmax and Tmin. The changes in Tmax tend to be always larger than for Tmin, except in some coastal regions. Other authors also found that higher temperature values are are projected to increase more than lower temperature values (Kjellström et al., 2007; Sánchez et al., 2004). The assessment of very extreme values of Tmax and Tmin was also carried out. The WRF simulations projected a clear tendency towards more pronounced temperature extremes, particularly for the Tmax ones. For example the number of days where Tmax is particularly high is likely to increase significantly. Beniston et al. (2007) provided similar results, although the areas exposed to higher changes were not exactly the same since WRF simulations tend to project the largest changes in the southwest and over the mountainous areas.

As exposed above, the climate change projections obtained with WRF are overall consistent with previous studies, which indicates that the projected changes are largely consistent. However, there are features of the climate, such as the precipitation extreme events, that are projected differently by other authors. Nonetheless, it should be stressed that high resolution has a beneficial impact on the model estimates that tend to compare better with rainfall observations, especially in terms of spatial distribution (Grubišić et al., 2005; Mass et al., 2002; Sánchez et al., 2009), and hence the projections at higher resolution might be more reliable. In any case, the differences with previous works are only minor, and the main advantage of the unprecedented resolution used to perform the climate change projections in this Thesis are related to the spatial detail

of the projected changes. Furthermore, the assessment of the changes has been performed over a wide range of frequencies and hence the high spatial detail is complemented with a full picture of the entire temporal spectrum, from long term means to exceptional events.

Chapter 8

Conclusions

> Si hay algo seguro en nuestros
> conocimientos es la verdad de que todos
> los conocimientos actuales son parcial o
> totalmente equivocados.
>
> *Uno y el Universo*
> Ernesto Sábato

A number of climate 10-km resolution runs have been completed with WRF to elucidate the impact of global warming on the Iberian climate at regional scales. The climate change information provided by two GCMs has been dynamically downscaled by means of WRF to generate high-resolution future (2070-2099) projections of climate over the IP under different emission scenarios.

The motivation of this study relies on the necessity to asses the repercussion of global warming on regional climate at scales that are of paramount importance for population and natural environment. Furthermore, the issue of climate change at regional scales is seldom approached form a multi-temporal point of view and the studies are often limited to either long-term or large-scale mean values. In this Thesis, projected changes of precipitation, Tmax and Tmin have been explored, including not only annual, seasonal and monthly means but also high-order statistics.

Prior to perform the actual climate simulations (30 years), the model had to be adequately configured to represent the climate of the IP, a region particularly complex in terms of topography and spatio-temporal variability. To that purpose a set of decadal simulations (1990-1999) were completed to build a physical ensemble. In total, 12 simulations (of which 8 were fully examined) were carried out and the model outputs were compared with observations to determine an

appropriate model configuration for the region. In this first part of the study (Chapters 4 and 5), different key parameterization schemes (cumulus, PBL and microphysics) were tested and the model was suited to correctly simulate precipitation and temperature at climate scales. The main conclusions regarding the model parameterizations and their configuration are:

- **The selection of an appropriate combination of physics schemes is of major importance and the model estimates vary dramatically between different configurations**. This especially applies to complex-terrain regions where processes that are not adequately resolved by the model dynamics play a crucial role in the simulation of local climate. Furthermore, the results do not exclusively depend on single physics options but on the overall combination of them, since the feedbacks between different parameterized processes might be more decisive than the performance of a particular scheme.

- **There is no optimal configuration that outperforms the others over the entire region, for all variables and at every timescale**. Indeed, the same configuration might simulate dissimilarly the mechanisms that predominate over areas with clearly differentiated climate regimes, and thus produce completely opposite results. Furthermore, not all variables are equally affected by the parameterizations. A compromise solution has to be attempted to reproduce main features of climate over most of the regions under survey and considering its impact on each variable. For the IP, it has been concluded that precipitation results should prevail over temperature ones because the parameterization configuration has larger impact on the former.

- **Not all parameterizations are equally determining**. The choice of the cumulus and the PBL schemes are crucial to accurately describe precipitation. On the other hand, the microphysics option do not have significant impact on the results and thus the use of higher-complexity and computationally demanding schemes might not be justified.

- **Overall, the BA3 configuration is the most appropriate to study the Iberian climate.** The configuration that uses BMJ for cumulus, ACM2 for the PBL and WSM3 for the microphysics was proposed to conduct the climate simulations. Nonetheless, other configurations showed

good agreement with observations too. All combinations of BMJ cumulus scheme, and YSU and ACM2 PBL schemes yielded better estimates for precipitation. In the case of temperature, the local PBL scheme (MYJ) compared better with Tmin observations because local schemes tend to simulate stable conditions more realistically. The mixed (local and non-local) ACM2 also produced good results in terms of Tmin.

- **WRF is able to clearly improve the information provided by the boundary data**. WRF generates significant added-value information with respect to the 'perfect boundary data' (ERA-40 reanalysis). The model estimates outperforms ERA-40 reanalysis outputs at every timescale. In addition, WRF supplies with deeper detail of temperature and precipitation spatial distribution. The use of WRF thus constitutes an important advance in the simulation of regional climate.

The second part (Chapter 6) is devoted to simulate present climate (1970-1999) and evaluate the WRF ability to reproduce a wide range of climate features of the IP. Three climate simulations driven by ERA-40 reanalysis, ECHAM5 and CCSM3.0 were completed to ascertain the model reliability and generate a baseline to quantify the future changes. The main findings of this evaluation are outlined below:

- **The WRF model is an extremely valuable tool to investigate the climate and explore the regional implications of climate change over the IP.** WRF is able to resolve spatial scales that go unnoticed by GCMs. The major benefit of using WRF is its ability to accurately distribute precipitation and temperature across the IP. It does not only capture the broad gradients that characterized the large scale but also incorporates the topographical effects on regional climate.

- **WRF enables the study of both mean climate and extreme events**. The simulation of the upper percentiles and the extreme indices are among WRF most remarkable strengths. The results obtained with respect to the high-order statistics makes WRF a suitable tool to address changes in both the long-term means and the extreme events.

- **The description of precipitation is highly dependent on the boundary conditions.** The shape of the annual cycle is overall reproduced, but differences between the GCM-driven simulations and the observations are

sometimes noteworthy. When driven by ERA-40, the model provides excellent results and reproduces most of the annual cycle details over nearly the entire IP. Some significant seasonal and annual biases were obtained for certain regions. The misrepresentation of the SLP by the boundary conditions might be at the origin of these biases, although the model dynamics must also play a primary role, as observed in the spatial patterns of the biases and the topographically-induced precipitation.

- **In general, WRF produces too much light-to moderate precipitation, whereas the heavy rainfall events are slightly underestimated over most of the IP.** In particular, the upper percentiles of precipitation are markedly underestimated over the Mediterranean area, where the extreme events are often caused by localized rainstorm. For the rest of the IP, WRF is able to provide very good estimates of heavy rainfall episodes.

- **Temperature is accurately simulated at all timescales**, and most of the errors between the model estimates and observations are characterized by systematic deviations, which are probably the less troublesome errors to deal with. These biases are mostly negative, except for some regions where positive deviations were obtained for Tmin.

- **WRF accurately represents the probability distribution of Tmax and Tmin.** It simulates most of the features that characterize the PDFs at the different regions, such as the bimodality and skewness of the distributions, particularly when driven by ERA-40. The extreme events are exceptionally well reproduced by WRF in nearly all situations, as evidenced by the analysis of percentiles and extreme indices, which is essential to assess the changes in the distribution tails.

In the third part (Chapter 7) the future climate projections are generated and analyzed. A set of 6 future (2070-2099) runs driven by the aforementioned GCMs and under three different emissions scenarios (B1, A1B and A2) conform the high-resolution climate change projections. The spatial resolution adopted in these simulations (10 km) together with the wide spectrum of timescales that were examined, made possible to provide detailed information about the projected changes and build up a full picture of future climate. The main conclusion drawn from these climate runs and concerning the changes with respect to present climate (1970-1999) are summarized below:

- **Total annual precipitation is very likely to substantially decrease by the end of the century over nearly the entire IP.** All simulations project important decreases over the IP that in average range from -18% to -42%. The most affected regions are the mountainous areas with changes that exceed -30%. Minor decreases or even slight increases in precipitation are projected along the east coast, although they are not significative.

- **Precipitation changes vary from season to season.** Precipitation decreases are more pronounced during the summer (between -32% and -71%), whereas in the winter, minor decreases and marked increases are projected. Nonetheless, winter changes are mostly non-significative except for the Cantabrian range. Although spring and autumn changes are not as significative as summer changes in percentage terms, their contribution to total annual precipitation is larger. On average over the IP, spring precipitation changes are projected to range between -24% to -58%, and autumn changes between -23% and -50%.

- **The frequency of extreme precipitation events is not projected to change substantially.** The precipitation events over the 95th percentiles are likely to explain larger amounts of total precipitation, especially along the east coast. However, this change is due to decreases in light-to-moderate precipitation events rather than increases in the heavy rainfall. The evidences of changes in the frequency and intensity of the extreme events are weak and spatially inconsistent, except for the Northern Central Plateau, where events above 20 mm/day are systematically projected to increase.

- **Larger precipitation decreases are projected over the IP as the radiative forcing increases.** The changes might be expected to be more significant under the assumptions of the A2 scenario. The changes are progressively more moderate under the A1B and B1 scenarios. Annual, seasonal and monthly precipitation changes show a large dependence on the selected scenario, but changes in the distribution tails of daily precipitation do not seem to be affected by the emission scenario.

- **The length of dry (wet) periods are consistently projected to increase (decrease).** The CDD* index is projected to increase over the entire IP (except confined locations along the Cantabrian coast), particularly under the A2 scenario and over the northern half of the IP. On the other hand, the CWD* index is likely to decrease in most of the IP, except

places in the east coast, where increases are also projected. The largest changes might be expected in the south (Baetic System) and over areas near the northern coast.

- **The entire IP is very likely to suffer from increases in both Tmax and Tmin by the end of this century.** On average over the IP, Tmax changes (2.0°C-4.3°C) are projected to be larger than Tmin changes (1.4°C-3.4°C).

- **The interior of the IP might be exposed to the largest Tmax changes**, being particularly severe over the mountainous areas (> 3.5°C), whereas the coastal regions might be expected to experience more moderate changes due to the sea thermal inertia. Tmin changes are also projected to be more pronounced over the high-altitude regions, but there are plain differences between the interior and the coast.

- **The largest changes for both Tmax and Tmin are projected to occur during the summer.** Tmax summer changes are likely to exceed 4.0°C in most of the IP. There is no clear tendency that indicates whether the autumn or spring are prone to larger changes, but Tmax is projected to increase substantially during both seasons. Winter changes are likely to be much milder. On the other hand, Tmin summer changes are projected to be much more moderate (between 2.0°C and 4.5°C). During the winter and spring, Tmin changes barely exceed 3.0°C.

- **Both the mean and the variability of daily temperature might increase in the future.** Tmax and Tmin PDFs are projected to move towards higher values. In addition, the variability is also projected to increase, since PDFs are somehow flattened and the changes in the upper tail of distribution are larger than in the lower one. The transition from cold to warm seasons might also be faster in the future over the southern and eastern regions, as indicated by the enhanced bimodality of distributions.

- **Temperature extremes are likely to be substantially warmer in the future over the entire IP.** The upper percentiles of both Tmax and Tmin are projected to change more than the means. The lower Tmin percentiles show a similar behavior over most of the regions (except in the south). Basically none of the regions is projected to experience daily Tmax values below the freezing point (ID) and those days with Tmin below 0°C are

considerably reduced. On the other hand, the number of days when Tmax exceeds 35°C might be expected to reach up to 80 days/year over areas in the southwest (Guadalquivir river basin) even under the least severe scenario. The tropical nights (Tmin > 20°C) are projected to increase dramatically in the southern half of the IP, and more specifically at locations in the southern coast.

- **The warm spells are projected to markedly increase and the cold spells are projected to decrease over the entire IP.** The number of consecutive warm days are projected to experience a remarkable increase and more particularly over the southwest and the Pyrenees, where the WSDI index could reach up to 90 days/year. Additionally, the number of consecutive cold days might be dramatically reduced and the CSDI index might drop to zero.

- **The projected changes for temperature present a large dependence on the emissions scenario.** In general, the changes are larger as the GHGs atmospheric concentrations increase and the radiative forcing intensifies. Nonetheless the differences between A1B and A2 scenarios highly depend upon the GCM used to drive the model. The A1B radiative forcing exceeds that of the A2 until approximately 2065 and ECHAM5 tend to prolong its effect into de 2070-2079 decade producing about the same conditions for both scenarios. On the other hand, the CCSM3.0 clear differentiates between the three scenarios and the changes progressively increase from B1 to A2. ECHAM5 also project the most moderate changes under the B1 scenario.

Outlook and future research

This Thesis has revealed that use of WRF, and more generally the RCMs, constitutes an extraordinary advance in the study of regional climate and the regional implications of global warming. However, it should also be admitted that dynamical downscaling by means of RCMs is not yet the definitive answer to investigate the effects of climate change at fine scales. In fact, RCMs still suffer from errors that must be identified in order understand current deficiencies of the models and facilitate upcoming improvements.

Furthermore, current climate change projections are usually restricted to a few variables (e.g. precipitation, temperature, wind) mainly because they have

a direct impact on human activity. Nonetheless, other variables should be also explored to shed light on the underlying processes that drive these changes. For example, a brief analysis of annual and seasonal SLP was performed in this study, but other fields such as relative humidity, upper-level pressure or SST would provide a beneficial insight of the mechanisms that affect regional climate.

The increase in the spatial resolution is currently hampered by computational resources, but finer grids are recently becoming more feasible. It would be very interesting to explore the performance of the model at very high-resolution (up to 1 km) over climate periods, particularly in areas with complex terrain or frequent convective precipitation. At such resolution, the cumulus scheme would not be necessary and the model dynamics could be further tested.

The new GCMs have substantially increased their resolution, incorporated new processes and feedbacks, and improved their simulation of certain features. The outputs are now becoming available and further simulations driven by these outputs could be performed in order to evaluate possible benefits and further determine the model dependency on the boundary conditions.

As exposed at the beginning of this study, the major advantage of dynamical downscaling is that the results are not limited to a few variables or locations, but describe the entire simulated domain and provide a large number of variables. Therefore, these outputs are of great value not only to explore the climate but also to feed other models that simulate very local processes, such as the hydrological model. The WRF outputs generated in this study are also aimed at driving a hydrological model that would enable the study of changes in the Iberian river flows.

Appendix A

Mathematical details of principal components analysis

The multi-step regionalization is composed of three main stages: (1) a S-mode PCA, (2) an agglomerative CA and (3) a non-hierarchical CA. A brief description of the methods is provided in the text (Sec. 3.3) but the former might require additional details to adequately understand the mathematical concepts behind it.

Principal Component Analysis

The Principal Component Analysis (PCA) or Empirical Orthogonal Function (EOF) analysis is a methodology that was mainly designed to reduce the dimensions of an observational matrix. In particular, it facilitates the interpretation of dependencies among large sets of variables that otherwise are very difficult to comprehend. If we are interested in the variance of the variables and correlations between them, PCA is a useful tool to generate illustrative information on the matter.

Mathematically speaking, the PCA is an orthogonal linear transformation that transform the original set of interrelated data to a new coordinate system such that the new variables are uncorrelated and are ordered so that the first few retain most of the variation present in the original dataset (Jolliffe, 2002).

Therefore, if only the few first new variables are kept, most of the variation is still retained and a considerable reduction of the dimensionality of the data is achieved. As a consequence, the interpretation of the dependencies between variables is much more straightforward. Another advantage that is significant within the regionalization framework is that it helps to stabilize measurements for additional statistical analysis such as cluster analysis (Timm, 2002) by reduction of information redundancy.

Suppose a dataset containing K variables that have been measured M times. Let us define a M by K matrix X where according to the standard nomenclature for PCA, the rows represent measurements (or observations) and the columns the different variables. In the particular case of S-Mode PCA, the rows might be the times (days) and the columns the different locations (stations).

Let us also define the matrix of anomalies formed by the K column vectors $X'_k = X_k - \overline{X}_k$, where $\overline{X}_k$ are the means calculated over the M elements of column k.

The new variables or *principal components* are then defined as linear combinations of the K $\mathbf{x'}_k$ that have certain properties:

$$u_m = \sum_{k=1}^{K} (e_{k,1} \cdot \mathbf{x'}_k), \quad m = 1...M \tag{A.1}$$

The new base is composed by the $\mathbf{e}_m$ eigenvectors and the first one $\mathbf{e}_1$ is aligned in the direction in which the data vectors jointly exhibit the most variability. This the primary property of the *principal components*: the first linear combinations is calculated so that it has the maximum variance, the second one is calculated so that it is orthogonal to the previous *principal component* and explain as much variance as possible, and so on.

Therefore, the largest eigenvalue λ_1 corresponds to the first eigenvector $\mathbf{e}_1$. The second-largest eigenvalue λ_2 corresponds to the second eigenvector $\mathbf{e}_2$, which is forced to be orthogonal to $\mathbf{e}_1$ and points to the direction in which $\mathbf{x'}_k$ show the next largest variations. Subsequent eigenvectors are defined similarly, associated with eigenvalues of decreasing magnitude and orthogonal to the previous eigenvectors. The matrix of the transformation can thus be written:

$$U = [E]^T X' \tag{A.2}$$

Owing to the fact that principal components are orthogonal and thus uncorrelated, the covariance matrix of U is diagonal. Taking into account this property,

the covariance matrix for the principal components can be obtained by diagonalization of the covariance matrix for the original dataset:

$$[S_x] = X'X'^T$$

$$[S_u] = [E^T][S_x][E] = [E^{-1}][S_x][E] = [\Lambda] \tag{A.3}$$

Which is equal to solve the equation:

$$det([S_x] - \lambda[I]) = 0 \tag{A.4}$$

that allow us to determine the eigenvectors and then calculate the *principal components*. In addition, the eigenvalues indicate the variance explained by each of the *principal components*. The fraction of total variation in the original $\mathbf{x}_k$ vectors explained by a certain principal component is proportional to its eigenvalue:

$$\text{Percentage of variance} = \frac{\lambda_m}{\sum\limits_{k=1}^{K}(\lambda_k)} \times 100\% \tag{A.5}$$

The transformation can be reverted and thus the original anomaly vectors can be retrieved from the *principal components*:

$$X' = [E]U \tag{A.6}$$

Truncation of the principal components

Bearing in mind that the objective of PCA is to reduce the information contained in the original data, the number of principal components can be truncated and keep only a fraction of the total variance. There are as many principal components as elements in the vector $\mathbf{x'}_m$. However, atmospheric data usually contain redundant information that is removed by approximating the original vectors by linear combinations of $K*$ eigenvectors, where $K^* < K$:

$$\mathbf{x'}_m \approx \sum_{k=1}^{K^*}(e_{m,k} \cdot \mathbf{u}_k), \quad m = 1...M \tag{A.7}$$

The fraction of the total variance explained by the new reduced base of eigen-

vectors is thus computed as:

$$\text{Variance explained } (\%) = \frac{\sum_{k=1}^{K^*}(\lambda_k)}{\sum_{k=1}^{K}(\lambda_k)} \tag{A.8}$$

In the atmospheric data, selecting $K^* << K$ usually leads to large variance explained and thus the original large dataset can be reduced to a base composed of very few eigenvectors that explain a substantial proportion of the total variance and thus are easier to interpret. The number of *principal components* to be retained are still a matter of controversy and different method have been proposed. A widespread method called the North Rule of Thumb (North et al., 1982) is based the degeneration of eigenvalues. That is, if the spacing between two consecutive eigenvalues is smaller than the error of the the first one, then they cannot be considered as different *true* eigenvalues, where the error of the eigenvalues is calculated as:

$$\Delta\lambda_k \approx \sqrt{\frac{2}{K}}\lambda_k \tag{A.9}$$

Only *principal components* with non-degenerated eigenvalues are thus maintained.

Rotation of the principal components

Once the reduced number of *principal components* is selected, the eigenvectors are normally plotted geographically and the corresponding *principal components* are interpreted physically. However, bearing in mind that the atmospheric processes are not independent, the orthogonality constraint might sometimes hamper the physical interpretation because the examination of independent modes of variability might not be justified (North, 1984; Wilks, 2006). In order to circumvent this problem, the retained eigenvectors after truncation are often rotated with the aim to produce a simple structure in the results. Namely, the elements of the resulting rotated vectors are either large or very close to zero, with few intermediate values.There are different techniques to rotate the eigenvectors (e.g. *varimax,orthomax,oblique*) of which the details can be found in Richman (1986).

Very good references that address the issue of PCA can be found in Preisendorfer (1988), Jolliffe (2002) or, more generally, Wilks (2006).

Appendix B

Description of statistical parameters

In all these parameters M refers to model estimates, O to observed values including both gridded and site-specific. Unless anything else is specified, the index i refers to times and N to the total number of events, either days, months, season or years. Additionally, $\bar{O}$ and $\bar{M}$ represents the observational and the modeled means.

Bias: The bias represents the difference between the model mean and the observed mean.

$$\text{BIAS} = N^{-1} \sum_{i=1}^{N} M_i - O_i = \bar{M} - \bar{O} \qquad \text{(B.1)}$$

Relative Bias: The relative bias is the bias divided by the observed mean and provides information of the differences in relative terms.

$$\text{relative BIAS} = N^{-1} \frac{\sum_{i=1}^{N} M_i - O_i}{\sum_{i=1}^{N} O_i} = \frac{\bar{M} - \bar{O}}{\bar{O}} \qquad \text{(B.2)}$$

MAE: The mean absolute error represent the average of the absolute errors between the model and the observations. It is very stable and little sensitive to extremes.

$$\text{MAE} = N^{-1} \sum_{i=1}^{N} |M_i - O_i| \tag{B.3}$$

Correlation: The Pearson Correlation, also known as simply correlation, evaluates the linear dependence between two variables. Therefore, it determines if the model and the observations vary similarly in time, that is to say if the model captures the observations timing.

$$\text{CORR(M,O)} = \frac{Cov(M,O)}{s_M s_O} =$$

$$= \frac{\frac{1}{(N-1)} \sum_{i=1}^{N} [(M_i - \bar{M})(O_i - \bar{O}]}{[\frac{1}{(N-1)} \sum_{i=1}^{N} (M_i - \bar{M})^2]^{1/2}[\frac{1}{(N-1)} \sum_{i=1}^{N} (O_i - \bar{O})^2]^{1/2}} \tag{B.4}$$

$$= \frac{\sum_{i=1}^{N} (M_i' O_i')}{[\sum_{i=1}^{N} (M_i')^2]^{1/2}[\sum_{i=1}^{N} (O_i')^2]^{1/2}}$$

The Pearson correlation is usually employed to compare how similar are two time series, but it can also be used to compare two maps (snapshots) and is calculated over the space. In that case, it is called **Pattern correlation**:

$$\text{PattC(M,O)} = \frac{\sum_{l=1}^{L} (M_l' O_l')}{[\sum_{l=1}^{L} (M_l')^2]^{1/2}[\sum_{l=1}^{L} (O_l')^2]^{1/2}} \tag{B.5}$$

Where l covers all the locations (L) in the map. Alternatively, the pattern

correlations can be calculated using the anomalies in place of the absolute value. A climatological value (C_M *and* C_O) is calculated for each location and the so-called **Anomaly spatial correlation** reads

$$AC(M,O) == \frac{\sum_{l=1}^{L}[(M_l - C_M)(O_l - C_O)]}{[\sum_{l=1}^{L}(M_l - C_M)^2]^{1/2}[\sum_{l=1}^{L}(O_l - C_O)^2]^{1/2}} \quad \text{(B.6)}$$

RMSE: The root-mean-squared error calculates an average of the squared differences between the model and the observations that is then root-squared to maintain the original units. It is interpretable as an error magnitude. Its estimation of the model validity weights individual high errors in excess.

$$\text{RMSE} = (N^{-1}\sum_{i=1}^{N}(M_i - O_i)^2)^{1/2} \quad \text{(B.7)}$$

The relative RMSE is identical to RMSE except that the result is divided by the observed mean. This provides an estimation of the error with respect to the actual value of the variable.

$$\text{relRMSE} = \frac{RMSE}{\bar{O}} \quad \text{(B.8)}$$

Perkins Skill Score (SS) (Perkins et al., 2007): This skill score is a measure of the common area between two PDFs. It is defined as:

$$\text{SS} = \sum_{i=1}^{N}\min(Z_m, Z_o) \quad \text{(B.9)}$$

where n are the number of bins used to describe the empirical PDF, Z_m and Z_o are the frequency of values in a given bin from the model and the observations respectively.

References

Ahrens, C., 1998: *Meteorology Today. An Introduction to Weather, Climate and the Environment..* West Publishing Company, Minneapolis, 5th edition, 591 pp. 113

Ainslie, B. and P. L. Jackson, 2010: Downscaling and Bias Correcting a Cold Season Precipitation Climatology over Coastal Southern British Columbia Using the Regional Atmospheric Modeling System (RAMS). *Journal of Applied Meteorology and Climatology*, **49**, 937–953. 150

Alexandru, A., R. de Elía, and R. Laprise, 2008: Internal variability in regional climate downscaling at the seasonal scale. *Monthly Weather Review*, **135**, 3221–3238. 74

Amengual, A., R. Romero, V. Homar, C. Ramis, and S. Alonso, 2007: Impact of the lateral boundary conditions resolution on dynamical downscaling of precipitation in Mediterranean spain. *Climate Dynamics*, **29**, 487–499. 86

Anav, A., P. M. Ruti, V. Artale, and R. Valentini, 2010: Modelling the effects of land-cover changes on surface climate in the Mediterranean region. *Climate Resesearch*, **41**, 91–104. 11

Antic, S., R. Laprise, B. Denis, and R. de Elía, 2006: Testing the downscaling ability of a one-way nested regional climate model in regions of complex topography. *Climate Dynamics*. 10, 21, 60

Argüeso, D., J. Hidalgo-Muñoz, S. Gámiz-Fortis, M. Esteban-Parra, and Y. Castro-Díez, -: Evaluation of WRF mean and extreme precipitation over Spain: present climate (1970-1999), Under revision in *Journal of Climate* (REF: JCLI-D-11-00276). 105

— 2009: Análisis de la respuesta del MM5 frente a diferentes parametrizaciones físicas para el sur de la Península Ibérica. *CLIVAR-ES.Clima en España: Pasado, presente y futuro. Contribución a un informe de Evaluación del Cambio Climático Regional*, February 11th–13th, Madrid (Spain)., URL: http://clivar.iim.csic.es/?q=es/node/269/. 91

Argüeso, D., J. M. Hidalgo-Muñoz, S. R. Gámiz-Fortis, M. J. Esteban-Parra, J. Dudhia, and Y. Castro-Díez, 2011: Evaluation of WRF parameterizations for climate studies over Southern Spain using a multi-step regionalization. *Journal of Climate*, *In Press*. 79

Bärring, L., 1987: Spatial patterns of daily rainfall in central Kenya - Application of Principal Component Analysis, Common Factor Analysis and spatial correlation. *Journal of Climatology*, **7**, 267–289. 44

Bell, J., L. Sloan, and M. Snyder, 2004: Regional changes in extreme climatic events: A future climate scenario. *Journal of Climate*, **17**, 81–87. 84

Beniston, M., D. B. Stephenson, O. B. Christensen, C. A. T. Ferro, C. Frei, S. Goyette, K. Halsnaes, T. Holt, K. Jylhä, B. Koffi, J. Palutikof, R. Schöll, T. Semmler, and K. Woth, 2007: Future extreme events in European climate: an exploration of regional climate model projections. *Climatic Change*, **81**, 71–95. 9, 90, 223

Betts, A., 1986: A New Convective Adjustment Scheme. Part I: Observational and Theoretical Basis. *Quarterly Journal Of The Royal Meteorological Society*, **112**, 677–691. 32

Betts, A. and M. Miller, 1986: A New Convective Adjustment Scheme. Part II: Single Column Tests Using Gate Wave, Bomex, Atex and Arctic Air-Mass Data Sets. *Quarterly Journal Of The Royal Meteorological Society*, **112**, 693–709. 32

Boé, J., L. Terray, F. Habets, and E. Martin, 2007: Statistical and dynamical downscaling of the Seine basin climate for hydro-meteorological studies. *International Journal of Climatology*, **27**, 1643–1655. 4, 150

Borge, R., V. Alexandrov, J. del Vas, J. Lumbreras, and E. Rodríguez, 2008: A comprehensive sensitivity analysis of the WRF model for air quality applications over the Iberian Peninsula. *Atmospheric Environment*, **42**, 8560–8574. 60

Boulanger, J.-P., G. Brasseur, A. F. Carril, M. de Castro, N. Degallier, C. Ereno, H. L. Treut, J. A. Marengo, C. G. Menéndez, M. N. Nuñez, O. C. Penalba, A. L. Rolla, M. Rusticucci, and R. Terra, 2010: A Europe-South America network for climate change assessment and impact studies. *Climate Change*, **98**, 307–329. 10

Brunet, M., P. D. Jones, J. Sigró, O. Saladié, E. Aguilar, A. Moberg, P. M. Della-Marta, D. Lister, A. Walther, and D. López, 2007: Temporal and spatial temperature variability and change over Spain during 1850–2005. *Journal of Geophysical Research*, **112**, 1–28. 222

Bukovsky, M. S. and D. J. Karoly, 2009: Precipitation Simulations Using WRF as a Nested Regional Climate Model. *Journal of Applied Meteorology and Climatology*, **48**, 2152–2159. 80

— 2011: A Regional Modeling Study of Climate Change Impacts on Warm-Season Precipitation in the Central United States. *Journal of Climate*, **24**, 1985–2002. 60, 119

Bunkers, M., J. Miller, and A. DeGaetano, 1996: Definition of climate regions in the Northern Plains using an objective cluster modification technique. *Journal of Climate*, **9**, 130–146. 43

Caldwell, P., H.-N. S. Chin, D. C. Bader, and G. Bala, 2009: Evaluation of a WRF dynamical downscaling simulation over California. *Climatic Change*, **95**, 499–521. 11, 21, 43, 60, 107

Calinski, R. and J. Harabasz, 1974: A dendrite method for cluster analysis. *Communications in Statistics*, **3**, 1–27. 49

Casado, M. J. and M. A. Pastor, 2011: Use of variability modes to evaluate AR4 climate models over the Euro-Atlantic region. *Climate Dynamics*, doi:10.1007/s00382-011-1077-2. 113

Castro, C., R. A. Pielke, and G. Leoncini, 2005: Dynamical downscaling: Assessment of value retained and added using the Regional Atmospheric Modeling System (RAMS). *Journal of Geophysical Research*, **110**, 1–21. 9

Chen, F. and J. Dudhia, 2001: Coupling an Advanced Land Surface-Hidrology Model with the Penn State-NCAR MM5 Modeling System Part I: Model Implementation and Sensitivity. *Monthly Weather Review*, **129**, 569–585. 35

Christensen, J., B. Hewitson, A. Busuioc, A. Chen, X. Gao, I. Held, R. Jones, R. Kolli, W.-T. Kwon, R. Laprise, V. M. Rueda, C. M. L. Mearns, J. Räisänen, A. Rinke, A. Sarr, and P. Whetton, 2007a: *Regional Climate Projections. In: Climate Change 2007: The Physical Science Basis. Contribution of Working Group I to the Fourth Assessment Report of the Intergovernmental Panel on Climate Change*. [Solomon, S. and D. Qin and M. Manning and Z. Chen and M. Marquis and K.B. Averyt and M. Tignor and H.L. Miller(eds)]. Cambridge University Press, Cambridge,United Kingdom and New York, NY, USA. 3, 7, 11, 21, 156, 212, 222, 223

Christensen, J. H., T. Carter, and M. Rummukainen, 2007b: Evaluating the performance and utility of regional climate models: the PRUDENCE project. *Climatic Change*, **81**, 1–6. 10

Christensen, J. H., T. R. Carter, M. Rummukainen, and G. Amanatidis, 2007c: A summary of the PRUDENCE model projections of changes in European climate by the end of this century. *Climatic Change*, **81**, 1–6. 10, 65, 222

Collins, W. D., C. M. Bitz, M. L. Blackmon, G. B. Bonan, C. S. Bretherton, J. A. Carton, P. Chang, S. C. Doney, J. J. Hack, T. B. Henderson, J. T. Kiehl, W. G. Large, D. S. McKenna, B. D. Santer, and R. D. Smith, 2006: The Community Climate System Model version 3 (CCSM3). *Journal of Climate*, **19**, 2122–2143. 68, 70

Collins, W. D., P. J. Rasch, B. A. Boville, J. J. Hack, J. R. McCaa, D. L. Williamson, J. T. Kiehl, B. Briegleb, C. Bitz, S.-J. Lin, M. Zhang, and Y. Dai, 2004: Description of the NCAR Community Atmosphere Model (CAM 3.0). *NCAR/TN-464+STR NCAR Technical Note*, 1–226. 30

Compagnucci, R. H. and M. B. Richman, 2008: Can principal component analysis provide atmospheric circulation or teleconnection patterns? *International Journal of Climatology*, **28**, 703–726. 46

Correia, F. W. S., R. C. S. Alvalá, and A. O. Manzi, 2008: Modeling the impacts of land cover change in Amazonia: a regional climate model (RCM) simulation study. *Theoretical and Applied Climatology*, **93**, 225–244, doi:10.1007/s00704-007-0335-z. 9

Cubasch, U., J. Waszkewitz, G. Hegerl, and J. Perlwitz, 1995: Regional climate

changes as simulated in time-slice experiments. *Climatic Change*, **31**, 273–304.
4

Davies, H. C., 1976: A lateral boundary formulation for multi-level prediction models. *Quarterly Journal of the Royal Meteorological Society*, **102**, 405–5128.
16

Davies, T., A. Staniforth, N. Wood, and J. Thuburn, 2003: Validity of anelastic and other equation sets as inferred from normal-mode analysis. *Quarterly Journal of the Royal Meteorological Society*, **129**, 2761–2775, doi:10.1256/qj.02.195.
22, 28

Deb, S., T. Srivastava, and C. Kishtawal, 2008: The WRF model performance for the simulation of heavy precipitating events over Ahmedabad during August 2006. *Journal of Earth System Science*, **117**, 589–602. 79

DeMott, C. A., D. A. Randall, and M. Khairoutdinov, 2007: Convective precipitation variability as a tool for general circulation model analysis. *Journal of Climate*, **20**, 91–112. 119

Denis, B., R. Laprise, and D. Caya, 2003: Sensitivity of a regional climate model to the resolution of the lateral boundary conditions. *Climate Dynamics*, **20**, 107–126. 59, 75

Denis, B., R. Laprise, D. Caya, and J. Côte, 2002: Downscaling ability of one-way nested regional climate models: the Big-Brother Experiment. *Climate Dynamics*, **18**, 627–646, doi:10.1007/s00382-001-0201-0. 18, 21, 60

Déqué, M. and J. P. Piedelievre, 1995: High resolution climate simulation over Europe. *Climate Dynamics*, **11**, 321–339. 4, 9

Déqué, M., D. P. Rowell, D. Lüthi, F. Giorgi, J. H. Christensen, B. Rockel, D. Jacob, E. Kjellström, M. de Castro, and B. van den Hurk, 2007: An intercomparison of regional climate simulations for Europe: assessing uncertainties in model projections. *Climate Change*, **81**, 53–70, doi:10.1007/s10584-006-9228-x.
19

Dickinson, R., R. Errico, F. Giorgi, and G. Bates, 1989: A regional climate model for the western United States. *Climatic Change*, **15**, 383–422. 9

Dimitrijevic, M. and R. Laprise, 2005: Validation of the nesting technique in a regional climate model and sensitivity tests to the resolution of the lateral boundary conditions during summer. *Climate Dynamics*, **25**, 555–580. 60

Dosio, A. and P. Paruolo, 2011: Bias correction of the ENSEMBLES high-resolution climate change projections for use by impact models: Evaluation on the present climate. *Journal of Geophysical Research*, **116**. 150

Douville, H., F. Chauvin, S. Planton, J. Royer, D. Salas-Melia, and S. Tyteca, 2002: Sensitivity of the hydrological cycle to increasing amounts of greenhouse gases and aerosols. *Climate Dynamics*, **20**, 45–68. 156

Errasti, I., A. Ezcurra, J. Sáenz, and G. Ibarra-Berastegi, 2010: Validation of IPCC AR4 models over the Iberian Peninsula. *Theoretical and Applied Climatology*, **103**, 61–79. 68, 113

Esteban-Parra, M. J., F. S. Rodrigo, and Y. Castro-Díez, 1998: Spatial and temporal patterns of precipitation in Spain for the period 1880-1992. *International Journal of Climatology*, **18**, 1557–1574. 108

Evans, J. and M. McCabe, 2010: Regional climate simulation over Australia's Murray-Darling basin: A multitemporal assessment. *Journal of Geophysical Research*. 10, 60, 107

Fernández, J., 2004: *Statistical and dynamical downscaling models applied to winter precipitation on the Cantabrian coast*. Ph.D. thesis, Universidad del País Vasco - Euskal Herriko Unibertsitatea. 75

Fernández, J., J. P. Montávez, J. Sáenz, J. González-Rouco, and E. Zorita, 2007: Sensitivity of the MM5 mesoscale model to physical parameterizations for regional climate studies: Annual cycle. *Journal of Geophysical Research*, **112**, D04101. 65, 82, 94

Fita, L. and J. Fernández, 2010: *CLWRF: WRF modifications for regional climate simulation under future scenarios*. 11th WRF Users' Workshop, NCAR, Boulder (CO), USA. 30, 77

Fovell, R., 1997: Consensus clustering of US temperature and precipitation data. *Journal of Climate*, **10**, 1405–1427. 44, 47

Fovell, R. and M. Fovell, 1993: Climate zones of the conterminous United States defined using cluster analysis. *Journal of Climate*, **6**, 2103–2135. 44, 50

Fowler, H., M. Ekström, C. Kilsby, and P. Jones, 2005: New estimates of future changes in extreme rainfall across the UK using regional climate model integrations. 1. Assessment of control climate. *Journal of Hydrology*, **300**, 212–233. 90

Frei, C., J. H. Christensen, M. Déqué, D. Jacob, R. G. Jones, and P. L. Vidale, 2003: Daily precipitation statistics in regional climate models: Evaluation and intercomparison for the European Alps. *Journal of Geophysical Research*, **108**, D3, 4124. 84

Frei, C., R. Schöll, S. Fukutome, and J. Schmidli, 2006: Future change of precipitation extremes in Europe: Intercomparison of scenarios from regional climate models. *Journal of Geophysical Research*, **111**. 60, 223

Fu, C., S. Wang, Z. Xiong, W. Gutowski, D. Lee, J. McGregor, Y. Sato, H. Kato, J. Kim, and M. Suh, 2005: Regional climate model intercomparison project for Asia. *Bulletin Of The American Meteorological Society*, **86**, 257–266. 10

Gallardo, C., A. Arribas, J. Prego, M. A. Gaertner, and M. Castro, 2001: Multi-year simulations using a regional climate model over the Iberian Peninsula: current climate and 2xCO2 scenario. *Quarterly Journal of the Royal Meteorological Society*, **126**, 1659–1682. 222

Gallus Jr, W. and J. Bresch, 2006: Comparison of impacts of WRF dynamic core, physics package, and initial conditions on warm season rainfall forecasts. *Monthly Weather Review*, **134**, 2632–2641. 80

Gao, X., J. Pal, and F. Giorgi, 2006: Projected changes in mean and extreme precipitation over the Mediterranean region from a high resolution double nested RCM simulation. *Geophysical Research Letters*, **33**, L03706. 222, 223

Ge, J., J. Qi, B. Lofgren, N. Moore, and N. Torbick, 2007: Impacts of land use/cover classification accuracy on regional climate simulations. *Journal of Geophysical Research*, **112**, D05107. 21

Gerstengarbe, F.-W., P. Werner, and K. Fraedrich, 1999: Applying Non-Hierarchical Cluster Analysis Algorithms to Climate Classification: Some Problems and their Solution. *Theoretical and Applied Climatology*, **64**, 143–150. 44

Gesch, D. B., K. L. Verdin, and S. K. Greenlee, 1999: New Land Surface Digital Elevation Model Covers the Earth. *EOS,Transaction, American Geophysical Union*, **80**, 69–70. 61

Giorgi, F., 1990: Simulation of regional climate using a limited area model nested in a general circulation model. *Journal of Climate*, **3**, 941–964. 9

— 2005: Climate change prediction. *Climate Change*, **73**, 239–265. 21

— 2006a: Climate change hot-spots. *Geophysical Research Letters*, **33**. 8

— 2006b: Regional climate modeling: Status and perspectives. *Journal of Physique IV*, **139**, 101–118. 10, 84

Giorgi, F. and G. Bates, 1989: The Climatological Skill of a Regional Model over Complex Terrain. *Monthly Weather Review*, **117**, 2325–2347. 9

Giorgi, F. and X. Bi, 2000: A study of internal variability of a regional climate model. *Journal of Geophysical Research*, **105**, 29503–29521. 19

Giorgi, F., C. Brodeur, and G. Bates, 1994: Regional Climate Change Scenarios over the United States Produced with a Nested Regional Climate Model. *Journal of Climate*, **7**, 375–399. 9

Giorgi, F., B. Hewitson, J. Christensen, M. Hulme, H. von Storch, P. Whetton, R. Jones, L. Mearns, and C. Fu, 2001: *Regional climate information - Climate Change 2001. The Scientific basis. Contribution of working group I to the third assesment report of the IPCC*. JT Houghton and Y Ding and DJ Griggs and M Noguer and PJ van der Linden and X Dai and K Maskell and CA Johnson (eds.) Cambridge University Press, Cambridge, United Kingdom. 10

Giorgi, F. and P. Lionello, 2008: Climate change projections for the Mediterranean region. *Global and Planetary Change*, **63**, 90–104. 222

Giorgi, F. and L. Mearns, 1999: Introduction to special section: Regional climate modeling revisited. *Journal of Geophysical Research*, **104**, 6335–6352. 4, 75

Giorgi, F., L. Mearns, C. Shields, and L. McDaniel, 1998: Regional nested model simulations of present day and 2 x CO2 climate over the central plains of the US. *Climatic Change*, **40**, 457–493. 91

Göber, M., E. Zsótér, and D. Richardson, 2008: Could a perfect model ever satisfy a naïve forecaster? On grid box mean versus point verification. *Meteorological Applications*, **15**, 359–365. 10, 39

Gong, X. and M. Richman, 1995: On the application of cluster analysis to growing season precipitation data in North America east of the Rockies. *Journal of Climate*, **8**, 897–931. 49

Good, P. and J. Lowe, 2006: Emergent behavior and uncertainty in multimodel climate projections of precipitation trends at small spatial scales. *Journal of Climate*, **19**, 5554–5569. 3

Grell, G. A., J. Dudhia, and D. R. Stauffer, 1995: A Description of the Fifth-Generation Penn State/NCAR Mesoscale Model (MM5). *NCAR/TN-398+STR NCAR Technical Note*, 122 pp.
URL http://www.mmm.ucar.edu/mm5/documents/mm5-desc-doc.html 22

Grubišić, V., R. Vellore, and A. Huggins, 2005: Quantitative precipitation forecasting of wintertime storms in the Sierra Nevada: sensitivity to the microphysical parameterization and horizontal resolution. *Monthly Weather Review*, **133**, 2834–2859. 223

Gutowski Jr, W., S. Decker, R. Donavon, Z. Pan, R. Arritt, and E. Takle, 2003: Temporal-spatial scales of observed and simulated precipitation in central U.S. climate. *Journal of Climate*, **16**, 3841–3847. 119

Harris, L. M. and D. R. Durran, 2010: An Idealized Comparison of One-Way and Two-Way Grid Nesting. *Monthly Weather Review*, **138**, 2174–2187. 60

Hay, L., R. Wilby, and G. Leavesley, 2000: A comparison of delta change and downscaled GCM scenarios for three mountainous basins in the United States. *Journal of the American Water Resources Association*, **36**, 387–397. 150, 158

Haylock, M. R., N. Hofstra, A. M. G. K. Tank, E. J. Klok, P. D. Jones, and M. New, 2008: A European daily high-resolution gridded data set of surface temperature and precipitation for 1950-2006. *Journal of Geophysical Research-Atmospheres*, **113**, 1–12. 40

Heikkilä, U., A. Sandvik, and A. Sorteberg, 2010: Dynamical downscaling of ERA-40 in complex terrain using the WRF regional climate model. *Climate Dynamics*, 10.1007/s00382–010–0928–6. 65, 74

Herrera, S., L. Fita, J. Fernández, and J. M. Gutiérrez, 2010a: Evaluation of the mean and extreme precipitation regimes from the ENSEMBLES regional climate multimodel simulations over Spain. *Journal of Geophysical Research*, **115**, D21117. 107

Herrera, S., J. Gutiérrez, R. Ancell, M. R. Pons, M. D. Frías, and J. Fernández, 2010b: Development and analysis of a 50-year high-resolution daily gridded precipitation dataset over Spain (Spain02). *International Journal of Climatology*, doi:10.1002/joc.2256. 41, 43, 87

Hidalgo-Muñoz, J., D. Argüeso, S. Gámiz-Fortis, M. Esteban-Parra, and Y. Castro-Díez, 2011: Trends of extreme precipitation and associated synoptic patterns over the southern Iberian Peninsula. *Journal of Hydrology*, *In Press.* 41

Hong, S., V. Lakshmi, E. E. Small, F. Chen, M. Tewari, and K. W. Manning, 2009: Effects of vegetation and soil moisture on the simulated land surface processes from the coupled WRF/Noah model. *Journal of Geophysical Research-Atmospheres*, **114**, D18118. 21, 80

Hong, S. and H. Pan, 1996: Nonlocal boundary layer vertical diffusion in a Medium-Range Forecast Model. *Monthly Weather Review*, **124**, 2322–2339. 34

Hong, S.-Y., J. Dudhia, and S. Chen, 2004: A revised approach to ice microphysical processes for the bulk parameterization of clouds and precipitation. *Monthly Weather Review*, **132**, 103–120. 31

Hong, S.-Y. and J. Lim, 2006: The WRF single-moment 6-class microphysics scheme (WSM6). *Journal of the Korean Meteorological Society*, **42**, 129–151. 33

Hu, X.-M., J. W. Nielsen-Gammon, and F. Zhang, 2010: Evaluation of Three Planetary Boundary Layer Schemes in the WRF Model. *Journal of Applied Meteorology and Climatology*, **49**, 1831–1844. 80

Huth, R., 1999: Statistical downscaling in central Europe: evaluation of methods and potential predictors. *Climate Research*, **13**, 91–101. 4

Ines, A. V. M. and J. W. Hansen, 2006: Bias correction of daily GCM rainfall for crop simulation studies. *Agricultural and Forest Meteorology*, **138**, 44–53. 151

IPCC, 2001: *Climate Change 2001: The Scientific Basis. Contribution of Working Group I to the Third Assessment Report of the Intergovernmental Panel on Climate Change*. [Houghton, J.T., Y. Ding, D.J. Griggs, M. Noguer, P.J. van der Linden, X. Dai, K. Maskell, and C.A. Johnson (eds.)]. Cambridge University Press, Cambridge, United Kingdom and New York, NY, USA, 881 pp. 72, 73

— 2007: *Climate Change 2007: The Physical Science Basis. Contribution of Working Group I to the Fourth Assessment Report of the Intergovernmental Panel on Climate Change*. [Solomon, S. and D Qin and M Manning and Z Chen and M Marquis and K B Averyt and Tignor and H L Miller (eds.)].Cambridge University Press, Cambridge, United Kingdom and New York, NY, USA, Cambridge University Press, Cambridge, United Kingdom and New York, NY, USA. 2, 74, 107

Jacob, D., L. Bärring, O. B. Christensen, J. H. Christensen, M. de Castro, M. Déqué, F. Giorgi, S. Hagemann, M. Hirschi, R. G. Jones, E. Kjellström, G. Lenderink, B. Rockel, E. Sánchez, C. Schär, S. I. Seneviratne, S. Somot, A. van Ulden, and B. V. D. Hurk, 2007: An inter-comparison of regional climate models for Europe: model performance in present-day climate. *Climatic Change*, **81**, 31–52. 91, 107

Janjic, Z., 1994: The Step-Mountain Eta Coordinate Model - Further Developments of the Convection, Viscous Sublayer, and Turbulence Closure Schemes. *Monthly Weather Review*, **122**, 927–945. 32

Janjic, Z. I., 1990: The Step-Mountain Coordinate - Physical Package. *Monthly Weather Review*, **118**, 1429–1443. 32, 34

— 2002: Nonsingular implementation of the Mellor–Yamada level 2.5 scheme in the NCEP Meso Model. *NCEP Office Note*. 34

Jankov, I., W. Gallus Jr, M. Segal, B. Shaw, and S. Koch, 2005: The impact of different WRF model physical parameterizations and their interactions on warm season MCS rainfall. *Weather and Forecasting*, **20**, 1048–1060. 80

Jiménez, P. A., E. Garcia-Bustamante, J. Gonzéalez-Rouco, F. Valero, J. P. Montávez, and J. Navarro, 2008: Surface wind regionalization in complex terrain. *Journal of Applied Meteorology and Climatology*, **47**, 308–325. 11, 43

Jiménez, P. A., J. F. González-Rouco, E. García-Bustamante, J. Navarro, J. P. Montávez, J. Vilà-Guerau, J. Dudhia, and A. Muñoz-Roldán, 2010: Surface wind regionalization over complex terrain: Evaluation and analysis of a high-resolution wrf simulation. *Journal of Applied Meteorology and Climatology*, **49**, 268–287, doi:10.1175/2009JAMC2175.1. 9

Jolliffe, I., 2002: *Principal Component Analysis*. Springer-Verlag., 2nd edition, 487 pp. 233, 237

Jones, R., J. Murphy, M. Noguer, and A. Keen, 1997: Simulation of climate change over Europe using a nested regional-climate model. II: Comparison of driving and regional model responses to a doubling of carbon dioxide. *Quarterly Journal of the Royal Meteorological Society*, **123**, 265–292. 9

Jones, R. G., J. Murphy, and M. Noguer, 1995: Simulation of climate change over Europe using a nested regional-climate model. I: Assessment of control climate, including sensitivity to location of lateral boundaries. *Quarterly Journal of the Royal Meteorological Society*, **121**, 1413–1449. 9, 17

Jungclaus, J. H., N. Keenlyside, M. Botzet, H. Haak, J. J. Luo, M. Latif, J. Marotzke, U. Mikolajewicz, and E. Roeckner, 2006: Ocean circulation and tropical variability in the coupled model ECHAM5/MPI-OM. *Journal of Climate*, **19**, 3952–3972. 68

Kain, J., 2004: The Kain-Fritsch convective parameterization: An update. *Journal of Applied Meteorology*, **43**, 170–181. 32

Kain, J. and J. Fritsch, 1990: A One-Dimensional Entraining Detraining Plume Model and Its Application in Convective Parameterization. *Journal of the Atmospheric Sciences*, **47**, 2784–2802. 32

Kain, J. S., S. Weiss, J. Levit, and M. Baldwin, 2006: Examination of Convection-Allowing Configurations of the WRF Model For the Prediction of Severe Convective Weather: The SPC/NSSL Spring Program 2004. *Weather and Forecasting*. 80

Kalkstein, L., G. Tan, and J. Skindlov, 1987: An Evaluation of Three Clustering Procedures for Use in Synoptic Climatological Classification. *Journal of Applied Meteorology*, **26**, 717–730. 44, 49

Kalnay, E., M. Kanamitsu, R. Kistler, W. Collins, D. Deaven, L. Gandin, M. Iredell, S. Saha, G. White, J. Woollen, Y. Zhu, M. Chelliah, W. Ebisuzaki, W. Higgins, J. Janowiak, K. Mo, C. Ropelewski, J. Wang, A. Leetmaa, R. Reynolds, R. Jenne, and D. Joseph, 1996: The NCEP/NCAR 40-year re-analysis project. *Bulletin of the American Meteorological Society*, **77**, 437–471. 64

Kjellström, E., L. Bärring, D. Jacob, R. G. Jones, G. Lenderink, and C. Schär, 2007: Modelling daily temperature extremes: recent climate and future changes over Europe. *Climatic Change*, **81**, 249–265. 223

Kjellström, E., F. Boberg, M. Castro, J. Christensen, G. Nikulin, and E. Sánchez, 2010: Daily and monthly temperature and precipitation statistics as performance indicators for regional climate models. *Climate Research*, **44**, 135–150. 121

Klemp, J. B., W. C. Skamarock, and J. Dudhia, 2007: Conservative split-explicit time integration methods for the compressible nonhydrostatic equations. *Monthly Weather Review*, **135**, 2897–2913, d. 23, 28

Köppen, W., 1923: *Die Klimate der Erde: Grundriss der Klimakunde*. De Greyter, Berlin. 44

Kostopoulou, E., K. Tolika, I. Tegoulias, C. Giannakopoulos, S. Somot, C. Anagnostopoulou, and P. Maheras, 2009: Evaluation of a regional climate model using in situ temperature observations over the Balkan Peninsula. *Tellus A*, **61**, 357–370. 11, 43, 107

Kunkel, K., R. Pielke Jr, and S. A. Changnon, 1999: Temporal fluctuations in weather and climate extremes that cause economic and human health impacts: A review. *Bulletin Of The American Meteorological Society*, **80**. 185

Kusaka, H., T. Takata, and Y. Takane, 2010: Reproducibility of Regional Climate in Central Japan Using the 4-km Resolution WRF Model. *Sola*, **6**, 113–116. 10

Kwun, J., Y. Kim, J. Seo, J. Jeong, and S. You, 2009: Sensitivity of MM5 and WRF mesoscale model predictions of surface winds in a typhoon to planetary boundary layer parameterizations. *Natural Hazards*, **51**, 63–77. 80

Laprise, R., 2008: Regional climate modelling. *Journal of Computational Physics*, **227**, 3641–3666. 21

Laprise, R., D. Caya, M. Giguere, G. Bergeron, G. Boer, and N. McFarlane, 1998: Climate and climate change in western Canada as simulated by the Canadian regional climate model. *Atmosphere-Ocean*, 119–167. 9

Leduc, M. and R. Laprise, 2009: Regional climate model sensitivity to domain size. *Climate Dynamics*, **32**, 833–854. 17

Leggett, J., W. Pepper, and R. Swart, 1992: *Emissions Scenarios for IPCC: An Update. In: Climate Change 1992. The Supplementary Report to the IPCC Scientific Assessment*. [Houghton, J.T., B.A. Callander and S.K. Varney (eds.)].Cambridge University Press, Cambridge, United Kingdom, 69-95 pp. 72, 73

Leung, L. R., L. Mearns, F. Giorgi, and P. H. Wilby, 2003: Regional climate research: needs and opportunities. *Bulletin of the American Meteorological Society*, **84**, 89–95. 107

Li, X. and Z. Pu, 2009: Sensitivity of Numerical Simulations of the Early Rapid Intensification of Hurricane Emily to Cumulus Parameterization Schemes in Different Model Horizontal Resolutions. *Journal of the Meteorological Society of Japan*, **87**, 403–421. 80

Liang, X., K. Kunkel, and A. Samel, 2001: Development of a regional climate model for US midwest applications. Part I: Sensitivity to buffer zone treatment. *Journal of Climate*, **14**, 4363–4378. 17

Lund, R. and B. Li, 2009: Revisiting Climate Region Definitions via Clustering. *Journal of Climate*, **22**, 1787–1800. 44

Lutgens, F. K. and E. J. Tarbuck, 1998: *The Atmosphere: An Introduction to Meteorology*. Prentice Hall, New Jersey, 7th edition edition, 434 pp. 113

Marsland, S., H. Haak, J. Jungclaus, M. Latif, and F. Roske, 2003: The Max-Planck-Institute global ocean/sea ice model with orthogonal curvilinear coordinates. *Ocean Modelling*, **5**, 91–127. 69

Mass, C., D. Ovens, K. Westrick, and B. Colle, 2002: Does increasing horizontal resolution produce more skillful forecasts? The results of two years of real-time numerical weather prediction over the Pacific northwest. *Bulletin Of The American Meteorological Society*, **83**, 407–430. 91, 223

McGregor, J., 1997: Regional climate modelling. *Meteorology and Atmospheric Physics*, **63**, 105–117. 4

McGregor, J., J. Katzfey, and K. Nguyen, 1998: Fine resolution simulations of climate change for southeast Asia. Final report for a Research Project commissioned by Southeast Asian Regional Committee for START (SARCS), Aspendale, Vic. Technical report, CSIRO Atmospheric Research. 9

McGregor, J. L. and K. Walsh, 1993: Nested Simulations of Perpetual January Climate over the Australian Region. *Journal of Geophysical Research-Atmospheres*, **98**, 23283–23290. 9

Mearns, L. O., R. Arritt, G. Boer, D. Caya, P. Duffy, F. Giorgi, W. J. Gutowski, I. M. Held, R. Jones, R. Laprise, L. R. Leung, J. Pal, J. Roads, L. Sloan, R. Stouffer, G. Takle, and W. Washington, 2005: NARCCAP, North American Regional Climate Change Assessment Program. *Preprints of the American Meteorological Sociecty 16th Conference on Climate Variability and Change.*, 9–13 January 2005, Paper J6.10 pp 235–238. 10

Mellor, G. and T. Yamada, 1982: Development of a turbulence closure model for geophysical fluid problems. *Reviews of Geophysics and Space Physics*, **20**, 851–875. 34

Míguez-Macho, G., G. L. Stenchikov, and A. Robock, 2004: Spectral nudging to eliminate the effects of domain position and geometry in regional climate model simulations. *Journal of Geophysical Research*, **109**, D13104. 17, 74

— 2005: Regional climate simulations over North America: Interaction of local processes with improved large-scale flow. *Journal of Climate*, **18**, 1227–1246. 74

Milligan, G., 1980: An examination of the effect of six types of error perturbation on fifteen clustering algorithms. *Psychometrika*, **45**, 325–342. 47

Milligan, G. and M. Cooper, 1985: An examination of procedures for determining the number of clusters in a data set. *Psychometrika*, **50**, 159–179. 49

Mitchell, T., T. Carter, P. Jones, M. Hulme, and M. New, 2004: A comprehensive set of high-resolution grids of monthly climate for Europe and the globe: the observed record (1901–2000) and 16 scenarios (2001–2100). *Tyndall Centre for Climate Change Research, Working Paper no. 55*, 30 pp. 40

Moberg, A. and P. D. Jones, 2004: Regional climate model simulations of daily maximum and minimum near-surface temperatures across Europe compared with observed station data 1961–1990. *Climate Dynamics*, **23**, 695–715. 39, 60

Nakicenovic, N., J. Alcamo, G. Davis, B. de Vries, J. Fenhann, S. Gaffin, K. Gregory, A. Grübler, T. Y. Jung, T. Kram, E. L. L. Rovere, L. Michaelis, S. Mori, T. Morita, W. Pepper, H. Pitcher, L. Price, K. Riahi, A. Roehrl, H.-H. Rogner, A. Sankovski, M. Schlesinger, P. Shukla, S. Smith, R. Swart, S. van Rooijen, N. Victor, and Z. Dadi, 2000: Special Report on Emissions Scenarios. Technical report, IPCC. 20, 68, 71, 74

Nieto, S. and C. Rodríguez-Puebla, 2006: Comparison of precipitation from observed data and general circulation models over the Iberian Peninsula. *Journal of Climate*, **19**, 4254–4275. 68

Nolan, D. S., J. A. Zhang, and D. P. Stern, 2009: Evaluation of Planetary Boundary Layer Parameterizations in Tropical Cyclones by Comparison of In Situ Observations and High-Resolution Simulations of Hurricane Isabel (2003). Part I: Initialization, Maximum Winds, and the Outer-Core Boundary Layer. *Monthly Weather Review*, **137**, 3651–3674. 80

North, G., 1984: Empirical orthogonal functions and normal modes. *Journal of the Atmospheric Sciences*, **41**, 879—887. 236

North, G., T. Bell, R. Cahalan, and F. Moeng, 1982: Sampling errors in the estimation of empirical orthogonal functions. *Monthly Weather Review*, **110**, 699–706. 47, 236

Nuñez, M. N., S. A. Solman, and M. F. Cabré, 2008: Regional climate change experiments over southern South America. II: Climate change scenarios in the late twenty-first century. *Climate Dynamics*, 15, doi:10.1007/s00382-008-0449-8. 11

Osborn, T. and M. Hulme, 1998: Evaluation of the European daily precipitation characteristics from the Atmospheric Model Intercomparison Project. *International Journal of Climatology*, **18**, 505–522. 39

Paeth, H., K. Born, R. Girmes, R. Podzun, and D. Jacob, 2009: Regional Climate change in tropical and northern Africa due to greenhouse forcing and land use changes. *Journal of Climate*, **22**, 114–132. 11

Perkins, S. E., A. J. Pitman, N. J. Holbrook, and J. McAneney, 2007: Evaluation of the AR4 climate models' simulated daily maximum temperature, minimum temperature, and precipitation over Australia using probability density functions. *Journal of Climate*, **20**, 4356–4376. 121, 241

Piani, C., J. Haerter, and E. Coppola, 2010: Statistical bias correction for daily precipitation in regional climate models over Europe. *Theoretical and Applied Climatology*, **99**, 187–192. 150, 151

Pleim, J. E., 2007: A combined local and nonlocal closure model for the atmospheric boundary layer. Part II: Application and evaluation in a mesoscale meteorological mode. *Journal of Applied Meteorology and Climatology*, **46**, 1396–1409. 34

Preisendorfer, R., 1988: *Principal Components Analysis in Meteorology and Oceanography*. Elsevier, New York, NY, U.S.A ., 1st edition, 425 pp. 44, 237

Radu, R., M. Déqué, and S. Somot, 2008: Spectral nudging in a spectral regional climate model. *Tellus A*, **60**, 898–910. 74

Räisänen, J., 2007: How reliable are climate models? *Tellus A*, **59**, 2–29. 150, 158

Räisänen, J., M. Rummukainen, A. Ullerstig, B. Bringfelt, U. Hansson, and U. Willén, 1999: The first Rossby Centre regional climate scenario - dynamical downscaling of CO2-induced climate change in the HadCM2 GCM. SMHI Reports Meteorology and Climatology. Technical report, Swedish Meterological and Hydrological Institute, SE-601 76 Norrköping, Sweden. 9

Rauscher, S. A., E. Coppola, C. Piani, and F. Giorgi, 2010: Resolution effects on regional climate model simulations of seasonal precipitation over Europe. *Climate Dynamics*, **35**, 685–711. 65

Reid, S. and R. Turner, 2001: Correlation of real and model wind speeds in different terrains. *Weather and Forecasting*, **16**, 620–627. 43

Richardson, L. F., 1922: *Weather Prediction by Numerical Processes*. Cambridge University Press, Cambridge, UK. 9

Richman, M. and P. Lamb, 1985: Climatic pattern analysis of three-and seven-day summer rainfall in the central United States: Some methodological considerations and a regionalization. *Journal of Applied Meteorology and Climatology*, **24**, 1325–1343. 44

Richman, M. B., 1986: Rotation of principal components. *Journal of Climatology*, **6**, 293–335. 236

Rivington, M., D. Miller, K. Matthews, G. Russell, G. Bellocchi, and K. Buchan, 2008: Evaluating regional climate model estimates against site-specific observed data in the UK. *Climatic Change*, **88**, 157–185. 38, 39

Roeckner, E., G. Bäuml, L. Bonaventura, R. Brokopf, M. Esch, M. Giorgetta, S. Hagemann, I. Kirchner, L. Kornblueh, E. Manzini, A. Rhodin, U. Schlese, U. Schulzweida, and A. Tompkins, 2003: The atmospheric general circulation model ECHAM5. *MPI-Report 349*, Hamburg, Germany. 68

Romero, R., C. Ramis, and J. Guijarro, 1999a: Daily rainfall patterns in the Spanish Mediterranean area: an objective classification. *International Journal of Climatology*, **19**, 95–112. 50, 51

Romero, R., C. Ramis, J. Guijarro, and G. Sumner, 1999b: Daily rainfall affinity areas in Mediterranean Spain. *International Journal of Climatology*, **19**, 557–578. 44, 53

Rosenberg, E. A., P. W. Keys, D. B. Booth, D. Hartley, J. Burkey, A. C. Steinemann, and D. P. Lettenmaier, 2010: Precipitation extremes and the impacts of climate change on stormwater infrastructure in Washington State. *Climatic Change*, **102**, 319–349. 90, 107, 150

Ruiz, J. J., C. Saulo, and J. Nogués-Paegle, 2010: WRF Model Sensitivity to Choice of Parameterization over South America: Validation against Surface Variables. *Monthly Weather Review*, **138**, 3342–3355. 80

Rummukainen, M., 2010: State-of-the-art with regional climate models. *Wiley Interdisciplinary Reviews: Climate Change*, **1**, 82–96. 16, 21, 60, 150

Salathé Jr, E. P., L. Leung, Y. Qian, and Y. Zhang, 2010: Regional climate model projections for the State of Washington. *Climatic Change*, **102**, 51–75. 11

Salathé Jr, E. P., R. Steed, C. F. Mass, and P. H. Wilby, 2008: A High-Resolution Climate Model for the U.S. Pacific Northwest: Mesoscale Feedbacks and Local Responses to Climate Change. *Journal of Climate*, **21**, 5708. 60

Sánchez, E., M. Domínguez, R. Romera, N. López de la Franca, M. Gaertner, C. Gallardo, and M. Castro, 2011: Regional modeling of dry spells over the Iberian Peninsula for present climate and climate change conditions. *Climatic Change*, **107**, 625–634. 223

Sánchez, E., M. Gaertner, and C. Gallardo, 2009: Dynamical downscaling of daily precipitation over the Iberian Peninsula: a spatial resolution analysis for present and future climate conditions . *Física de la Tierra*, **21**, 207–218. 222, 223

Sánchez, E., M. A. Gaertner, C. Gallardo, E. Padorno, A. Arribas, and M. Castro, 2007: Impacts of a change in vegetation description on simulated European summer present-day and future climates. *Climate Dynamics*, **29**, 319–332. 21

Sánchez, E., C. Gallardo, M. Gaertner, A. Arribas, and M. de Castro, 2004: Future climate extreme events in the Mediterranean simulated by a regional climate model: a first approach. *Global and Planetary Change*, **44**, 163–180. 90, 223

Schär, C., P. L. Vidale, D. Lüthi, C. Frei, and C. Häberli, 2004: The role of increasing temperature variability in European summer heatwaves. *Nature*, doi:10.1038/nature02300. 222

Seth, A. and F. Giorgi, 1998: The effects of domain choice on summer precipitation simulation and sensitivity in a regional climate model. *Journal of Climate*, **11**, 2698–2712. 17

Skamarock, W. C., J. B. Klemp, J. Dudhia, D. O. Gill, D. M. Barker, M. G. Duda, X.-Y. Huang, W. Wang, and J. G. Powers, 2008: A Description of the Advanced Research WRF Version 3. *NCAR/TN-475+STR NCAR Technical note*, 125 pp.
URL http://www.mmm.ucar.edu/wrf/users/docs/arw_v3.pdf 22, 24, 28

Solman, S. A., M. N. Nuñez, and M. F. Cabré, 2008: Regional climate change experiments over southern South America. I: present climate. *Climate Dynamics*, **30**, 533–552. 9

Solomon, S., D. Qinand, M. Manningand, R. B. Alleyand, T. Berntsenand, N. L. Bindoffand, Z. Chenand, A. Chidthaisongand, J. M. Gregoryand, G. C. Hegerland, M. Heimannand, B. Hewitsonand, B. Hoskinsand, F. Joosand, J. Jouzeland, V. Kattsovand, U. Lohmannand, T. Matsunoand, M. Molinaand, N. Nichollsand, J. Overpeckand, G. Ragaand, V. Ramaswamyand, J. Renand, M. Rusticucciand, R. Somervilleand, T. Stockerand, P. Whettonand, R. Wood, and D. Wratt, 2007: *Technical Summary. In: Climate Change 2007: The Physical Science Basis. Contribution of Working Group I to the Fourth Assessment Report of the Intergovernmental Panel on Climate Change*. [Solomon, S. and D Qin and M Manning and Z Chenand M Marquis and K B Averyt and Tignor and H L Miller (eds.)].Cambridge University Press, Cambridge, United Kingdom and New York, NY, USA. 68

Staniforth, A., 1997: Regional modeling: A theoretical discussion. *Meteorology and Atmospheric Physics*, **63**, 15–29. 16, 23

Stensrud, D. J., 2007: *Parameterization Schemes: Keys to Understanding Numerical Weather Prediction*. Cambridge University Press, Cambridge, United Kingdom, 459pp. 29, 31, 80

Stull, R. B., 1988: *An Introduction to Boundary Layer Meteorology*. Kluwer Academic Publisher, Dordrecht, the Netherlands, 1st edition, 670 pp. 33

Tapiador, F. J., E. Sánchez, and R. Romera, 2009: Exploiting an ensemble of regional climate models to provide robust estimates of projected changes in monthly temperature and precipitation probability distribution functions. *Tellus A*, **61A**, 57–71. 222

Terink, W., R. T. W. L. Hurkmans, P. J. J. F. Torfs, and R. Uijlenhoet, 2010: Evaluation of a bias correction method applied to downscaled precipitation and temperature reanalysis data for the Rhine basin. *Hydrology and Earth System Sciences*, **14**, 687–703. 150

Thompson, G., R. M. Rasmussen, and K. W. Manning, 2004: Explicit forecasts of winter precipitation using an improved bulk microphysics scheme. Part I:

Description and sensitivity analysis. *Monthly Weather Review*, **132**, 519–542.
31

Thornthwaite, C., 1931: The climates of North America: according to a new
classification. *Geographical Review*, **21**, 633–655. 44

— 1948: An approach toward a rational classification of climate. *Geographical
Review*, **38**, 55–94. 44

Timm, N. H., 2002: *Applied Multivariate Analysis*. Springer-Verlag. New York,
NY, USA,, 1st edition, 720 pp. 50, 234

Trigo, R. M. and J. P. Palutikof, 2001: Precipitation Scenarios over Iberia: A
Comparison between Direct GCM Output and Different Downscaling Tech-
niques. *Journal of Climate*, **14**, 4422–4446. 222

Unal, Y., T. Kindap, and M. Karaca, 2003: Redefining the climate zones of
Turkey using cluster analysis. *International Journal of Climatology*, **23**, 1045–
1055. 44, 50

Uppala, S., P. Kallberg, A. Simmons, U. Andrae, V. Bechtold, M. Fiorino,
J. Gibson, J. Haseler, A. Hernandez, G. Kelly, X. LI, K. Onogi, S. Saari-
nen, N. Sokka, R. Allan, E. Andersson, K. Arpe, M. Balmaseda, A. Beljaars,
L. Van De Berg, J. Bidlot, N. Bormann, S. Caires, F. Chevallier, A. Dethof,
M. Dragosavac, M. Fisher, M. Fuentes, S. Hagemann, E. Holm, B. Hoskins,
L. Isaksen, P. Janssen, R. Jenne, A. McNally, J. Mahfouf, J. Morcrette,
N. Rayner, R. Saunders, P. Simon, A. Sterl, K. Trenberth, A. Untch, D. Vasil-
jevic, P. Viterbo, and J. Woollen, 2005: The ERA-40 re-analysis. *Quarterly
Journal Of The Royal Meteorological Society*, **131**, 2961–3012. 64

van der Linden, P. and J. F. Mithchell, 2009: *ENSEMBLES: Climate Change and
its Impacts: Summary of research and results from the ENSEMBLES project*.
Met Office Hadley Centre, FitzRoy Road, Exeter EX1 3PB, UK, 160pp pp. 10,
65, 222

van Ulden, A., G. Lenderink, B. van den Hurk, and E. van Meijgaard, 2007: Cir-
culation statistics and climate change in Central Europe: Prudence simulations
and observations. *Climatic Change*, **81**, 179–192. 8

Vidale, P. L., D. Lüthi, C. Frei, S. I. Seneviratne, and C. Schär, 2003: Predictability and uncertainty in a regional climate model. *Journal of Geophysical Research*, **108**. 91

von Storch, H., H. Langenberg, and F. Feser, 2000: A spectral nudging technique for dynamical downscaling purposes. *Monthly Weather Review*, **128**, 3664–3673. 16

von Storch, H., E. Zorita, and U. Cubasch, 1993: Downscaling of global climate change estimates to regional scales: an application to Iberian rainfall in wintertime. *Journal of Climate*, **6**, 1161–1171. 3, 4

Waldron, K., J. Paegle, and J. Horel, 1996: Sensitivity of a spectrally filtered and nudged limited-area model to outer model options. *Monthly Weather Review*, **124**, 529–547. 16

Walsh, K. and J. McGregor, 1997: An assessment of simulations of climate variability over Australia with a limited area model. *International Journal of Climatology*, **17**, 201–223. 108

Wang, G., 2005: Agricultural drought in a future climate: results from 15 global climate models participating in the IPCC 4th assessment. *Climate Dynamics*, **25**, 739–753. 156

Wang, M., J. Paegle, and S. DeSordi, 1999: Global variable resolution simulations of Mississippi River basin rains of summer 1993. *Journal of Geophysical Research-Atmospheres*, **104**, 19399–19414. 4

Wang, Y., L. R. Leung, J. L. McGregor, D.-K. Lee, W.-C. Wan, Y. Ding, and F. Kimura, 2004: Regional climate modeling: Progress, challenges, and prospects. *Journal of the Meteorological Society of Japan*, **82**, 1599–1628. 21

Wicker, L. and W. Skamarock, 2002: Time-splitting methods for elastic models using forward time schemes. *Monthly Weather Review*, **130**, 2088–2097. 28

Wilby, R., L. Hay, and G. Leavesley, 1999: A comparison of downscaled and raw GCM output: implications for climate change scenarios in the San Juan River basin, Colorado. *Journal of Hydrology*, **225**, 67–91. 4

Wilby, R. and T. Wigley, 1997: Downscaling general circulation model output: a review of methods and limitations. *Progress in Physical Geography*, **21**, 530–548. 4

Wilks, D. S., 2006: *Statistical Methods in the Atmospheric Sciences*, volume 100 of *International Geophysics*. Academic Press, Elsevier, 2nd edition, 648 pp. 159, 236, 237

Zahn, M., H. von Storch, and S. Bakan, 2008: Climate mode simulation of North Atlantic polar lows in a limited area model. *Tellus A*, **60**, 620–631. 74

Zhang, Y., V. Duliére, P. W. Mote, and E. P. Salathe Jr, 2009: Evaluation of WRF and HadRM Mesoscale Climate Simulations over the US Pacific Northwest. *Journal of Climate*, **22**, 5511–5526. 91, 99